RUHR-UNIVERSITÄT BOCHUM
FAKULTÄT FÜR CHEMIE UND BIOCHEMIE
LEHRSTUHL FÜR THEORETISCHE CHEMIE

RUB

Implementation of Coupled Cluster Excitation Energies and Gradients using Pair Natural Orbitals

Dissertation

zur Erlangung des Doktorgrades der Naturwissenschaften

von

Marius Sebastian Frank

I. ACKNOWLEDGEMENTS

First of all, I would like to thank Prof. Dr. Christof Hättig most sincerely for leaving this interesting topic to me, his competent supervision and for being very helpful in the origination process of this thesis.
Furthermore, I would like to give many thanks to the whole quantum chemistry group in Bochum for a nice working atmosphere and, especially, to Alireza Marefat Khah and Sarah Khani for many fruitful discussions.
Many thanks also to my girlfriend Özlem Yönder for being understanding and supportive during the creation process of this thesis. And of course, thanks for proof-reading.
Last but not least, I want to give profuse thanks to my immediate family for constantly supporting me in every possible way during my whole study. Without them I would not have come that far.

CONTENTS

I. Acknowledgements II

II. Introduction 1

A. Coupled Cluster Methods For Excited States 8

B. Local Correlation Methods for the Ground State 13

C. Local Correlation Methods for Excited States 19

III. Theory 25

A. Coupled Cluster Theory 25

B. Computation of Molecular Properties and Excitation Energies for Non-Variational Waverunctions 27

1. Computation of Ground State Properties 27

2. Excitation Energies within the Linear Response Framework 29

C. Coupled Cluster Models for Excited States 36

1. The Coupled Cluster Models CCSD and CCSDT 36

2. The CC2 Approximation to the CCSD Model 38

3. The CIS(D) Approximation to CCSD 39

4. The CC3 Approximation to the CCSDT Model 40

D. Local Correlation Domains 42

1. Pair Natural Orbitals for the Ground State 42

2. Orbitals Specific Virtuals for the Ground State 44

3. Local Resolution of the Identity Approximation for the Ground State 45

4. Combination of PNOs and OSVs: The Hybrid OSV-PNO Approach 47

5. Excited State PNOs 49

6. Excited State OSVs 51

7. Hybrid OSV-PNO approach for Excited States 52
8. Local Resolution of the Identity Approximation for Excited States 53
E. Solution of the Excited State Eigenvalue Problem in a Truncated PNO Basis 53

IV. The PNO-MP2 Gradient and its Application to Molecular Geometry Optimizations 58

V. PNO-CCSD excitation energies within a Linear Response Framework 79

VI. PNO-CC3 Excitation Energies using Laplace Transformation Techniques 91

VII. Conclusions and Outlook 131

References 136

II. INTRODUCTION

Quantum chemistry employs the laws of quantum mechanics to make predictions about properties and structures of molecular systems. For this the (time-independent) Schrödinger equation

$$H_{\text{full}}\Psi(\mathbf{r}_1,\ldots,\mathbf{r}_N,\mathbf{R}_1,\ldots,\mathbf{R}_n) = E\Psi(\mathbf{r}_1,\ldots,\mathbf{r}_N,\mathbf{R}_1,\ldots,\mathbf{R}_n) \tag{1}$$

needs to be solved to obtain the energy E of a system with a wavefunction Ψ which depends on the coordinates $\mathbf{R}$ and $\mathbf{r}$ of, respectively, n nuclei and N electrons. It should be noted that the use of the Schrödinger equation already is an approximation, in the sense that relativistic effects are neglected. The exact solution of the Schrödinger equation is only possible for systems consisting of two particles. Hence, a variety of approximations has been introduced in order to make it possible to treat systems with several electrons and nuclei. For chemistry, the most fundamental one of these approximations is the Born-Oppenheimer approximation[1], which decouples the electronic and nuclear wave functions. Hence, the electronic Schrödinger equation for the electronic wavefunction ϕ only carries a parametric dependence on nuclear coordinates:

$$H(\mathbf{r}_1,\ldots,\mathbf{r}_N;\mathbf{R}_1,\ldots,\mathbf{R}_n)\phi = E\phi(\mathbf{r}_1,\ldots,\mathbf{r}_N;\mathbf{R}_1,\ldots,\mathbf{R}_n) \tag{2}$$

Solving this equation for different configurations of the nuclei $\mathbf{R}$ yields the potential energy surface (PES) of a molecule. The quantities of interest for this work are vertical excitation energies, molecular properties, as well as nuclear gradients. These quantities are directly related to the electronic energy and its derivatives with respect to an external perturbation. Hence, only the electronic Schrödinger equation will be considered here.

Even with the reduced parameter space obtained by the Born-Oppenheimer approximation, the exact analytical solution of the electronic Schrödinger equation is still only possible for systems consisting of one electron. Thus, further approximations

have to be introduced to solve the electronic Schrödinger equation for chemically relevant molecular systems.

These different approximations can roughly be divided into two categories: Wavefunction and density based methods. The basis for all wavefunction based methods is the Hartree Fock method[2,3]. Here, the N-electron wavefunction is represented by a single Slater determinant which consists of one-electron wavefunctions (orbitals) expanded in a finite basis set[4]. This single-determinant approach only takes the so-called Fermi correlation of electrons into account, i.e. the fact that two electrons with the same spin quantum number cannot occupy the same point in space. Hence, within Hartree Fock theory only electrons of the same spin are correlated in a trivial manner since each electron is only exposed to the mean field of all other electrons. Even though the simple description of the Hartree-Fock model accounts for the main contributions to the energy, the missing contributions are often crucial to obtain sufficiently accurate energies, geometries, or other properties. To account for the missing contributions another kind of electron correlation has to be taken into account, which is called dynamic electron correlation or Coulomb correlation. The dynamic electron correlation takes into account that electrons, as Coulombic particles, repel each other, and hence, the correlation of the electrons with the same spin is also taken into account. The consequence of the dynamic electron correlation is that the probability of two electrons occupying the same region in space is reduced compared to the spatially uncorrelated (only spin correlated) movement of electrons in the Hartree-Fock picture.

One way to account for the dynamic electron correlation is the use of density-based methods, i.e. density functional theory (DFT). Like Hartree-Fock, DFT is a one-particle theory, but it includes the dynamic electron correlation via an effective exchange-correlation (XC) functional[5,6]. Unfortunately, the exact XC functional is not known. In practice, the XC functional is therefore often approximated by assuming a functional form and performing a parametrization of this functional

against external parameters obtained from either experiments or high level *ab initio* method calculations. The lack of knowledge of the exact XC makes it impossible to define a hierarchy of functionals which systematically improve the results. Therefore, it is often mandatory to first carry out benchmark calculations to determine the most suitable functional for the system/property of interest. Especially, the treatment of London-dispersion interactions is not accounted for in the standard (semi-local) DFT functionals. Special corrections like Grimme's DFT-D3[7] and DFT-D4[8] dispersion corrections have to be used in such cases. When it comes to the computation of excitation energies, time-dependent DFT[9,10] (TDDFT), which is derived from linear response theory, is mostly used. Besides the aforementioned weaknesses of DFT methods, TDDFT is not able to describe charge-transfer and Rydberg states correctly[11] with the standard functionals. Also for these deficiencies there exist specialized functionals and methods like Coulomb attenuating functionals (e.g. CAM-B3LYP[12–15]) or constrained DFT[16] (CDFT) which are able to overcome these problems but again at the expense of corrupting the *ab initio* idea of quantum chemistry. However, DFT and TDDFT are nowadays still very widely used. This is mostly due to their low computational demands and fast convergence to the basis set limit. This makes these methods still highly attractive when the system of interest has to be treated at a quantum mechanical level but the more accurate wavefunction-based methods are prohibitive due to their high computational demands.

Wavefunction-based post-HF methods are built upon a Hartree-Fock reference determinant. Dynamic electron correlation is taken into account by forming excited configurations out of the reference determinant. This can be interpreted as excitations of electrons to unoccupied orbitals (with a certain probability given by the wavefunction parameters). By taking higher excitation levels (double, triple, quadruple,... excitation corresponding to pair-, three-, four-, ... electron correlations) into account the accuracy of wavefunction-based methods can systematically

be improved, i.e. the description of the N-electron basis is improved. Taking all possible excitations up to a level N of a system consisting of N electrons into account leads to the full CI (FCI) solution which is the best possible solution within a given basis set.

The maybe oldest wavefunction-based model which takes dynamic electron correlation into account is the configuration interaction (CI) model. The wavefunction ansatz for this approach is a linear combination of determinants whose expansion coefficients are determined variationally (in the following, only single-reference CI will be discussed). The hierarchy of these models is called according to the excitation classes included. For example, the CI singles and doubles (CISD) model includes single and double excitations out of the reference determinant (it is truncated after double excitations). Due do its lack of size-extensivity (for truncated CI models) and slow convergence towards the FCI limit with respect to the excitation class the CI model is nowadays not used anymore in practical applications.

By now, the CI model has mostly been replaced by the coupled cluster (CC) model[17–21] which uses an exponential parameterization of the wavefunction instead of a linear one. The exponential wavefunction ansatz ensures that the CC hierarchy of models remains size-extensive also for truncated CC models like CC with singles and doubles (CCSD). Additionally, it enhances the convergence towards the FCI limit. Both of these advantages of CC theory can be attributed to the inclusion of products of excitation operators, so-called disconnected excitations, which are a result of the exponential parameterization. However, the standard DFT, CI and CC models only yield meaningful results if a single determinant (HF) is a reasonable approximation for the ground state wavefunction (so-called single-reference models). If this is not the case, the reference wavefunction has to be composed of several configurations (determinants) which leads to e.g. the complete active space self-consistent field (CASSCF) model. Like HF is usually used as reference wavefunction for single reference models, the CASSCF wavefunction is usually used

TABLE I. Formal scaling of operation counts and disk space demands for different quantum chemical models as function of the system size $\mathcal{N}$.

Models	Operation count	Disk space
MP2/CC2	$\mathcal{O}(\mathcal{N}^5)$	$\mathcal{O}(\mathcal{N}^2)$
CCSD	$\mathcal{O}(\mathcal{N}^6)$	$\mathcal{O}(\mathcal{N}^4)$
CCSD(T)/CC3	$\mathcal{O}(\mathcal{N}^7)$	$\mathcal{O}(\mathcal{N}^4)$
CCSDT	$\mathcal{O}(\mathcal{N}^8)$	$\mathcal{O}(\mathcal{N}^6)$

as reference for multi-reference models. In addition to the Fermi correlation, the CASSCF model also incorporates the so-called static electron correlation which arises due to near-degeneracies and strong correlation between orbitals. However, the CASSCF model is usually not used to take dynamic electron correlation into account. For this, multi-reference versions of the aforementioned single-reference models have been developed such as multi-reference CI (MRCI), multi-reference CC (MRCC), second order perturbation correction to CASSCF (CASPT2), etc. Single- and multi-reference models converge towards the same FCI result with respect to the excitation class but the truncated multi-reference models are generally computationally much more demanding than their single-reference analogues. Multi-reference models such MRCC are not well-established yet and still subject to on-going research. Therefore, in the following the single-reference models will be focused.

Even though, wavefunction-based methods offer a way to systematically improve a result towards the exact solution, the high computational demands (floating point operations (FLOPs), memory, and disk space) of wavefunction-based methods dramatically limits their applicability. Improving the description of the N-electron basis comes at the cost of increasing the computational demands as summarized in table I for different quantum chemical models. These models will be discussed in more detail in the forthcoming sections.

However, the steep scaling is not an inherent physically based property of these models but only arises from the delocalized character of the usually employed canonical molecular orbitals. It is straightforward to show that dynamic electron correlation is a short-range effect which decays as $\mathcal{O}(\mathcal{R}^{-6})$ with the distance between two electrons, i.e. it is a dispersion interaction. Hence, it is, in principle, possible to implement the aforementioned wavefunction-methods (with additional approximations) in a linear scaling fashion if the short-range character of electron correlation is taken into account such that the number of correlated electrons pairs, triples, etc. scales linearly with the system size. Such methods are consequently called local correlation methods. There exist many different ways to exploit the locality of electron correlation, each with its own challenges, weaknesses and opportunities. These will be discussed in Chapter II B.

The application of local correlation methods for the computation to excitation energies and nuclear gradients is not straightforward. Both of these properties can be seen as a response to an external perturbation. For excitation energies the perturbation is due to the application of an external electric field which excites the molecule from the ground to an excited state. The challenge for local correlation methods arises due to the fact that the electronic excitation process is often non-local. While the electron correlation in the ground and the excited states are still local in the sense that only nearby electrons are correlated, the excitation process itself can be highly non-local. However, the correlated electrons involved in the excitation process still constitute a sparse set. To account for this sparsity of electron correlation in the excitation process, distance-based criteria for the selection of correlation domains as they were used for ground state local correlation methods are unsuitable.

The computation of gradients which take the response of orbitals to a change in the geometry into account imposes a different set of challenges for local correlation methods. First of all, the PES has to be (sufficiently) smooth (i.e. without

discontinuities) in order to obtain a physically meaningful derivative for geometry optimizations. When approximations are introduced to the energy, this may result in discontinuities in the PES due to the varying correlation domains at different geometries. Furthermore, it has to be investigated to which extent the contributions from the local approximations to the gradient have to be taken into account in order to obtain accurate geometries.

Hence, the aim of the present of work is to implement and analyze the results obtained flrom the local correlation treatment of excitation energies and nuclear gradients. Therefore, we will make use of the pair natural orbital (PNO) approximation (*vide infra*). The part on excitation energies builds upon previous work published by Hättig and Helmich[22] who implemented and analyzed the PNO approximation up to methods which do not take any doubles-doubles coupling into account (second order methods like coupled cluster singles with approximate doubles[23] (CC2) and the extended second algebraic diagrammatic construction scheme[24] (ADC(2)-x)). Thus, here the main goal is to extent this work to CCSD which takes the doubles-doubles coupling into account and to arrive at the first implementation of excitation energies for a model which takes triple excitations into account. For this, we will use the CC3 model (*vide infra*). The goal of the other part of this work is to arrive at the first implementation of a gradient within the PNO framework. For this purpose the simplest wavefunction-based model which takes electron correlation into account, i.e. second-oder Møller-Plesset perturbation theory (MP2), will be used. The focus here is to investigate the general applicability of the PNO approximation for molecular geometry optimizations while neglecting contributions to the gradient which are expected to be negligible compared to the PNO truncation errors.

A. Coupled Cluster Methods For Excited States

Extending the advantages of the coupled cluster theory (the black-box character, accuracy and fast convergence towards the FCI limit) from ground state to excited state calculations has been quite a challenge for theoretical chemists. This is also the reason why the first implementations of CCSD excitation energies, which were able to fully exploit the aforementioned advantages of coupled cluster theory, were only presented approximately 10 years after the ground state energies have been published.[25,26] It may seem straightforward to first compute the ground state energy and in an analogous fashion the energy of the excited state to obtain the excitation energy as difference between the ground state and the excited state energy. However, this approach requires that the wavefunction is obtained using a linear variational principle. This is done in multireference models (and in the determination of the amplitudes in CI models) but not in methods like DFT, MP2 or CC. Hence, such methods require different routes to obtain excitation energies.

Fortunately, theoretical work from Monkhorst[27,28], Mukherjee[29–31], Jørgensen[26,32], Koch[26], Bartlett[25,33,34] and co-workers made it possible to derive coupled cluster methods for excited states which do not have to rely on a single-state treatment. Around 1990, the first implementations of excitation energies[25,26] within the full CCSD model have been presented which employed these techniques, namely equation of motion coupled cluster[25,33,34] (EOM-CC) and linear reponse theory based coupled cluster[26–28,32,35] (LR-CC). These methods, presented back then, are still the most widely used ones nowadays for CC excitation energy and excited state property calculations. The idea of the EOM-CC ansatz is the application of a linear excitation operator on the coupled cluster wavefunction which results in the creation of the excited state configuration. Excitation energies are then straightforwardly obtained by diagonalizing a similarity transformed Hamiltonian. Response theory, in contrast, is derived from time-dependent perturbation theory. Here, excitation energies correspond to singularities of linear response functions which are

obtained by expanding a time-dependent expectation value in orders of the time-dependent electromagnetic perturbation. It can be shown that the EOM-CC and LR-CC ansatz are equivalent for excitation energies[25]. But for excited state properties the EOM-CC ansatz does not scale correctly with the system size whereas LR-CC does. Even though LR-CC leads to a slightly more complicated formalism, the fact that it scales for properties and transition moments correctly with the system size makes it for general purpose applications more attractive.

Both approaches generalize the hierarchy of standard coupled cluster models (CCSD, CCSDT, ...) to excited state calculations. But in the past more than 25 years, a significant amount of work has been put into the development of approximate coupled cluster methods. The motivation is to approximate the CCSD or CCSDT models in such a way that the time-determining $\mathcal{O}(\mathcal{N}^6)$- and $\mathcal{O}(\mathcal{N}^8)$-scaling operation counts and $\mathcal{O}(\mathcal{N}^4)$- and $\mathcal{O}(\mathcal{N}^6)$-scaling storage demands, respectively, of these models is avoided while the accuracy is not significantly deteriorated.

For ground state calculations the second order Moller-Plesset perturbation[36] (MP2) and coupled cluster singles and doubles with approximate triples[37] (CCSD(T)) are among the most widely used and reliable approximations to CCSD and CCSDT (even though, it should be noted that MP2 was initially not designed to approximate CCSD but was developed prior to coupled cluster theory). For most ground state properties they provide accurate results[38,39]. However, the extension of the success of these methods to excited state is still an on-going area of research for several reasons which will be briefly discussed in the following.

Since MP2 is a perturbative correction to Hartree-Fock, the MP2 response function has a spurious pole structure which is not consistent with the general pole structure in response theory[40]. Therefore, a variety of approaches has been presented which aim at approximating CCSD excitation energies (and excited state properties) with the same success as MP2 does for the ground state. The most popular of these approaches are the linear response based CC2 model from Christiansen *et al*[41],

the EOM-CCSD(2) model from Stanton and Gauss[42], the partitioned EOM many-body perturbation theory to second order (EOM-p-MBPT2) from Gwaltney *et al.*[43], and the configuration interactions singles with perturbative doubles (CIS(D)) from Head-Gordon *et al*[44]. While most of these models perform very similar to MP2 for ground state calculations[39] or are even built upon a MP2 ground state wavefunction they can show quite a different behavior in excited state calculations. This was shown in recent benchmark calculations from Kannar *et al.*[45] and coworkers and also by Goings *et al.*[46] where it was found that the CC2 and CIS(D) models have difficulties in describing Rydberg states while the EOM-CCSD(2) and EOM-p-MBPT2 models do yield more accurate results for such states. On the other hand, CC2 and CIS(D) are more accurate in describing local excitations[46]. The drawback of the EOM-based models is that the time-determining steps scale as $\mathcal{O}(\mathcal{N}^6)$ (indicating an unbalanced treatment of ground and excited state correlation effects) while the second order models obtained from linear response theory show the same scaling as MP2.

The aforementioned problems in approximating LR-CCSD and EOM-CCSD also transfer directly to excited state triples models which aim at approximating EOM-CCSDT and LR-CCSDT. Unfortunately, the success of the so-called gold standard of quantum chemitry for ground state calculations, CCSD(T), is not straightforwardly extendable to excited state calculations due to the existence of additional CCSD poles in the CCSD(T) response function[40]. This implies that CCSD(T) excitation energies do formally not exist[47] since the poles of the response function are only of CCSD quality[40]. For the ground state, CCSD(T) can be seen as a first iteration of the CCSDT-1 model[48] introduced by Bartlett and coworkers[49,50]. For ground state energy calculations both models were shown to perform equally well in terms of correcting the CCSD energy. However, extending the iterative CCSDT-1 model to excited state calculations (EOM-CCSDT-1[51]) results in improved results, compared to CCSD, only for the states with a significant double

excitation character[52]. For singly excited states the CCSDT-1 barely improves the CCSD results since both methods are correct through second order in the fluctuation potential for such states[52]. Also, attempts to extend the applicability of CCSD(T) to excited state calculations by drawing analogies between CCSD(T) and CCSDT-1, and generalizing them to excited states have failed since the resulting method (called EOM-CCSD(T)[51]) is correct only through first order in the fluctuation potential for singly excited states[47]. Christiansen *et al*[47] demonstrated the importance of a through analysis based on perturbation theory based arguments. By performing a perturbational analysis of the contributions to the CCSDT excitation energy they derived the noniterative models CCSDR(T) and CCSDR(3)[47], both of which are correct through third order in the fluctuation potential for singly excited states. Furthermore, Matthews and Stanton[53] recently presented the noniterative EOM-CCSD(T)(a*) (and EOM-CCSD(T)(a)) models which are computationally not more demanding than the CCSDR(T) and CCSDR(3) models but seems to be more accurate[45].

The iterative CC3[48,52] model can be seen as an extension of CC2 to triple excitations where the singles amplitudes are treated as zeroth-order parameters and all contributions arising from third or high order in the triples amplitudes are neglected. Like the CCSDR(T) and CCSDR(3) models, also the CC3 model is correct through third order in the fluctuation potential for singly excited states. The iterative EOM-CCSDT-1 can be seen as a special case of the CC3 model where certain contributions are neglected which leads to the poor performance for singly excited states. This finding led Bartlett and coworkers to develop the CCSDT-3 model[54,55]. Again, for ground state calculations this model performs similar to CCSD(T), CCSDT-1 and CC3. But even though, it is formally the most complete triples model (with respect to CCSDT) it does not improve the CC3 results with respect to excitation energies[56]. The same holds for the corresponding noniterative triples correction EOM-CCSD($\tilde{\text{T}}$)[55] obtained from analyzing the CCSDT-3 model.

This is most probably due to an imbalanced treatment of the doubles amplitudes in the CCSDT-3 model[52] in terms of perturbation theory.

For this work perturbative triples corrections CCSDR(T), CCSDR(3), and EOM-CCSD(T)(a*) have not been considered since their implementation within a local correlation framework is far more involved since they require the computation of the left CCSD eigenvectors. Among the iterative models, the hierarchy CC2 < CCSD < CC3 probably yields the most balanced description of excitation energies due to its thorough grounding in perturbation theory. As it was already shown by Hättig and coworkers[24,57] the introduction of (local) approximations in a model which does not describe ground and excited state correlation effects on an equal footing may result in spurious errors. Excitation energies for the models PNO-CC2[23] and PNO-ADC(2) have already been implemented in our group. Hence, in the present work we extend this framework towards the models CCSD and CC3.

So far, four different layers of approximations have been discussed: (1) The Born-Oppenheimer approximation which allows the separation of nuclear and electronic motion and is the basis of quantum chemistry, (2) the truncation of the cluster operator which makes quantum chemical calculations feasible by avoiding the exponential scaling of a FCI calculation, (3) the expansion of the one-electron basis in terms of finite discrete basis sets, and (4) the introduction of approximations to the cluster equations/Jacobian in order to avoid the time-determining steps of methods like CCSD and CCSDT.

There also exist other ways to further reduce the computational demands for ground and excited state calculations like the multilevel treatment by Myhre and Koch[58,59], where only a subset of orbitals is correlated a high level (e.g. CC3) and the other orbitals are treated at a lower level (e.g. CCSD). Even though, such methods may lead to significant computational savings, they do not address the inherent problem/bottleneck of quantum chemical calculations based on delocalized MOs: The unphysical scaling of computational demands with respect to the system size.

To address this issue, the so-called local correlation methods will be discussed in the next section.

B. Local Correlation Methods for the Ground State

Already in the early days of quantum chemistry, it has been realized that (dynamic) electron correlation is a local phenomenon. However, at that time it was not possible to take advantage of this in a practical sense due to the limited computational resources which made it impossible to perform calculations on sufficiently large (molecular) systems.

Nowadays, that the computational power is available and even converges to its limits, these local correlation methods have gained more and more attention since they enable the application of highly accurate *ab initio* calculations to large systems which would otherwise be out of reach for any conventional post-HF method. Being able to perform highly accurate and systematically improvable calculations on extended molecular systems without relying on empirical parameters, which are e.g. in many exchange correlation functionals in the DFT framework obtained by fitting to experimental data or e.g. high level CC results, is of great importance for the understanding of many chemical phenomena.

In the recent decades, two main families of local correlation approaches have emerged: Fragment based and the so-called direct[60] local correlation approaches. The basic concept behind the fragment-based local correlation approaches is the fragmentation of a molecular system into subsystems and to perform individual calculations on each of these subsystems (or depending on the method also on pair, triples, ... of the subsystems). These energies are then combined to obtain the total (correlation) energy of the whole molecular system. If the occupied orbitals are localized, the individual fragments can be interpreted as local correlation domains where only the electron correlation between spatially close electrons is considered.

Since the number of fragments scales linearly with the system size this makes it possible to develop linear scaling variants of canonical coupled cluster models even though the calculation of the individual fragments scale as the corresponding canonical method with the fragment size. This results in the need for an efficient fragmentation scheme which takes the most important electron correlation effects into account but avoids that the fragments become too large. Many different flavors of fragmentation schemes have been proposed in the past decade, like the cluster-in-molecule[61–64] (CIM), divide-expand-consolidate (DEC)[65–67], divide-and-conquer (DC)[68,69], fragment molecular orbital based[70,71] (FMO), natural linear scaling coupled cluster[72] (NSCCC), and the incremental scheme[73–78]. Roughly speaking, these approaches mainly differ in the way the molecule is partitioned and the subsystem energies are combined. The incremental method also requires to take fragment pairs, triples, ... into account whereas the DEC method only requires the computation of fragment and pair fragment energies in a truncated local orbital space. For most of the above mentioned methods, efficient approximate triples models[64,79–82] and partially also implementations for their explicitly correlated versions[83,84] have been presented. The main advantage of the fragment-based local correlation methods is that they can be trivially parallelized since the calculation on individual fragments are independent from each other. Furthermore, standard canonical codes can be used for the calculations of the fragments. A drawback of this method is that it involves a large number of redundant calculations, since the fragments need to have some amount of overlap in order to achieve accurate results. Even though fragmentation-based local correlation methods can in principle be implemented in a linear scaling fashion, they are only able to outperform direct local correlation methods (of the same model) through parallelization, i.e. through massively parallel calculations on high-end computer clusters which are not suitable/accessible for routine applications.

The family of direct local correlation methods does not define local correlation meth-

ods by a fragmentation of the system but by restricting the correlated wavefunction of the total system to local correlation domains. Hence, calculations are performed on the whole molecule but the wavefunction parameter space is truncated.

The maybe oldest of these approaches is based on the ideas of Saebø and Pulay[85–90] who proposed to use localized molecular orbitals (LMOs) for the occupied orbitals and then span the virtual space by projected atomic orbitals (PAOs). The projected atomic orbitals are obtained by projecting the AOs onto the virtual space. Since the AOs are generally local (if no diffuse functions are included) this results in a local but nonorthogonal representation of the virtual space. Local correlation domains are then defined by restricting excitation from LMOs to PAOs which are spatially close to each other. For double and triple excitations two and three of these domains are merged where the corresponding LMOs are close to each other. Werner and Schütz refined and implemented this scheme for MP2, CCSD and CCSD(T) and this way they were able to achieve a linear scaling of the computational demands with the system size. However, the determination of local correlation domains chosen[91,92] within the early PAO-based methods is based on parameters like distance or the number of connecting bonds, which requires that the PAO domains are specified prior to a calculation and cannot adapt themselves to the specific electronic structure problem at hand. Furthermore, the inclusion of diffuse basis functions can result in large correlation domains.

Another approach is based on the ideas by Almlöf and Häser[93–96] who showed that lower-scaling and yet accurate variants of MP2 can be obtained by a reformulation of the energy expression in the AO basis in combination with Laplace transformation techniques. Using efficient (multipole-based) integral screening techniques developed by Ochsenfeld[97,98], several groups were able to present lower-scaling versions of MP2[99–101]. Unfortunately, this technique can not be generalized to methods beyond second order since such methods involve more complicated expressions for the doubles amplitudes and using multipole estimates for the required integrals is

not always useful in reducing the number of required integrals.

A different approach in the realm of direct local correlation methods has already been proposed in 1956 by Löwdin[102] and was then later implemented by Meyer, Staemmler, Ahlrichs, Kutzelnigg, Lischka, and coworkers[103–106] in the context of CI and coupled electron pair approximation (CEPA) methods. The idea is to represent the virtual space by pair natural orbitals (PNOs). PNOs offer a way to represent the virtual space by pair-specific virtual orbitals, i.e. each electron pair gets its own virtual space assigned. The expansion coefficients are the eigenvectors of the pair contribution to an (approximate) one-electron density matrix and the eigenvalues correspond to the natural occupation numbers and, hence, indicate the importance of a given PNO to describe the electron correlation of a given pair of electrons. If the occupied space is spanned by LMOs, the natural occupation numbers decay rapidly (given that they are sorted in descending order) and are only significant if two electrons are sufficiently close to each other. Thus, it is possible to define local correlation domains by truncating the PNO expansion based on a threshold T_{PNO} which determines the accuracy of a calculation. This results in a linear scaling number of relevant pairs while the number of PNOs per pair is asymptotically independent of the system size. The advantage over PAOs is that no spatial information and *a priori* selection of domains are needed since the PNOs are constructed by analyzing an approximate model wavefunction and, hence, adapt themselves to the given system. Another important advantage is that the localization of the virtual space does not directly depend on the AO basis but mainly on the localization of the occupied space and the correlation length in the quantum system. Hence, if diffuse functions can be localized well with the given localization method also the PNOs will be localized close to the electron pair which results in smaller correlation domains.

At the time the PNOs were introduced, it was not possible to take full advantage of this local correlation method due to the high computational demands of

the two-electron integral transformations to the PNO basis which soon became prohibitive and led to a fading interest in this method. Only about 50 years after their introduction they have been revived by Neese *et al*[107,108] who realized that the aforementioned bottleneck can be circumvented by making use of the resolution-of-the-identity approximation[109] which makes it possible to approximate four-index integrals into products of three-index integrals. They also made use of the fact that the PAO basis as intermediate basis for the PNO construction can cover larger domains[110] and still speedup a calculation significantly. Combining the PNO and PAO approaches led then to the development of the so-called domain based PNO (DLPNO) method which has been used to arrive at highly efficient (near-) linear-scaling local variants of the single-reference models CCSD[111] and CCSD(T)[112–114], as well as of the multi-reference Mukherjee (Mk) coupled cluster models MkCCSD[115,116] and MkCCSD(T)[117].

Since the revival of the PNO approximation it has also gained much interest from other groups. Based on the idea to span the virtual space by pair-specific orbitals, Chan and coworkers introduced the concept of orbital specific virtuals[118–120] (OSVs) which constitute an orbital specific representation of the virtual space. Schmitz *et al* as well as Krause and Werner pointed out that the PNO, OSV, and PAO representations are just different tensor decompositions of the doubles amplitudes. Based on this, they combined the PAO, OSV and PNO approaches to reduce the computational complexity of the PNO construction. They also extended the concept of PNOs to explicitly correlated F12 methods which led to highly efficient implementations of MP2, CCSD and CCSD(T) and their explicitly correlated counterparts[121–131].

Recently, the PNO framework has been extended by several groups to multi-reference models. The resulting PNO-based implementations of CASPT2[132,133], NEVPT2[134] and Mukherjees multi-reference coupled cluster (MkCC)[115–117] yield highly accurate results, are (partially) linear scaling with respect to the system size

(provided a small and constant sized active space) and, hence, pave the way to make the PNO approximation a general purpose approach also for multi-reference models.

Compared to the fragment-based local correlation approach, the advantage of the direct local correlation approach is that it does not require massively parallel calculations in order to fully take advantage of it since redundant calculations on overlapping fragments are not needed and the computational demands for a calculation within a fragment/correlation domain do not have the same computational demands as a canonical calculation due to the reduced parameter space. However, a natural next step is the combination of fragment based and local correlation methods in order to combine the advantages of both methods[135,136].

So far, only total energy calculations have been discussed. Even though total energy can be seen as the key quantity, for a general purpose local correlation method other properties should also be efficiently reachable and with a high accuracy. Hence, part of this work aims at this extension of the PNO approach. Therefore, the computation of orbital relaxed gradient (first derivatives of the energy) of the simplest correlated wavefunction model MP2 is considered to investigate the applicability of the PNO approximation to molecular geometry optimizations. As a result, we presented the first implementation of analytic gradients for PNO-MP2 geometry optimizations. So far, gradient and molecular property calculations have been less intensively investigated in the context local correlation methods than the computation of total energies. For PAO based methods the MP2 and CC2 gradients[137–139] have been analyzed and applied to molecular geometry optimizations for ground and excited states and also ground state CCSD gradient have been presented[140]. Furthermore, ground and excited state properties were investigated within the context of PAOs[139,141–143]. Moreover, Werner and Dornbach[144] recently investigated the use of intrinsic bond orbitals[145] (IBOs) as localization method for the occupied space within the context of a PAO-based MP2 gradient. Also for the DEC and

CIM methods efficient MP2 gradients have only been presented very recently[146–148]. Ochsenfeld and coworkers[149,150] extended their AO-MP2 framework towards gradient and molecular property calculations. Furthermore, following the approximate PNO-MP2 gradient presented in this work, Pinski and Neese[151,152] presented a version of the DLPNO-MP2 gradient which additionally takes the relaxation of the PNOs as well as the gradient of the (pair and PNO) energy corrections into account. Their results show that taking these additional contributions to the orbital relaxed gradient into account does neither improve the convergence behavior in molecular geometry optimizations nor the accuracy compared to the results presented in this work. But for certain molecular properties such as electric field gradients they found that the inclusion of the PNO relaxation is necessary for obtaining accurate results.

Ground state energy derivatives are important for the understanding of many chemical phenomena and the interpretation of experimental results. Obtaining excited state properties and geometries requires, as a first step, being able to compute the excitation energies, which can be interpreted as a response of the wavefunction to an external frequency dependent electromagnetic field. In order to arrive at a generally applicable local correlation method which is equally reliable for ground and excited state calculations, it first has to be shown that it is able to give highly accurate results for excitation energies with high-order wavefunction based methods.

C. Local Correlation Methods for Excited States

The computation of excitation energies within a local correlation framework is anything but straightforward and local correlation methods which work impressively well for ground state energies may fail miserably when it comes to the computation of excitation energies. The difficulty emerges from the often non-local nature of the excitation process which may either lead to deficiencies in accuracy or efficiency for local correlation methods.

The first local correlation method applied to excited states was in 2002 presented by Crawford and King[153]. They used the ground state PAO domains and applied it to excited state EOM-CCSD calculations. The results were rather disappointing since the errors obtained with this approach were in the range of 0.2 - 0.3 eV. But they also mentioned that the results may be improved by constructing the excited state domains from analyzing a CIS vector. This idea was then taken up by Korona and Werner[154]. They chose to use the union of excited state domains obtained by an analysis of the natural transition orbitals (NTOs) and the ground state domains. This approach to a local version of EOM-CCSD also failed to transfer the success of ground state local correlation methods to excited state since the errors for singly excited states were still in the range of 0.06 eV - 0.15 eV even though the excited state domains were significantly larger than the ground state domains which led to a rather inefficient implementation. These findings led Schütz and coworkers[155] to the conclusion that due to the extended pair lists/correlation domains the implementation of CCSD excitation energies within the PAO framework is computationally too demanding and, hence, they proposed to restrict the local correlation treatment of excited states to second-order methods like CC2 whose computational demands only scale as $\mathcal{O}(\mathcal{N}^2)$ with the domain size (instead of $\mathcal{O}(\mathcal{N}^4)$ for CCSD). Within this context they succeeded in the implementation of excited state properties, transition moments and orbital relaxed gradients in the LR framework[139,141–143]. However, also the CC2 implementations were rather inefficient due to the extended excited state domains and for that reason the implementation of PAO-based CCSD excitation energies has been given up.

Similar difficulties have been reported by Mata and Stoll[156] in the context of the incremental scheme. They partitioned the occupied space into LMOs and NTOs and performed the partitioning into fragments by including the whole NTO and nearby LMOs into a single fragment. As the distance to the occupied NTO increases, the fragments are allowed to become smaller. Using this fragmentation

scheme leads to errors in excitation energies of typically 0.09 eV with respect to canonical EOM-CCSD. Clearly, this accuracy is not satisfactory for highly accurate calculations and can again be attributed to a non-optimal domain/fragment selection. Especially, due to the neglect of the virtual NTO in the fragment determination, it is not (yet) applicable to charge transfer excitations. Furthermore, a prohibitive loss of efficiency is expected for exciton coupling between two spatially distant chromophores. Up-to-date, the work of Mata and Stoll constitutes the only investigation of the applicability of fragment-based local correlation methods to the computation of excitation energies. But similar difficulties can also be expected for other fragmentation schemes like CIM or DEC.

In recent years, more and more research groups have tried to tackle the local correlation problem for excited states: Kallay and coworkers[157,158] attempted to truncate the virtual space by making use of state-averaged natural orbitals (NOs) and a truncated auxiliary basis to reduce the computational demands of CC2 calculations. This approach is similar to the reduced-virtual-space (RVS) approach presented by Sundholm and co-workers[159] which uses a truncation of the virtual space directly based on orbital energies and has been applied to CC2 excitation energies. The problem with such approaches is that the sparsity in the pair list of occupied orbitals cannot be exploited, the use of NOs or a RVS leads to a far less compact representation of the virtual space and the density matrices for the determination of the NOs have to be evaluated in the full MO basis.

Kristensen and coworkers[160–162] aimed at a complementary approach. They define local correlation domains by real-space cutoffs based on the distance between LMOs and the dominant NTOs for a transition but the virtual space is not truncated. This leads to computational saving only for cases where the chromophore is small compared to the molecular size but for chromophores which are extended over the whole molecular systems this approach does not lead anymore to significant computational savings. However, for many molecular systems of practical interest

the chromophore region is rather small and for such cases they have shown efficient implementations of excitation energies with the CC2[162,163] and CCSD[164] models. NO based approaches from Crawford[165] and coworkers as well as Bartlett[166] and coworkers suffer from similar drawbacks as mentioned above.

Neese and coworkers follow a different route to avoid the need to define separate domains for excited states. They introduced the concept of back-transformed PNOs[167] (bt-PNOs) which are usual ground state PNOs projected onto the canonical virtual space. The idea is to solve the ground state CCSD equations in the PNO basis and to use bt-PNOs for the solution of the excited state eigenvalue problem. Furthermore, they combine this approach with STEOM-CCSD[168] which requires the calculation of ionization and electron attachment potentials (IPs and EAs) for the amplitudes of the second similarity transformation. Since such calculations do not require a specialized set of excited state local correlation domains, it is possible to perform these calculations in the PNO basis of the ground state[169,170]. While the ground state, IP, and EA calculations can be performed in a linear scaling fashion, the computation of the excitation energy within the bt-PNO basis scales with STEOM-CCSD still as $\mathcal{O}(\mathcal{N}^5)$. Hence, also this approach does not yield a satisfying solution to the computation of excitation energies. Furthermore, it inherits some severe limitations of the STEOM method itself like the poor description of doubly excited states and the need to define an active space even though Dutta *et al*[171,172] recently proposed an automated active space selection scheme. The maybe most severe limitation of this approach is that it is not extendable towards approximate triples models like CCSDR(3) or CC3 and inherently non-linear scaling.

Very recently, also state-sepcific (and multistate) implementations of the multireference methods MkCCSD[116], MkCCSD(T)[117] and CASPT2[133] have been presented. Such an approach has the advantage that the non-local excitation process does not need to be described explicitly since the ground and excited state energies can be computed separately which makes the computation of excitation energies far less

problematic. The domains for the excited state can in principle be computed in the same way as they are computed for the single-reference ground state case. On the other hand, the usage of such multi-reference methods is much more involved (from a users point-of-view, these are not blackbox methods) and also the extension to excited gradients and properties is far more demanding from a developers point-of-view. The maybe most severe limitation of the combination of multireference methods with local correlation methods arises from the exponential scaling of computational costs with the size of the active space.

Helmich and Hättig, in contrast, proposed a PNO-based approach for the computation of excitation energies within the single-reference linear response framework which is efficient for local as well as non-local excitations. They proposed to construct separate state-specific PNOs for each excited state[22]. These PNOs are constructed by analyzing approximate CIS(D)-like densities which can be computed with close to linear-scaling costs from a pre-truncated basis. Using these state-specific PNOs ensures that the excited state PNO basis adapts itself to the nature of the excited state, irrespective of the locality of the excitation. Another advantage of this approach is that in principle a linear scaling of computational demands in terms of FLOPs, hard disk, and memory requirements can be achieved. This is in our eyes the most promising approach to compute excitation energies within the coupled cluster response framework and it has already been shown for CC2[23] and the extended ADC(2) method ADC(2)-x[24] that it yields highly accurate excitation energies for local as well as charge transfer excitations.

The aim of the present work to explore the extension of this approach to response methods that include connected triple excitations. As an intermediate step we have also developed the first fully PNO-based implementation of CCSD excitation energies which is highly efficient and accurate for local, charge transfer, and Rydberg excitations. As last part of this work the state-specific PNO framework is extended to the CC3 method which includes connected triple excitations in an approximate

way, similar as CC2 does for connected double excitations.

In the following section (section III) the underlying theoretical basis of this work will be explained. Then, in sections IV, V, and VI the results and implementations of the PNO-MP2 gradient, PNO-CCSD and PNO-CC3 excitation energies will be discussed based on the publications originated from this work. Concluding, the results will be summarized and an outlook on possible future developments will be given in section VII.

III. THEORY

A. Coupled Cluster Theory

In coupled cluster theory the ansatz for the correlated wavefunction is

$$|\mathrm{CC}\rangle = e^{T}|\mathrm{HF}\rangle \tag{3}$$

where $|\mathrm{HF}\rangle$ denotes the Hartree-Fock reference determinant and the cluster operator T is defined as

$$T = \sum_{i} T_i = T_1 + T_2 + T_3 + T_4 + \dots . \tag{4}$$

The operators $T_i = \sum_{\mu_i} t_{\mu_i} \tau_{\mu_i}$ excite i electrons out of the reference determinant with the amplitudes t_{μ_i}. For example, the one-, two and three electron contributions to the cluster operator are given by

$$T_1 = \sum_{ai} t_a^i \tau_{ai} \tag{5}$$

$$T_2 = \frac{1}{2} \sum_{aibj} t_{ab}^{ij} \tau_{ai} \tau_{bj} \tag{6}$$

$$T_3 = \frac{1}{6} \sum_{aibjck} t_{abc}^{ijk} \tau_{ai} \tau_{bj} \tau_{ck} \tag{7}$$

where the operator τ_{ai} correspond to excitation operator which excite an electron from an occupied orbital i to an unoccupied orbital a. Since this work is restricted to closed-shell systems the spin-free excitation operators

$$\tau_{ai} = E_{ai} = a_{a\alpha}^{\dagger} a_{i\alpha} + a_{a\beta}^{\dagger} a_{i\beta} \tag{8}$$

where $a_{a\alpha}^{\dagger}$ and $a_{i\alpha}$ are, respectively, electron creation and annhilation operators in the second quantization formalism, respectively, and the indices α and β refer to the two different minor spin quantum numbers, M_S, of electrons.

Inserting the coupled cluster wavefunction ansatz into the time-independent Schrödinger equation and multiplying from the left with e^{-T} leads to

$$e^{-T}He^{T}|\mathrm{HF}\rangle = E|\mathrm{HF}\rangle \tag{9}$$

where the similarity-transformed Hamiltonian can be evaluated using the Baker-Campbell-Hausdorff (BCH) expansion:

$$e^{-T}He^{T} = H + [H,T] + \frac{1}{2!}[[H,T],T] + \frac{1}{3!}[[[H,T],T],T] + \frac{1}{4!}[[[[H,T],T,]T],T] \ . \tag{10}$$

The coupled cluster energy can be obtained by projecting equation (9) onto the Hartree-Fock reference determinant

$$E = \langle \mathrm{HF}|He^{T}|\mathrm{HF}\rangle \tag{11}$$

and the cluster amplitudes t_{μ_i} can be obtained by projecting equation (9) onto the excited determinants $\langle\mu_i| = \langle \mathrm{HF}|\tau_{\mu_i}^{\dagger}$:

$$\Omega_{\mu_i} = \langle\mu_i|e^{-T}He^{T}|\mathrm{HF}\rangle = 0 \tag{12}$$

where Ω_{μ_i} is in the following referred to as ground state vector function.
Evaluating the coupled cluster energy as described here (so-called linked coupled cluster equations), leads to a non-variational energy evaluation for a truncated cluster operator, i.e. the coupled cluster energy is not an upper bound to the exact energy. Computing the coupled cluster energy variationally (variational coupled cluster (VCC)), i.e. minimizing

$$E = \frac{\langle \mathrm{CC}|H|\mathrm{CC}\rangle}{\langle \mathrm{CC}|\mathrm{CC}\rangle} = \frac{\langle \mathrm{HF}|e^{T^{\dagger}}He^{T}|\mathrm{HF}\rangle}{\langle \mathrm{HF}|e^{T^{\dagger}}e^{T}|\mathrm{HF}\rangle}, \tag{13}$$

with respect to the cluster amplitudes, is computationally involved since the expansion of $\langle \mathrm{HF}|e^{T^{\dagger}}He^{T}|\mathrm{HF}\rangle$ does not truncate before N_{el}-fold excitations, where N_{el} is the number of electrons. However, for practical applications the non-variational

nature of the coupled cluster energy is not a problem and the standard coupled cluster models, CCSD, CCSDT, ... use the projected Schrödinger equation. The linked form of the cluster equations used in this work is for formal derivations preferable over the alternative unlinked form as it gives term-wise size-consistent expressions[173].

B. Computation of Molecular Properties and Excitation Energies for Non-Variational Waverunctions

The non-variational nature of the coupled cluster energy has important consequences when it comes to the computation of molecular properties, gradients and excitation energies which will be discussed here.

1. Computation of Ground State Properties

Since the coupled cluster energy is not variational in its parameters, the first partial derivatives with respect to the wavefunction parameters λ do not vanish, i.e. $\frac{\partial E}{\partial \lambda} \neq 0$. For example, the total derivative of the energy with respect to a perturbation X would have to be computed as

$$\frac{dE(X,\lambda)}{dX} = \frac{\partial E}{\partial X} + \sum_i \frac{\partial E}{\partial \lambda_i}\frac{\partial \lambda_i}{\partial X} \tag{14}$$

where the vector λ contains all wavefunction parameters and the summation in the second term runs over all components of λ. Equation (14) requires the computation of the zeroth-order response of the wavefunction parameters $\lambda_i^{(0),X} = \frac{\partial \lambda_i}{\partial X}$. Hence, also the $2n+1$ rule, which states that the wavefunction parameters up to order n determine the energy up to order $2n+1$, does not hold.

In order to arrive at a formulation which obeys the $2n+1$ rule and, hence, avoids the computation of the parameter responses, the technique of Lagrange multipliers is used as suggested by Jørgensen and co-workers[174]. For this, a Lagrangian is set

up

$$\mathcal{L}(X,\lambda,\bar{\lambda}) = E + \sum_i \bar{\lambda}_i f_i(X,\lambda) \tag{15}$$

where $\bar{\lambda}_i$ denotes the Lagrange multiplier for the constraint f_i of the wavefunction parameters λ_i. The constraints are chosen such that the wavefuuction parameters can be determined as usual (i.e. for coupled cluster f_i are the residuals Ω_{μ_i}) and the Lagrange multipliers are determined by requiring the Lagrangian to be stationary with respect to variations of the wavefunction parameters. The wavefunction parameters can then be obtained similarly by requiring the Lagrangian to be stationary with respect to variations of the Lagrange multipliers:

$$\frac{\partial\mathcal{L}(X,\lambda,\bar{\lambda})}{\partial\lambda_i} = \frac{\partial E}{\partial\lambda_i} + \sum_i \bar{\lambda}_i \frac{\partial f_i(X,\lambda)}{\partial\lambda_i} = 0 \tag{16}$$

$$\frac{\partial\mathcal{L}(X,\lambda,\bar{\lambda})}{\partial\bar{\lambda}_i} = f_i(X,\lambda) = 0 \tag{17}$$

Determining the parameters of the Lagrangian this way makes it possible to evaluate the derivative of the Lagrangian with respect to an external perturbation in the same way as the derivative of the energy for a variational wavefunction:

$$\frac{\partial\mathcal{L}(X,\lambda,\bar{\lambda}))}{\partial X} = \frac{\partial E(X,\lambda)}{\partial\lambda} \tag{18}$$

For coupled cluster theory, equations (16) and (17) can be written as (if orbital relaxation is not taken into account)

$$\begin{aligned}\frac{\partial\mathcal{L}(X,\mathbf{t},\bar{\mathbf{t}})}{\partial t_{\mu_i}} &= \frac{\partial E}{\partial t_{\mu_i}} + \sum_{i\nu_j} \bar{t}_{\nu_j} \frac{\partial\Omega_{\nu_j}(X,\mathbf{t})}{\partial t_{\mu_i}} \\ &= \eta + \bar{\mathbf{t}}\mathbf{A} = 0 \end{aligned} \tag{19}$$

$$\frac{\partial\mathcal{L}(X,\mathbf{t},\bar{\mathbf{t}})}{\partial\bar{t}_{\mu_i}} = \Omega_{\mu_i}(X,\lambda) = 0 \tag{20}$$

where

$$\eta = \frac{\partial E}{\partial t_{\mu_i}} \ . \tag{21}$$

The Jacobian **A** introduced in the above equation can also be expressed as a mixed derivative with respect to the wavefunction parameters and the Lagrange multipliers:

$$A_{\mu_i\nu_j} = \frac{\partial \Omega_{\mu_i}}{\partial t_{\nu_j}} = \frac{\partial^2 \mathcal{L}(X, \mathbf{t}, \bar{\mathbf{t}})}{\partial \bar{t}_{\mu_i} \partial t_{\nu_j}} \tag{22}$$

Hence, coupled cluster properties (and similarly gradients) can in a Lagrangian formulation be computed by first solving the amplitude equations (20), subsequently computing the Lagrange multipliers by solving the linear equation (19) which involves the left transformation of the Lagrange multipliers with the Jacobian. Finally, the property of interest can be computed in a variational fashion using equation (18).

For the computation of gradients, the HF equations need to be considered as additional constraint. However, as soon as local approximations are introduced such as a truncation of the virtual space or the neglect of LMO pairs, the correlation energy is e.g. no longer invariant under rotations among the occupied MOs. Such local approximations, hence, result in the requirement to account for additional constraints. Within this work, only the aforementioned localization constraint which takes the non-invariance among occupied-occupied LMO rotations into account has been considered since the effect of other constraints on the gradient and molecular properties were expected to be small compared to the geometry dependence of the PNO selection[175] (*vide infra*). Hence, a PNO-based MP2 gradient augmented with this localization constraint has been implemented and thoroughly tested. The results of this study will be presented in section IV.

2. Excitation Energies within the Linear Response Framework

The computation of excitation energies (and excited state properties) requires similar techniques as described in the previous section for ground state properties. However, the transition from static propterties like dipole or quadrupole moments,

which can be evaluated as energy derivatives with respect to a static electromagnetic field (see above), to frequency or time-dependent properties requires a generalization of the techniques presented above. This will here be discussed in the framework of response theory.

The basis of linear response theory is the time-dependent Schrödinger equation

$$H(t,\epsilon)\Psi(t,\epsilon) = i\frac{d}{dt}\psi(t,\epsilon) \tag{23}$$

where the perturbed Hamiltonian is partitioned as

$$H(t,\epsilon) = H_0 + V(t,\epsilon) \tag{24}$$

with the unperturbed time-independent Hamiltonian H_0 and a time-dependent perturbation[40]

$$V(t,\epsilon) = \sum_{k=-N}^{N} e^{-i\omega_k t} \sum_X \epsilon_X(\omega_k) X \tag{25}$$

where ω_k is the frequency of an perturbing oscillating electromagnetic field, $\epsilon_X(\omega_k)$ is the field strength and X are the perturbation operators. The conditions $\omega_{-k} = -\omega_k$ and $\epsilon_X(\omega_{-k}) = \epsilon_X^*(\omega_k)$ have to be fulfilled such that $V(t,\epsilon)$ is Hermitian[40]. It should be stressed that the following derivations only hold for periodic a time-dependence. The wavefunction also is time-dependent and depends on the field strength:

$$\Psi(t,\epsilon) = \tilde{\Psi}(t,\epsilon) \exp\left(-i\int_{t_0}^{t_0+\tau} \mathcal{W}(t')dt'\right) \tag{26}$$

In equation (26) the wavefunction has been split into a phase-isolated part $\tilde{\Psi}(t,\epsilon)$ and an oscillating phase factor. The function $\mathcal{W}(t)$ of the phase factor is defined as

$$\mathcal{W}(t) = \langle\tilde{\Psi}(t,\epsilon)|H(t,\epsilon) - i\frac{d}{dt}|\tilde{\Psi}(t,\epsilon)\rangle \tag{27}$$

where it was assumed that the phase-isolated wavefunction is normalized.

Inserting this wavefunction ansatz into the time-dependent Schrödinger equation and multiplying with the complex conjugate of the phase factor yields the

Schrödinger equation for the phase-isolated wavefunction:

$$\left(H - i\frac{d}{dt}\right)\tilde{\Psi}(t,\epsilon) = \mathcal{W}(t,\epsilon)\tilde{\Psi}(t,\epsilon) \tag{28}$$

Multiplication with an arbitrary variation of the phase-isolated wavefunction $\delta\tilde{\Psi}$ from the left, integration of the real part

$$Re\langle\tilde{\Psi}(t,\epsilon)|H - i\frac{d}{dt} - \mathcal{W}(t,\epsilon)|\tilde{\Psi}(t,\epsilon)\rangle = 0 \tag{29}$$

and time-averaging over one period τ leads to the time-dependent variational principle

$$\delta\frac{1}{\tau}\int_{t_0}^{t_0+\tau}\mathcal{W}(t,\epsilon)dt = \delta\{\mathcal{W}\}_T = 0 \tag{30}$$

from which it can be deduced that the time-average of $\mathcal{W}$, which will in the following be denoted as $\{\mathcal{W}\}_T$ plays in the time-dependent case the same role as the energy does in the time-independent case[40]. Hence, $\{\mathcal{W}\}_T$ is also referred to as quasi-energy[40].

Response functions can be obtained by differentiating the quasi-energy with respect to the field strength at zero field strength. For example, the linear response function is given by[40]

$$\langle\langle X_0; X_1\rangle\rangle = \left.\frac{d^2\mathcal{W}\}_T}{d\epsilon_0 d\epsilon_1}\right|_0 \tag{31}$$

Hence, the above equation shows that the derivatives of the quasi-energy with respect to an electromagnetic field are in the time-dependent case connected to frequency-dependent molecular properties in a similar way as the derivatives of the energy are connected to static molecular properties in the time-independendent case[40].

Evaluating the response functions as derivatives of the quasi-energy is only possible if the wavefunction is variational with respect to its parameters. If the wavefunction is not variational with respect to its parameters the variational condition can

be enforced by the technique of Lagrange multipliers as described in the previous section. The corresponding Lagrange function can be set up by replacing the energy in equation (15) by the quasi-energy[40]

$$\mathcal{L}(\lambda(t), \bar{\lambda}(t), t) = \mathcal{W}(t) + \sum_i \bar{\lambda}_i(t) f_i(\lambda(t)) \tag{32}$$

where the wavefunction parameters λ as well as the Lagrange multipliers $\bar{\lambda}$ are time-dependent and the constraining functions f_i make the Lagrangian a variational quantity by the conditional equations for the Lagrange multipliers. It should be stressed that the Lagrangian defined above can be comlex whereas the quasi-energy of a variational method is real. Hence, the variational conditions are only applied to the real part of the Lagrangian $\mathrm{Re}(\mathcal{L})$.

Performing a Fourier component variational perturbation expansion of the Lagrangian and its parameters leads to the following expansion of the parameters and the Lagrangian with respect to the perdiodic perturbation[40]

$$\lambda(t) = \lambda^{(0)} + \lambda^{(1)}(t) + \lambda^{(2)}(t) + \ldots \tag{33}$$

$$\bar{\lambda}(t) = \bar{\lambda}^{(0)} + \bar{\lambda}^{(1)}(t) + \bar{\lambda}^{(2)}(t) + \ldots \tag{34}$$

$$\mathcal{L}(t) = \mathcal{L}^{(0)} + \mathcal{L}^{(1)}(t) + \mathcal{L}^{(2)}(t) + \ldots \tag{35}$$

where the zeroth-order parameters are time-independent (they are equal to the ones obtained in the previous section: $\lambda^{(0)} = \lambda^{(0),X}$) and the higher order parameters are given by[40]

$$\lambda^{(1)} = \sum_{k=-N}^{N} e^{-i\omega_{k_1} t} \lambda^{(1)}(\omega_{k_1}) \tag{36}$$

$$\lambda^{(2)} = \sum_{k=-N}^{N} e^{-i(\omega_{k_1} + \omega_{k_2}) t} \lambda^{(2)}(\omega_{k_1}, \omega_{k_2}) \tag{37}$$

The Fourier components $\lambda^{(n)}(\omega_{k_1}, \ldots, \omega_{k_n})$

$$\lambda^{(1)}(\omega_{k_1}) = \sum_X \epsilon_X(\omega_{k_1})\lambda^X(\omega_{k_1}) \tag{38}$$

$$\lambda^{(2)}(\omega_{k_1}, \omega_{k_2}) = \frac{1}{2}\sum_X Y\epsilon_X(\omega_{k_1})\epsilon_Y(\omega_{k_2})\lambda^{XY}(\omega_{k_2}, \omega_{k_2}) \tag{39}$$

in which the wavefunction parameters are expanded in include the parameters response $\lambda^{X\cdots}$ to the perturbation. The Lagrange multipliers are expanded in the same way[40].

For the time-averaged quasi-energy Lagrangian similar expressions are obtained[40]:

$$\{\mathcal{L}^{(0)}\}_T = \mathcal{L}^{(0)}(0) \tag{40}$$

$$\{\mathcal{L}^{(1)}\}_T = \sum_X \epsilon_X(0)\mathcal{L}^X(0) = \sum_X \epsilon_X(0)\langle X\rangle \tag{41}$$

$$\{\mathcal{L}^{(2)}\}_T = \frac{1}{2}\sum_{XYk_1} \epsilon_X(\omega_{k_1})\epsilon_Y(-\omega_{k_1})\mathcal{L}^{XY}(\omega_{k_1}) = \frac{1}{2}\sum_{XYk_1} \epsilon_X(\omega_{k_1})\epsilon_Y(-\omega_{k_1})\langle\langle X;Y\rangle\rangle_{\omega_{k_1}} \tag{42}$$

where $\mathcal{L}^{(0)}(0)$ corresponds to the Lagrangian given in equation (15) in the previous section for the time-independent case.

Hence, the response functions can be identified as the Fourier components of the quasi-energy Lagrangian[40]. The responses of the wavefunction parameters to a perturbation can be obtained by requiring the time-dependent variational (equation (30)) principle to hold in any order for the real part of the time-averaged Lagrangian:

$$\delta\{\mathrm{Re}(\mathcal{L}^{(n)})\}_T = 0 \tag{43}$$

This again is similar to requiring the time-independent Lagrangian to satisfy the usual time-independent variational principle to determine its parameters $\lambda^{(0)}$ and $\bar{\lambda}^{(0)}$.

The zeroth-order response parameters can be obtained by requiring the time-dependent variational principle to hold for the second-order parameters[40] (yielding

zeroth-order response equations given in the previous section in terms of equations (16) and (17))

$$\frac{\partial \mathcal{L}^{XY}(\omega_{k_1}, -\omega_{k_1})}{\partial \lambda^{XY}(\omega_{k_1}, -\omega_{k_1})} = \frac{\partial \{\mathcal{L}^{(2)}\}_T}{\partial \lambda^{(2)}(\omega_{k_1}, -\omega_{k_1})} = 0 \tag{44}$$

$$\frac{\partial \mathcal{L}^{XY}(\omega_{k_1}, -\omega_{k_1})}{\partial \bar{\lambda}^{XY}(\omega_{k_1}, -\omega_{k_1})} = \frac{\partial \{\mathcal{L}^{(2)}\}_T}{\partial \bar{\lambda}^{(2)}(\omega_{k_1}, -\omega_{k_1})} = 0 \tag{45}$$

Imposing the same condition for the first-order parameters

$$\begin{aligned}\frac{\partial \mathcal{L}^{XY}(\omega_{k_1}, -\omega_{k_1})}{\partial \lambda^{X}(\omega_{k_1})} &= \frac{\partial^2 \{\mathcal{L}^{(2)}\}_T}{\partial \lambda^{(1)}(\omega_{k_1}) \partial \epsilon_Y(-\omega_{k_1})} + \frac{\partial^2 \{\mathcal{L}^{(2)}\}_T}{\partial \lambda^{(1)}(\omega_{k_1}) \partial \lambda^{(1)}(-\omega_{k_1})} \lambda^Y(\omega_{k_1}) \\ &\quad + \bar{\lambda}^Y(-\omega_{k_1}) \frac{\partial^2 \{\mathcal{L}^{(2)}\}_T}{\partial \lambda^{(1)}(\omega_{k_1}) \partial \bar{\lambda}^{(1)}(-\omega_{k_1})} \\ &= \eta^Y + F(\omega_{k_1}) \lambda^Y(\omega_{k_1}) + \bar{\lambda}^Y(-\omega_{k_1}) A(\omega_{k_1}) = 0 \end{aligned} \tag{46}$$

$$\begin{aligned}\frac{\partial \mathcal{L}^{XY}(\omega_{k_1}, -\omega_{k_1})}{\partial \bar{\lambda}^{X}(\omega_{k_1})} &= \frac{\partial \{\mathcal{L}^{(2)}\}_T}{\partial \bar{\lambda}^{(1)}(\omega_{k_1}) \partial \epsilon_Y(-\omega_{k_1})} + \frac{\partial \{\mathcal{L}^{(2)}\}_T}{\partial \bar{\lambda}^{(1)}(\omega_{k_1}) \partial \lambda^{(1)}(-\omega_{k_1})} \lambda^Y(-\omega_{k_1}) \\ &\quad \chi^Y + A(\omega_{k_1}) \lambda^Y(\omega_{k_1}) = 0 \end{aligned} \tag{47}$$

gives the equations for them[40]. The intermediates appearing in the above equations are defined in table II.

Inserting the equations for the first- and zeroth-order parameters into the time-averaged second-order Lagrangian leads to the following equation for the first-order response function[40]

$$\begin{aligned}\langle\langle X; Y \rangle\rangle_{\omega_{k_1}} &= L^{XY}(\omega_{k1}, -\omega_{k_1}) = \frac{\partial^2 \{L^{(2)}\}_T}{\partial \epsilon_X(\omega_{k_1}) \partial \epsilon_Y(-\omega_{k_1})} \\ &= C^{\pm\omega} P\left(X(\omega_{k_1}), Y(-\omega_{k_1})\right) \left[\eta^X + \frac{1}{2} F(\omega_{k_1}) \lambda^X(-\omega_{k_1})\right] \lambda^Y(\omega_{k_1}) \end{aligned} \tag{48}$$

where

$$P\left(X(\omega_{k_1}), Y(-\omega_{k_1}))\right) f\left(X(\omega_{k_1}), Y(-\omega_{k_1}))\right) = f\left(X(\omega_{k_1}), Y(-\omega_{k_1})\right) + f\left(Y(-\omega_{k_1}), X(\omega_{k_1})\right) \tag{49}$$

and

$$C^{\pm\omega} f^{XY}(\omega_{k_1}, -\omega_{k_1}) = \frac{1}{2}\left[f^{XY}(\omega_{k_1}, -\omega_{k_1}) + f^{*XY}(-\omega_{k_1}, \omega_{k_1})\right] \tag{50}$$

TABLE II. Definion of the intermediates[40] appearing in equations (47) and (46).

Intermediate
$\eta^Y = \dfrac{\partial^2\{\mathcal{L}^{(2)}\}_T}{\partial\lambda^{(1)}(\omega_{k_1})\partial\epsilon_Y(-\omega_{k_1})}$
$F(\omega_{k_1}) = \dfrac{\partial^2\{\mathcal{L}^{(2)}\}_T}{\partial\lambda^{(1)}(\omega_{k_1})\partial\lambda^{(1)}(-\omega_{k_1})}$
$A(\omega_{k_1}) = \dfrac{\partial^2\{\mathcal{L}^{(2)}\}_T}{\partial\lambda^{(1)}(\omega_{k_1})\partial\bar{\lambda}^{(1)}(-\omega_{k_1})}$
$\chi^Y = \dfrac{\partial\{\mathcal{L}^{(2)}\}_T}{\partial\bar{\lambda}^{(1)}(\omega_{k_1})\partial\epsilon_Y(-\omega_{k_1})}$

The evaluation of the first-order response function, hence, requires (besides the zeroth-order parameters) the first-order response of the wavefunction parameter λ^Y to the perturbation. These can be obtained by solving equation (47).

In order to deduce excitation energies from the linear response function of an approximate (non-variational) wavefunction, the response function of the exact wavefunction has to be considered (since in linear response theory excitation energies and molecular properties are for approximate wavefunctions obtained by drawing analogies to the response functions of an exact wavefunction[40])

$$\langle\langle X;Y\rangle\rangle_{\omega_{k_1}} = \sum_{J\neq 0}\frac{\langle 0|X|J\rangle\langle J|Y|0\rangle}{\omega_{k_1}-\Delta E_{J0}} - \frac{\langle 0|Y|J\rangle\langle J|X|0\rangle}{\omega_{k_1}+\Delta E_{J0}} \tag{51}$$

where the states $|J\rangle$ correspond to the eigenstates of the unperturbed Hamiltonian and ΔE_{J0} denotes the energy difference between the ground state $|0\rangle$ and an excited state $|J\rangle$, i.e. an excitation energy. Obviously, the exact response function has poles where the frequency of the monochromatic perturbation is equal to the excitation frequency. Equation (47) shows that the wavefunction parameters of an approximate wavefunction, and hence, the response functions, have poles if the frequency becomes equal to an eigenvalue of the Jacobian[40] $A(0) = A(\omega_{k_1}) + \omega_{k_1}$ where $A(0)$ corresponds to the Jacobian defined in equation (22). Hence, by induction it can be concluded that the excitation energies for an approximate wavefunction can be obtained as eigenvalues of Jacobian.

C. Coupled Cluster Models for Excited States

In the previous section it was shown that excitation energies are in the linear response framework given by the eigenvalues of the Jacobian. Hence, the solution of an eigenvalue problem

$$\mathbf{AR} = \omega\mathbf{R} \tag{52}$$

is required where $\mathbf{R}$ refers to the eigenvectors which are, similar to the cluster amplitudes partitioned into single R_{μ_1}, double R_{μ_2}, triple R_{μ_3} ... excitation components. The storage or direct diagonalization of the full Jacobian matrix is computationally not feasible since already for methods including double excitations the Jacobian is a rank-8 tensor. Since the full spectrum is usually not of interest but only a few of the lowest eigenvalues, the eigenvalue problem is usually solved iteratively. Therefore, most implementations make use of a Davidson algorithm[176] for the determination of the Jacobian eigenvalues. The Davidson algorithm only requires the computation of linear transformations of trial vector $\mathbf{E}$ with the Jacobian

$$\rho_{\mu_i} = \sum_{\nu_j} A_{\mu_i\nu_j} E_{\nu_j}. \tag{53}$$

1. The Coupled Cluster Models CCSD and CCSDT

For the coupled cluster model CCSDT the cluster operator is truncated after triple excitations, i.e. $T = T_1 + T_2 + T_3$. The vector function for the singles, doubles and triples amplitudes is given by

$$\Omega_{\mu_1}^{\mathrm{CCSDT}} = \langle\mu_1|e^{-T_2-T_3}\hat{H}e^{T_2+T_3}|\mathrm{HF}\rangle = \Omega_{\mu_1}^{\mathrm{CCSD}} + \langle\mu_1|[H,T_3]|\mathrm{HF}\rangle \tag{54}$$

$$\Omega_{\mu_2}^{\mathrm{CCSDT}} = \langle\mu_2|e^{-T_2-T_3}\hat{H}e^{T_2+T_3}|\mathrm{HF}\rangle = \Omega_{\mu_2}^{\mathrm{CCSD}} + \langle\mu_2|[\hat{H},T_3]|\mathrm{HF}\rangle \tag{55}$$

$$\Omega_{\mu_3}^{\mathrm{CCSDT}} = \langle\mu_3|e^{-T_2-T_3}\hat{H}e^{T_2+T_3}|\mathrm{HF}\rangle \tag{56}$$

$$= \langle\mu_3|[\hat{H},T_3] + [\hat{H},T_2]|\mathrm{HF}\rangle + \langle\mu_3|[[H,T_3],T_2] + \frac{1}{2}[[\hat{H},T_2],T_2]|\mathrm{HF}\rangle \tag{57}$$

where $\Omega_{\mu_i}^{\mathrm{CCSD}}$ refers to the CCSD vector function

$$\Omega_{\mu_1}^{\mathrm{CCSD}} = \langle \mu_1 | \hat{H} + [\hat{H}, T_2] | \mathrm{HF} \rangle \tag{58}$$

$$\Omega_{\mu_2}^{\mathrm{CCSD}} = \langle \mu_2 | \hat{H} + [\hat{H}, T_2] + \frac{1}{2}[[\hat{H}, T_2]T_2] | \mathrm{HF} \rangle \tag{59}$$

and the $\exp(\hat{T}_1)$ similarity-transformed Hamiltonian $\hat{H}$ is given by

$$\hat{H} = e^{-T_1} H e^{T_1} \tag{60}$$

The Jacobian, which plays the central role in the computation of excitation energies within the linear response framework, is for CCSDT obtained as

$$A_{\mu_i\nu_j}^{\mathrm{CCSDT}} = \begin{pmatrix} A_{\mu_1\nu_1}^{\mathrm{CCSD}} & A_{\mu_1\nu_2}^{\mathrm{CCSD}} & \langle \mu_1 | [\hat{H}, \tau_{\nu_3}] | \mathrm{HF} \rangle \\ A_{\mu_2\nu_1}^{\mathrm{CCSD}} + \langle \mu_2 | [[\hat{H}, T_3], \tau_{\nu_1}] | \mathrm{HF} \rangle & A_{\mu_2\nu_2}^{\mathrm{CCSD}} & \langle \mu_2 | [\hat{H}, \tau_{\nu_3}] | \mathrm{HF} \rangle \\ \langle \mu_3 | [\hat{H} + T_3 & \langle \mu_3 | [\hat{H} + [\hat{H}, T_2] & \langle \mu_3 | [\hat{H} \\ \quad + \frac{1}{2}[[\hat{H}, T_2], T_2], \tau_{\nu_1}] | \mathrm{HF} \rangle & \quad + [\hat{H}, T_3], \tau_{\nu_2}] | \mathrm{HF} \rangle & \quad + [\hat{H}, T_2], \tau_{\nu_3}] | \mathrm{HF} \rangle \end{pmatrix}$$

where $A_{\mu_i\nu_j}^{\mathrm{CCSD}}$ refers to the CCSD-like Jacobian given by

$$A_{\mu_i\nu_j}^{\mathrm{CCSD}} = \begin{pmatrix} \langle \mu_1 | [\hat{H} + [\hat{H}, T_2], \tau_{\nu_1}] | \mathrm{HF} \rangle & \langle \mu_1 | [\hat{H}, \tau_{\nu_2}] | \mathrm{HF} \rangle \\ \langle \mu_2 | [\hat{H} + [\hat{H}, T_2], \tau_{\nu_1}] | \mathrm{HF} \rangle & \langle \mu_2 | [\hat{H} + [\hat{H}, T_2], \tau_{\nu_2}] | \mathrm{HF} \rangle \end{pmatrix} \tag{61}$$

but evaluated for CCSDT with the singles and doubles amplitudes from the CCSDT calculation. The opertation counts for CCSDT and CCSD scale as $\mathcal{O}(\mathcal{N}^8)$ and $\mathcal{O}(\mathcal{N}^6)$, respectively. In addition to the steep scaling, also the storage requirements of $\mathcal{O}(\mathcal{N}^6)$ (for the CCSDT triples amplitudes) and $\mathcal{O}(\mathcal{N}^4)$ (for the CCSD doubles amplitudes), respectively, can become prohibitive for many applications. To circumvent these potential bottlenecks of both methods, different approximations to these methods have been proposed. However, approximate methods like MP2 and CCSD(T) which work well for ground state calculations cannot be used for excited state calculations due to the reasons given in Section II A. Therefore, alternative approximate models for excited states have been developed which some of (CC2, CIS(D) and CC3) will be discussed in the following.

2. The CC2 Approximation to the CCSD Model

The CC2 approximation[41] aims at approximating the CCSD model such that the $\mathcal{O}(\mathcal{N}^6)$-scaling operation counts and the $\mathcal{O}(\mathcal{N}^4)$-scaling storage demands are avoided while the accuracy for excitation energies is as much as possible maintained. The basis is the partitioning of the Hamiltonian as

$$H = F + \phi \tag{62}$$

with the Fock operator F and the fluctuation potential ϕ. The singles amplitudes are treated as zeroth order parameters due to their special importance in coupled cluster response theory for a balanced description of properties and energies since they respond to zeroth-order in ϕ to an external perturbation[41] if the perturbation is described by a one-electron operator. The doubles amplitudes are required to be correct to first order in the flutuation potential which leads to the following equations for the ground state vector function

$$\Omega_{\mu_1}^{\mathrm{CC2}} = \langle \mu_1 | \hat{H} + [\hat{H}, T_2] | \mathrm{HF} \rangle = \Omega_{\mu_1}^{\mathrm{CCSD}} \tag{63}$$

$$\Omega_{\mu_2}^{\mathrm{CC2}} = \langle \mu_2 | \hat{H} + [F, T_2] | \mathrm{HF} \rangle \tag{64}$$

which shows that the singles equations of the CCSD model stay unaltered. The doubles equations are significantly simplified since $[[F,T],T] = [[[F,T],T],T] = \cdots = 0$ (assuming a closed-shell system) and

$$[F, T_i] = \sum_{\mu} t_{\mu_i} E_{\mu_i} \epsilon_{\mu_i} = \sum_{\mu} T_i \epsilon_{\mu_i} \tag{65}$$

where ϵ_{μ_i} refers to (Hartree-Fock) orbital energy differences, e.g. $\epsilon_{aibj} = \epsilon_a + \epsilon_b - \epsilon_i - \epsilon_j$. With these simplifications an analytic expression for the doubles amplitudes can be obtained as

$$t_{\mu_2} = \epsilon_{\mu_2}^{-1} \langle \mu_2 | \hat{H} | \mathrm{HF} \rangle. \tag{66}$$

Equation (66) only involves the computation of two-electron integrals and, hence, the computation of the doubles vector function only scales as $\mathcal{O}(\mathcal{N}^5)$ instead of $\mathcal{O}(\mathcal{N}^6)$ for CCSD. Furthermore, the storage of the doubles amplitudes which scales as $\mathcal{O}(\mathcal{N}^4)$ can be avoided since these amplitudes can be computed on-the-fly from equation (66) whenever needed[41]. However, it should be noted that this is only feasible if the RI approximation for the two-electron integrals appearing in the amplitude equations is used.

The CC2 Jacobian is from equations (63) and (64) readily obtained as[41]

$$A^{\mathrm{CC2}}_{\mu_i\nu_j} = \begin{pmatrix} \langle\mu_1|[\hat{H}+[\hat{H},T_2],\tau_{\nu_1}]|\mathrm{HF}\rangle & \langle\mu_1|[\hat{H},\tau_{\nu_2}]|\mathrm{HF}\rangle \\ \langle\mu_2|[\hat{H},\tau_{\nu_1}]|\mathrm{HF}\rangle & \delta_{\mu\nu}\epsilon_{\nu_2} \end{pmatrix} \tag{67}$$

Due to the diagonal structure of the doubles-doubles block of the Jacobian the CC2 eigenvalue problem can be expressed in terms of the singles space only

$$\sum_{\nu_1} A^{\mathrm{eff}}_{\mu_1\nu_1}(\omega) R_{\nu_1} = \sum_{\nu_1}\left[A_{\mu_1\nu_1} + \sum_{\kappa_2}\frac{A_{\mu_1\kappa_2}A_{\kappa_2\nu_1}}{\omega-\epsilon_{\kappa_2}}\right] R_{\nu_1} = \omega R_{\mu_2} \tag{68}$$

where the excited state doubles amplitudes can be computed as[41]

$$R_{\mu_2} = (\omega-\epsilon_{\mu_2})^{-1}\sum_{\nu_1} A_{\mu_2\nu_1}R_{\nu_1} = (\omega-\epsilon_{\mu_2})^{-1}\sum_{\nu_1}\langle\mu_2|[\hat{H},\tau_{\nu_1}]|\mathrm{HF}\rangle R_{\nu_1} \tag{69}$$

$$= (\omega-\epsilon_{\mu_2})^{-1}\langle\mu_2|[\bar{H}|\mathrm{HF}\rangle \tag{70}$$

In equation (70) the effective Hamiltonian $\bar{H} = [\hat{H}, R_1]$ with the auxiliary operator $R_1 = \sum_\nu \tau_{\nu_1} R_{\nu_1}$ has been introduced. Hence, the computatin of the excited state doubles amplitudes only scales as $\mathcal{O}(\mathcal{N}^5)$ and the storage of the excited states doubles amplitudes can be avoided by partitioning the eigenvalue problem according to equation (68).

3. The CIS(D) Approximation to CCSD

Even though the CC2 approximation significantly reduces the computational demands compared to CCSD, it still is an iterative procedure, i.e. each iteration

scales as $\mathcal{O}(\mathcal{N}^5)$, and the partitioning technique results in a nonlinear eigenvalue problem. To further reduce the computational demands, a noniterative correction to the excitation energy and the doubles eigenvector can be employed like it is done in the CIS(D) model[44].

As in the CC2 model, the Hamiltonian is partitioned as $H = F + \phi$. The aim is to correct the CIS excitation energies and eigenvectors for the CCSD doubles contributions. Therefore, the CIS solution is treated as zeroth-order solution $\mathbf{A}^{\mathrm{CIS}}\mathbf{R}^{(0)} = \omega\mathbf{R}^{(0}$ with $A^{\mathrm{CIS}}_{\mu_1\nu_1} = \langle\mu_1|[H,\tau_{\nu_1}],|\mathrm{HF}\rangle$. The CCSD Jacobian is expanded in terms of of the fluctuation potential[44]

$$\begin{aligned} A^{\mathrm{CCSD}}_{\mu_i\nu_j} &= A^{(0)}_{\mu_i\nu_j} + A^{(1)}_{\mu_i\nu_j} + A^{(2)}_{\mu_i\nu_j} + \dots \\ &= \begin{pmatrix} A^{\mathrm{CIS}}_{\mu_1\nu_1} & 0 \\ 0 & \delta_{\mu\nu}\epsilon_{\nu_2} \end{pmatrix} + \begin{pmatrix} 0 & \langle\mu_1|[\phi,\tau_{\nu_2}]|\mathrm{HF}\rangle \\ \langle\mu_2|[\phi,\tau_{\nu_1}]|\mathrm{HF}\rangle & \langle\mu_2|[\phi,\tau_{\nu_2}]|\mathrm{HF}\rangle \end{pmatrix} \\ &+ \begin{pmatrix} \langle\mu_1|[[\phi,T_2],\tau_{\nu_1}]|\mathrm{HF}\rangle & 0 \\ \langle\mu_2|[[\phi,T_2],\tau_{\nu_1}]|\mathrm{HF}\rangle & 0 \end{pmatrix} + \dots \end{aligned} \tag{71}$$

The second-order correction to the excitation energy is then given by[44]

$$\begin{aligned} \omega^{(2)} &= \sum_{\mu_1\nu_1} R^{(0)}_{\mu_1} A^{(2)}_{\mu_1\nu_1} R^{(0)}_{\nu_1} + \sum_{\mu_1\nu_1} R^{(0)}_{\mu_1} A^{(1)}_{\mu_1\nu_2} R^{(1)}_{\nu_2} \\ &= \sum_{\nu_1} \langle R^{(0)}_{\mu_1}|[[\phi,T_2],\tau_{\nu_1}|\mathrm{HF}\rangle R^{(0)}_{\nu_1} + \sum_{\nu_1} \langle R^{(0)}_{\mu_1}|[\phi,\tau_{\nu_1}]|\mathrm{HF}\rangle R^{(1)}_{\nu_1} \end{aligned} \tag{72}$$

with $\langle R^{(0)}_{\mu_1}| = \sum_{\mu_1}\langle\mu_1|R^{(0)}_{\mu_1}$ and $\mathrm{R}^{(0)}$) refers to the CIS eigenvectors while $\mathrm{R}^{(1)}$ are the first-order approximations to the CCSD eigenvectors[44]

$$R^{(1)}_{\mu_2} = (\omega - \epsilon_{\mu_2})^{-1} \sum_{\nu_1} A^{(1)}_{\mu_2\nu_1} R^{(0)}_{\nu_1} = (\omega - \epsilon_{\mu_2})^{-1} \sum_{\nu_1} \langle\mu_2|[\phi,\tau_{\nu_1}]|\mathrm{HF}\rangle R^{(0)}_{\nu_1} \tag{73}$$

4. The CC3 Approximation to the CCSDT Model

The CC3 approximation[48,52] to CCSDT is designed very similar to the CC2 approximation to CCSD. Like for CC2, the singles amplitudes are treated as zeroth-order

parameters due to their special role in response theory. The triples amplitudes are required to be correct to second order in the fluctuation potential, i.e. they are correct in the lowest non-vanishing order[41]. This leads to the following equations for the CC3 ground state vector function

$$\Omega_{\mu_1}^{\mathrm{CC3}} = \langle \mu_1 | \hat{H} + [\hat{H}, T_2] + [\hat{H}, T_3] | \mathrm{HF} \rangle \tag{74}$$

$$\Omega_{\mu_2}^{\mathrm{CC3}} = \langle \mu_2 | \hat{H} + [\hat{H}, T_2] + \frac{1}{2}[[\hat{H}, T_2]T_2] + [\hat{H}, T_3] | \mathrm{HF} \rangle \tag{75}$$

$$\Omega_{\mu_3}^{\mathrm{CC3}} = \langle \mu_3 | [F, T_3] + [\hat{H}, T_2] | \mathrm{HF} \rangle \tag{76}$$

From equation (76) it can be seen that the ground state triples amplitudes can be computed analytically (similar to the CC2 doubles amplitudes) as

$$t_{\mu_3} = \epsilon_{\mu_3}^{-1} \langle \mu_3 | [\hat{H}, T_2] | \mathrm{HF} \rangle \tag{77}$$

The Jacobian is from equations (74) - (76) obtained as[52]

$$\mathbf{A}_{\mu_i \nu_j}^{\mathrm{CC3}} = \begin{pmatrix} \langle \mu_1 | [\hat{H} + [\hat{H}, T_2], \tau_{\nu_1}] | \mathrm{HF} \rangle & \langle \mu_1 | [\hat{H}, \tau_{\nu_2}] | \mathrm{HF} \rangle & \langle \mu_1 | [\hat{H}, \tau_{\nu_3}] | \mathrm{HF} \rangle \\ \langle \mu_2 | [\hat{H} + [\hat{H}, T_2 + T_3], \tau_{\nu_1}] | \mathrm{HF} \rangle & \langle \mu_2 | [\hat{H} + [\hat{H}, T_2], \tau_{\nu_2}] | \mathrm{HF} \rangle & \langle \mu_2 | [\hat{H}, \tau_{\nu_3}] | \mathrm{HF} \rangle \\ \langle \mu_3 | [[\hat{H}, T_2], \tau_{\nu_1} | \mathrm{HF} \rangle & \langle \mu_3 | [\hat{H}, \tau_{\nu_2}] | \mathrm{HF} \rangle & \delta_{\mu\nu} \epsilon_{\mu_3} \end{pmatrix}$$

Due to the diagonal structure of the triples-triples block of the Jacobian, the eigenvalue problem can be solved in the singles and doubles space only using the following effective Jacobian

$$\sum_{j=1}^{2} \sum_{\nu_j} A_{\mu_i \nu_j}^{\mathrm{eff}}(\omega) R_{\nu_j} = \sum_{j=1}^{2} \sum_{\nu_j} \left(A_{\mu_i \nu_j} + \sum_{\kappa_3} \frac{A_{\mu_i \kappa_3} A_{\kappa_3 \nu_j}}{\Delta_{\kappa_3} + \omega} \right) R_{\nu_j} = \omega R_{\mu_i} \ , \tag{78}$$

where the excited state triples amplitudes can be computed analytically from[52]

$$\begin{aligned} R_{\mu_3} &= (\omega - \epsilon_{\mu_3})^{-1} \sum_{j}^{2} \sum_{\nu_j} A_{\mu_3 \nu_j}^{\mathrm{CC3}} R_{\nu_j} \\ &= (\omega - \epsilon_{\mu_3})^{-1} \left[\sum_{\nu_1} \langle \mu_3 | [[\hat{H}, T_2], \tau_{\nu_1}] | \mathrm{HF} \rangle R_{\nu_1} + \sum_{\nu_2} \langle \nu_3 | [\hat{H}, \tau_{\nu_2}] | \mathrm{HF} \rangle R_{\nu_2} \right] \\ &= (\omega - \epsilon_{\mu_3})^{-1} \langle \mu_3 | [\bar{H}, T_2] + [\hat{H}, R_2] | \mathrm{HF} \rangle \ , \end{aligned} \tag{79}$$

with the auxiliary operator $R_2 = \sum_\nu R_{\mu_2}\tau_{\nu_2}$. Using the effective Jacobian makes it possible to avoid the explicit treatment of the triples amplitudes and, hence, they do not have to be stored on disc. Furthermore, the contributions to the CC3 linear transformations only scales as $\mathcal{O}(\mathcal{N}^7)$ instead of $\mathcal{O}(\mathcal{N}^8)$ for CCSDT.
The CC2 model has already been implemented and applied to excitation energy calculations by Helmich and Hättig[23] in the context of state-spefcific PNOs[22] (*vide infra*). In addition, also the extended PNO-ADC(2) model (PNO-ADC(2)-x) has been been tested by them[24]. Based on this, the present work aims at extending PNO framework for excitation energies towards the CCSD and CC3 models. For this, the next sections will briefly summarize the theory of ground excited state PNOs and the solution of the eigenvalue problem for excitation energies in a state-specific PNO basis which this work is based on.

D. Local Correlation Domains

As previously mentioned, there exists a wide variety of local correlation methods with different advantages, challenges and perspectives. This work will focus on the use of the so-called direct local correlation methods which aim at a truncation of the virtual space while performing the calculations on the whole molecule without fragmentation. For this, PNOs and OSVs will be used in this work.

1. Pair Natural Orbitals for the Ground State

PNOs are defined as linear combinations of virtual orbitals

$$|\bar{a}_{ij}\rangle = \sum_a d^{ij}_{a\bar{a}_{ij}} |a\rangle. \tag{80}$$

Here and in the following, indices $i, j, k, l, \ldots$ denote occupied MOs and indices $a, b, c, d, \ldots$ denote virtual MOs. PNOs and OSVs will be denoted by a bar and a tilde over the virtual index, respectively. For the sake of clarity the LMO pair

indices ij of the PNOs will be omitted if it is clear from the context which LMO pair a PNO belongs to.

The PNOs constitute a pair-specific representation of the virtual space, i.e. each pair of LMOs is assigned a separate virtual space. In case of a non-truncated virtual space the virtual space assigned to each pair is the full virtual space. No cost-reduction would be obtained in such a case. Hence, the goal is to truncate the PNO expansion such that the most important virtual orbitals, which are needed to describe the electron correlation of a given pair, are included without a significant loss in accuracy. This is achieved by analyzing a correlated model wavefunction. Since the simplest and cheapest correlated wavefunction based model MP2 already yields the most important contributions to the correlation energy, the analysis of this wavefunction should be adequate to obtain sufficient information about the electron correlation of a pair ij. Hence, the PNO coefficients are obtained as eigenvectors of the pair contribution to the MP2 density[107]

$$\sum_{ab} d^{ij}_{a\bar{a}} D^{\mathrm{MP2},ij}_{ab} d^{ij}_{b\bar{b}} = \delta_{\bar{a}\bar{b}} \eta^{ij}_{\bar{a}} \tag{81}$$

which is defined as

$$D^{\mathrm{MP2},ij}_{ab} = \sum_{c} \left(\tilde{t}^{ij,(1)}_{ac} t^{ij,(1)}_{bc} + \tilde{t}^{ij,(1)}_{ca} t^{ij,(1)}_{cb} \right) \tag{82}$$

with $\tilde{t}^{ij,(1)}_{ab} = 2t^{ij,(1)}_{ab} - t^{ij,(1)}_{ba}$ and the approximate MP1 amplitudes

$$t^{ij,(1)}_{ab} = \frac{(ai|bj)}{\epsilon_i + \epsilon_j - \epsilon_a - \epsilon_b}. \tag{83}$$

The eigenvalues $\eta^{ij}_{\bar{a}}$ correspond to the natural occupation numbers. These natural occupation numbers indicate the importance of a PNO $\bar{a}_{ij}$ for the correlation treatment of a pair ij. Hence, it becomes possible to truncate the virtual space based on these occupation numbers where only PNOs with a natural occupation number above a certain threshold T_{PNO} are considered in the correlation treatment. However, if the occupied orbital space is spanned by delocalized canonical orbitals,

the natural occupation numbers only decay slowly with the distance of a PNO from its MO pair. This can be rationalized by considering that the integrals $(ai|bj)$ in the nominator of the MP1 amplitudes decay as $\mathcal{O}(\mathcal{R}^{-3})$ with the distance $\mathcal{R}$ between the charge distributions (ai) and (bj). If the occupied orbital space consists of orbitals, delocalized over the whole molecule, this short-range character of the electron correlation cannot be exploited. But if localized MOs (LMOs) are used for the occupied orbital space, the natural occupation numbers decay very rapidly and LMO pairs with very distant LMOs do not have any significant occupation numbers. The resulting PNO basis also is local and spatially close to the corresponding LMO pair.

However, in a LMO basis the occupied-occupied block of the Fock matrix is no longer diagonal ($F_{ii} \neq \epsilon_i$). As a consequence, the MP1 amplitudes can no longer be computed according to equation (83) but would have to be computed iteratively. To avoid this, the amplitudes are approximated as

$$t_{ab}^{ij,(1)} \approx \frac{(ai|bj)}{F_{ii} + F_{jj} - \epsilon_a - \epsilon_b} \tag{84}$$

where F_{ii} are the diagnoal elements of the Fock matrix in a LMO basis.

2. Orbitals Specific Virtuals for the Ground State

The OSV approximation[118] is very similar to the PNO approximation: Instead of creating a pair-specific representation, the OSV approach introduces on a orbital specific representation of the virtual space. Hence, a possible choice[177] for the OSVs[118] are the PNOs for diagonal pairs ii,

$$|\tilde{a}_{ii}\rangle = \sum_a d^{ii}_{a\tilde{a}_{ii}} |a\rangle \tag{85}$$

The OSV coefficients can consequently be obtained by diagonalizing the contribu-

tion of a diagonal pair ii to the MP2 pair density

$$\sum_{ab} d^{ii}_{a\tilde{a}} D^{\mathrm{MP2},ii}_{ab} d^{ii}_{b\tilde{b}} = \delta_{\tilde{a}\tilde{b}} \eta^{ii}_{\tilde{a}} \tag{86}$$

where

$$D^{\mathrm{MP2},ii}_{ab} = 2 \sum_{c} t^{ii}_{ac} t^{ii}_{cb} \tag{87}$$

The diagonalization of $\mathbf{D}^{\mathrm{MP2},ii}$ is equivalent to the diagonalization of the amplitude matrix $\mathbf{t}^{ii}$

$$\sum_{ab} d^{ii}_{a\tilde{a}} t^{ii}_{ab} d^{ii}_{b\tilde{b}} = \delta_{\tilde{a}\tilde{b}} \kappa^{ii}_{\tilde{a}} \tag{88}$$

which have the same eigenvectors and the eigenvalues of $\mathbf{t}^{ii}$ (denoted as $\kappa^{ii}_{\tilde{a}}$) are related to the ones of $\mathbf{D}^{\mathrm{MP2},ii}$ by $\kappa^{ii}_{\tilde{a}} = \frac{1}{2}\sqrt{\eta^{ii}_{\tilde{a}}}$. To ensure the equivalence between diagonal PNOs and OSVs and to use a single threshold T_{PNO} for the truncation of the virtual space, the OSVs are also selected[178] based on $\eta^{ii}_{\tilde{a}}$.

3. Local Resolution of the Identity Approximation for the Ground State

The PNO and OSV construction can be significantly sped up by making use of the resolution of the identity (RI approximation[109] which is often also referred to as density-fitting (DF) approximation). The usual RI approximation approximates two-electron integrals as

$$(ai|bj) \approx (ai|bj)^{\mathrm{RI}} = \sum_{PQ} (ai|Q) \left[\mathbf{V}\right]^{-1}_{QP} (P|bj) \tag{89}$$

where P and Q are auxiliary functions. The metric matrix in the above equation is here chosen as the inverse of the Coulomb matrix

$$V_{PQ} = (P|Q) \ . \tag{90}$$

The auxiliary basis is usually 4 - 5 times larger than the AO basis since the auxiliary functions need to be able to approximate different kinds of products (ai). In a local-correlation method the evaluation of integrals in the full auxiliary basis can therefore become a computational bottleneck and hamper a linear-scaling of computational resources with respect to the system size.. Hence, a local version of the RI approximation (local-RI) is used to only consider the auxiliary function close to the local-correlation domain. The selection of such auxiliary function which are spatially close to products ai is based on[178] the Schwartz estimate for the three-index overlap integrals (Qai)

$$\frac{|(Qai)|}{\sqrt{(QQ)}} \leq \frac{\sqrt{(QQii)}\sqrt{(aa)}}{\sqrt{(QQ)}} = \frac{\sqrt{(QQii)}}{\sqrt{(QQ)}} = S_{Qi} \tag{91}$$

where normalized MOs have been assumed.

For the generation of the OSVs, each LMO is assigned a separate auxiliary basis which only includes auxiliary functions[178]

$$Q_i = \{Q|S_{Qi} \geq T_{RI}\} \tag{92}$$

where T_{RI} is the selection threshold for the local-RI domains which is chosen such that errors of the local-RI approximation is small compared to the PNO truncation error[178].

For the PNO construction pair-specific auxiliary functions are needed which are close to the PNO domains and the orbital products. These are obtained by selecting auxiliary functions according to[178]

$$Q_{ij} = \{Q|f_{ij} \cdot S_{Qi} \geq T_{RI} \text{ or } f_{ij} \cdot S_{Qj} \geq T_{RI}\} \tag{93}$$

where $f_{ij} = 10 \cdot (e_{ij}^{(2)})^{\frac{1}{3}}$ is a damping factor connected to the pair energy estimate $e_{ij}^{(2)}$ which ensures that distant LMO pairs have less auxiliary functions assigned[178] (With $f_{ij} = 1$ distant pairs would have the largest RI basis).

4. Combination of PNOs and OSVs: The Hybrid OSV-PNO Approach

PNOs and OSVs are different types of tensor factorizations of the doubles amplitudes[118,177]. PNOs yield the most compact representation of the virtual space but also have the highest costs of construction. If they are computed by diagonalizing the density matrix in the full virtual space, the construction of the PNOs scales as $\mathcal{O}(\mathcal{N}^5)$ which is equal to the scaling of the MP2 method itself. On the other hand, OSVs offer a less compact representation of the virtual space but are computationally less demanding to construct. Their construction scales as $\mathcal{O}(\mathcal{N}^4)$ if they are computed by diagonalizing the full density/amplitude matrix in a non-truncated basis.

However, combining the OSV and PNO approaches with some further approximations makes it already possible to arrive at a $\mathcal{O}(\mathcal{N}^2)$-scaling implementation[178] of the PNO construction as will be shown in this section.

Due to the shared properties of PNOs and OSVs, it is possible to combine them to reduce the complexity of the PNO construction. Therefore, the OSV spaces of two LMOs i and j are merged and reorthogonalized to obtain a pair-specific truncated orthonormal basis for the PNO construction. The resulting basis will in the following be referred to as pre-PNO basis[178] $\{\tilde{a}_{ij}\}$. After construction of the pre-PNO basis, approximate amplitudes and densities can be evaluated in this basis as:

$$t^{ij,(1)}_{\tilde{a}_{ij}\tilde{b}_{ij}} = \frac{(\tilde{a}_{ij}i|\tilde{b}_{ij})}{F_{ii} + F_{jj} - \epsilon_{\tilde{a}_{ij}} - \epsilon_{\tilde{b}_{ij}}} \tag{94}$$

To not dominate the errors introduced by the PNO approximation itself, the OSV selection threshold has to be chosen one order of magnitude smaller than the PNO threshold ($T_{\mathrm{OSV}} = 0.1 \cdot T_{\mathrm{PNO}}$) as shown by Schmitz *et al.*[178].

The construction of PNOs for pairs which do not have any significant occupation

numbers is avoided by estimating[178] the second-order pair correlation energy

$$e_{ij}^{(2)} = \sum_{\tilde{a}_i \tilde{b}_j} \frac{\left[(\tilde{a}_i i|\tilde{b}_j j)\right]^2}{F_{ii} + F_{jj} - \epsilon_{\tilde{a}_i} - \epsilon\tilde{b}_j} \tag{95}$$

for each pair in the OSV basis and consequently only constructing PNOs for pairs whose pair correlation energy is above a threshold $e_{ij}^{(2)} \geq \frac{1}{3} T_{\text{pair}}$ where the factor of $\frac{1}{3}$ ensures that no pairs are discarded which might have PNOs with significant occupation numbers and $T_{\text{pair}} = (0.1 \cdot T_{\text{PNO}})^{\frac{2}{3}}$. All other pairs are discarded, i.e. they are not included in the correlation treatment.

Computing the PNOs as described above results in a complexity of the PNO construction of $\mathcal{O}(\mathcal{N}^4)$. The time-determining step is the computation of the integrals $(ai|bi)$ for the amplitude matrix $\mathbf{t}^{ii}$ to determine the OSVs. Schmitz *et al.*[178] realized that this step can be evaluated in a lower-scaling manner by using Laplace transformation techniques combined with an iterative diagonalization of the amplitude matrix and the local RI approximation. Since the full eigenbasis of $\mathbf{t}^{ii}$ is usually not of interest but only the few dominant eigenvectors (OSV coefficients) with occupation numbers above T_{OSV} are needed. This led to the approach to determine the OSV coefficients iteratively[178] using a block-Davidson-type algorithm, which successively computes the dominant eigenvectors in a reduced space. This algorithm requires the computation of the linear transformations of a trial vector $\mathbf{b}^{ii}$ (which converges to the OSV coefficients) with the amplitude matrix $\sum_c t_{ac}^{ii} b_{c\bar{c}}^{ii}$. Using equation (84) for the amplitudes does not lead to a cost-reduction since it still requires the computation of all integrals $(ai|bi)$. Instead, the numerical Laplace transform of the energy denominator[93–95]

$$\frac{1}{\epsilon_a + \epsilon_b - \epsilon_i - \epsilon_j} = \int_0^\infty e^{-(\epsilon_a + \epsilon_b - \epsilon_i - \epsilon_j)t} dt = \sum_z w_z e^{-(\epsilon_a + \epsilon_b - \epsilon_i - \epsilon_j)t_z} \tag{96}$$

where n_L refers to the number of Laplace grid points, w_z to the Laplace weights and t_z to the Laplace grid points, is used to transform the expression for the matrix

vector products into a factorizable form[178]

$$\sum_{c} t_{ac}^{ii} b_{c}^{ii} = \sum_{z}^{n_L} w_z \sum_{\nu} C_{\nu a}^{z} \sum_{Q} (Q|\nu i^z) \sum_{P} \left[\mathbf{V}^{-1}\right]_{PQ} \sum_{\mu} (P|\mu i^z) \sum_{c} C_{\mu c}^{z} b_{c}^{ii} \tag{97}$$

The grid point-dependent integrals and MO coefficients in the above equation are given by

$$C_{\nu a}^{z} = e^{-\epsilon_a t_z} C_{\mu a} \tag{98}$$

$$(Q|\mu i^z) = \sum_{\nu} (Q|\mu\nu) C_{\nu i}^{z} = \sum_{\nu} (Q|\mu\nu) \sum_{j} C_{\nu i} e^{\epsilon_i t_z} T_{ji} \tag{99}$$

where T_{ji} is the matrix which transforms from the MO to the LMO basis. Equation (97) can be evaluated as a sequence of matrix-vector products. Hence, the scaling of the OSV construction is reduced to $\mathcal{O}_(\mathcal{N}^3)$. Making use of the local-RI approximation and integral-screening further reduces the computational demands[178] to $\mathcal{O}(\mathcal{N}^2)$. However, a linear scaling could only be achieved with the use of a local basis for the truncated virtual basis which b_c^{ii} can be restricted to.

Throughout this work, the (iterative) PNO construction as described above has been used for CCSD and CC3 ground state calculations. However, for triples methods like CCSD(T) and CC3 a suitable basis for the triples amplitudes needs to be defined (similar to the PNO basis which the doubles amplitudes are restricted to). For this, the triple natural orbitals (TNOs) approach proposed by Riplinger *et al.*[179] was employed which has already been implemented and appied by Schmitz and Hättiig[130,180] in the context of their PNO-CCSD(F12*)(T) implementation.

5. Excited State PNOs

As already stressed through this work, the computation of excitation energies requires different techniques and approaches than the computation of ground state energies. This also translates to the definition of local correlation domains which have to fulfill different requirements than the ones for the ground state due to the potential non-local character of the excitation process.

Even though, the excited state correlation domains have different requirements than the ones for the ground state, it still is possible to transfer most of the techniques discussed in the previous section to also determine the excited state PNOs in an efficient manner.

To account for the potential non-local character of the excitation process, the excited state domains cannot be obtained by analyzing the approximate MP2 density introduced in the previous section since this density only accounts for spatially close LMO pairs and PNOs. Instead, a separate excited state PNO basis is obtained by diagonalizing excited state CIS(D)-like densities[22]

$$D_{ab}^{ij,\mathrm{ex}} = \sum_c \left(\tilde{R}_{ac}^{ij,(1)} R_{bc}^{ij,(1)} + \tilde{R}_{ca}^{ij,(1)} R_{cb}^{ij,(1)} \right) \tag{100}$$

which are computed from approximate CIS(D)-like excited state first-order amplitudes

$$R_{ab}^{ij,(1)} = \frac{(a\tilde{i}|bj)}{F_{ii} + F_{jj} - \epsilon_a - \epsilon_b + \omega} = \frac{P_{ab}^{ij} \left[\sum_k R_a^k (ki|bj) - \sum_c R_c^i (ac|bj) \right]}{F_{ii} + F_{jj} - \epsilon_a - \epsilon_b + \omega} \tag{101}$$

and $\tilde{R}_{ab}^{ij,(1)} = 2R_{ab}^{ij,(1)} - R_{ba}^{ij,(1)}$.

The integrals $(a\tilde{i}|bj)$ take the potential long-range character of the excitation process into account since they are also non-vanishing if i and j are spatially distant or the PNOs are spatially distant from the corresponding LMO pair ij. This can be rationalized by considering the case of a long-range charge-transfer excitation where the excited state singles amplitudes can be decomposed in terms of a single pair of natural transition orbitals (NTOs)

$$R_a^i = \beta_{a\sigma^v} \beta_{i\sigma^o} \tag{102}$$

where $\beta_{a\sigma^v}$ are the coefficients of the virtual NTO $|\sigma^v\rangle = \sum_c \beta_{c\sigma^v} |c\rangle$ (the electron acceptor) and $\beta_{i\sigma^o}$ are the coefficients of the occupied NTO $|\sigma^o\rangle = \sum_k \beta_{k\sigma^o} |k\rangle$ (the electron donor). Inserting this into the expression for the integrals the excited state PNOs are constructed from, yields[23]

$$(a\tilde{i}|bj) = P_{ab}^{ij} \left[\beta_{a\sigma^v} (\sigma^o i|bj) - \beta_{i\sigma^o} (a\sigma^v|bj) \right] \tag{103}$$

The contributions $\beta_{a\sigma^v}(\sigma^o i|bj)$ are only non-vanishing if the LMOs i and j are close to each other and close to the occupied NTO and the corresponding PNOs are either close to the occupied or the virtual NTO such that neither $\beta_{a\sigma^v}$ nor $(\sigma^o i|bj)$ vanish[23]. On the other hand, $\beta_{i\sigma^o}(a\sigma^v|bj)$ only contributes if the PNOs of a pair ij are close to each other and close to the virtual NTO and i is close to the occupied NTO while j is close to the virtual NTO[23]. Hence, the excited state PNO basis of a pair can be delocalized over the whole chromophore.

As for the ground state case, also for the excited state the PNO construction scales as $\mathcal{O}(\mathcal{N}^5)$ if the PNOs are constructed from the full MO basis. A cost-reduction can here also be obtained by constructing the excited state PNOs in a truncated OSV basis.

6. Excited State OSVs

Computing the excited state OSVs from the diagonal elements $R_{ab}^{ii,(1)}$ of the excited state first-order amplitudes would not result in an adequate OSV basis for excited states[23]. The reason is that the integrals

$$\widetilde{(ai|bi)} = P_{ab}^{ii}\left[\sum_k R_a^{k,(0)}(ki|bi) - \sum_c R_c^{i,(0)}(ac|bi)\right] \tag{104}$$

$$= P_{ab}^{ij}\left[\beta_{a\sigma^v}(\sigma^o i|bi) - \beta_{i\sigma^o}(a\sigma^v|bi)\right] \tag{105}$$

are only non-vanishing if i is close to the occupied NTO. If i is close to the virtual NTO, $\beta_{a\sigma^v}(\sigma^o i|bi)$ vanishes and $\beta_{i\sigma^o}(a\sigma^v|bi)$ cannot contribute in any case since it requires i to be close to the virtual and the occupied NTO at the same time which cannot be the case for a long-range charge-transfer state. Constructing the PNO basis from this OSV basis would only account for pairs ij where both LMOs are close to the occupied NTO but the case where one LMO is close to the occupied and the other is close to the virtual NTO could not be covered[22].

Hence, the excited state OSV basis is constructed from the modified amplitudes[23]

$$R'^{ii,(1)}_{ab} = \frac{(ai|bj) + (\overline{ai|bj})}{F_{ii} + F_{jj} - \epsilon_a - \epsilon_b + \omega} \tag{106}$$

with

$$(\overline{ai|bj}) = \sum_{kl} R^{k,(0)}_a (ki|lj) R^{l,(0)}_b + \sum_{cd} R^{i,(0)}_c (ac|bd) R^{j,(0)}_d - P^{ij}_{ab} \sum_{kc} R^{k,(0)}_a (ki|bc) R^{j,(0)}_c \tag{107}$$

Constructing the OSVs from these modified amplitudes yields a suitable basis which the excited state PNOs can be expanded in without neglecting important contributions.

Having defined a suitable PNO and OSV basis for excited states, the reduced scaling algorithm described in section III D 4 is straightofrward to extend to excited state calculations.

7. Hybrid OSV-PNO approach for Excited States

Similar to the ground state procedure, the excited state doubles amplitudes are expanded in an excited state pre-PNO basis[23]

$$R^{ij,(1)}_{\tilde{a}_{ij}\tilde{b}_{ij}} = \frac{(\tilde{a}_{ij} i|\tilde{b}_{ij} j)}{F_{ii} + F_{jj} - \epsilon_{\tilde{a}_{ij}} - \epsilon_{\tilde{b}_{ij}} + \omega} \tag{108}$$

and the list of relevant pairs is pre-screened based on the second-order contribution to the correlation energy evaluated in the excited state OSV basis[23]

$$\omega^{(2)}_{ij} = \sum_{\tilde{a}_{ij}\tilde{b}_{ij}} \frac{(\tilde{a}_i i|\tilde{b}_j j)}{F_{ii} + F_{jj} - \epsilon_{\tilde{a}_i} - \epsilon_{\tilde{b}_j} + \omega} \tag{109}$$

Only excited state pairs with $\omega^{(2)}_{ij} \geq \frac{1}{3} T_{pair}$ are kept and all for all other pairs no PNOs are constructed.

The iterative determination of the excited state OSVs is directly transferable to excited state calculations[23,181]. With the use of a local-RI approximation for excited states this results in a $\mathcal{O}(\mathcal{N}^2)$-scaling for the excited state PNO construction.

8. Local Resolution of the Identity Approximation for Excited States

Equations (101) and (106) suggest that the excited state local-RI basis not only needs to be able to approximate orbital products (ai) but also orbitals products $\sum_c R_c^{i,(0)}(ac) = (a\breve{i})$ and $\sum_c R_a^{k,(0)}(ki) = (\breve{a}i)$. In Ref. 181 it was shown that the local-RI domains of the ground state are not suitable for approximating these products in the case of non-local excitations where e.g. $|\breve{i}\rangle$ and $|a\rangle$ can be far away from each other.

Instead, it was suggested to determine the local-RI domains for the OSVs and PNOs by

$$Q_i = \{Q| \max(S_{Qi}, S_{Q\breve{i}}) \geq T_{RI}\} \tag{110}$$

$$Q_{ij} = \{Q|f'_{ij} \max(S_{Qi}, S_{Q\breve{i}}) \geq T_{RI} \text{ or } f'_{ij} \cdot \max(S_{Qj}, S_{Q\breve{j}}) \geq T_{RI}\} \tag{111}$$

with

$$\frac{|(Qa\breve{i})|}{\sqrt{(QQ)}} \leq \frac{(QQ\breve{i}\breve{i})(aa)}{\sqrt{(QQ)}} = \frac{(QQ\breve{i}\breve{i})}{\sqrt{(QQ)}} = S_{Q\breve{i}} \tag{112}$$

The overlap $(Q\breve{a}i)$ can be neglected if normalized excited state singles vectors are used[181] since then $(\breve{a}\breve{a}) = 1$ and, hence, $(Q\breve{a}i) \leq (QQii)(\breve{a}\breve{a}) = S_{Qi}$ Like in the ground state case, the damping factor $f'_{ij} = 10 \cdot (\omega_{ij}^{(2)})^{\frac{1}{3}}$ is directly connected to the estimate of the pair correlation energy to the excitation energy[181] $\omega_{ij}^{(2)}$.

E. Solution of the Excited State Eigenvalue Problem in a Truncated PNO Basis

The equations for the excited state local correlation domains, i.e. the excited state PNOs, OSVs and the local-RI basis, show that these domains depend on the nature of the excited state. This is due to their dependence on the excitation energy ω and the excited state singles amplitudes R_{μ_1}. These quantities are not known prior to a calculation but could only be guessed by e.g. a canonical CIS calculation

as it was done by Korona and Werner[154] in their PAO-based implementation of CCSD exctation energies. This bears, however, the problem that only states which are similar to the CIS states could be found if the excited state PAO basis is fixed. Using a more sophisticated method like CIS(D) or CC2 for the reference calculation would, on the other hand, strongly limit the applicability of the local correlation treatment of excited states.

Another problem for the local correlation treatment of excited states is directly connected to the Davidson algorithm itself. While most canonical methods determine the eigenvalues of several states simultaneously (so-called multistate Davidson algorithms), this is not possible for a truncated state-specific PNO basis without loss of accuracy or efficiency[181]. This can be attributed to the fact that the Davidson algorithm requires the computation of the Jacobian in a reduced space $A^{\text{red}}_{\alpha\beta} = (\mathbf{E}^{\alpha})^T \mathbf{A}\mathbf{E}^{\beta}$ which involves the calculation of linearly transformed trial vectors which depend on two PNO bases of two different states α and β. This would result in a quadratic scaling with the number of states to be computed[181]. Valeev and co-workers[182] proposed to use a state-averaged PNO basis which is obtained by averaging the the CIS(D) densities of all states, and, hence, able to span the virtual space of all states equally well to circumvent this problem. However, this results in an unnecessarily large PNO basis for most states, especially in the case of a molecule with different spatially separated chromophores. Furthermore, this approach results in the fact that the errors do not only depend on the PNO truncation but also on the number of states averaged over to obtain this PNO basis. Even though, this approach is compatible with the excited state PNO construction described in the previous sections, it will not be considered here due to the unphysical PNO basis.

Instead, this work will use the techniques presented by Helmich and Hättig[22,23] to circumvent the aforementioned problems. They proposed to construct state-specific PNOs, i.e. a separate PNO basis for each excited state, to obtain the most compact and physically meaningful representation for each excited state. To ensure that

the PNO basis adapts itself to the excited state and does not have to rely on the overlap with a reference state, the excited state eigenvalue problem is solved self-consistently[23]. Therefore, the overlap of the excited state singles trial vectors ${}^{(0)}E_{\mu_1}$ (initially, these are the CIS singles vectors) the PNOs are constructed from (reference singles amplitudes) and the excited state singles vectors in the j-th Davidson iteration (from now on referred to as microiteration) ${}^{(j)}E_{\mu_1}$ is computed as[23]

$$ {}^{(j)}s = \frac{{}^{(0)}E_{\mu_1} \cdot {}^{(j)}E_{\mu_1}}{||{}^{(0)}E_{\mu_1}|| \cdot ||{}^{(j)}E_{\mu_1}||} \tag{113} $$

in each microiteration. The singles trial vectors are normalized in each microiteration. If the overlap between the reference singles amplitudes and the singles amplitudes in the j-th microiteration deviates significantly from 1, i.e. if

$$ 1 - {}^{(j)}s \geq 10 \cdot ||{}^{(j)}\sigma|| \tag{114} $$

is no longer fulfilled, the microiterations are stopped and new PNOs are generated with new amplitudes[23]

$$ R_{ab}^{ij,(1)} = \frac{P_{ab}^{ij} \left[\sum_k {}^{(j)}E_a^k(ki|bj) - \sum_c {}^{(j)}E_c^i(ac|bj)\right]}{F_{ii} + F_{jj} - \epsilon_a - \epsilon_b + {}^{(j)}\omega} \tag{115} $$

from the current guess of the singles amplitudes and the excitation energy ${}^{(j)}\omega$. The microiterations are then restarted with this new PNO basis until the PNO basis is not self-consistent anymore, i.e. until equation (114) is not satisfied. This procedure is repeated for one state at a time[23] and until the residual vector fulfills $||\sigma|| < T_{\text{conv}}$ where T_{conv} is the convergence threshold for the Davidson iterations.

However, this self-consistent determination of a suitable PNO basis for each excited state separately (single-state approach) requires modifications if more than one state is of interest. This is due to the fact that the Davdison algorithm without modifications always converges to the lowest eigenvalue of the Jacobian and, hence, higher excited states are not accessible. To be able to converge within this single-state approach to higher excited states, Helmich and Hättig[23] proposed the use

of Wielandt-Deflation[183] to modify the Jacobian such that states beyond the first excited state can be found.

The basic idea of Wielandt-Deflation is to project out the previously found eigenvectors of the Jacobian, i.e. to modify $\mathbf{A}$ by a rank-1 update such that its dominant eigenvalue is shifted to the next higher one,

$$\mathbf{A}^{(k)} = \mathbf{A} - \mu \sum_{i=1}^{k-1} \mathbf{q}^{(i)} \left(\mathbf{q}^{(i)}\right)^T \tag{116}$$

The vectors $\mathbf{q}^{(i)}$ are the Schur vectors of the i-th state[181] of which decompose $\mathbf{A}$ as

$$\mathbf{AQ} = \mathbf{QT} \tag{117}$$

where $\mathbf{Q}$ is a Hermitian (here: orthogonal) matrix containing the Schur vectors of $\mathbf{A}$ and $\mathbf{T}$ is an upper triangular matrix with $T_{kk} = \omega^{(k)}$ The Schur vectors are invariant under the rank-1 update from $\mathbf{A}$ to $\mathbf{A}^{(k)}$ similar to the eigenvalues $\omega^{(i)}$ which show the same invariance for $i < k$ and are shifted by $\omega^{(i)} - \mu$ for $i \geq k$. The shift parameter μ is in general related to the spectrum of $\mathbf{A}$ but, as sugggested by Helmich[181], chosen as a constant, $\mu = 1.5 \cdot \max\left(\omega^{\text{CIS}}\right)$.

The Schur vectors span, thus, span the same eigenspace for $\mathbf{A}^{(k)}$ and $\mathbf{A}$, in contrast to the eigenvectors, which are different for a non-Hermitian deflated Jacobian. This kind of deflation is in this work used for all methods including only up to doubles excitations (here: primarily CCSD).

For a nonlinear (non-polynomial) eigenproblem of the form $\mathbf{A}(\omega)\mathbf{R} = \omega(R)$ as it is for CC3 obtained by diagonalizing the effective Jacobian (equation (78)) the Wielandt deflation (as well as other deflation techniques used for linear eigenvalue problems) as described above is no longer applicable. The reason is that the Schur vector $\mathbf{q}^{(i)}$ is obtained by orthogonalizing the eigenvector $\mathbf{b}^{(i)}$ of $\mathbf{A}^{(i)}$ against all previously found Schur vectors $\mathbf{q}^{(j)}$ $(j < i)$. Hence, the eigenvectors of $\mathbf{A}$ are assumed to be linearly independent. But for nonlinear eigenvalue problems the eigenvectors of $\mathbf{A}(\omega)$ are no longer restricted to form a linearly independent set. Consequently,

if the standard deflation techniques are used to compute the eigenvalues of $\mathbf{A}(\omega)$ it might lead to missing some of the eigenvalues.

While the doubles part of the eigenvectors are usually sufficiently compact in a PNO basis to be treated explicitly in the Davidson algorithm, the triples part can even in a local basis become prohibitively large such that for e.g. the storage of triples amplitudes can become a computational bottleneck. Therefore, this work uses the partitioned formulation of the CC3 eigenvalue problem which is, however, not compatible with the Wielandt-deflation. Therefore, in this work a different strategy of obtaining the CC3 excitation energies will be used which will be described in Section VI.

This work utilized the framework for excited state PNOs as described in the preceeding sections for the determination of PNO-CCSD and PNO-CC3 excitation energies. However, Hättig and Helmich already found for their PNO-CC2 implementation[23] that charge-transfer states need to be treated with special care in a state-specific PNO basis. Using the standard PNO construction for excited states as described above led to a very slow convergence of the PNO-CC2 errors[23] (with respect to canonical CC2). Therefore they needed to modify the PNOs for excited states for certain LMO pairs[23]. Such difficulties were also found in this work for PNO-CCSD excitation energies. To obtain for charge-transfer states a similar behavior of the errors in PNO-CCSD excitation energies (with respect to canonical CCSD), the excited state PNO construction had to be generalized further[57]. This will be described in section V. Furthermore, the implementation of PNO-CC3 excitation energies required the extension of the concept of TNOs towards excited states. For this, a multipole-based analysis has been performed to define a suitable TNO basis for excited states. This analysis revealed that the choice of a suitable TNO basis for long-range charge-transfer states is a delicate task. These findings will be presented in section VI in the realm of the implementation of PNO-CC3 excitation energies.

IV. THE PNO-MP2 GRADIENT AND ITS APPLICATION TO MOLECULAR GEOMETRY OPTIMIZATIONS

In this publication we present the first implementation of a PNO-based (orbital relaxed) MP2 gradient. The gradient is applied to geometry optimizations on a large and diverse test set of molecules in order to investigate the accuracy and applicability of PNO-MP2-based geometry optimizations in different bonding situations. Since the strength of MP2 (compared to computationally cheaper methods such as DFT or HF) is the ability to also yield reliable results for systems which are dominated by dispersion interactions, we also apply the gradient to geometry optimizations of different water clusters.

The gradient presented here is not the fully analytical gradient but an approximation to it. The contributions neglected are the PNO and OSV relaxation and the gradient of the energy correction for the neglected PNOs and LMO pairs. Instead, we chose to only include the relaxation of the LMOs since this should be more dominant than the aforementioned orbital responses and energy contribtutions.

This project is a follow-up project from my Master Thesis which has been supervised by Dr. Gunnar Schmitz and Prof. Dr. Christof Hättig. Within the Master Thesis the gradient has been implemented and tested without taking the LMO localization constraint into account.

Then, the work done within the PhD project has been done under the supervision of Prof. Dr. Christof Hättig. All coding and the mathematical derivation of the localization constraint has been done by myself. Furthermore, all numbers, figures and the publication itself have been created by myself.

After completion of the publication, further effort has been spent on the MPI parallelization of the PNO-MP2 gradient and the gradient has also been adapted for the usage of exact HF exchange integrals instead of using the RI approximation for these integrals as it was the case for the publication. Due to time constraints, these parts of my implementation have not yet been applied to chemically relevant

systems.

The publication presented in the following, is an Accepted Manuscript of an article published by Taylor & Francis in Molecular Physics on 12/21/2017, available online: http://www.tandfonline.com/10.1080/00268976.2016.1263762

The PNO-MP2 Gradient and its Application to Molecular Geometry Optimizations

Marius Frank[a*], Gunnar Schmitz[b] and Christof Hättig[a]

[a]Lehrstuhl für Theoretische Chemie, Ruhr-Universität Bochum, D-44801 Bochum, Germany;
[b] Deparment of Chemistry, Aarhus University, DK-8000 Aarhus C, Denmark

ARTICLE HISTORY
Compiled July 16, 2019

ABSTRACT
A preliminary implementation of a gradient for MP2 based on the pair natural orbital approximation (PNO-MP2) is presented. The accuracy of the PNO approximation for geometries is investigated by comparing bond lengths and bond angles of the PNO-MP2 structures with results from canonical MP2. Special emphasis is put on the optimization of weakly bound complexes, such as differently sized water clusters. It is found that the error introduced by the PNO approximation is already for moderate PNO thresholds negligible compared to the inherent error of MP2. However, too loose PNO thresholds lead to convergence difficulties in geometry optimizations. This is observed in particular for floppy groups as e.g. methyl groups with low rotational barriers. Compared to optimizations with canonical MP2 the convergence thresholds have to be mainly energy and less coordinate based to comply with the slight roughness of the potential energy surface which is introduced by the PNO selection.

KEYWORDS
local MP2; PNO-MP2 gradient; geometry optimizations; accuracy

1. Introduction

One of the major challenges of modern quantum chemistry is to find highly accurate and systematically improvable methods for the calculation of energies, geometries and properties, which are applicable to large molecular systems. This is due to the fact that well-established canonical methods, which are known to be very precise, show a steep scaling of the computational costs with the system size $\mathcal{N}$. Hence, canonical post Hartree-Fock (HF) wave function methods are restricted to small or medium sized systems.

Fortunately, new approaches to reduce the cost-scaling of wave function methods came up during the past decade. Most methods that aim at a reduced scaling are based on the fact that the dynamical electron correlation is a short-range effect. These methods are called local correlation methods. Many local correlation methods aim to achieve a truncation of the virtual space, while performing the calculation on the whole molecule. There exist different schemes for the truncation of the virtual space. The maybe most popular and refined one was originally developed by Saebø and Pulay [1–6] and later extended and implemented by Werner, Schütz and coworkers [7–11]. According to the ideas of Saebø and Pulay the virtual orbital space is spanned by projected atomic orbitals (PAOs), which differ from the AOs only from orthogonalization tails introduced by the projection onto the virtual space. Using this approach, Schütz and Werner succeeded in implementing linear scaling local versions of MP2 [7, 8], CCSD [9–14] and CCSD(T) [13–17]. Although these methods have a low cost-scaling, a major drawback is that the local domains need to be specified prior to a calculation, what results in a limited error control. Furthermore, the local domains soon become very large for highly accurate calculations, what then diminishes the computational savings obtained by the PAO approach.

*Corresponding author. Email: Marius.Frank@rub.de

2. Theory and Implementation

2.1. *The conventional RI-MP2 Gradient*

For MP2 the (orbital-relaxed) Lagrange function is given by

$$\mathcal{L}^{\mathrm{MP2}} = \langle \mathrm{HF}|H + [H, T_2]|\mathrm{HF}\rangle + \sum_{\mu_2} \bar{t}_{\mu_2} \langle \mu_2|H + [F, T_2]|\mathrm{HF}\rangle + \sum_{\mu_0} \bar{\kappa}_{\mu_0} F_{\mu_0}, \tag{1}$$

where the operators F and H denote the Fock- and Hamilton operators and $T_2 = \sum_{\mu_2} t_{\mu_2} \tau_{\mu_2}$ the cluster operator. The index μ_2 runs over double replacements. In this work we assume closed-shell systems and use the spin-free operators [47] $\tau_{aibj} = E_{ai}E_{bj}$ and $\bar{t}^{ij}_{ab} = 4t^{ij}_{ab} - 2t^{ji}_{ab}$. Here and in the following we use the convention that indices $a, b, c, \ldots$ denote active virtual molecular orbitals (MOs) and $i, j, k, \ldots$ active occupied MOs (in the frozen core approximation). General MOs will be labeled with $p, q, r, \ldots$ and atomic orbitals (AOs) with $\mu, \nu, \kappa, \ldots$. To denote the complete, i.e. active + inactive, virtual and occupied MO subspace we use, respectively, the capital letters A, B and I, J. The Hartree-Fock (HF) reference determinant $|\mathrm{HF}\rangle$ is parametrized as

$$|\mathrm{HF}\rangle = \exp\left(\sum_{\mu_0} \kappa_{\mu_0} (E_{\mu_0} - E^{\dagger}_{\mu_0})\right) |\mathrm{HF}_0\rangle, \tag{2}$$

where $|\mathrm{HF}_0\rangle$ is chosen such that the orbital rotation parameters κ_{μ_0} vanish for the unperturbed system. The first term in equation (1) corresponds to the total MP2 energy. The second term accounts for the MP2 amplitude equations while the last term includes a sum over the Fock matrix elements which are required to vanish. The index range of μ_0 depends on the constraints applied to the Fock operator. Here, we use a non-canonical condition and only require that the Fock matrix is block-diagonal in the occupied/virtual and active/inactive sub blocks.

After some rearrangements the RI-MP2 gradient can be written as

$$\mathcal{L}^{\mathrm{MP2}} = \frac{1}{2} \sum_{pq} D^{\mathrm{SCF}}_{pq} h_{pq} + \sum_{pq} \left(\tfrac{1}{2} D^{\mathrm{SCF}}_{pq} + D^{\mathrm{MP2}}_{pq} + \bar{\kappa}_{pq}\right) F_{pq} + \frac{1}{2} \sum_{aibj} d^{nsep}_{aibj} (ai|bj)^{\mathrm{RI}} \tag{3}$$

with the SCF and the unrelaxed MP2 one-particle densities, D^{SCF}_{pq} and D^{MP2}_{pq}, the non-separable part of the two-electron density d^{nsep}_{aibj} and the one-electron (core) Hamiltonian matrix h_{pq}. Explicit expressions for the densities can be found e.g. in Ref. [48]. The two-electron repulsion integrals $(ai|bj)^{\mathrm{RI}}$ are evaluated within the resolution-of-the-identity (RI) approximation:

$$(ai|bj)^{\mathrm{RI}} = \sum_{Q} C_{Qbj} (Q|ai) \ , \tag{4}$$

with

$$C_{Qbj} = \sum_{P} (P|bj) \left[\mathbf{V}^{-1}\right]_{PQ} \ , \tag{5}$$

and the Coulomb metric

$$V_{PQ} = (P|Q). \tag{6}$$

Here, and in the following capital indices P, Q, R, ... denote auxiliary basis functions and $(Q|ai)$ and $(P|Q)$ are three- and two-index electron repulsion integrals.

2.2. *Pair Natural Orbitals*

Pair natural orbitals are defined as linear combination of virtual orbitals:

$$|\bar{a}\rangle = \sum_a |a\rangle d^{ij}_{a\bar{a}} \ , \tag{7}$$

with the expansion coefficient $d^{ij}_{a\bar{a}}$ chosen such that they diagonalize the contribution D^{ij}_{ab} of the pair ij to an one-electron density matrix [49]

$$\sum_{ab} d^{ij}_{a\bar{a}} D^{ij}_{ab} d^{ij}_{b\bar{b}} = \delta_{\bar{a}\bar{b}} n^{ij}_{\bar{a}} . \tag{8}$$

For D^{ij}_{ab} we choose the MP2 density which is given by

$$D^{ij}_{ab} = 2 \sum_c \left(u^{ij}_{ac} t^{ij}_{bc} + u^{ij}_{ca} t^{ij}_{cb} \right) \ , \tag{9}$$

with

$$u^{ij}_{ab} = 2t^{ij}_{ab} - t^{ij}_{ba} \ . \tag{10}$$

The PNO coefficients are obtained by diagonalizing D^{ij}_{ab} in a quasicanonical pair-specific basis $\{\tilde{a}_{ij}\}$, which is obtained by merging and orthonormalizing the OSV sets of i and j: Firstly, the OSV coefficients $d^{ii}_{a\tilde{a}_i}$ (which are equal to the PNO coefficients of a diagonal pair) are determined by solving the OSV eigenvalue problem

$$\sum_b D^{ii}_{ab} d^{ii}_{b\tilde{a}_i} = n_{\tilde{a}_i} d^{ii}_{a\tilde{a}_i} \tag{11}$$

iteratively. For details we refer to Ref. [36]. After building the aforementioned quasicanonical pair-specific basis the PNO coefficients are obtained by solving the PNO equations in this basis:

$$\sum_{\tilde{a}_{ij}\tilde{b}_{ij}} d^{ij}_{\tilde{a}_{ij}\bar{a}_{ij}} D^{ij}_{\tilde{a}_{ij}\tilde{b}_{ij}} d^{ij}_{\tilde{b}_{ij}\bar{b}_{ij}} = \delta_{\bar{a}_{ij}\bar{b}_{ij}} n^{ij}_{\tilde{a}_{ij}} \tag{12}$$

The approximate amplitudes are then calculated as

$$t^{ij}_{\tilde{a}_{ij}\tilde{b}_{ij}} = \frac{(\tilde{a}_{ij} i | \tilde{b}_{ij} j)}{F_{ii} - \epsilon_{\tilde{a}_{ij}} + F_{jj} - \epsilon_{\tilde{b}_{ij}}} \ , \tag{13}$$

where F_{ii} are the diagonal elements of the (non-diagonal) Fock matrix in the LMO basis and $\epsilon_{\tilde{a}_{ij}}$ the eigenvalues of the Fock matrix (diagonalized) in the unified OSV space. The eigenvalues $n^{ij}_{\bar{a}}$ of D^{ij}_{ab} are the natural occupation numbers. When sorted in descending order these natural occupation numbers decrease rapidly to zero if i and j are localized molecular orbitals (LMOs).

2.3. *Lagrange Multipliers for Localized Orbitals*

2.3.1. The Localization Constraint

In a truncated PNO basis or if LMO pairs are neglected, the wave function is no longer invariant under rotations among the occupied MOs. To account for this, the Lagrangian in equation (3)

needs to be augmented with a localization constraint, in the current work for Forster-Boys [50] localization we get

$$\left(\frac{d}{d\lambda_{kl}} \sum_{i,j} \left(\langle \tilde{i} | \vec{r} | \tilde{i} \rangle - \langle \tilde{j} | \vec{r} | \tilde{j} \rangle \right)^2 \right)_{\lambda=0} = 0. \tag{14}$$

The perturbed localized MOs (LMOs) $\tilde{\phi}_i$ are obtained from the unperturbed LMOs ϕ_i by the unitary transformation

$$\tilde{\phi}_i = \exp\left(\sum_{i<j} \lambda_{ij} \left(E_{ij} - E_{ji} \right) \right) \phi_i. \tag{15}$$

The antisymmetric matrix $\boldsymbol{\lambda}$ describes the change of the localization coefficients with respect to an external perturbation, similar to the matrix $\boldsymbol{\kappa}$, which describes the change of the MO coefficients with respect to the perturbation (vide infra). Evaluation of equation (14) yields

$$0 = \left(\langle i | \vec{r} | i \rangle - \langle j | \vec{r} | j \rangle \right) \langle j | \vec{r} | i \rangle = B_{ij} \ . \tag{16}$$

Thus, the Lagrangian becomes:

$$\begin{aligned} \mathcal{L}^{\mathrm{MP2}} = & \frac{1}{2} \sum_{pq} D_{pq}^{\mathrm{SCF}} h_{pq} + \sum_{pq} \left(\tfrac{1}{2} D_{pq}^{\mathrm{SCF}} + D_{pq}^{\mathrm{MP2}} + \bar{\kappa}_{pq} \right) F_{pq} + \frac{1}{2} \sum_{aibj} d_{aibj}^{nsep} (ai|bj)^{\mathrm{RI}} \\ & + \sum_{i<j} \bar{\lambda}_{ij} B_{ij} \ . \end{aligned} \tag{17}$$

In principle, additional constraints which take the selection of the PNOs into account would have to be considered. In the current work we neglect these constraints since their effect on the gradient and the final geometries can be expected to be of similar size as the noise due to the geometry dependence of the PNO selection.

Furthermore it should at this point be mentioned that we do not take the gradient of the pair correction (evaluated in the OSV basis $\{\tilde{a}_i\}$)

$$\mathcal{E}_{ij} = c_{OS}(1 + \delta_{ij}) \sum_{\tilde{a}_i \tilde{b}_j} \frac{2K_{\tilde{a}_i \tilde{b}_j}^{ij} K_{\tilde{a}_i \tilde{b}_j}^{ij}}{F_{ii} - F_{\tilde{a}_i \tilde{a}_i} + Fjj - F_{\tilde{b}_j \tilde{b}_j}} \tag{18}$$

with $K_{\tilde{a}_i \tilde{b}_j}^{ij} = (\tilde{a}_i i | \tilde{b}_j j)$ and the diagonal elements of the (non-diagonal) Fock matrix evaluated in the OSV basis into account in our preliminary implementation. For the calculation of energies the above equation is used to screen the pair list and subsequently these estimated pair correlation energies of discarded pairs are added to the total energy. For further details it is referred to Refs. [34, 36].

2.3.2. The Coupled-Perturbed Hartree Fock and Localization Equations

Now that a suitable Lagrangian has been set up, the Lagrange multipliers can be determined. The matrix $\bar{\boldsymbol{\kappa}}$, whose only non-vanishing blocks are the virtual/occupied and inactive/active blocks is then obtained by solving the so-called Z-vector equations [51]. For the virtual/occupied

block they can be written as:

$$\sum_{BJ} \bar{\kappa}_{BJ} \left(\delta_{JI} F_{BA} - \delta_{BA} F_{IJ} + \frac{1}{2} A_{BJAI} \right) = -\eta^{\kappa}_{AI}, \tag{19}$$

with the Z-CPHF matrix $A_{pqrs} = 4(pq|rs)^{RI} - (pr|sq)^{RI} - (ps|rq)^{RI}$, which also is evaluated using the RI approximation (see section 2.4 for details), and the right-hand-side (RHS) vector

$$\eta^{\kappa}_{AI} = L_{IA} - L^{''}_{AI} + M_{AI} + \frac{1}{2} \sum_{pq} \left(D^{\mathrm{MP2}}_{pq} + \bar{\kappa}^{OO}_{pq} \right) A_{pqIA} \tag{20}$$

The intermediate M_{AI} stems from the differentiation of the localization constraint and has non-vanishing elements only if I is an active occupied orbital:

$$M_{qi} = \sum_{w=xyz} \sum_{l} \bar{\lambda}_{il} \left[\langle i|r_w|q\rangle \langle l|r_w|i\rangle + \frac{1}{2} \Big(\langle i|r_w|i\rangle - \langle l|r_w|l\rangle \Big) \langle l|r_w|q\rangle \right] \tag{21}$$

The intermediates L_{IA} and $L^{''}_{AI}$, which contain contractions with the non-separable part of the two–electron density (i.e. the doubles amplitudes), are evaluated in the PNO basis as follows:

$$L^{''}_{aq} = \sum_{\mu} C_{\mu q} \sum_{ij} \sum_{\bar{a}} d^{ij}_{a\bar{a}} \sum_{P} (\mu i|P) \Gamma^{ij}_{P,\bar{a}i} \ , \tag{22}$$

$$L_{iq} = \sum_{\nu} C_{\nu q} \sum_{j} \sum_{P\mu} (\mu\nu|P) \sum_{\bar{a}} C^{ij}_{\mu\bar{a}} \Gamma^{ij}_{P,\bar{a}i} \ , \tag{23}$$

with

$$\Gamma^{ij}_{P,\bar{a}i} = \sum_{\bar{b}j} t^{ij}_{\bar{a}\bar{b}} C^{ij}_{P,\bar{b}j} \ , \tag{24}$$

$$C^{ij}_{P,\bar{b}j} = \sum_{\mu} C_{P,\mu,j} C^{ij}_{\mu\bar{b}} \ , \tag{25}$$

and the coefficients $C^{ij}_{\mu\bar{b}} = \sum_b C_{\mu b} d^{ij}_{b\bar{b}}$, which transform from the AO to the PNO space of pair ij.

Furthermore, the unrelaxed MP2 density also needs to be evaluated from the amplitudes in the PNO basis. For the virtual/virtual block, this can be done straightforwardly as

$$D^{\mathrm{MP2}}_{ab} = 2 \sum_{ij} \sum_{\bar{a}\bar{b}} d^{ij}_{a\bar{a}} d^{ij}_{b\bar{b}} \sum_{\bar{c}} u^{ij}_{\bar{a}\bar{c}} t^{ij}_{\bar{b}\bar{c}} \ . \tag{26}$$

For the occupied/occupied block, additional transformations with PNO overlap matrices appear:

$$D^{\mathrm{MP2}}_{ij} = -2 \sum_{k\bar{a}_{jk}\bar{b}_{jk}} u^{jk}_{\bar{a}_{jk}\bar{b}_{jk}} \sum_{\bar{c}_{ik}} S^{ik,jk}_{\bar{c}_{ik}\bar{b}_{jk}} \sum_{\bar{d}_{ik}} S^{ik,jk}_{\bar{d}_{ik}\bar{a}_{jk}} \, t^{ik}_{\bar{d}_{ik}\bar{c}_{ik}} \ . \tag{27}$$

The overlap of PNOs belonging to different pairs ik and jk is defined as:

$$S^{ik,jk}_{\bar{a}\bar{b}} = \sum_{c} d^{ik}_{c\bar{a}} d^{jk}_{c\bar{b}} \ . \tag{28}$$

The matrix $\bar{\kappa}_{pq}^{OO}$ in eq. (20) contains the inactive-occupied/active-occupied block of $\bar{\boldsymbol{\kappa}}$. These Lagrange multipliers are determined by the equation:

$$\sum_K \left(\bar{\kappa}_{KJ} F_{KI} - \bar{\kappa}_{IK} F_{JK}\right) = -(L_{IJ} + M_{IJ}) \tag{29}$$

The Lagrange multipliers $\bar{\lambda}_{ij}$ are determined by the condition that the Lagrangian has to be stationary with respect to variations of the localization parameters λ_{ij}. This leads to the coupled-perturbed localization (Z-CPL) equations [52]:

$$\left(1 - \hat{P}_{kl}\right) \sum_{w=xyz} \sum_i \bar{\lambda}_{ki} \left[\langle k|r_w|l\rangle\langle i|r_w|k\rangle + \frac{1}{2}\Big(\langle k|r_w|k\rangle - \langle i|r_w|i\rangle\Big)\langle i|r_w|l\rangle\right] = -\theta_{kl} \tag{30}$$

with the usual permutation operator $\hat{P}_{kl} f_{kl} = f_{lk}$ and the RHS vector

$$\theta_{kl} = \left(1 - \hat{P}_{kl}\right) \sum_i \left(D_{il}^{\mathrm{MP2}} F_{ik} + \tfrac{1}{2} L_{lk}\right) \tag{31}$$

Since the Lagrange multipliers $\bar{\boldsymbol{\kappa}}$ do not contribute to the Z-CPL equations, the latter equations can be solved prior to the Z-CPHF equations.

2.4. *The PNO-MP2 gradient*

Now, that the Lagrange multipliers have been determined, the gradient can be evaluated in the AO basis as follows:

$$\begin{aligned}\left(\frac{d\mathcal{L}^{\mathrm{MP2}}}{dx}\right)_{x=0} &= \sum_{\mu\nu} D_{\mu\nu}^{eff} h_{\mu\nu}^{[x]} - \sum_{\mu\nu} F_{\mu\nu}^{eff} S_{\mu\nu}^{[x]} + \sum_{Q\mu\nu} \Delta_{Q,\mu\nu} (Q|\mu\nu)^{[x]} \\ &+ \sum_{PQ} \gamma_{PQ} (P|Q)^{[x]} + \sum_{Q'\mu\nu} \Delta_{Q',\mu\nu}^{\mathrm{SCF}} (Q'|\mu\nu)^{[x]} + \sum_{P'Q'} \gamma_{P'Q'}^{\mathrm{SCF}} (P'|Q')^{[x]} \\ &+ \sum_{w\in\{xyz\}} \sum_{\mu\nu} D_{\mu\nu}^{(w)} \langle\mu|r_w|\nu\rangle^{[x]}\end{aligned} \tag{32}$$

where P, Q denote auxiliary basis functions for the correlation part and P', Q' auxiliary basis functions for the RI-JK approximation [53] used in the HF part.
The effective Fock matrix $F_{\mu\nu}^{eff}$, also known as energy weighted density matrix, is defined as

$$\begin{aligned}F_{\mu\nu}^{eff} =& \sum_{pq} C_{\mu p} C_{\nu q} \sum_u D_{pu}^{eff} F_{qu} + \frac{1}{2} \sum_{Iq} C_{\mu I} C_{\nu q} \sum_{rs} \left(D_{rs}^{\mathrm{MP2}} + \bar{\kappa}_{rs}\right) A_{rsIq} \\ &+ \frac{1}{2} \sum_{pq} C_{\mu p} C_{\nu q} \left(L_{pq} + L_{pq}^{''}\right) + \sum_{Ij} C_{\mu I} C_{\nu j} M_{Ij}\end{aligned} \tag{33}$$

with the usual relaxed one-electron density $D_{\mu\nu}^{eff} = D_{\mu\nu}^{\mathrm{SCF}} + D_{\mu\nu}^{\mathrm{MP2}} + \bar{\kappa}_{\mu\nu}$. The three- and two-index two-particle densities for the correlation part are defined as [54]:

$$\begin{aligned}\gamma_{PQ} &= \sum_{i\mu} C_{P,\mu i} \Gamma_{Q,\mu i} \\ \Delta_{Q,\mu\nu} &= \sum_i \Gamma_{Q,\mu i} C_{\nu i}\end{aligned} \tag{34}$$

Table 1. Definition of the three- and two-index two-electron densities $\Delta^{\mathrm{SCF}}_{Q,\mu\nu}$ and $\gamma^{\mathrm{SCF}}_{PQ}$ for the SCF part of the gradient.

$$\Delta^{\mathrm{SCF}}_{Q,\mu\nu} = \left(D^{\mathrm{MP2}}_{\mu\nu} + \bar{\kappa}_{\mu\nu}\right) i^{\mathrm{SCF}}_{Q} + 2\sum_I \widetilde{\Gamma}^{\mathrm{SCF}}_{Q,\nu I} C_{\mu I}$$
$$\gamma^{\mathrm{SCF}}_{PQ} = \sum_{\mu I} \Gamma^{\mathrm{SCF}}_{P,\mu I} C_{Q,\mu I}$$
$$\widetilde{\Gamma}^{\mathrm{SCF}}_{Q,\nu I} = C_{\nu I} i^{eff}_{Q} - \sum_\mu \left(\tfrac{1}{2} D^{\mathrm{SCF}}_{\mu\nu} + D^{\mathrm{MP2}}_{\mu\nu} + \bar{\kappa}_{\mu\nu}\right) C_{Q,\mu I}$$
$$\Gamma^{\mathrm{SCF}}_{Q,\mu I} = 2C_{\mu I}\left(i^{eff}_{Q} - i^{\mathrm{SCF}}_{Q}\right) - \sum_\nu \left(\tfrac{1}{2} D^{\mathrm{SCF}}_{\nu\mu} + D^{\mathrm{MP2}}_{\nu\mu} + \bar{\kappa}_{\nu\mu}\right) C_{Q,\nu I}$$
$$i^{\mathrm{SCF}}_{Q} = \sum_{\mu\nu} D^{\mathrm{SCF}}_{\mu\nu} C_{Q,\mu\nu} = \sum_{\mu I} C_{Q,\mu I} C_{\mu I}$$
$$i^{eff}_{Q} = \sum_{\mu\nu} D^{eff}_{\mu\nu} C_{Q,\mu\nu} = i^{\mathrm{SCF}}_{Q} + \sum_P j^{\mathrm{MP2}}_{P} \left[\mathbf{V}^{-1}\right]_{PQ} + \sum_{IA\mu} C_{\mu A} \bar{\kappa}_{AI} C_{Q,\mu I}$$
$$j^{\mathrm{MP2}}_{Q} = \sum_{\mu\nu} (\mu\nu|Q) \sum_{pq} C_{\mu p} C_{\nu q} \widetilde{D}^{\mathrm{MP2}}_{pq}$$

Table 2. Geometry convergence thresholds used for the RI- and PNO-MP2 geometry optimizations.

	RI-MP2	PNO-MP2
$T_{\Delta E}$	$1 \cdot 10^{-6}$	$1 \cdot 10^{-6}$
$T_{RMS(G)}$	$5 \cdot 10^{-4}$	$5 \cdot 10^{-4}$
T_{MaxG}	$1 \cdot 10^{-3}$	$1 \cdot 10^{-3}$
T_{RMSD}	$5 \cdot 10^{-4}$	$5 \cdot 10^{-3}$
T_{MaxD}	$1 \cdot 10^{-3}$	$2 \cdot 10^{-2}$

The definition of the three- and two electron densities ($\Delta^{\mathrm{SCF}}_{Q,\mu\nu}$ and $\gamma^{\mathrm{SCF}}_{PQ}$) for the SCF part are summarized in table 1. The last term in equation (32) is the contribution from the localization constraint with the density $D^{(w)}_{\mu\nu}$, which is defined as

$$D^{(w)}_{\mu\nu} = \sum_{kl} C_{\mu k} C_{\nu l} \bar{\lambda}_{kl} \Big[\langle k|r_w|k\rangle + \langle l|r_w|k\rangle\Big] \tag{35}$$

This term is a direct consequence of the use of Boys localization (in the localization constraint). Since it only involves contractions with sparse one-electron integrals, the computational costs are insignificant compared to the overall costs for computing the gradient.

3. Computational Details

The PNO-MP2 gradient has been implemented in a development version of the TURBOMOLE quantum chemistry program package [55, 56]. The SCF calculations have been done with the ridft [53, 57–60] and reference MP2 calculations with the ricc2 [48, 61, 62] program. For the geometry optimizations the optimizer statpt, which is part of TURBOMOLE, was used. During the geometry optimizations five convergence criteria have been tested: The energy change ($T_{\Delta E}$); the root mean square displacement of the atoms (T_{RMSD}); the maximum displacement of the atoms (T_{MaxD}); the RMS of the gradient (T_{RMSG}) and the maximum component of the gradient (T_{MaxG}). Table 2 summarizes the different thresholds for PNO- and RI-MP2 geometry optimizations.

The thresholds for the displacements were increased for PNO-MP2 geometry optimizations compared to the defaults. This accounts for the fact that the PNO approximation and the neglect of the PNO equations as constraint in the Lagrangian hinder such tight convergence of the geometry as it is default for the statpt program (see also section 4.1 for details).

The actual (PNO-)MP2 geometry optimizations have been carried out using the def2-SVP [63, 64], def2-TZVPP [64], def2-QZVPP [64, 65] aug-cc-pVTZ and aug-cc-pVQZ [66–68] orbital basis sets and the corresponding auxiliary basis sets for RI-MP2 [69, 70] and RI-JK. [53, 60]. Furthermore, the frozen core approximation has been used in all calculations.

4. Results

4.1. *Application of PNO-MP2 to Baker's Test Set for Geometry Optimizations*

For the investigation of the convergence behavior and the accuracy of PNO-MP2 geometries in a broad variety of bonding situations, we use Baker's test set for geometry optimizations [71]. The molecules included in this test set are listed in table 3.
The errors introduced by the PNO approximation are investigated as function of the PNO threshold ($T_{PNO} = 10^{-6} \dots 10^{-9}$) and the basis set size (def2-SVP, def2-TZVPP, def2-QZVPP). As statistical measures we use the mean error $\bar{\Delta}$, mean absolute error $\bar{\Delta}^{abs}$, maximum error Δ^{max} and the standard deviation σ.

For these statistical measures of the errors in bond lengths and angles, each covalent bond (angle) in all molecules has been considered: First, the statistical measures have been calculated for each molecule and subsequently, these molecule specific statistical data have then been used to obtain the statistical data over the whole test set.

4.1.1. Bond lengths

Before considering the statistical measures, which are calculated over the whole test set, it is interesting to investigate how the errors introduced by the PNO approximation behave for different bonding situations. For this purpose, characteristic bonds in a subset of molecules have been selected (see table 3). The errors of PNO-MP2 in these bond lengths in the def2-QZVPP basis set are shown in figure 1.

From this figure it obvious that the errors usually decrease with decreasing PNO thresholds. But this observation does not hold for all cases. For example, the error in the C=C bond in allene slightly increases from $T_{PNO} = 10^{-6}$ to $T_{PNO} = 10^{-8}$ and only decreases by further lowering the PNO threshold. A similar behavior can be seen for the error in the C $\equiv$ C bond in acetylene. Here, the error significantly increases by about 0.45 pm going from $T_{PNO} = 10^{-6}$ to $T_{PNO} = 10^{-7}$. This non-monotonic behavior is a result of the superposition of errors with different sign. But compared to the MP2 intrinsic errors (maximum and typical errors of 0.46 pm and 1.70 pm for first row elements [47, 72] (in the cc-pCVQZ basis) and 0.71 pm and 3.49 pm (in the cc-pCVQZ basis) for second row elements [73], respectively), this effect is small.

The statistical measures are shown in figure 2 and table 4. From the mean errors, it can be seen that there is no systematic trend concerning over- or underestimation of bond lengths with respect to RI-MP2 in the small def2-SVP basis, while in the larger triple-ζ and quadruple-ζ basis sets the PNO results tend to overestimate bond lengths, as it is expected as a consequence of the partial neglect of dynamic correlation. The mean absolute and maximum errors, in contrast, systematically decrease for tighter PNO thresholds. Already for $T_{PNO} = 10^{-6}$ both of these

Table 3. The molecules included in the Baker test set for geometry optimizations and the individual bonds with the corresponding labels considered for the calculation of the deviations shown in figure 1.

Molecule	Bond	Label	Molecule
Dimethylpentane	C-C	1	Water
Naphtalene	C=C	2	Ammonia
Acetylene	C $\equiv$ C	3	Ethane
Allene	C=C	4	Ethanol
Benzidine	C-C	5	Methylamine
1,3,5-Trisilacyclohexane	Si-C	6	Benzene
Disilylether	Si-O	7	Acetone
ACANIL01	N-CO	8	Benzaldehyde
Caffeine	N-CO	9	1,3-Difluorobenzene
Histidine	N=C	10	1,3,5-Trifluorobenzene
2-Hydroxzbicyclopentane	C-O	11	Neopentane
Menthone	C=O	12	Furan
Mesityloxide	C=O	13	ACHTAR10
Difuropyrazine	O-C	14	Pterin
1,5-Difuloronaphtalene	C-F	15	
Hydrosulphane	S-O	16	

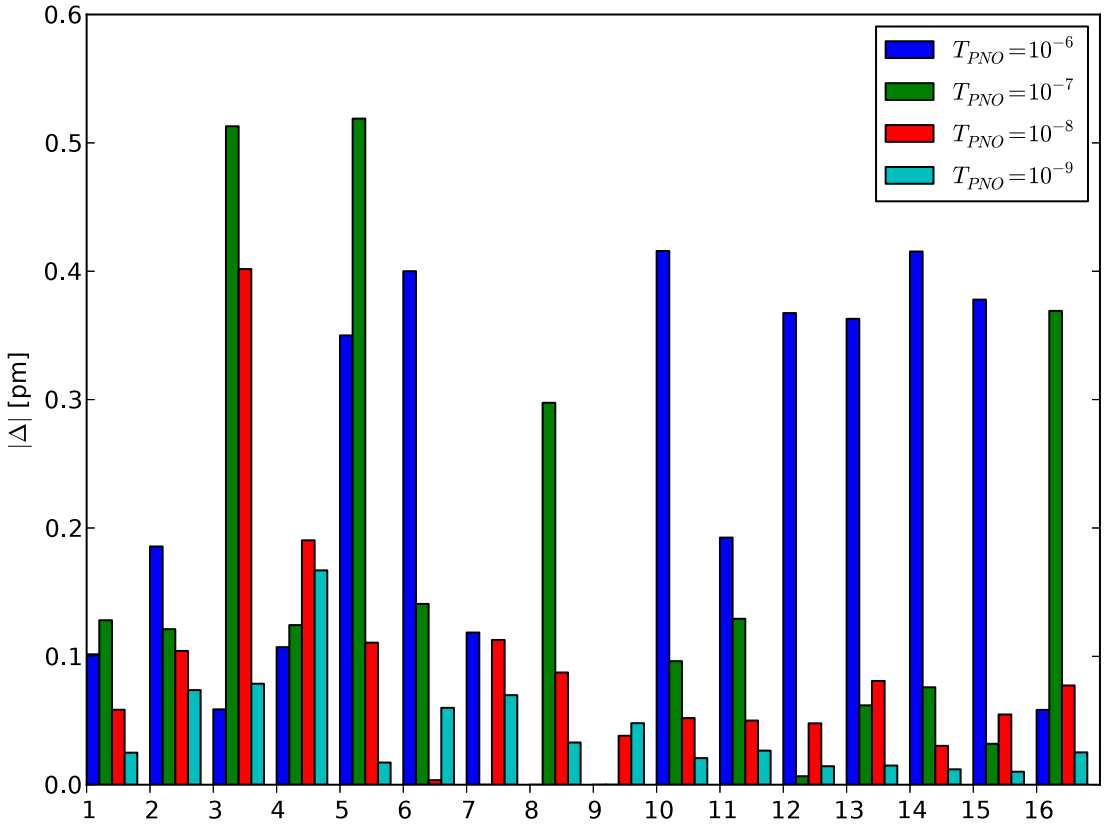


Figure 1. Errors in individual bonds in the def2-QZVPP basis set. The numbers on the x-axis refer to the numbering of molecules/bonds in table 3.

measures are below the respective MP2 intrinsic errors observed by Helgaker and coworkers [47] for first row elements (with one exception for the maximum error with $T_{PNO} = 10^{-6}$ in def2-TZVPP). In addition, the mean absolute and maximum errors increase in most cases with the size of the basis set. This is reasonable, since the virtual space increases with basis set size. This then leads to a more truncated virtual space if the same PNO threshold is applied for a calculation in a larger basis set. But compared to the MP2 intrinsic errors, this effect is small.

To better understand the origin of the relatively large maximum error of 2.26 pm with $T_{PNO} = 10^{-6}$ in the def2-TZVPP basis, we analyzed the structure of benzidine where this error occurs. The problematic bond is the C-C bond that connects the two phenyl rings. A competition between steric repulsion and dispersion interactions leads at the MP2 level to a dihedral angle between the phenyl rings of around 142° and a bond length of 147 pm (see also table 5). With $T_{PNO} = 10^{-6}$ and the def2-TZVPP basis the truncation of the virtual space apparently is too harsh to capture the dispersion interaction accurately enough and the geometry optimization converges to an almost perpendicular structure.

The normal distributions shown in figure 3 give a nice overview of the observations made so far. While being rather narrow and minimally displaced in the def2-SVP basis set for all PNO thresholds studied, they are broader for the larger basis sets. The curves become more sharply peaked with decreasing PNO thresholds, indicating the expected convergence towards the canonical results.

Furthermore, it is important to mention at this point that even though the statistical measures for $T_{PNO} = 10^{-6}$ and $T_{PNO} = 10^{-7}$ overall look promising (even for $T_{PNO} = 10^{-6}$ about 99.9 % of the errors lie within the MP2 error bar), for a few molecules and basis set sets, however, the optimizations did not convergence within the thresholds defined in table 2. This was

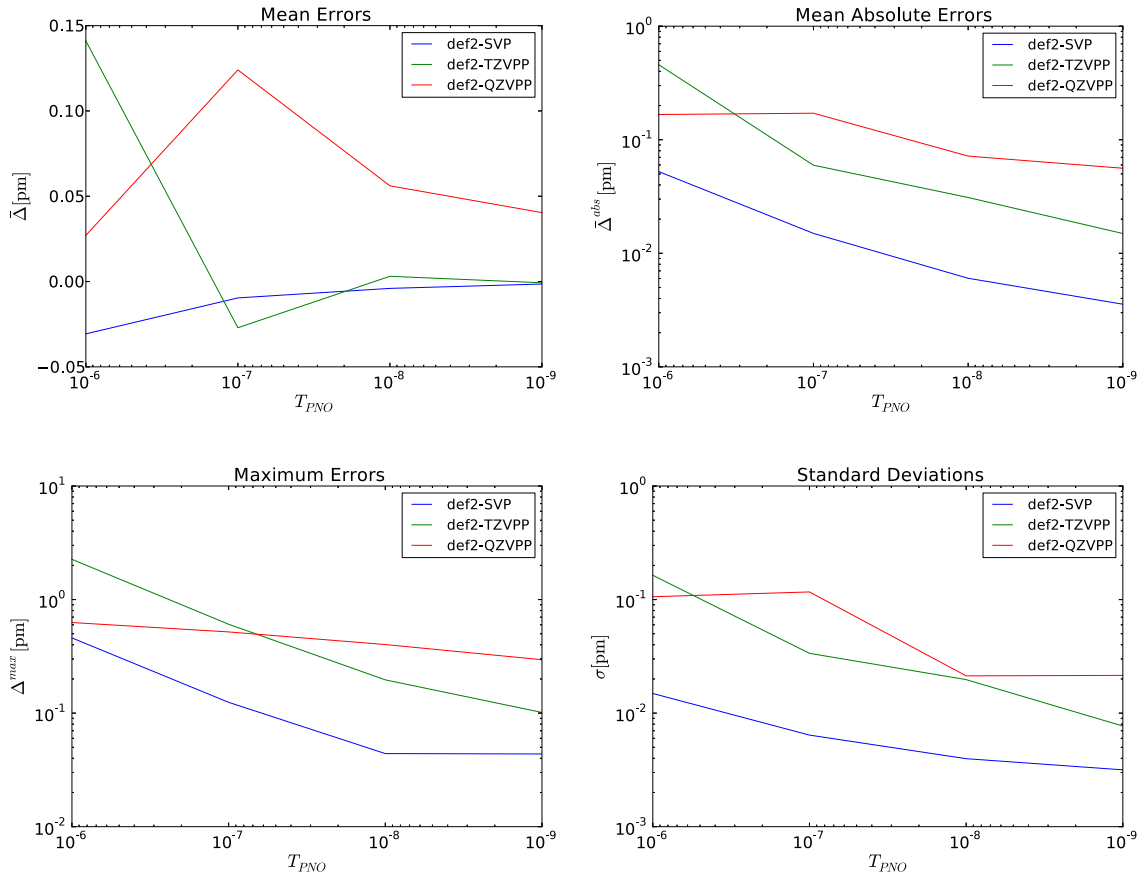


Figure 2. Graphical visualization of the statistical measures obtained for the errors in bond lengths.

Table 4. Statistical measures of errors in bond lengths [pm].

T_{PNO}		def2-SVP	def2-TZVPP	def2-QZVPP
10^{-6}	$\bar{\Delta}$	-0.03	0.14	0.03
	$\bar{\Delta}^{abs}$	0.05	0.46	0.17
	$\bar{\Delta}^{max}$	0.46	2.26	0.63
	σ	0.01	0.16	0.11
10^{-7}	$\bar{\Delta}$	$\lvert\bar{\Delta}\rvert < 0.01$	-0.03	0.12
	$\bar{\Delta}^{abs}$	0.01	0.06	0.17
	$\bar{\Delta}^{max}$	0.12	0.61	0.52
	σ	< 0.01	0.03	0.12
10^{-8}	$\bar{\Delta}$	$\lvert\bar{\Delta}\rvert < 0.01$	$\lvert\bar{\Delta}\rvert < 0.01$	0.06
	$\bar{\Delta}^{abs}$	< 0.01	0.03	0.07
	$\bar{\Delta}^{max}$	0.04	0.20	0.40
	σ	< 0.01	0.02	0.02
10^{-9}	$\bar{\Delta}$	$\lvert\bar{\Delta}\rvert < 0.01$	$\lvert\bar{\Delta}\rvert < 0.01$	0.04
	$\bar{\Delta}^{abs}$	< 0.01	0.01	0.06
	$\bar{\Delta}^{max}$	0.04	0.10	0.30
	σ	< 0.01	< 0.01	0.02

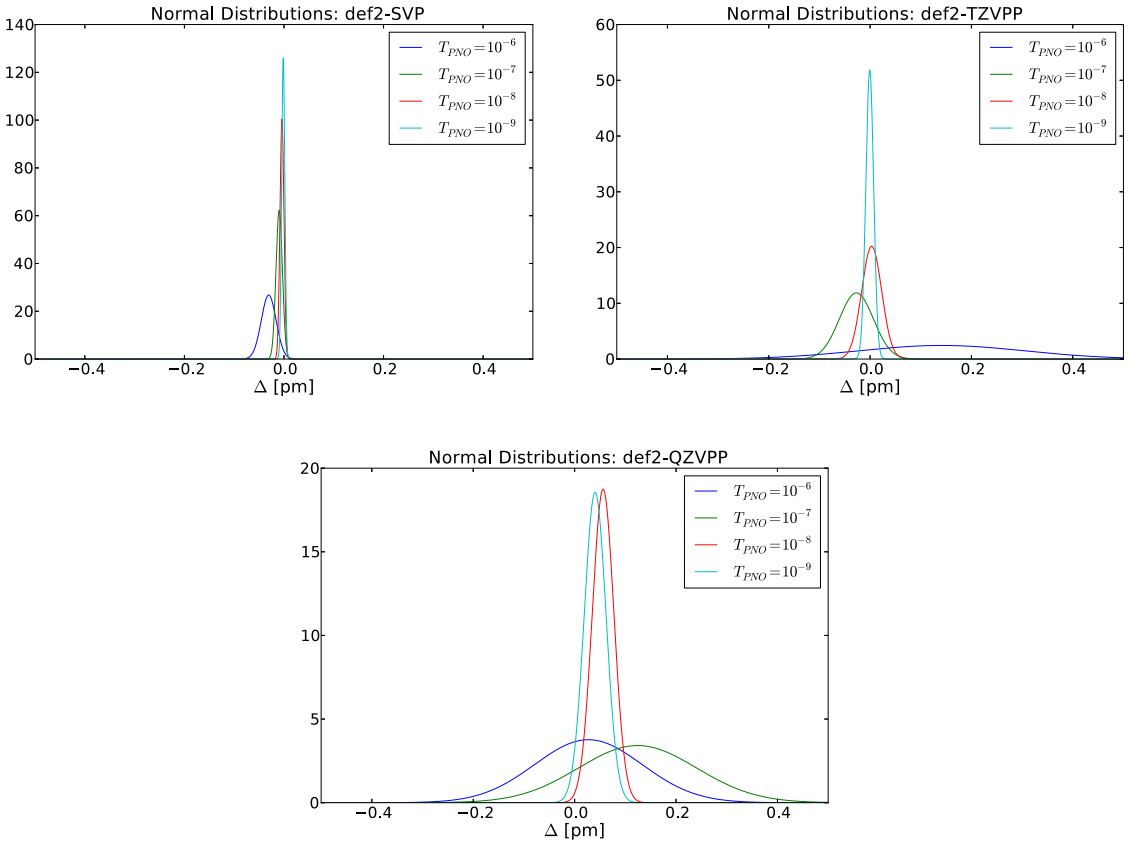


Figure 3. Normal distributions of the PNO errors (in bond lengths) in different basis sets.

Table 5. Comparison of the RI-MP2 and the PNO-MP2 C-C bond length and the dihedral angle between the two phenyl groups in benzidine.

	Dihedral angle [°]		C-C bond length [pm]	
	def2-TZVPP	def2-QZVPP	def2-TZVPP	def2-QZVPP
$T_{PNO} = 10^{-6}$	92.6	138.4	149.4	147.3
$T_{PNO} = 10^{-7}$	143.8	145.7	147.7	147.5
$T_{PNO} = 10^{-8}$	143.2	141.3	147.3	147.1
$T_{PNO} = 10^{-9}$	142.3	140.6	147.2	147.0
RI-MP2	142.0	142.0	147.1	147.0

the case for pterin ($T_{PNO} = 10^{-6}$) and caffeine ($T_{PNO} = 10^{-6}$ and $T_{PNO} = 10^{-7}$) in all basis sets. Additionally, disilylether could not be converged for $T_{PNO} = 10^{-6}$ in def2-TZVPP and for $T_{PNO} = 10^{-7}$ in def2-QZVPP and ACANIL01 could not be converged for $T_{PNO} = 10^{-6}$ in def2-QZVPP. Caffeine, ACANIL01 and disilylether are rather floppy molecules (especially due to the methyl groups) with many local minima on a flat potential energy surface. For these molecules, the rotation of the methyl groups prevents the energy or the gradient from convergence: After an initial decrease of the energy, the optimization starts to oscillate. Similar observations have been made for pterin. It is, however, unclear whether this is a problem of the PNO approximation itself or of the neglect of the PNO equations as constraints in the Lagrangian in the current preliminary implementation.

4.1.2. Bond Angles

Statistical measures for the errors in bond angles are given in figure 4 and table 6. They have been evaluated in a similar way as the bond lengths before. For the angles we present, however, no results for the mean error, since the errors in individual angles tend to cancel each other,

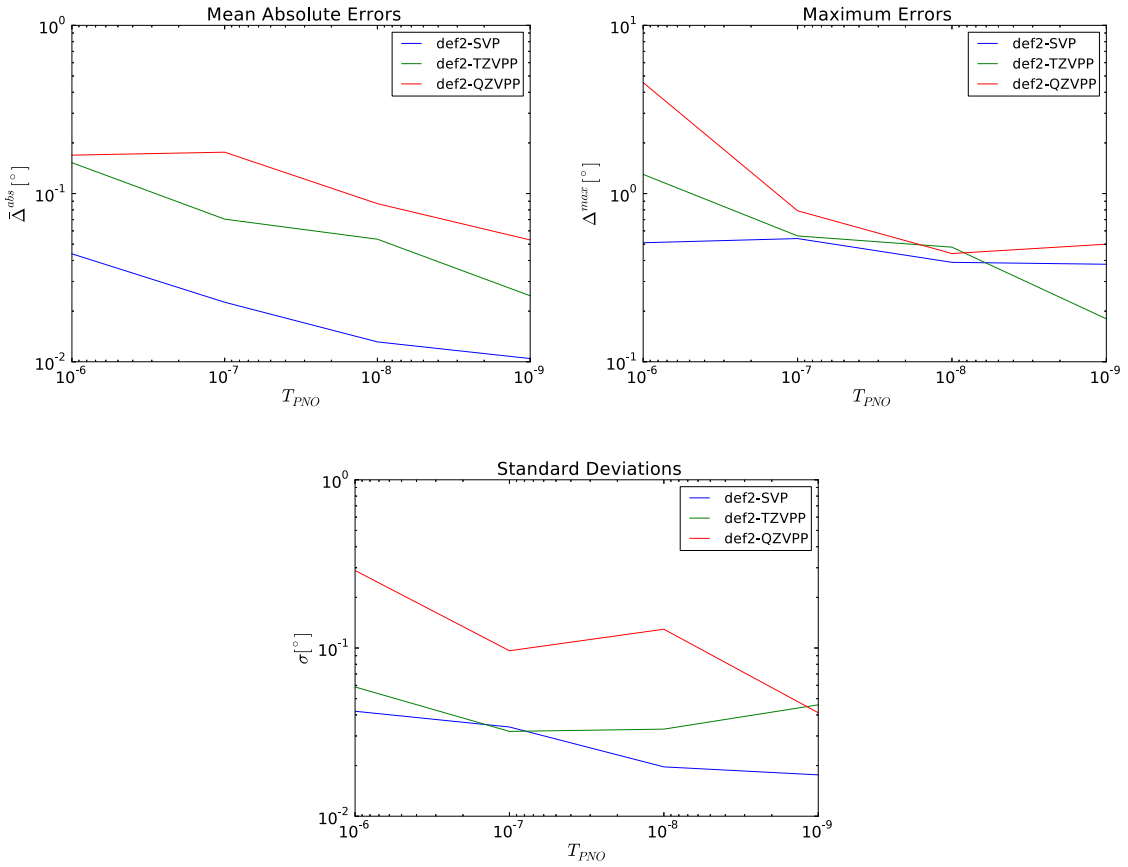


Figure 4. Graphical visualization of the statistical measures obtained for the errors in bond angles.

as e.g. for the three bond angles at a sp^2 hybridized central atom. All in all, the curves show a similar behavior as the ones for the bond lengths. Again, the mean absolute errors are below the MP2 intrinsic errors (0.19° for first row elements [47, 72] and 0.12° for second row elements [73]) in every case. The maximum error at $T_{PNO} = 10^{-6}$ and $T_{PNO} = 10^{-9}$ in the def2-QZVPP basis both occur in the Si-O-Si bond of disilylether. The large error at $T_{PNO} = 10^{-6}$ and the significant decrease at $T_{PNO} = 10^{-9}$ suggest that somewhat tighter thresholds should be used for molecules containing second row elements, even though the errors in the bond lengths are small.

4.2. *The Structure of Water Clusters*

One of the key areas, where MP2 or related double hybrid DFT functionals are applied, are geometry optimizations of molecular clusters and complexes, with geometries that are vastly determined by weak interactions, as e.g. hydrogen bonding. To investigate the accuracy of PNO-MP2 on such intermolecular complexes different water hexa- and octamers have been optimized.

The error between canonical and PNO-MP2 in the nearest neighbor O-O distances has been used as a measure for the description of hydrogen bonds, since these are also commonly used measures to describe water complexes in the literature [74–76] (see table 4). Furthermore, the errors in H-O-H, O-H$\cdots$O and H$\cdots$O-H($\cdots$O) have been been analyzed (see table 8) to obtain a more complete overview of the similarity of the structures. The same statistical measures as described above have been used. But in this case the statistical measures have been evaluated by averaging only over the errors at each water cluster to obtain a more complete overview of the similarity of the structures.

Table 6. Statistical measures of errors in bond angles [°].

T_{PNO}		def2-SVP	def2-TZVPP	def2-QZVPP
10−6	$\bar{\Delta}^{abs}$	0.04	0.15	0.17
	$\bar{\Delta}^{max}$	0.51	1.30	4.57
	σ	0.04	0.06	0.29
10−7	$\bar{\Delta}^{abs}$	0.02	0.07	0.18
	$\bar{\Delta}^{max}$	0.54	0.56	0.79
	σ	0.03	0.03	0.10
10−8	$\bar{\Delta}^{abs}$	0.01	0.05	0.09
	$\bar{\Delta}^{max}$	0.39	0.48	0.44
	σ	0.02	0.03	0.13
10−9	$\bar{\Delta}^{abs}$	0.01	0.02	0.05
	$\bar{\Delta}^{max}$	0.38	0.18	0.50
	σ	0.02	0.05	0.04

As a general trend it can be seen from tables 7 and 8 that the errors in the aug-cc-pVQZ basis set are somewhat larger than those in the aug-cc-pVTZ basis for the same PNO threshold. Similar to the observations made for Baker's test set, we observe that for tight PNO thresholds, i.e. $T_{PNO} = 10^{-8}$ and $T_{PNO} = 10^{-9}$, the O-O distances converge in the quadruple-zeta basis set from below.

Furthermore, it was found that the influence of basis set superposition error (BSSE) on PNO-MP2 and canonical MP2 geometries is similar for practically relevant PNO thresholds (see below). Similar observations can be made by comparing the counterpoise-corrected (CP-corrected) [77] and uncorrected MP2 and PNO-MP2 binding energies (table 9). Hence, only the errors referring to the uncorrected results will be discussed in the following.

Concerning the accuracy, tables 7 and 8 clearly show that PNO thresholds as loose as $T_{PNO} = 10^{-6}$ do lead to unacceptable errors in geometries in almost all water clusters. This can be rationalized by the fact that the dispersion effect from weak pairs contributes substantially to hydrogen bonds. Apparently, the weak pairs needed for the description of hydrogen bonds are discarded at loose PNO thresholds which leads to the overestimation of intermolecular distances. Tightening the PNO threshold to 10^{-7} already yields a significant improvement for all water clusters and basis sets. The mean absolute errors in O-O distances fall below 2 pm. The MP2 intrinsic error also was found to be in the range of 2 pm for water clusters up to water hexamers. These errors were determined by comparing CCSD(T) to MP2 geometries [78]. Further lowering the PNO threshold does not lead to a significant decrease of errors in neighbor O-O distances.

The bond angles, however, still improve further with lower PNO thresholds of 10^{-8} or 10^{-9} when large basis sets are used. While in the aug-cc-pVTZ basis the results for the bond angles change only little between $T_{PNO} = 10^{-7}$ and $T_{PNO} = 10^{-8}$, this is not yet the case in the aug-cc-pVQZ basis set. Especially for the water octamers, where the mean absolute error is still 3.4 ° – 3.8 ° with $T_{PNO} = 10^{-7}$. With a PNO threshold of 10^{-8} the mean absolute errors drop below 0.7 °. The maximum errors also decrease significantly, especially for the water octamers.

Since the maximum errors all occur in O-H$\cdots$O and H$\cdots$O-H($\cdots$O) angles, which are, compared to covalent bond angles, rather loose degrees of freedom, the accuracy achieved with $T_{PNO} = 10^{-7}$ might already be sufficient. This might in particular be the case for the binding energies where the differences between MP2 and PNO-MP2 are already with $T_{PNO} = 10^{-7}$ in all cases below 1 kcal/mol per hydrogen bond.

4.3. *Performance of the Implementation*

To investigate the performance of the implementation, calculations on increasingly large glycine chains have been done. The wall times for the computation of the correlation contributions to the one- and two-particle densities are shown for canonical RI-MP2 and PNO-MP2 in figure 5. At this point it should also be mentioned that the local RI approximation, which we do not yet exploit in our preliminary implementation, will lead to a further reduction of the scaling.

Table 7. Statistical measures for the errors in the nearest neighbor O-O distances [pm] in different water clusters. The errors were obtained by comparing the results for canonical and PNO-MP2 results without counterpoise correction.

T_{PNO}		aug-cc-pVTZ					aug-cc-pVQZ				
		$(H_2O)_6$			$(H_2O)_8$		$(H_2O)_6$			$(H_2O)_8$	
		Prism	Cage	Book	D_{2d}	S_4	Prism	Cage	Book	D_{2d}	S_4
10^{-6}	$\bar{\Delta}$	5.05	4.66	4.75	5.72	5.51	9.32	10.12	-[a]	11.87	-[b]
	$\bar{\Delta}^{abs}$	5.05	4.66	4.75	5.72	5.51	9.32	10.12	-[a]	11.87	-[b]
	$\bar{\Delta}^{max}$	6.58	8.44	6.53	5.95	5.75	12.91	14.52	-[a]	15.10	-[b]
	σ	1.19	1.60	0.91	0.16	0.31	2.83	2.08	-[a]	1.53	-[b]
10^{-7}	$\bar{\Delta}$	-0.44	-0.50	0.23	0.08	0.34	1.25	0.98	1.66	0.44	0.42
	$\bar{\Delta}^{abs}$	0.88	0.98	0.44	0.52	0.62	1.30	1.38	1.66	0.44	0.83
	$\bar{\Delta}^{max}$	1.89	1.64	0.93	0.66	0.94	5.17	2.65	2.84	0.52	1.10
	σ	0.96	0.96	0.46	0.52	0.55	1.60	1.30	0.63	0.06	0.74
10^{-8}	$\bar{\Delta}$	0.13	-0.25	-0.25	0.12	$\lvert\bar{\Delta}\rvert < 0.01$	-0.93	-0.96	-0.85	-2.60	-2.54
	$\bar{\Delta}^{abs}$	0.72	0.50	0.36	0.13	0.43	1.18	1.00	0.85	2.60	2.54
	$\bar{\Delta}^{max}$	2.92	1.36	0.61	0.27	0.82	2.70	2.32	1.46	2.70	2.71
	σ	1.10	0.59	0.32	0.11	0.47	1.06	0.70	0.41	0.07	0.09
10^{-9}	$\bar{\Delta}$	0.23	0.15	0.15	0.28	0.19	-0.43	-0.12	-0.66	-0.54	-0.63
	$\bar{\Delta}^{abs}$	0.40	0.16	0.23	0.28	0.21	1.09	0.61	0.68	0.54	0.63
	$\bar{\Delta}^{max}$	0.87	0.35	0.38	0.36	0.37	2.81	1.33	1.21	0.91	1.00
	σ	0.41	0.13	0.21	0.06	0.13	1.24	0.68	0.38	0.25	0.27
MP2[c]	$\bar{\Delta}$	-2.50	-2.48	-2.54	-2.55	-2.56	-1.30	-1.36	-1.42	-1.36	-1.36
	$\bar{\Delta}^{abs}$	2.50	2.48	2.54	2.55	2.56	1.30	1.36	1.42	1.36	1.36
	$\bar{\Delta}^{max}$	2.91	3.08	2.83	2.61	2.67	1.42	1.55	1.51	1.38	1.39
	σ	0.26	0.25	0.14	0.07	0.11	0.07	0.09	0.05	0.02	0.01

[a]No reasonable geometry found

[b]No convergence achieved

[c]Refers to the deviations between MP2 and CP-corrected MP2 structures

Table 8. Statistical measures for the errors in inter- and intramolecular bond angles of different water clusters. All possible H-O-H, O-H$\cdots$O and H$\cdots$O-H($\cdots$O) angles [°] have been included in the analysis to give a more complete overview over the similarities of the structures.

T_{PNO}		aug-cc-pVTZ					aug-cc-pVQZ				
		$(H_2O)_6$			$(H_2O)_8$		$(H_2O)_6$			$(H_2O)_8$	
		Prism	Cage	Book	D_{2d}	S_4	Prism	Cage	Book	D_{2d}	S_4
10^{-6}	$\bar{\Delta}^{abs}$	1.44	2.33	1.76	2.84	2.52	2.61	1.72	-[a]	3.14	-[b]
	$\bar{\Delta}^{max}$	4.54	9.67	3.83	4.34	3.93	17.25	5.91	-[a]	13.90	-[b]
10^{-7}	$\bar{\Delta}^{abs}$	0.68	0.75	0.74	0.78	0.92	1.61	1.70	1.67	3.80	3.43
	$\bar{\Delta}^{max}$	1.97	1.67	1.61	1.37	1.95	4.56	3.56	9.01	5.89	7.54
10^{-8}	$\bar{\Delta}^{abs}$	0.71	0.47	0.46	0.23	0.37	0.68	0.80	0.63	0.42	0.47
	$\bar{\Delta}^{max}$	2.19	1.32	2.20	0.67	1.36	3.96	2.37	1.70	0.84	1.48
10^{-9}	$\bar{\Delta}^{abs}$	0.22	0.26	0.24	0.13	0.12	0.76	0.61	0.51	0.76	0.75
	$\bar{\Delta}^{max}$	1.12	1.48	1.64	0.39	0.47	2.97	1.67	2.14	1.27	1.31
MP2[c]	$\bar{\Delta}^{abs}$	0.26	0.27	0.34	0.22	0.23	0.11	0.12	0.13	0.09	0.10
	$\bar{\Delta}^{max}$	0.67	0.64	1.22	0.36	0.42	0.25	0.31	0.33	0.19	0.25

[a]No reasonable geometry found

[b]No convergence achieved

[c]Refers to the deviations between MP2 and CP-corrected MP2 structures

Table 9. Comparison of the PNO-MP2 and MP2 binding energies for different water clusters with and without CP-correction. The binding energies have been calculated at geometries optimized with the respective method/PNO threshold given in the second column.

		aug-cc-pVTZ		aug-cc-pVQZ	
		E_{int}	E_{int}^{CP}	E_{int}	E_{int}^{CP}
$(H_2O)_6$ (Prism)	$T_{PNO} = 10^{-6}$	-47.9	-44.0	-45.2	-43.3
	$T_{PNO} = 10^{-7}$	-50.0	-45.7	-48.6	-46.5
	$T_{PNO} = 10^{-8}$	-49.8	-45.6	-49.0	-46.9
	$T_{PNO} = 10^{-9}$	-49.7	-45.5	-49.0	-46.9
	MP2	-49.8	-45.6	-48.9	-46.8
$(H_2O)_6$ (Cage)	$T_{PNO} = 10^{-6}$	-47.7	-43.9	-44.9	-43.0
	$T_{PNO} = 10^{-7}$	-49.9	-45.6	-48.4	-46.3
	$T_{PNO} = 10^{-8}$	-49.7	-45.5	-48.9	-46.8
	$T_{PNO} = 10^{-9}$	-49.6	-45.4	-48.9	-46.8
	MP2	-49.7	-45.5	-48.9	-46.8
$(H_2O)_6$ (Book)	$T_{PNO} = 10^{-6}$	-47.3	-43.7	-[a]	-[a]
	$T_{PNO} = 10^{-7}$	-49.3	-45.2	-47.8	-45.8
	$T_{PNO} = 10^{-8}$	-49.4	-45.4	-48.5	-46.5
	$T_{PNO} = 10^{-9}$	-49.3	-45.2	-48.7	-46.7
	MP2	-49.4	-45.3	-48.6	-46.6
$(H_2O)_8$ (D_{2d})	$T_{PNO} = 10^{-6}$	-75.6	-69.5	-70.2	-67.3
	$T_{PNO} = 10^{-7}$	-79.5	-72.7	-77.0	-73.6
	$T_{PNO} = 10^{-8}$	-79.4	-72.6	-78.4	-75.0
	$T_{PNO} = 10^{-9}$	-79.3	-72.5	-78.0	-74.7
	MP2	-79.5	-72.6	-77.8	-74.5
$(H_2O)_8$ (S_4)	$T_{PNO} = 10^{-6}$	-75.7	-69.5	-[b]	-[b]
	$T_{PNO} = 10^{-7}$	-79.4	-72.6	-77.0	-73.6
	$T_{PNO} = 10^{-8}$	-79.4	-72.6	-78.5	-75.0
	$T_{PNO} = 10^{-9}$	-79.3	-72.4	-78.0	-74.7
	MP2	-79.5	-72.6	-77.8	-74.5

[a]No reasonable geometry found

[b]No convergence achieved

From figure 5 it can be seen that canonical RI-MP2 and PNO-MP2 show a reasonably early break even point at approximately 1060 basis functions. The asymptotic scaling of canonical MP2 is in the order of $\mathcal{O}(\mathcal{N}^5)$ (the effective scalling obtained from a linear regression between 706 and 2650 basis functions is in the order of $\mathcal{O}(\mathcal{N}^{4.7})$). The scaling of our PNO-MP2 implementation, in contrast, is only in the order of $\mathcal{O}(\mathcal{N}^{3.2})$. Since our iterative PNO construction also shows a very similar scaling behavior, this suggests that no additional bottleneck is introduced when computing the correlation contribution to the gradient.

Concerning the dependence of the efficieny on the PNO threshold, it should be noted that the computational costs increase quadratically with the number of PNOs per pair and linearly with the number of pairs.

5. Conclusions

We presented an implementation of the PNO-MP2 gradient. The equations have been derived by augmenting the canonical RI-MP2 Lagrangian with the localization constraint and restricting the doubles amplitudes to the PNO space. A statistical analysis of the errors relative to canonical RI-MP2 demonstrates that the errors introduced by the PNO approximation are negligible with respect to the intrinsic error of the MP2 method. Geometry optimizations for water clusters of different size show that the errors are larger for weakly bound systems. Since also the intrinsic error of MP2 is larger for intermolecular distances and effects such as the BSSE increase the uncertainty, it can be stated, that also here PNO thresholds of 10^{-7} to 10^{-8} are sufficient to obtain accurate geometries.

The convergence may be improved in the future by including the PNO and OSV equations

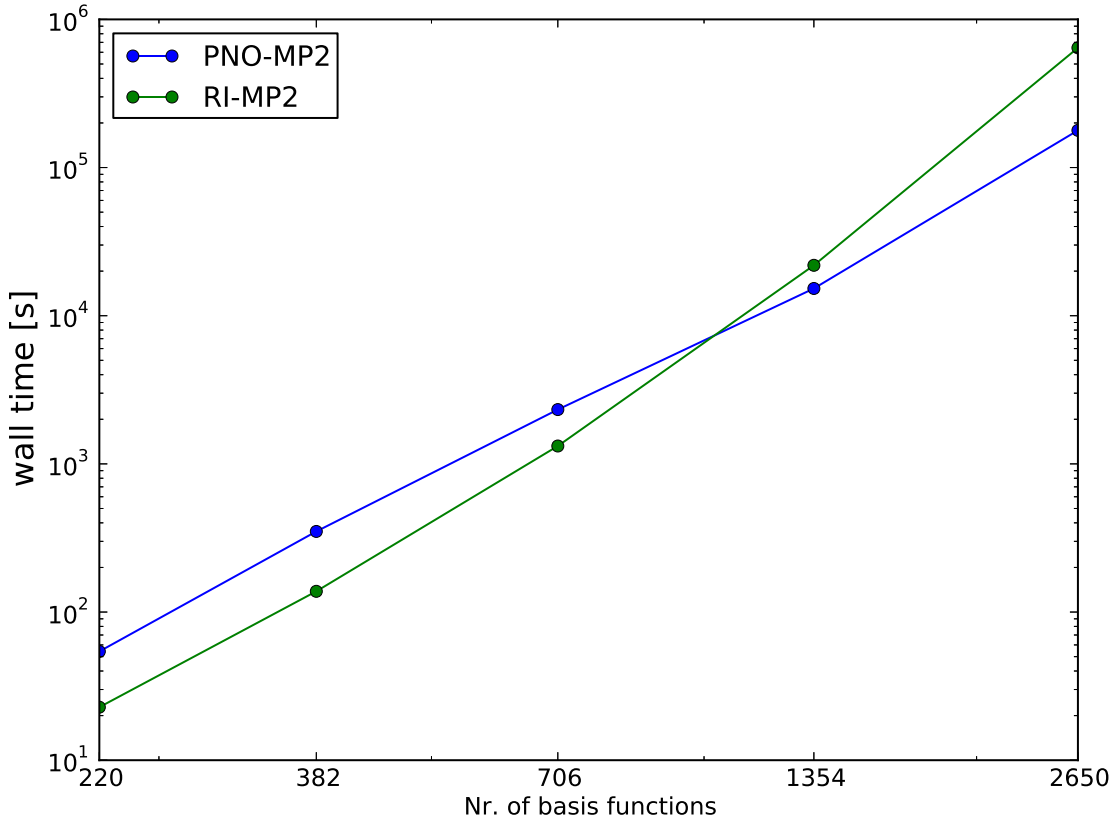


Figure 5. Comparison of the performance of canonical RI-MP2 and PNO-MP2 on gly_n chains ($n = 1, 2, 4, 8, 16$) in the cc-pVTZ basis set. The PNO-MP2 calculation has been carried out using a PNO threshold of $T_{PNO} = 10^{-8}$. For this comparison the time for the solution of he Z-CPHF equations has not been considered.

as additional constraints in the Lagrangian. Furthermore, the correction for neglected pairs and PNOs have not been considered in the preliminary implementation reported here. Whether these points will enhance the efficiency or merely increase the computational costs is subject of ongoing work.

6. Acknowledgements

This work was supported by the Deutsche Forschungsgemeinschaft (DFG) under Grant HA2588/7-1.

References

[1] P. Pulay, Chem Phys Lett **100**, 151 (1983).
[2] S. Saebø and P. Pulay, Chem. Phys. Lett. **113**, 13 (1985).
[3] S. Saebø and P. Pulay, Ann. Rev. Phys. Chem **44**, 213 (1993).
[4] P. Pulay and S. Saebø, Theor Chim Acta **69**, 357 (1986).
[5] S. Saebø and P. Pulay, J Chem Phys **86**, 914 (1987).
[6] S. Saebø and P. Pulay, J Chem Phys **88**, 1884 (1988).
[7] G. Rauhut, P. Pulay and H.J. Werner, J Comput Chem **19**, 1241 – 1254 (1998).
[8] M. Schütz, G. Hetzer and H.J. Werner, J. Chem. Phys. **111**, 5691 (1999).
[9] C. Hampel and H.J. Werner, J Chem Phys **104**, 6286 – 6297 (1996).
[10] M. Schütz, Phys Chem Chem Phys **4**, 3941 – 3347 (2002).

[11] M. Schütz and F.R. Manby, Phys Chem Chem Phys **5**, 3349 – 3358 (2003).
[12] G.D. Purvis and R.J. Bartlett, J Chem Phys **76**, 1910 (1982).
[13] H.J. Werner and M. Schütz, J Chem Phys **135**, 144116 (2011).
[14] M. Schütz, O. Masur and D. Usvyat, J Chem Phys **140**, 244107 (2014).
[15] K. Raghafavachari, G.W. Trucks, J.A. Pople and M. Head-Gordon, Chem Phys Lett **157**, 479 (1989).
[16] R.J. Bartlett, J.D. Watts, S.A. Kucharski and J. Noga, Chem Phys Lett **165**, 513 (1990).
[17] M. Schütz and H.J. Werner, J Chem Phys **2000**, 9986 (2000).
[18] W. Meyer, *Methods of Electronic Structure Theory*, 3rd ed. (Plenum Press, New York, 1977).
[19] W. Meyer, Theor Chem Acc **35**, 277 – 292 (1974).
[20] W. Meyer, J Chem Phys **58**, 1017 – 1035 (1973).
[21] W. Meyer, Int J Quantum Chem **S5**, 341 – 348 (1971).
[22] R. Ahlrichs, F. Driessler, H. Lischka, V. Staemmler and W. Kutzelnigg, J Chem Phys **62**, 1235 – 1247 (1975).
[23] R. Ahlrichs and F. Driessler, Theor Chem Acc **36**, 275 – 287 (1975).
[24] V. Staemmler and R. Jaquet, Theor Chem Acc **59**, 487 – 500 (1981).
[25] J.L. Whitten, J Chem Phys **58**, 4496 (1973).
[26] B.I. Dunlap, J.W.D. Conolly and J.R. Sabin, J Chem Phys **71**, 3396 (1973).
[27] F. Neese, A. Hansen and D.G. Liakos, J Chem Phys **131**, 064103 – 15 (2009).
[28] F. Neese, A. Hansen and F. Wennmohs, S Acc Chem Res **42**, 641 – 648 (2009).
[29] F. Neese., Wennmohs and A. Hansen, J. Chem. Phys. **130**, 114108 (2009).
[30] D.G. Liakos, A. Hansen and F. Neese, J Chem Theory Comput **7**, 76 – 87 (2011).
[31] A. Hansen, D.G. Liakos and F. Neese, J Chem Phys **135**, 214102 – 20 (2011).
[32] C. Riplinger and F. Neese, J Chem Phys **138**, 034106 (2013).
[33] J. Yang, G.K.L. Chan, F.R. Manby, M. Schütz and H.J. Werner, J Chem Phys **136**, 144105 (2012).
[34] C. Hättig, D.P. Tew and B. Helmich, J Chem Phys **136** (20), 204105 (2012).
[35] C. Krause and H.J. Werner, Phys Chem Chem Phys **14**, 7591 – 7604 (2012).
[36] G. Schmitz, B. Helmich and C. Hättig, Mol Phys **111**, 2463 – 2476 (2013).
[37] B. Helmich and C. Hättig, J Chem Phys (2013).
[38] B. Helmich and C. Hättig, Computational and Theoretical Chemistry (2014).
[39] D.P. Tew and C. Hättig, International Journal of Quantum Chemistry **113** (3) (2013).
[40] D.P. Tew and C. Hättig, J Chem Phys **135** (7), 074107 (2011).
[41] G. Schmitz, C. Hättig and D.P. Tew, Phys Chem Chem Phys **16** (2014).
[42] C. Riplinger, B. Sandhoefer, A. Hansen and F. Neese, J Chem Phys **139**, 134101 (2013).
[43] H.J. Werner, G. Knizia, C. Krause, M. Schwilk and M. Dornbach, J Chem Theor Comput **11**, 484 – 507 (2015).
[44] Q. Ma and H.J. Werner, J Chem Theor Comput **11**, 5291 – 5304 (2015).
[45] P. Pinski, C. Riplinger, E.F. Valeev and F. Neese, J Chem Phys **143**, 034108 (2015).
[46] C. Riplinger, P. Pinski, U. Becker, E.F. Valeev and F. Neese, J Chem Phys **144**, 024109 (2016).
[47] T. Helgaker, P. Jørgensen and J. Olsen, *Molecular Electronic-Structure Theory* (Wiley, Chichester, 2000).
[48] C. Hättig, J Chem Phys **118** (17), 7751 (2003).
[49] B. Helmich and C. Hättig, J Chem Phys **135** (21), 214106 (2011).
[50] S.F. Boys, Rev. Mod. Phys. **32**, 296–299 (1960).
[51] N.C. Handy and H.F. Schaefer, J Chem Phys **81**, 5031 (1984).
[52] M. Schütz, H.J. Werner, R. Lindh and F.R. Manby, J Chem Phys **121**, 737 (2004).
[53] F. Weigend, J Comput Chem **30;29** (2), 167 – 175 (2008).
[54] C. Hättig, A. Hellweg and A. Köhn, Phys. Chem. Chem. Phys. **8**, 1159–1169 (2006).
[55] TURBOMOLE GmbH, *TURBOMOLE V7.1 2014, a development of University of Karlsruhe and Forschungszentrum Karlsruhe GmbH, 1989–2007, TURBOMOLE GmbH, since 2007; available from* `http://www.turbomole.com`. (Forschungszentrum Karlsruhe GmbH, Karlsruhe, Germany, 2014).
[56] F. Furche, R. Ahlrichs, C. Hättig, W. Klopper, M. Sierka and F. Weigend, Wiley Interdisciplinary Reviews: Computational Molecular Science **4** (2), 91–100 (2014).
[57] M. v Arnim and R. Ahlrichs, J Comput Chem **19**, 1746 (1998).
[58] M. Häser and R. Ahlrichs, J Comput Chem **10**, 104 (1989).
[59] F. Weigend, Phys Chem Chem Phys **8**, 1057 (2006).
[60] F. Weigend, Phys Chem Chem Phys **4**, 4285 (2002).
[61] C. Hättig and F. Weigend, J. Chem. Phys. **113**, 5154 (2000).
[62] C. Hättig, A. Hellweg, and A. Köhn, Phys Chem Chem Phys **8**, 1159 (2006).

[63] A. Schäfer, H. Horn and R. Ahlrichs, J Chem Phys **97**, 2571 (1992).
[64] F. Weigend and R. Ahlrichs, Phys Chem Chem Phys **7**, 3297 (2005).
[65] F. Weigend, F. Furche and R. Ahlrichs, J Chem Phys **119**, 12753 (2003).
[66] T.H. Dunning Jr., J. Chem. Phys. **90**, 1007 (1989).
[67] R.A. Kendall, T.H. Dunning Jr. and R.J. Harrison, J. Chem. Phys. **96**, 6796–6806 (1992).
[68] D.E. Woon and T.H. Dunning Jr., J. Chem. Phys. **98**, 1358–1371 (1993).
[69] F. Weigend, A. Köhn and C. Hättig, J. Chem. Phys. **116** (8), 3175 (2002).
[70] F. Weigend, M. Häser, H. Patzelt and R. Ahlrichs, Chem Phys Lett **294**, 143 (1998).
[71] J. Baker, J. Comput. Chem. **14** (9), 1085–1100 (1993).
[72] K.L. Bak, J. Gauss, P. Jørgensen, J. Olsen, T. Helgaker and J.F. Stanton, J. Chem. Phys. **6548**, 114 (2001).
[73] S. Coriani, D. Marchesan, J. Gauss, C. Hättig, T. Helgaker and P. Jørgensen, J. Chem. Phys. **123**, 184107 (2005).
[74] C. Pérez, M.T. Muckle, D.P. Zaleski, N.A. Seifert, B. Temelso, G.C. Shields, Z. Kisiel and B.H. Pate, Science **336**, 897 (2012).
[75] I.M.B. Nielsen, E.T. Seidl and C.L. Janssen, J. Chem. Phys. **110** (19), 9435 (1999).
[76] M. Schütz, H.J. Werner, R. Lindh and F.R. Manby, J. Chem. Phys. **121** (2), 737 (2004).
[77] S. Boys and F. Bernadi, Molecular Physics **19**, 553 – 566 (1970).
[78] E. Miliordos, E. Aprà and S.S. Xantheas, J. Chem. Phys. **139**, 114302 (2013).

V. PNO-CCSD EXCITATION ENERGIES WITHIN A LINEAR RESPONSE FRAMEWORK

The aim of this project is the investigation of the performance and accuracy of PNO-CCSD in the determination of excitation energies within a linear response theory framework. Since other local correlation methods such as PAOs and the fragment based incremental scheme failed due to the large domain sizes needed for accurate calculations and, hence, their development for methods beyond second order such as CCSD is hindered, it is a natural step to investigate the performance of the state-specific PNO approach for obtaining CCSD excitation energies. The resulting publication is the first application of the PNO approximation to CCSD excitation energies.

This work has been performed under the supervision of Prof. Dr. Christof Hättig. The implementation is based on an existing framework for excited state PNO calculations which has previously been implemented by Hättig and Helmich[22–24]. The implementation of the contributions to the PNO-CCSD Jacobian right transformation beyond CC2/ADC(2)-D has been done by myself. Method development in the sense of deriving several working equations, implementing integrals screening for several terms and implementing the local RI approximation in an efficient manner was done by me. For the publication, I created all numbers, graphics and wrote the text.

The publication presented in the following, is reproduced from M.S. Frank and C. Hättig. A pair natural orbital based implementation of CCSD excitation energies within the framework of linear response theory. J. Chem. Phys. **148**, 134102 (2018), with the permission of AIP Publishing

THE JOURNAL OF CHEMICAL PHYSICS **148**, 134102 (2018)

A pair natural orbital based implementation of CCSD excitation energies within the framework of linear response theory

Marius S. Frank[a] and Christof Hättig[b]
Lehrstuhl für Theoretische Chemie, Ruhr-Universität Bochum, D-44801 Bochum, Germany

(Received 7 December 2017; accepted 13 March 2018; published online 3 April 2018)

We present a pair natural orbital (PNO)-based implementation of coupled cluster singles and doubles (CCSD) excitation energies that builds upon the previously proposed state-specific PNO approach to the excited state eigenvalue problem. We construct the excited state PNOs for each state separately in a truncated orbital specific virtual basis and use a local density-fitting approximation to achieve an at most quadratic scaling of the computational costs for the PNO construction. The earlier reported excited state PNO construction is generalized such that a smooth convergence of the results for charge transfer states is ensured for general coupled cluster methods. We investigate the accuracy of our implementation by applying it to a large and diverse test set comprising 153 singlet excitations in organic molecules. Already moderate PNO thresholds yield mean absolute errors below 0.01 eV. The performance of the implementation is investigated through the calculations on alkene chains and reveals an at most cubic cost-scaling for the CCSD iterations with the system size. *Published by AIP Publishing.* https://doi.org/10.1063/1.5018514

I. INTRODUCTION

One of the severe limitations for computational chemistry is the steep scaling of the required computational resources (i.e., time and memory demands) of accurate wavefunction-based methods with the system size $\mathcal{N}$. This unphysical behavior arises from the fact that the canonical molecular orbitals (MOs) are delocalized. The non-local MO basis makes it difficult to exploit that dynamic electron correlation is a local phenomenon and decays with the interelectronic distance R as R^{-6}.

Local correlation methods exploit the sparsity of electron correlation by neglecting excitations between spatially distant MOs. This is achieved by a transformation of the occupied orbitals to a localized MO (LMO) basis and by restricting excitations to a subspace of the full virtual space, i.e., to local correlation domains. Different local correlation methods mainly differ by the way the virtual subspaces are determined and represented. Pioneering work on these methods has been done by Saebø and Pulay[1–6] by introducing projected atomic orbitals (PAOs) as representation for the virtual space. Later, Werner, Schütz, and co-workers[7–12] implemented, refined, and extended these ideas to linear-scaling local coupled cluster (CC) methods implemented in the Molpro[13] package. An alternative approach to exploit the locality of electron correlation uses pair natural orbitals (PNOs) where each pair of occupied orbitals gets its own virtual space assigned which is truncated based on an analysis of approximate densities. The idea was already proposed and implemented in the 1970s by Meyer,[14–17] Ahlrichs,[18,19] Kutzelnigg,[18] and Staemmler and co-workers[18,20] but was then discontinued due to large computational demands for the transformation of two-electron integrals from the atomic orbital (AO) to the PNO basis. In 2008, Neese *et al.* realized that the aforementioned computational bottleneck can be circumvented by making use of the resolution-of-the-identity (RI) approximation[21,22] also known as density-fitting (DF). Combining the PNO and PAO approaches led Neese and co-workers to the development of improved linear scaling coupled cluster variants.[23–28]

Werner and co-workers[29] as well as Hättig and co-workers[30,31] proposed to use orbital specific virtuals[32] (OSVs) as an intermediate basis to reduce the computational costs for the construction of PNOs. An advantage of OSVs is that they share many properties with PNOs and can straightforwardly be generalized to different orbital spaces which is exploited in explicitly correlated F12 variants of PNO-MPn and PNO-CC methods.[30,33–35] This is also crucial for PNO-based coupled cluster response methods with state- or perturbation-specific PNOs and OSVs.[36–38]

The extension of PAO-based local correlation methods to excited states in the framework of response theory is not straightforward since excitation processes are usually delocalized over at least one chromophore. Describing ground and excited states with common domains for the virtual space would result in huge correlation domains that would need to contain local and non-local excitations (depending on the character of the excited states) and would grow in size with the number of states included. Apart from the CC2 method,[39,40] where an explicit treatment of the double excitation space can be avoided by partitioning techniques, the development of PAO-based response methods, e.g., coupled cluster singles and doubles (CCSD),[41,42] has been given up.

[a]Author to whom correspondence should be addressed: Marius.Frank@rub.de
[b]christof.haettig@rub.de

Dutta *et al.* recently presented an implementation[43] of equation of motion CCSD (EOM-CCSD) for excitation energies where domain-based local PNO-CCSD (DLPNO-CCSD) is used to solve the ground state amplitude equations with linear-scaling costs in the PNO basis and then the cluster amplitudes and other intermediates are back-transformed to the canonical virtual basis, the so-called back-transformed PNOs (bt-PNOs). The excited state problem is then solved in the canonical basis. This approach requires only minor modifications of an existing canonical code. On the other hand, it only reduces the prefactor of the computational costs but not the scaling with the system size. Combining the bt-PNO approach with similarity transformed EOM-CCSD (STEOM-CCSD) reduces the cost scaling but sacrifices important advantages of EOM-CCSD as, e.g., a qualitatively correct description of double excitations and its black-box character due to the introduction of an active space for single excitations.

Multilevel coupled cluster methods[44] also aim at a reduction of the prefactor of the computational costs. They divide the orbital space into active and inactive MOs which are treated at different levels of coupled cluster theory. Myhre and Koch[45] presented a multilevel CC3 model where CCSD is used for the inactive orbital space while the (smaller) active orbital space is treated at the computationally more demanding CC3 level. Even though this leads to a significant reduction of the prefactor of the computational costs, it does not reduce the steep scaling of the costs with the size of the chromophore and partially sacrifices the black-box character of the standard coupled-cluster methods.

Approaches to reduce the computational costs of coupled cluster response methods for excitation energy calculations that employ natural orbitals[46] and natural transition orbitals (NTOs)[47] either do not achieve the cost reductions and the compactness of the wavefunction parameters of PNO-based methods or only yield computational savings for local excitations which limits their applicability.

Hättig and Helmich,[36] in contrast, proposed to solve the eigenvalue problem for the excitation energies in a state-specific PNO basis to fully exploit the compactness of the parameter space that is achieved with PNOs in coupled cluster response calculations. In this approach, the excited state PNOs are generated separately for each excited state from densities calculated from configuration interaction singles with perturbative doubles [CIS(D)]-like doubles amplitudes. The number of amplitudes then scales linearly with the chromophore size and, equally important, the PNO truncation errors are small and decrease rapidly[36] for the perturbative CIS(D) method as well as for the iterative second order methods ADC(2) and CC2.[37] At the example of ADC(2)-x, it was furthermore shown that this strategy can straightforwardly be applied to higher-order methods with a non-diagonal doubles-doubles block of the Jacobian matrix. The most important feature of the state-specific PNO ansatz is that there are no conceptual limitations to achieve linear scaling operation counts and memory and disk space demands. In the present paper, we report the extension of this approach to the CCSD model including an analysis of the convergence of the PNO truncation errors with the occupation number threshold and demonstrate its computational efficiency compared to a canonical implementation.

II. THEORY AND IMPLEMENTATION

A. The coupled cluster singles and doubles model

In the following, we follow the notation introduced by Christiansen *et al.*[48] for the coupled cluster singles and doubles (CCSD) model[49–53] within the framework of linear response theory. In the CCSD model, the cluster operator is truncated after the double excitation operator T_2. This leads to the following cluster equations for the singles and doubles amplitudes:[54]

$$\Omega_{\mu_1} = \langle \mu_1 | \hat{H} + [\hat{H}, T_2] | \mathrm{HF} \rangle, \tag{1}$$

$$\Omega_{\mu_2} = \langle \mu_2 | \hat{H} + [\hat{H}, T_2] + \frac{1}{2}[[\hat{H}, T_2], T_2] | \mathrm{HF} \rangle, \tag{2}$$

where the T_1-similarity transformed Hamiltonian[54]

$$\hat{H} = e^{-T_1} H e^{T_1} = \sum_{pq} \hat{h}_{pq} E_{pq} + \sum_{pqrs} (pq\hat{|}rs) e_{pqrs}, \tag{3}$$

with $T_1 = \sum_{\mu_1} t_{\mu_1} \tau_{\mu_1}$ and $T_2 = \sum_{\mu_2} t_{\mu_2} \tau_{\mu_2}$, has been used. Here and in the following we present the equations for the closed-shell case and use the spin-free one- and two-electron operators E_{pq} and e_{pqrs} and the excitation operators $\tau_{ai} = E_{ai}$ and $\tau^{ij}_{ab} = E_{ai} E_{bj}$. Greek letters denote atomic orbitals (AOs), Latin letters denote molecular orbitals (MOs), and capital letters P, Q auxiliary functions. The indices μ_1 and μ_2 run over, respectively, all single and double replacements.

The T_1-transformed integrals $\hat{h}_{pq}$ and $(pq\hat{|}rs)$ can be evaluated from the respective AO integrals using $\mathbf{t}_1$-dressed particle and hole MO transformation matrices,[54]

$$\mathbf{\Lambda}^p = \mathbf{C} \left(\mathbf{1} - \mathbf{t}_1^T \right), \tag{4}$$

$$\mathbf{\Lambda}^h = \mathbf{C} \left(\mathbf{1} + \mathbf{t}_1 \right), \tag{5}$$

as

$$(pq\hat{|}rs) = \sum_{\mu\nu\kappa\lambda} \Lambda^p_{\mu p} \Lambda^p_{\nu r} \Lambda^h_{\kappa q} \Lambda^h_{\lambda s} (\mu\kappa|\nu\lambda). \tag{6}$$

The matrix $\mathbf{t}_1$ in the above equations is defined as[54]

$$\mathbf{t}_1 = \begin{pmatrix} 0 & 0 \\ \{t^i_a\} & 0 \end{pmatrix}. \tag{7}$$

In response theory, excitation energies are obtained as eigenvalues of the Jacobian,[55] which for CCSD is readily obtained from the cluster equations (1) and (2) as[48]

$$A_{\mu_i \nu_j} = \frac{\partial \Omega_{\mu_i}}{\partial t_{\nu_j}} = \begin{pmatrix} \langle \mu_1 | [\hat{H} + [\hat{H}, T_2], \tau_{\nu_1}] | \mathrm{HF} \rangle & \langle \mu_1 | [\hat{H}, \tau_{\nu_2}] | \mathrm{HF} \rangle \\ \langle \mu_2 | [\hat{H} + [\hat{H}, T_2], \tau_{\nu_1}] | \mathrm{HF} \rangle & \langle \mu_2 | [\hat{H} + [\hat{H}, T_2], \tau_{\nu_2}] | \mathrm{HF} \rangle \end{pmatrix}. \tag{8}$$

The eigenvalue problem is solved iteratively—usually using a block Davidson algorithm[56]—which requires an implementation of linear transformations of trial vectors with the Jacobian,

$$\rho_{\mu_i} = \sum_{\nu_j} A_{\mu_i\nu_j} R_{\nu_j}. \tag{9}$$

To obtain a compact notation for the transformed vectors ρ_{μ_i}, we introduce the operators $R_i = \sum_{\mu_i} R_{\mu_i} \tau_{\mu_i}$ and the R_1-dressed Hamiltonian

$$\bar{H} = \left[\hat{H}, R_1\right] = \sum_{pq} \bar{h}_{pq} E_{pq} + \sum_{pqrs} (pq|rs) e_{pqrs}, \tag{10}$$

with corresponding integrals

$$(pq|rs) = P^{pr}_{qs} \sum_{\mu\nu\kappa\lambda} \left(\bar{\Lambda}^p_{\mu p} \Lambda^h_{\nu q} + \Lambda^p_{\mu p} \bar{\Lambda}^h_{\nu q}\right) \Lambda^p_{\kappa r} \Lambda^h_{\lambda s} (\mu\nu|\kappa\lambda), \tag{11}$$

and modified particle/hole MO transformation matrices

$$\bar{\Lambda}^p_{\mu a} = -\sum_i R^i_a C_{\mu i}, \tag{12}$$

$$\bar{\Lambda}^h_{\mu i} = \sum_a R^i_a C_{\mu a}. \tag{13}$$

In Eq. (11), the symmetrization operator P^{qs}_{pr} is defined by $P^{qs}_{pr} f^{qs}_{pr} = f^{pr}_{qs} + f^{sq}_{rp}$. With this notation the transformed vectors ρ_{μ_i} can be written as

$$\rho_{\mu_1} = \langle \mu_1 | \bar{H} + [\bar{H}, T_2] + [\hat{H}, R_2] | \mathrm{HF} \rangle, \tag{14}$$

$$\rho_{\mu_2} = \langle \mu_2 | \bar{H} + [\bar{H}, T_2] + [\hat{H} + [\hat{H}, T_2], R_2] | \mathrm{HF} \rangle. \tag{15}$$

B. Ground and excited state PNOs

PNOs are defined as linear combinations of virtual orbitals

$$|\bar{a}_{ij}\rangle = \sum_a |a\rangle d^{ij}_{a\bar{a}}, \tag{16}$$

where the expansion coefficients are the elements of the eigenvectors of the contribution D^{ij}_{ab} of a LMO pair ij to a one-electron density matrix,

$$\sum_{ab} d^{ij}_{a\bar{a}} D^{ij}_{ab} d^{ij}_{b\bar{b}} = n^{ij}_{\bar{a}} \delta_{\bar{a}\bar{b}}. \tag{17}$$

Here and in the following, indices i, j, k, l denote occupied orbitals, a, b, c, d virtuals and PNOs and OSVs are denoted by, respectively, bar and tilde accents.

For the ground state, D^{ij}_{ab} are approximate MP2 densities calculated as

$$D^{ij}_{ab} = 2 \sum_c \left(\tilde{t}^{ij,(1)}_{ac} t^{ij,(1)}_{bc} + \tilde{t}^{ij,(1)}_{ca} t^{ij,(1)}_{cb}\right), \tag{18}$$

with $\tilde{t}^{ij,(1)}_{ab} = 2t^{ij,(1)}_{ab} - t^{ij,(1)}_{ba}$ and the first order amplitudes

$$t^{ij,(1)}_{ab} = \frac{(ai|bj)}{F_{ii} + F_{jj} - \epsilon_a - \epsilon_b}, \tag{19}$$

where F_{ii} are the diagonal Fock matrix elements in a localized molecular orbital (LMO) basis and ϵ_a are canonical orbital energies.

For excited state PNOs, the MP1 ground state amplitudes in Eq. (18) are replaced by first-order doubles amplitudes

$$R^{ij,(1)}_{ab} = \frac{(ai|\bar{b}j)}{F_{ii} + F_{jj} - \epsilon_a - \epsilon_b + \omega} \tag{20}$$

calculated in a CIS(D)-like way from the current guess for the excitation energy ω and the singles amplitudes via the R_1-transformed integrals $(ai|\bar{b}j)$. The pair density is then constructed analogously to the ground state as

$$D^{ij}_{ab} = 2 \sum_c \left(\tilde{R}^{ij,(1)}_{ac} R^{ij,(1)}_{bc} + \tilde{R}^{ij,(1)}_{ca} R^{ij,(1)}_{cb}\right), \tag{21}$$

with $\tilde{R}^{ij,(1)}_{ab} = 2R^{ij,(1)}_{ab} - R^{ij,(1)}_{ba}$. In addition, pairs for which the second-order correlation energy contribution evaluated with $t^{ij,(1)}_{ab}$ for the ground state and with $R^{ij,(1)}_{ab}$ for excited states is less than a pair energy threshold T_{pair} are discarded.

The construction of the pair densities has the complexity $\mathcal{O}(\mathcal{N}^5)$ if done for all pairs ij and in the full virtual basis. To reduce the complexity the pair densities are constructed in a preselected pair-specific semi-canonical pre-PNO basis $\{\tilde{a}_{ij}\}$ obtained by merging the OSV spaces for the LMOs i and j and then diagonalizing the Fock matrix in this space. The approximate doubles amplitudes for Eqs. (18) and (21) are then evaluated as

$$t^{ij,(1)}_{\tilde{a}_{ij}\tilde{b}_{ij}} = \frac{(\tilde{a}_{ij}i|\tilde{b}_{ij}j)}{F_{ii} + F_{jj} - \epsilon_{\tilde{a}_{ij}} - \epsilon_{\tilde{b}_{ij}}}, \tag{22}$$

$$R^{ij,(1)}_{\tilde{a}_{ij}\tilde{b}_{ij}} = \frac{(\tilde{a}_{ij}i|\bar{\tilde{b}}_{ij}j)}{F_{ii} + F_{jj} - \epsilon_{\tilde{a}_{ij}} - \epsilon_{\tilde{b}_{ij}} + \omega}, \tag{23}$$

where $\epsilon_{\tilde{a}_{ij}}$ are the eigenvalues of the Fock matrix in the pre-PNO basis.

In addition we pre-screen the list of pairs ij based on an estimate for the second-order pair contributions to the correlation energies for the ground $e^{(2)}_{ij}$ or the excited state $\omega^{(2)}_{ij}$ which is evaluated in the OSV basis,

$$e^{(2)}_{ij} = \sum_{\tilde{a}_i\tilde{b}_j} \frac{(\tilde{a}_i i|\tilde{b}_j j)^2}{F_{ii} + F_{jj} - \epsilon_{\tilde{a}_i} - \epsilon_{\tilde{b}_j}}, \tag{24}$$

$$\omega^{(2)}_{ij} = \sum_{\tilde{a}_i\tilde{b}_j} \frac{(\tilde{a}_i i|\bar{\tilde{b}}_j j)^2}{F_{ii} + F_{jj} - \epsilon_{\tilde{a}_i} - \epsilon_{\tilde{b}_j} + \omega}. \tag{25}$$

The ground state pairs with $e^{(2)}_{ij} < \frac{1}{3} T_{pair}$ and the excited state pairs with $\omega^{(2)}_{ij} < \frac{1}{3} T_{pair}$ are discarded. The factor $\frac{1}{3}$ ensures that in this step no pairs are discarded for which the more accurate pair correlation energy estimates obtained from $t^{ij,(1)}_{ab}$ for the ground state and from $R^{ij,(1)}_{ab}$ for excited states are above T_{pair}.

Combined with a local RI approximation this leads to a quadratic cost scaling of the PNO construction for ground and excited states.[31,37,57]

TABLE I. Explicit expressions for the contributions to the doubles result vector. ρ_{μ_2} is split into contributions as $\rho_{\mu_2} = \rho^A_{\mu_2} + \rho^B_{\mu_2} + \rho^C_{\mu_2} + \rho^D_{\mu_2} + \rho^E_{\mu_2} + \rho^F_{\mu_2}$ and P_{ij} is a permutation operator defined by $P_{ij} f_{ij} = f_{ji}$.

	Scaling	
Contribution	CCSD	PNO-CCSD
$\rho^{A,ij}_{\bar{a}\bar{b}} = \sum_{kl} \Gamma^{T_2+E,ij}_{kl} \sum_{\bar{a}'} S^{ij,kl}_{\bar{a}\bar{a}'} \sum_{\bar{b}'} S^{ij,kl}_{\bar{b}\bar{b}'} R^{kl}_{\bar{a}'\bar{b}'}$ $+ \sum_{kl} \Gamma^{R_2+\tilde{E},ij}_{kl} \sum_{\bar{a}^0} S^{ij,kl}_{\bar{a}\bar{a}^0} \sum_{\bar{b}^0} S^{ij,kl}_{\bar{b}\bar{b}^0} t^{kl}_{\bar{a}^0\bar{b}^0}$ $+ \sum_{kl} t^k_{\bar{a}} t^l_{\bar{b}} \sum_{\bar{c}\bar{d}} R^{ij}_{\bar{c}\bar{d}} \sum_{\bar{c}^0\bar{d}^0} S^{ij,kl}_{\bar{c}\bar{c}^0} K^{kl}_{\bar{c}^0\bar{d}^0} S^{kl,ij}_{\bar{d}^0\bar{d}}$	$\mathcal{O}(\mathcal{N}^6)$	$\mathcal{O}(\mathcal{N})$
$\rho^{B,ij}_{\bar{a}\bar{b}} = \sum_{\bar{c}\bar{d}} R^{ij}_{\bar{c}\bar{d}} (\bar{a}\bar{c}\vert\bar{b}\bar{d}) - P^{ij}_{\bar{a}\bar{b}} \sum_k t^k_{\bar{b}} \Omega^{B(R2),ij}_{\bar{a}k} - P^{ij}_{\bar{a}\bar{b}} \sum_k R^k_{\bar{a}} \Omega^{B(T2),ij}_{k\hat{b}}$	$\mathcal{O}(\mathcal{N}^4)$	$\mathcal{O}(\mathcal{N}^2)$
$\rho^{C,ij}_{\bar{a}\bar{b}} = -P^{ij}_{\bar{a}\bar{b}} \left(\frac{1}{2} + P_{ij}\right) \sum_k \sum_{\bar{c}} C^{ik}_{\bar{a}_{ij}\bar{c}_{kj}} \sum_{\bar{b}'} R^{jk}_{\bar{c}\bar{b}'} S^{jk,ij}_{\bar{b}'\bar{b}}$ $- P^{ij}_{\bar{a}\bar{b}} \left(\frac{1}{2} + P_{ij}\right) \sum_k \sum_{\bar{c}^0} \bar{C}^{ik}_{\bar{a}_{ij}\bar{c}^0_{kj}} \sum_{\bar{b}^0} t^{jk}_{\bar{c}^0\bar{b}^0} S^{jk,ij}_{\bar{b}^0\bar{b}}$	$\mathcal{O}(\mathcal{N}^6)$	$\mathcal{O}(\mathcal{N})$
$\rho^{D,ij}_{\bar{a}\bar{b}} = \frac{1}{2} P^{ij}_{\bar{a}\bar{b}} \sum_k \sum_{\bar{c}} D^{ik}_{\bar{a}_{ij}\bar{c}_{kj}} \sum_{\bar{b}'} \tilde{R}^{jk}_{\bar{c}\bar{b}'} S^{jk,ij}_{\bar{b}'\bar{b}}$ $+ \frac{1}{2} P^{ij}_{\bar{a}\bar{b}} \sum_k \sum_{\bar{c}^0} \bar{D}^{ik}_{\bar{a}_{ij}\bar{c}^0_{kj}} \sum_{\bar{b}^0} \tilde{t}^{jk}_{\bar{c}^0\bar{b}^0} S^{jk,ij}_{\bar{b}^0\bar{b}}$	$\mathcal{O}(\mathcal{N}^6)$	$\mathcal{O}(\mathcal{N})$
$\rho^{E,ij}_{\bar{a}\bar{b}} = P^{ij}_{\bar{a}\bar{b}} \sum_{\bar{c}} R^{ij}_{\bar{a}\bar{c}} \sum_b d^{ij}_{b\bar{b}} \sum_c E_{bc} d^{ij}_{c\bar{c}}$ $+ P^{ij}_{\bar{a}\bar{b}} \sum_{\bar{a}^0} S^{ij,ij}_{\bar{a}\bar{a}^0} \sum_{\bar{c}^0} t^{ij}_{\bar{a}^0\bar{c}^0} \sum_b d^{ij}_{b\bar{b}} \sum_c \bar{E}_{bc} d^{ij}_{c\bar{c}^0}$	$\mathcal{O}(\mathcal{N}^5)$	$\mathcal{O}(\mathcal{N}^3)$
$\rho^{F,ij}_{\bar{a}\bar{b}} = (\bar{a}i\vert\bar{b}j)$	$\mathcal{O}(\mathcal{N}^4)$	$\mathcal{O}(\mathcal{N})$

C. Implementation of transformations with the CCSD Jacobian in a PNO basis

For the transformations with the CCSD Jacobian, we follow a similar approach as proposed by Christiansen *et al.*,[48] i.e., we introduce global (t_{μ_i}-dependent) intermediates, which are only computed once after the ground state CC equations are converged, and local (R_{μ_i}-dependent) intermediates, which have to be computed for each trial vector. For an easier discussion, we split the doubles part of the transformed vector ρ_{μ_2} into contributions denoted by $\rho^A_{\mu_2}$, $\rho^B_{\mu_2}$, ..., $\rho^F_{\mu_2}$ (compare Table I).

To account for the different pair lists in ground and excited states and the state-specific PNOs, some of the t_{μ_i}-dependent intermediates become state specific and are recomputed for each state and whenever the excited state PNO basis is updated (*vide infra*). To distinguish between the different PNO basis sets we denote in the following ground state PNOs with $\bar{a}^0$ and excited state PNOs with $\bar{a}$.

The implementation of the CCSD ground state equations has been described in the context of PNO-CCSD[F12] in Ref. 34. The CCSD singles part of the transformed vectors is evaluated in the same way as for CC2. Therefore, we do not repeat the equations here but refer to Ref. 37 for further details. Table I summarizes how the contributions to the double excitation part of the transformed vectors ρ_{μ_2} are evaluated with state-specific PNOs. The intermediates used in Table I are defined in Tables III and IV in the Appendix. We follow a similar route as proposed by Neese and co-workers[23] for the residual of the ground state amplitude equations: The general strategy of the implementation is to pre-compute all integrals and intermediates for the Jacobian transformations which do not depend on R_{μ_i} prior to the Davidson procedure. Depending on the intermediates this is done for the ground or the excited state PNO basis and/or the respective pair lists. Some intermediates, as, e.g., the overlap matrices $S^{ij,kl}_{\bar{c}\bar{c}^0}$ and the intermediates $\bar{C}^{ik}$ and $\bar{D}^{ik}$ for the ring terms, are needed with some indices in the ground and some indices in the excited state PNO basis and for a combination of the respective pair lists. During the evaluation of the result vector ρ_{μ_2}, the amplitudes and intermediates are in some places projected from the PNO space of a pair ij to the PNO space of a pair kl using the PNO overlap matrices $S^{ij,kl}_{\bar{a}_{ij}\bar{b}_{kl}}$ or the respective matrices between ground and excited state PNOs.

As indicated in Table I, all steps which in a canonical implementation have operation counts scaling with $\mathcal{O}(\mathcal{N}^6)$ (the contributions $\rho^A_{\mu_2}$, $\rho^C_{\mu_2}$, and $\rho^D_{\mu_2}$) have in the PNO-based implementation a linear cost scaling. We currently still accept a cubic cost-scaling for the transformation of E_{bc} and $\bar{E}_{bc}$ from the full virtual basis to the PNO basis since this step has a very small prefactor and does not yet contribute significantly

to the overall wall time. The computation of the $\bar{E}$ intermediates themselves (see Table III) in each iteration also scales as $\mathcal{O}\left(\mathcal{N}^3\right)$ but again with a small prefactor. For large-scale calculations, the $\mathcal{O}\left(\mathcal{N}^3\right)$-scaling transformations of the Coulomb and exchange integrals $(ik|l\bar{c}_{kj}) = \sum_\mu d^{kj}_{\mu\bar{c}_{kj}}(ik|l\mu)$ and $(il|k\bar{c}_{kj}) = \sum_\mu d^{kj}_{\mu\bar{c}_{kj}}(il|k\mu)$ from the AO the PNO basis dominate in the current implementation the overall costs during the iterations.

The calculation of the state-specific two-electron integrals $(\bar{a}\bar{c}|\bar{b}\bar{d})$ currently scales quadratically with the system size due to the calculation of $(Q|\mu\nu)$ in the full auxiliary basis $\{Q\}$. But also this step has a very small prefactor. The calculation of the 3-index PNO integrals $(Q|\bar{a}\bar{c})$, their density fitting, and the final contractions to $(\bar{a}\bar{c}|\bar{b}\bar{d})$ are done in a pair-specific auxiliary basis. These steps are linear scaling but have a large prefactor and currently dominate together with the computation of $W^{ij}_{Q\bar{d}^0\bar{a}}$ for small to medium sized systems the costs for the calculation of the state-specific intermediates after each PNO reconstruction. For larger systems, the computation of $(Q_{ij}|k\bar{d}^0_{ij}) = \sum_\mu (Q_{ij}|\mu\bar{d}^0_{ij})C_{\mu k}$ becomes dominant due to its $\mathcal{O}\left(\mathcal{N}^3\right)$ scaling. This is then the computationally most demanding contribution to the B terms $\rho^B_{\mu_2}$. But it should be mentioned that these integrals only need to be computed once as global intermediates since they do not depend on any excited state quantities in contrast to the $\mathcal{O}\left(\mathcal{N}^2\right)$ scaling intermediate $W^{ij}_{Q\bar{d}^0\bar{a}}$. The time-determining steps for large-scale applications are in our current implementation the generation of some t_1- and R_1-dressed integrals for the ring terms, $\rho^C_{\mu_2}$, $\rho^D_{\mu_2}$, and $\rho^B_{\mu_2}$. The computation of all other global, local, and state-specific intermediates for the Jacobian transformations scales at most quadratically with the system size.

D. Solution of the eigenvalue problem in a PNO basis

For the solution of the eigenvalue problem, we use a single-state solver which determines the eigenvalues and eigenvectors of only one state at a time.[37] Because the space spanned by the excited state doubles amplitudes and thus the respective PNOs depend on the excited state singles amplitudes which are not known prior to solving the eigenvalue problem, we determine the PNOs in a self-consistent manner while solving the eigenvalue problem. Whenever the overlap $s = R^{(0)}_{\mu_1} R_{\mu_1} / (||R_{\mu_1}|| \cdot ||R^{(0)}_{\mu_1}||)$ between the singles part of the start vector $R^{(0)}_{\mu_1}$ for which the PNOs were constructed and the current singles guess R_{μ_1} significantly deviates from 1 so that

$$1 - s \geq 10 \cdot ||\sigma|| \tag{26}$$

is no longer fulfilled (where σ denotes the residual vector of the eigenvalue problem), updated PNOs are generated and the Davidson procedure is restarted.

To obtain a suitable start guess for the doubles part of the eigenvector in the new PNO basis, the solution vector from the previous iteration is projected onto the new PNO basis. To enhance the convergence rate and minimize the number of PNO reconstructions for PNO-CCSD, a PNO-ADC(2) calculation followed by the perturbative correction PNO-ADC(2)-(D)[38] is carried out prior to the PNO-CCSD calculation. The PNO-ADC(2) eigenvectors are then resorted according to the PNO-ADC(2)-(D)[38] excitation energies and used as start for the PNO-CCSD excitation energy calculation.

III. COMPUTATIONAL DETAILS

The calculation of PNO-CCSD excitation energies has been implemented in a development version of the pnoccsd program[31,34] of the TURBOMOLE package.[58] Hartree-Fock calculations have been carried out with the dscf program,[59] density functional theory (DFT)[60,61] geometry optimizations with ridft,[62–66] and canonical CCSD reference calculations with the ccsdf12 program of TURBOMOLE. For the DFT geometry optimizations of the alkene chains (see Sec. IV C), we have used the B3LYP functional,[67–71] the def2-TZVP orbital basis set,[72] and the corresponding auxiliary basis for the RI approximation of Coulomb integrals[73] (RI-J approximation). Test calculations have been done using the def2-TZVP,[72] cc-pVDZ,[74] and d-aug-cc-pVDZ[75] orbital basis sets. If not explicitly mentioned, the corresponding standard auxiliary basis sets[76,77] for the RI approximation of two electron integrals have been used in post-HF calculations. The occupied orbital basis has either been localized using Pipek-Mezey[78] localization or intrinsic bond orbitals (IBOs)[79] (*vide infra*). Furthermore, we used the frozen core approximation with the 1*s* orbitals of second row atoms excluded from the correlation treatment.

The thresholds for the pair correlation energy, T_{pair}, and the truncation of the OSV basis, T_{OSV}, are coupled to the PNO truncation threshold, T_{PNO}, as $T_{pair} = (0.1 \cdot T_{\mathrm{PNO}})^{2/3}$ and $T_{\mathrm{OSV}} = 0.1 \cdot T_{\mathrm{PNO}}$. In all calculations we use identical truncation thresholds for the ground and the excited states.

IV. RESULTS

A. Accuracy of PNO-CCSD

To investigate the accuracy of PNO-CCSD with respect to canonical CCSD we use the test set developed by Schreiber *et al.* in Ref. 80. It comprises 153 vertical singlet excitations in 28 organic molecules. The structures were taken from the supplementary material of Ref. 80.

The errors introduced by the PNO approximation were evaluated with respect to canonical CCSD as it is implemented in the ccsdf12 program in TURBOMOLE, where 4-index electron repulsion integrals are used for the ladder terms ($\rho^A_{\mu_2}$, $\rho^B_{\mu_2}$) and $\rho^F_{\mu_2}$ and the intermediates E_{ki} and $\bar{E}_{ki}$ and the RI approximation is used for all remaining electron repulsion integrals. Test calculations showed that the deviations due to the different use of the RI approximation in the PNO-based and the canonical implementation are in the order of 10^{-3} – 10^{-4} eV and thus irrelevant for practical purposes.

TABLE II. Statistical measures for the errors in PNO-CCSD excitation energies in the def2-TZVP basis. The abbreviations ME, MAE, and MAX stand for mean error, mean absolute error, and maximum error, respectively, and σ denotes the standard deviation with respect to the ME.

	ME	MAE	MAX	σ
$T_{\text{PNO}} = 10^{-6}$	0.040	0.041	0.089	0.022
$T_{\text{PNO}} = 10^{-7}$	0.007	0.008	0.033	0.008
$T_{\text{PNO}} = 10^{-8}$	−0.002	0.003	0.011	0.003

Table II and Fig. 1 summarize the results obtained from a statistical analysis of the PNO truncation error for the CCSD excitation energies. All statistical measures decrease monotonically with the PNO threshold. The mean errors (ME) reveal that loose and moderate PNO thresholds ($T_{\text{PNO}} = 10^{-6}, 10^{-7}$) tend to slightly overestimate the excitation energies. Already with the moderate PNO threshold $T_{\text{PNO}} = 10^{-7}$ the mean absolute error (MAE) drops below 0.01 eV which is a promising result for a future implementation of PNO excitation energies for methods including connected triple excitations where such an accuracy is required to maintain the intrinsic accuracy of these methods.

Figure 2 compares mean absolute and maximum PNO truncation errors of PNO-CCSD to those for PNO-CC2 and PNO-ADC(2)-x. The latter were taken from Refs. 37 and 38. The comparison shows that both statistical measures are for PNO-ADC(2)-x much larger than for PNO-CC2 and PNO-CCSD; only for the loose threshold $T_{\text{PNO}} = 10^{-6}$ the MAE for PNO-CCSD and PNO-ADC(2)-x are close. In general, we observe that the PNO truncation errors for PNO-CCSD are only by a factor of two larger than for PNO-CC2 and that the convergence to the canonical results is for both methods almost identical. The fact that the errors for PNO-ADC(2)-x are substantially larger than for PNO-ADC(2) or PNO-CC2 has already been observed previously.[38] In Ref. 38, it was argued that this is caused by an unbalanced treatment of correlation effects from the ground and excited state wavefunctions

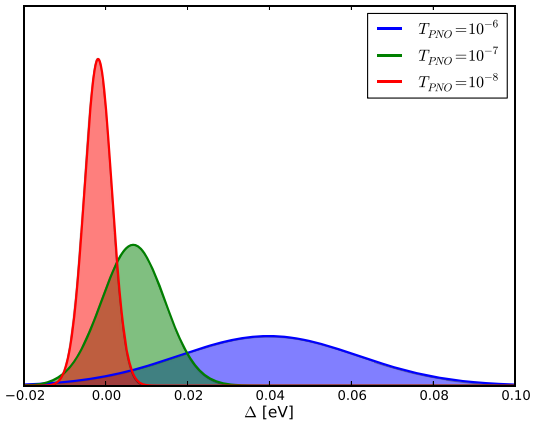


FIG. 1. Normal distributions of PNO errors in excitation energies from the test set of Schreiber *et al.*[80] (def2-TZVP basis).

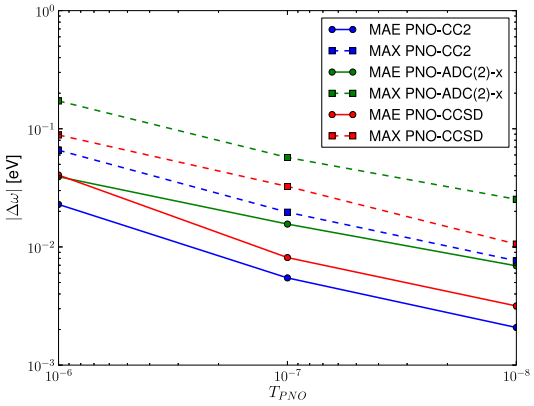


FIG. 2. Comparison of mean absolute and maximum errors of PNO-CC2, PNO-ADC(2)-x, and PNO-CCSD in the def2-TZVP basis.

on the excitation energies in the PNO-ADC(2)-x method. ADC(2)-x includes in the secular matrix $\langle\mu_2|[H,\tau_{\nu_2}]|\text{HF}\rangle$, which accounts for correlation effects from the excited state wavefunction on the excitation energy, but neglects its counterpart $\langle\mu_2|[[H,T_2],\tau_{\nu_1}]|\text{HF}\rangle$, which accounts for similar correlation effects from the ground state wavefunction on the excitation energy. Including only one of the two terms destroys an error balance between them which is reestablished at the PNO-CCSD level when both terms are included. As shown in Ref. 38, the unbalanced treatment of ground and excited state correlation effects in ADC(2)-x is also the source for the sizeable systematic red shift of ADC(2)-x excitation energies.

B. Charge transfer and Rydberg excitations

Charge transfer (CT) excitations are a challenge for local correlation methods since these excitations are not only by definition non-local but pose for PNO-based methods in addition the problem that due to a very low rank of R_{μ_1} the PNO basis obtained from the non-negligible eigenpairs of the density in Eq. (21) is very small and thus inflexible.[37] For long range CT states, R_{μ_1} has usually only a rank of 1 so that

$$R_a^i \approx \beta_{a\sigma^v}\beta_{i\sigma^o}, \tag{27}$$

where $\beta_{i\sigma^o}$ are the coefficients of the occupied natural transition orbital (NTO) and $\beta_{a\sigma^v}$ are the coefficients of the virtual NTO. The R_1-dressed integrals $(ai|\bar{bj})$ from which the doubles amplitudes and the densities for the PNO construction are evaluated become in this case

$$(ai|\bar{bj}) \approx P_{ab}^{ij}[\beta_{i\sigma^o}(a\sigma^v|bj) - \beta_{a\sigma^v}(\sigma^o i|bj)]. \tag{28}$$

They are non-negligible for only two kinds of pairs ij: Those where i is close to the occupied NTO and j is close to the virtual NTO or vice versa and those pairs where both i and j are close to the occupied NTO. The contribution $P_{ab}^{ij}\beta_{i\sigma^o}(a\sigma^v|bj)$ has a rank which can be as large as the number of virtuals (rank-V) in the electron acceptor chromophore but only contributes if one LMO is close to the virtual NTO and the other LMO is close to the occupied NTO. The contribution

$P^{ij}_{ab}\beta_{a\sigma^v}(\sigma^o i|bj)$ is of rank 1 and only non-negligible if both LMOs are close to the occupied NTO. If occupied and virtual NTOs are localized in the same chromophore, both terms contribute for all pairs close to this chromophore. For CT states where the virtual and the occupied NTO are spatially separated, in contrast, only rank-1 terms contribute to $(ai|bj)$ if both LMOs are close to the occupied NTO. For such rank-1 pairs, $(ai|bj)$ has only two non-negligible singular vectors and, hence, decreasing the PNO threshold will not enlarge the PNO basis for these pairs. To prevent that this effect limits the accuracy of PNO-based response calculations it is for the second-order methods CIS(D), ADC(2), and CC2 sufficient to ensure that the amplitudes, from which the density in Eq. (21) is computed, can converge to the correct limit which can be implemented, e.g., using a numerical Laplace transformation of the orbital energy denominators to avoid the neglect of off-diagonal elements of the Fock matrix.[37] For higher-order methods with a more complex doubles-doubles block of the secular matrix, it is, however, no longer feasible to ensure this convergence.

To investigate this problem at the PNO-CCSD level we chose the two lowest $\pi\pi^*$ CT states in the $C_2H_4\cdots C_2F_4$ model system in the cc-pVDZ basis and compared the convergence of the excitation energies with the PNO threshold with that for the two lowest lying local $\pi\pi^*$ excitations (LE). For these calculations, we used the large aug-cc-pVQZ auxiliary basis[76] to exclude that the analysis of the errors is affected by deviations from the different use of the RI approximation in the PNO and the canonical code. The black colored graphs in Fig. 3 show the results obtained for PNO-CCSD using the Laplace transformation (as implemented for PNO-CC2) for rank-1 pairs. Apparently, the LE states show errors and a convergence behavior very similar to the one observed for the Schreiber test set. For the $\pi_{C_2H_4} \rightarrow \pi^*_{C_2F_4}$ CT transition, the PNO truncation error decays similarly fast as for the LE states. For the $\pi_{C_2F_4} \rightarrow \pi^*_{C_2H_4}$ CT transition, the PNO truncation errors are significantly larger than for the other states and the convergence is much slower. That the results for the $\pi_{C_2F_4} \rightarrow \pi^*_{C_2H_4}$ transition are more sensitive to the PNO construction for the rank-1 pairs than the results for the other CT transition is due to the fact that for this transition the occupied NTO is located at C_2F_4 which has far more LMOs than C_2H_4 and, hence, the number of rank-1 pairs is much larger than for the $\pi_{C_2H_4} \rightarrow \pi^*_{C_2F_4}$ transition.

The red colored graphs in Fig. 3 show the results obtained using for rank-1 pairs the pre-PNO basis without further truncation of the virtual space, i.e., using for these pairs the pre-PNO basis as PNO basis.

That the error for the $\pi_{C_2H_4} \rightarrow \pi^*_{C_2F_4}$ transition is exceptionally small for $T_{\mathrm{PNO}} = 10^{-7}$ but for $T_{\mathrm{PNO}} = 10^{-8}$ again of the same order of magnitude as for the $\pi_{C_2H_4} \rightarrow \pi^*_{C_2F_4}$ transition is due to a fortunate error cancellation for this particular state and threshold. Figure 3 shows that the accuracy of the LE states is not affected by using the pre-PNOs without further truncation (due to the absence of rank-1 pairs). For both CT states, the errors are significantly reduced and decay rapidly.

We also investigated the accuracy of the excited state PNO construction for Rydberg states, which is a second class of non-local transitions where the occupied and virtual NTOs are located in different regions of space. As show case we chose the lowest lying Rydberg state (1^1A) of 1,1,2-trifluoro-1-hexene in the d-aug-cc-pVDZ[75] basis. For the occupied orbitals, we used IBOs. The red colored graph in Fig. 4 shows the errors obtained when using for rank-1 pairs the pre-PNO basis without further truncation as described above and the black colored graph shows the MAE obtained for Schreiber's test set (compare Sec. IV A and Table II). The convergence behavior for the Rydberg state is essentially the same as for CT states: If for rank-1 pairs the pre-PNO basis is used without further truncations, the PNO truncation errors decrease fast with T_{PNO}.

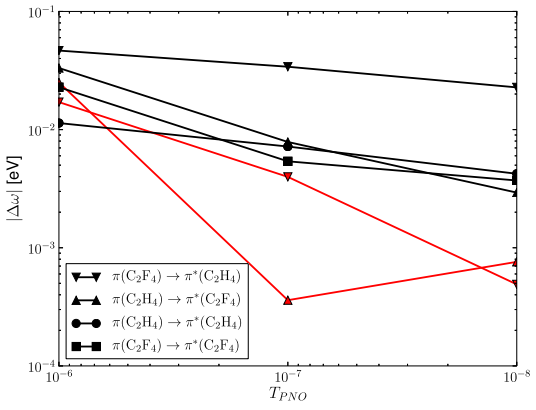


FIG. 3. Absolute errors in CT and LE states of $C_2H_4\cdots C_2F_4$ in the cc-pVDZ basis. The black lines show the results obtained with the PNO construction proposed in Ref. 37 for second-order methods. The red lines show the absolute error obtained by keeping for rank-1 pairs the pre-PNO basis without further truncation. For the LE states, there are no red lines visible since these are congruent with the black lines (due to the absence of rank-1 pairs).

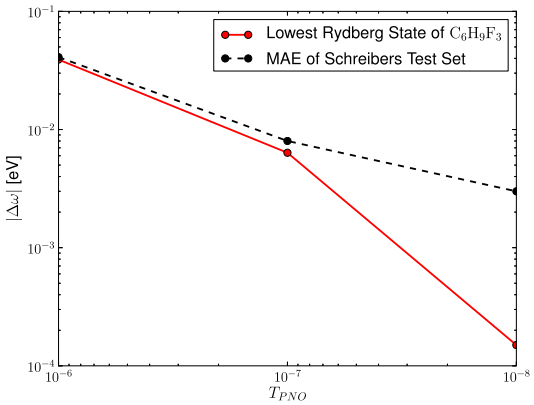


FIG. 4. Absolute errors of the first Rydberg state (1^1A) of 1,1,2-trifluoro-1-hexene in the d-aug-cc-pVDZ basis compared to the MAE obtained for Schreiber's test set (see Sec. IV A).

The results suggest that for rank-1 pairs the pre-PNO basis presents a simple and efficient possibility to obtain a PNO space which is flexible enough to allow for a reliable and rapid convergence of the PNO truncation errors in excitation energy calculations with higher-order methods. The identification of the rank-1 pairs is a simple and cheap black-box procedure described in Ref. 37. It should at this point be stressed that already the number of pre-PNOs scales linearly with the chromophore size. Hence, using for rank-1 pairs the pre-PNO basis without further truncation does not affect the scaling of the computational costs and increases the prefactor only insignificantly.

C. Performance of the implementation

To investigate the performance of the PNO-CCSD implementation for excitation energies we carried out calculations on alkene chains in the def2-TZVP basis set using IBOs for the occupied space. Figure 5 shows the wall times obtained for thread-parallel calculations on a machine with 2 Intel Xeon E5-2609 8-Core CPUs for the well-parallelized canonical CCSD code and the yet only partially parallelized PNO-CCSD implementation.

The Jacobian transformations for canonical CCSD scale for the largest systems as $\mathcal{O}\left(\mathcal{N}^{5.59}\right)$ with the chain size. In the PNO-CCSD implementation, the scaling is reduced to $\mathcal{O}\left(\mathcal{N}^{2.87}\right)$ (obtained from the last two points shown in Fig. 5). The time-determining steps in both the canonical and the PNO-CCSD calculations arise from the same terms but for different reasons: For canonical CCSD calculations on small- to medium-sized molecules, the calculation of the B term $\rho^{B}_{\mu_2}$ represents the time-determining step, while for larger systems this term becomes negligible compared to the ring terms C and D ($\rho^{C}_{\mu_2}$, $\rho^{D}_{\mu_2}$) due to an asymptotic $\mathcal{O}\left(\mathcal{N}^{4}\right)$-scaling for the contraction $\sum_{\mu\nu} t^{ij}_{\mu\nu}(\mu\kappa|\nu\lambda)$ which is evaluated in the AO basis. For large calculations, the strictly $\mathcal{O}\left(\mathcal{N}^{6}\right)$-scaling C and D terms become time-determining. For PNO-CCSD, the evaluation of the B terms also has a large prefactor and is time-determining for medium-sized molecules but these contributions soon become linear and quadratic scaling since they are rather short-ranged.[81] For larger systems, the time-determining step in our current PNO-CCSD implementation is the evaluation of the R_1-dressed integral matrices $\mathbf{J}^{R1o}$ and $\mathbf{L}^{R1o}$ in the PNO basis (compare Table III in the Appendix) which has a cubic cost-scaling. For example, for $C_{48}H_{50}$, about 50% of the wall time is spent for the calculation of these integrals. But still, the PNO-CCSD implementation performs impressingly well even when taking the computational costs for the PNO reconstruction and the recalculation of the state-specific intermediates into account. For example, for $C_{32}H_{34}$, the PNO-CCSD excitation energy calculation was completed before a single canonical CCSD ground state iteration was finished.

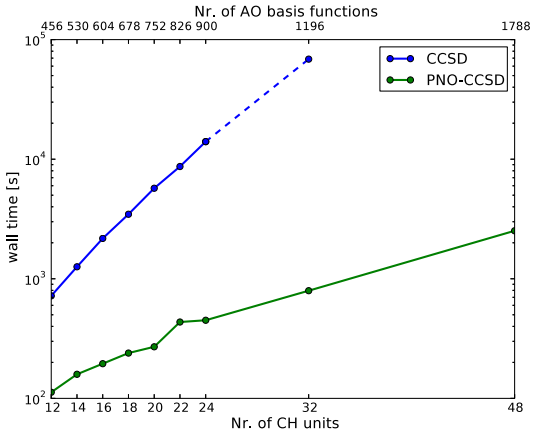


FIG. 5. Wall-time of a single Jacobian transformation for canonical and PNO-CCSD for alkene chains C_nH_{n+2} in the def2-TZVP basis. The calculations have been done Open-MP parallel on 2 Intel Xeon E5-2609 8-Core CPUs (1.7 GHz) and 64 GB of Ram. For the PNO-CCSD calculations, a PNO threshold of 10^{-7} has been used. The dashed line for canonical CCSD was obtained by an extrapolation according to the power law $4.4 \cdot 10^{-13} \cdot \mathcal{N}_{bf}^{5.59}$, where $\mathcal{N}_{bf}$ denotes the number of basis functions (for details see text).

V. SUMMARY AND CONCLUSIONS

We presented an efficient and accurate implementation of PNO-CCSD for the calculation of vertical excitation energies. Using state-specific PNOs to solve the excited state eigenvalue problem it could be demonstrated that the wall time for the Jacobian transformations scales at most cubically with the chromophore size and that PNO-CCSD outperforms canonical CCSD even for small molecular systems. For long-range charge transfer states, a smooth convergence with T_{PNO} is ensured by using for the problematic rank-1 pairs the pre-PNO basis, which is obtained from merging the OSVs of the respective LMOs without further truncation. This does not affect the scaling of the computational costs with the system size since already the pre-PNO basis scales linearly with the chromophore size.

We find a fast decay of the PNO truncation errors with the cutoff threshold. Already with a moderate threshold of $T_{\mathrm{PNO}} = 10^{-7}$ the mean absolute error in the excitation energies for a test set of 153 singlet excitations in 28 organic molecules decayed blow 0.01 eV. These are much smaller errors than observed previously for PNO-ADC(2)-x, for which apparently the unbalanced treatment of correlation effects from the ground and the excited state wavefunction retards the convergence with the PNO cutoff threshold.

These findings are encouraging for a future development of PNO-based iterative and perturbative triples methods such as CC3[82,83] and CCSDR(T) or CCSDR(3)[84] for highly accurate excitation energies which require PNO truncation errors of less than 0.01 eV to exploit the full accuracy of these methods.

ACKNOWLEDGMENTS

This work has been supported by the Deutsche Forschungsgemeinschaft (DFG) under Grant No. HA 2588/7.

APPENDIX: DEFINITION OF INTERMEDIATES FOR THE PNO-CCSD JACOBIAN RIGHT TRANSFORMATION

TABLE III. Global and local intermediates needed for the CCSD Jacobian right transformation. For ease of notation, the short-hand notation $L^{pq}_{rs} = 2(pr|qs) - (pq|rs)$ is used.

Global	Local
$E_{ki} = \hat{F}_{ki} + \sum_{j\bar{a}^0\bar{b}^0} \tilde{t}^{ij}_{\bar{a}^0\bar{b}^0} \sum_{\bar{c}^0\bar{d}^0} S^{ij,jk}_{\bar{b}^0\bar{c}^0} (\bar{c}^0 j|\bar{d}^0 k) S^{jk,ij}_{\bar{d}^0\bar{a}^0}$	$\bar{E}_{ki} = \bar{F}_{ki} + \sum_{j\bar{a}\bar{b}} \bar{R}^{ij}_{\bar{a}\bar{b}} \sum_{\bar{c}^0\bar{d}^0} S^{ij,jk}_{\bar{b}\bar{c}^0} (\bar{c}^0 j|\bar{d}^0 k) S^{jk,ij}_{\bar{d}^0\bar{a}}$
	$\bar{F}_{ki} = \sum_{c} \hat{F}_{kc} R^i_c + \sum_{\mu\nu} \Lambda^p_{\mu k} \Lambda^h_{\nu i} \tilde{F}_{\mu\nu}$
$E_{bc} = \hat{F}_{bc} - \sum_{ij\bar{b}^0} d^{ij}_{b\bar{b}^0} \sum_{\bar{a}^0} \tilde{t}^{ij}_{\bar{b}^0\bar{a}^0} \sum_{\bar{c}^0} K^{kj}_{\bar{a}^0\bar{c}^0} d^{ij}_{c\bar{c}^0}$	$\bar{E}_{bc} = \bar{F}_{bc} - \sum_{ij\bar{b}} d^{ij}_{b\bar{b}} \sum_{\bar{c}^0} d^{kj}_{c\bar{c}^0} \sum_{\bar{a}} \bar{R}^{ij}_{\bar{b}\bar{a}} \sum_{\bar{a}^0} K^{kj}_{\bar{a}^0\bar{c}^0} S^{kj,ij}_{\bar{a}^0\bar{a}}$
	$\bar{F}_{bc} = -\sum_{j} R_{bj} \hat{F}_{jc} + \sum_{\mu\nu} \tilde{F}_{\mu\nu} \Lambda^p_{\mu b} \Lambda^h_{\nu c}$
	$\tilde{F}_{\mu\nu} = \sum_{dl} [2(\mu\nu|ld) - (\mu d|l\nu)] R_{dl}$
$\Gamma^{T_2,+E,ij}_{kl} = (ik\hat{\|}jl) - \delta_{ki} E_{lj} - \delta_{lj} E_{ki} + \sum_{\bar{c}^0\bar{a}^0} t^{ij}_{\bar{c}^0\bar{a}^0} \sum_{\bar{c}'^0\bar{a}'^0} S^{ij,kl}_{\bar{c}^0\bar{c}'^0} (\bar{c}'^0 k|\bar{a}'^0 l) S^{kl,ij}_{\bar{a}'^0\bar{a}^0}$	$\Gamma^{R_2,+\bar{E},ij}_{kl} = (ik\bar{\|}jl) - \delta_{ki}\bar{E}_{lj} - \delta_{lj}\bar{E}_{ki} + \sum_{\bar{c}\bar{d}} \bar{R}^{ij}_{\bar{c}\bar{d}} \sum_{\bar{c}'^0\bar{a}'^0} S^{ij,kl}_{\bar{c}\bar{c}'^0} (\bar{c}'^0 k|\bar{a}'^0 l) S^{kl,ij}_{\bar{a}'^0\bar{a}}$
	$\bar{C}_{\bar{a}_{ij}\bar{c}^0_{kj}} = J^{R1o,ik}_{\bar{a}_{ij}\bar{c}^0_{kj}} + \sum_{\bar{a}'\bar{c}'} S^{ij,ki}_{\bar{a}_{ij}\bar{a}'_{ik}} C^{R2,ik}_{\bar{a}'_{ik}\bar{c}'_{ik}} S^{ki,kj}_{\bar{c}'_{ik}\bar{c}^0_{kj}}$
	$\bar{D}_{\bar{a}_{ij}\bar{c}^0_{kj}} = L^{R1o,ik}_{\bar{a}_{ij}\bar{c}^0_{kj}} + \sum_{\bar{a}'\bar{c}'} S^{ij,ki}_{\bar{a}_{ij}\bar{a}'_{ik}} D^{R2,ik}_{\bar{a}'_{ik}\bar{c}'_{ik}} S^{ki,kj}_{\bar{c}'_{ik}\bar{c}^0_{kj}}$
$C^{T2,ik}_{\bar{a}^0_{ik}\bar{c}^0_{ik}} = -\frac{1}{2} \sum_{l\bar{a}^0_{li}\bar{d}^0_{li}} (\bar{c}^0_{ki} l|\bar{d}^0_{li} k) \left(t^{li}_{\bar{a}^0_{li}\bar{d}^0_{li}} + 2 t^l_{\bar{a}^0_{li}} t^i_{\bar{d}^0_{li}} \right) S^{li,ik}_{\bar{a}^0_{li}\bar{a}^0_{ik}} + J^{T1v,ik}_{\bar{a}^0_{ik}\bar{c}^0_{ik}}$	$C^{R2,ik}_{\bar{a}_{ik}\bar{c}_{ik}} = -\frac{1}{2} \sum_{l\bar{a}_{li}\bar{d}_{li}} (\bar{c}_{ki} l|\bar{d}_{li} k) \left(R^{li}_{\bar{a}_{li}\bar{d}_{li}} + 2 R^l_{\bar{a}_{li}} t^i_{\bar{d}_{li}} + 2 t^l_{\bar{a}_{li}} R^i_{\bar{d}_{li}} \right) S^{li,ik}_{\bar{a}^0_{li}\bar{a}_{ik}} + J^{R1v,ik}_{\bar{a}_{ik}\bar{c}_{ik}}$
$D^{T2,ik}_{\bar{a}^0_{ik}\bar{c}^0_{ik}} = \frac{1}{2} \sum_{l\bar{a}^0_{li}\bar{d}^0_{li}} L^{k\bar{d}^0_{li}}_{\bar{c}^0_{ki} l} \left(t^{li}_{\bar{a}^0_{li}\bar{d}^0_{li}} - 2 t^l_{\bar{a}^0_{li}} t^i_{\bar{d}^0_{li}} \right) S^{li,ik}_{\bar{a}^0_{li}\bar{a}^0_{ik}} + L^{T1v,ik}_{\bar{a}^0_{ik}\bar{c}^0_{ik}}$	$D^{R2,ik}_{\bar{a}_{ik}\bar{c}_{ik}} = \frac{1}{2} \sum_{l\bar{a}_{li}\bar{d}_{li}} L^{k\bar{d}_{li}}_{\bar{c}_{ki} l} \left(R^{li}_{\bar{a}_{li}\bar{d}_{li}} - 2 R^l_{\bar{a}_{li}} t^i_{\bar{d}_{li}} - 2 t^l_{\bar{a}_{li}} R^i_{\bar{d}_{li}} \right) S^{li,ik}_{\bar{a}^0_{li}\bar{a}_{ik}} + L^{R1v,ik}_{\bar{a}_{ik}\bar{c}_{ik}}$
	$J^{R1o,ik}_{\bar{a}_{ij}\bar{c}^0_{kj}} = -\sum_{l} R^l_{\bar{a}_{ij}} \sum_{\mu} d^{kj}_{\mu\bar{c}^0_{kj}} (ik|l\mu)$
	$L^{R1o,ik}_{\bar{a}_{ij}\bar{c}^0_{kj}} = -2 \sum_{l} R^l_{\bar{a}_{ij}} \sum_{\mu} d^{kj}_{\mu\bar{c}^0_{kj}} (il|k\mu) - J^{R1o,ik}_{\bar{a}_{ij}\bar{c}^0_{kj}}$
$J^{T1v,ik}_{\bar{a}^0_{ik}\bar{c}^0_{ik}} = \sum_{\bar{d}^0_{ik}} (i\bar{d}^0_{ik}|\bar{a}^0_{ik}\bar{c}^0_{ik}) \sum_{d} d^{ik}_{d\bar{d}^0_{ik}} t^k_d$	$J^{R1v,ik}_{\bar{a}_{ik}\bar{c}_{ik}} = \sum_{\bar{d}_{ik}} (i\bar{d}_{ik}|\bar{a}_{ik}\bar{c}_{ik}) \sum_{d} d^{ik}_{d\bar{d}_{ik}} R^k_d$
$L^{T1v,ik}_{\bar{a}^0_{ik}\bar{c}^0_{ik}} = 2 \sum_{\bar{d}^0_{ik}} (i\bar{a}^0_{ik}|\bar{d}^0_{ik}\bar{c}^0_{ik}) \sum_{d} d^{ik}_{d\bar{d}^0_{ik}} t^k_d - J^{T1v,ik}_{\bar{a}^0_{ik}\bar{c}^0_{ik}}$	$L^{R1v,ik}_{\bar{a}_{ik}\bar{c}_{ik}} = 2 \sum_{\bar{d}_{ik}} (i\bar{a}_{ik}|\bar{d}_{ik}\bar{c}_{ik}) \sum_{d} d^{ik}_{d\bar{d}_{ik}} R^k_d - J^{R1v,ik}_{\bar{a}_{ik}\bar{c}_{ik}}$
	$\Omega^{B(R2),ij}_{\bar{a}k} = \sum_{\bar{c}\bar{d}} (\bar{a}\bar{c}|k\bar{d}) R^{ij}_{\bar{c}\bar{d}}$

TABLE IV. State-specific intermediates needed for the CCSD Jacobian right transformation. For ease of notation, the short-hand notation $L^{pq}_{rs} = 2(pq|rs) - (ps|rq)$ is used.

$C_{\bar{a}_{ij}\bar{c}_{kj}} = J^{T1o,ki}_{\bar{a}_{ij}\bar{c}_{kj}} + \sum_{\bar{a}^0\bar{c}^0} S^{ij,ki}_{\bar{a}_{ij}\bar{a}^0_{ki}} C^{T2,ik}_{\bar{a}^0\bar{c}^0} S^{ki,kj}_{\bar{c}^0_{ki}\bar{c}_{kj}}$
$D_{\bar{a}_{ij}\bar{c}_{kj}} = L^{T1o,ki}_{\bar{a}_{ij}\bar{c}_{kj}} + \sum_{\bar{a}^0\bar{c}^0} S^{ij,ki}_{\bar{a}_{ij}\bar{a}^0_{ki}} D^{T2,ik}_{\bar{a}^0\bar{c}^0} S^{ki,kj}_{\bar{c}^0_{ki}\bar{c}_{kj}}$
$J^{T1o,ik}_{\bar{a}_{ij}\bar{c}_{kj}} = (ik|\bar{a}_{ij}\bar{c}_{kj}) - \sum_{l} t^l_{\bar{a}_{ij}} \sum_{\mu} d^{kj}_{\mu\bar{c}_{kj}} (ik|l\mu)$
$L^{T1o,ik}_{\bar{a}_{ij}\bar{c}_{kj}} = L^{ik}_{\bar{a}_{ij}\bar{c}_{kj}} - 2 \sum_{l} t^l_{\bar{a}_{ij}} \sum_{\mu} d^{kj}_{\mu\bar{c}_{kj}} (il|k\mu) + \sum_{l} t^l_{\bar{a}_{ij}} \sum_{\mu} d^{kj}_{\mu\bar{c}_{kj}} (ik|l\mu)$
$\Omega^{B(T2),ij}_{k\bar{a}} = \sum_{P_{ij}Q_{ij}} \sum_{\bar{d}^0} W^{ij}_{P_{ij}\bar{d}^0\bar{a}} \left[\mathbf{V}^{-1}\right]_{P_{ij}Q_{ij}} (Q_{ij}|k\bar{d}^0)$
$W^{ij}_{Q_{ij}\bar{a}^0\bar{a}} = \sum_{\mu\nu} (Q_{ij}|\mu\nu) t^{ij}_{\mu\bar{a}^0} \Lambda^{p,ij}_{\nu\bar{a}}$

[1] P. Pulay, Chem. Phys. Lett. **100**, 151 (1983).
[2] S. Saebø and P. Pulay, Chem. Phys. Lett. **113**, 13 (1985).
[3] S. Saebø and P. Pulay, Annu. Rev. Phys. Chem. **44**, 213 (1993).
[4] P. Pulay and S. Saebø, Theor. Chim. Acta **69**, 357 (1986).
[5] S. Saebø and P. Pulay, J. Chem. Phys. **86**, 914 (1987).
[6] S. Saebø and P. Pulay, J. Chem. Phys. **88**, 1884 (1988).
[7] G. Rauhut, P. Pulay, and H.-J. Werner, J. Comput. Chem. **19**, 1241 (1998).
[8] M. Schütz, G. Hetzer, and H.-J. Werner, J. Chem. Phys. **111**, 5691 (1999).
[9] C. Hampel and H.-J. Werner, J. Chem. Phys. **104**, 6286 (1996).
[10] M. Schütz, Phys. Chem. Chem. Phys. **4**, 3941 (2002).
[11] M. Schütz and F. R. Manby, Phys. Chem. Chem. Phys. **5**, 3349 (2003).
[12] M. Schütz and H.-J. Werner, Chem. Phys. Lett. **318**, 370 (2000).
[13] H.-J. Werner, P. J. Knowles, G. Knizia, F. R. Manby, and M. Schütz, Wiley Interdiscip. Rev.: Comput. Mol. Sci. **2**, 242 (2012).
[14] W. Meyer, *Methods of Electronic Structure Theory*, 3rd ed. (Plenum Press, New York, 1977).
[15] W. Meyer, Theor. Chem. Acc. **35**, 277 (1974).
[16] W. Meyer, J. Chem. Phys. **58**, 1017 (1973).
[17] W. Meyer, Int. J. Quantum Chem. **S5**, 341 (1971).
[18] R. Ahlrichs, F. Driessler, H. Lischka, V. Staemmler, and W. Kutzelnigg, J. Chem. Phys. **62**, 1235 (1975).
[19] R. Ahlrichs and F. Driessler, Theor. Chem. Acc. **36**, 275 (1975).
[20] V. Staemmler and R. Jaquet, Theor. Chem. Acc. **59**, 487 (1981).
[21] J. L. Whitten, J. Chem. Phys. **58**, 4496 (1973).
[22] B. I. Dunlap, J. W. D. Conolly, and J. R. Sabin, J. Chem. Phys. **71**, 3396 (1979).
[23] F. Neese, A. Hansen, and D. G. Liakos, J. Chem. Phys. **131**, 064103 (2009).
[24] F. Neese, A. Hansen, F. Wennmohs, and S. Grimme, Acc. Chem. Res. **42**, 641 (2009).
[25] F. Neese, F. Wennmohs, and A. Hansen, J. Chem. Phys. **130**, 114108 (2009).
[26] D. G. Liakos, A. Hansen, and F. Neese, J. Chem. Theory Comput. **7**, 76 (2011).
[27] A. Hansen, D. G. Liakos, and F. Neese, J. Chem. Phys. **135**, 214102 (2011).
[28] C. Riplinger and F. Neese, J. Chem. Phys. **138**, 034106 (2013).
[29] C. Krause and H.-J. Werner, Phys. Chem. Chem. Phys. **14**, 7591 (2012).
[30] C. Hättig, D. P. Tew, and B. Helmich, J. Chem. Phys. **136**, 204105 (2012).
[31] G. Schmitz, B. Helmich, and C. Hättig, Mol. Phys. **111**, 2463 (2013).
[32] J. Yang, G. K. L. Chan, F. R. Manby, M. Schütz, and H.-J. Werner, J. Chem. Phys. **136**, 144105 (2012).
[33] D. P. Tew and C. Hättig, Int. J. Quantum Chem. **113**, 224 (2013).
[34] G. Schmitz, C. Hättig, and D. P. Tew, Phys. Chem. Chem. Phys. **16**, 22167 (2014).
[35] G. Schmitz and C. Hättig, J. Chem. Phys. **145**, 234107 (2016).
[36] B. Helmich and C. Hättig, J. Chem. Phys. **135**, 214106 (2011).
[37] B. Helmich and C. Hättig, J. Chem. Phys. **139**, 084114 (2013).
[38] B. Helmich and C. Hättig, Comput. Theor. Chem. **1040-1041**, 35 (2014).
[39] O. Christiansen, H. Koch, and P. Jørgensen, Chem. Phys. Lett. **243**, 409 (1995).
[40] D. Kats, T. Korona, and M. Schütz, J. Chem. Phys. **125**, 104106 (2006).
[41] T. Korona and H.-J. Werner, J. Chem. Phys. **118**, 3006 (2003).
[42] T. D. Crawford and R. A. King, Chem. Phys. Lett. **366**, 611 (2002).
[43] A. K. Dutta, F. Neese, and R. Izsák, J. Chem. Phys. **145**, 034102 (2016).
[44] R. H. Myhre, A. M. J. Sánchez de Merás, and H. Koch, J. Chem. Phys. **141**, 224105 (2014).
[45] R. H. Myhre and H. Koch, J. Chem. Phys. **145**, 044111 (2016).
[46] D. Mester, P. R. Nagy, and M. Kállay, J. Chem. Phys. **146**, 194102 (2017).
[47] P. Baudin and K. Kristensen, J. Chem. Phys. **144**, 224106 (2016).
[48] O. Christiansen, H. Koch, A. Halkier, P. Jørgensen, T. Helgaker, and A. Sánchez de Merás, J. Chem. Phys. **105**, 6921 (1996).
[49] G. D. Purvis and R. J. Bartlett, J. Chem. Phys. **76**, 1910 (1982).
[50] T. J. Lee and R. J. Rice, Chem. Phys. Lett. **150**, 406 (1988).
[51] G. E. Scuseria, C. L. Janssen, and H. L. Schaefer III, J. Chem. Phys. **89**, 7382 (1988).
[52] J. F. Stanton, J. Gauss, J. D. Watts, and R. J. Bartlett, J. Chem. Phys. **94**, 4334 (1991).
[53] C. Hampel, K. A. Peterson, and H.-J. Werner, Chem. Phys. Lett. **190**, 1 (1992).
[54] H. Koch, O. Christiansen, R. Kobayashi, P. Jørgensen, and T. Helgaker, Chem. Phys. Lett. **228**, 233 (1994).
[55] H. Koch and P. Jørgensen, J. Chem. Phys. **93**, 3333 (1990).
[56] E. R. Davidson, J. Comput. Phys. **17**, 87 (1975).
[57] B. Helmich, "Paarspezifische natürliche orbitale zur effizienten berechnung von coupled-cluster-anregungsenergien," Ph.D. thesis, Ruhr-Universität Bochum, 2014.
[58] R. Ahlrichs, M. Bär, M. Häser, H. Horn, and C. Kälmel, Chem. Phys. Lett. **162**, 165 (1989).
[59] M. Häser and R. Ahlrichs, J. Comput. Chem. **10**, 104 (1989).
[60] P. Hohenberg and W. Kohn, Phys. Rev. **136**, B864 (1964).
[61] W. Kohn and L. J. Sham, Phys. Rev. **140**, A1133 (1965).
[62] M. Von Arnim and R. Ahlrichs, J. Comput. Chem. **19**, 1746 (1998).
[63] M. Sierka, A. Hogekamp, and R. Ahlrichs, J. Chem. Phys. **118**, 9136 (2003).
[64] F. Weigend, J. Comput. Chem. **29**, 167 (2008).
[65] F. Weigend, Phys. Chem. Chem. Phys. **8**, 1057 (2006).
[66] F. Weigend, Phys. Chem. Chem. Phys. **4**, 4285 (2002).
[67] P. A. M. Dirac, Proc. R. Soc. London, Ser. A **123**, 714 (1929).
[68] J. C. Slater, Phys. Rev. **81**, 385 (1951).
[69] C. Lee, W. Yang, and G. Parr, Phys. Rev. B **37**, 785 (1988).
[70] A. D. Becke, Phys. Rev. A **38**, 3098 (1988).
[71] A. D. Becke, J. Chem. Phys. **98**, 5648 (1993).
[72] F. Weigend and R. Ahlrichs, Phys. Chem. Chem. Phys. **7**, 3297 (2005).
[73] K. Eichkorn, F. Weigend, O. Treutler, and R. Ahlrichs, Theor. Chem. Acc. **97**, 119 (1997).
[74] T. H. Dunning, J. Chem. Phys. **90**, 1007 (1989).
[75] D. E. Woon and T. H. Dunning, Jr., J. Chem. Phys. **100**, 2975 (1994).
[76] F. Weigend, A. Köhn, and C. Hättig, J. Chem. Phys. **116**, 3175 (2002).
[77] F. Weigend, M. Häser, H. Patzelt, and R. Ahlrichs, Chem. Phys. Lett. **294**, 143 (1998).
[78] J. Pipek and P. Mezey, J. Chem. Phys. **90**, 4916 (1988).
[79] G. Knizia, J. Chem. Theory Comput. **9**, 4834 (2013).
[80] M. Schreiber, M. R. Silva-Junior, S. P. A. Sauer, and W. Thiel, J. Chem. Phys. **128**, 134110 (2008).
[81] M. Schwilk, D. Usvyat, and H.-J. Werner, J. Chem. Phys. **142**, 121102 (2015).
[82] H. Koch, O. Christiansen, P. Jørgensen, A. M. J. Sánchez de Méras, and T. Helgaker, J. Chem. Phys. **106**, 1808 (1997).
[83] O. Christiansen, H. Koch, and P. Jørgensen, J. Chem. Phys. **103**, 7429 (1995).
[84] O. Christiansen, H. Koch, and P. Jørgensen, J. Chem. Phys. **105**, 1451 (1996).

VI. PNO-CC3 EXCITATION ENERGIES USING LAPLACE TRANSFORMATION TECHNIQUES

After the implementation of CCSD excitation energies the next step was to develop an efficient way to include triple excitations in excited state calculations. For this, we chose the CC3 model instead of the CCSDT-n model for the reasons given in section II A. Furthermore, we did not choose the computationally less demanding models CCSDR(T) or CCSDR(3) since these models require the computation of the left CCSD eigenvectors which will be considered in a forthcoming publication but were out-of-reach for this work.

All work regarding this publication has been performed under the supervision of Prof. Dr. Christof Hättig. For the implementation an existing framework for the computation of (ground state) PNO-CCSD(T0) and PNO-CCSD(T) energies has been used and modified. Furthermore, this framework has been completely restructured in order to avoid the input/output (I/O) of large integral files and to arrive at a better (OpenMP) parallel performance. This has partially been realized within a 2 weeks stay at Aarhus university with the help of Dr. Gunnar Schmitz who helped in shifting the loop over Laplace grid points inside the loop over LMO triples. His contribution was to adapt the driver routine where the triples correction is organized and the subroutines for the calculation of individual contributions to the triples amplitudes are invoked. My contribution within that 2-week-stay was the adaption of the routines which compute the integrals. However, after this stay where the aformentioned loop was reorganized, I was responsible myself for adapting the code further to avoid the I/O of any integral files and triples amplitudes.

The computation of the CC3 ground state vector function and the CC3 Jacobian right transformation was implemented by me. Method development in the sense of analyzing and defining suitable TNOs and selecting the subset of significant triples for excited states, designing an algorithm which avoids the computation of redundant contributions to the CC3 vector function and Jacobian right transformation

transformed vector was done by me. Furthermore, all figures, numbers and the manuscript itself have been created by me.
The work presented in the following is a manuscript under construction.

Implementation of the Iterative Triples Model CC3 for Excitation Energies using Pair Natural Orbitals and Laplace Transformation Techniques

Marius S. Frank,[1, a)] Gunnar Schmitz,[2, b)] and Christof Hättig[1, c)]

[1)] *Lehrstuhl für Theoretische Chemie, Ruhr-Universität Bochum, D-44801 Bochum, Germany*

[2)] *Deparment of Chemistry, Aarhus University, DK-8000 Aarhus C, Denmark*

(Dated: 17 July 2019)

We present a PNO-based implementation of CC3 excitation energies which extends our previously published state-specific pair natural orbital (PNO) ansatz for the solution of the excited state eigenvalue problem to methods including connected triple excitations. A thorough analysis of the equations for the excited state triples amplitudes is presented from which we derive a suitable state-specific triple natural orbital (TNO) basis for the excited state eigenvector. Furthermore, we employ a Laplace transformation of the energy denominators of the triples amplitudes to take the coupling between into account. The accuracy of the implementation is evaluated for a test set of 153 singlet excitations in 27 molecules. We find that for states with small contributions from double excitations already a T0 approximation to PNO-CC3 gives accurate results with a mean absolute error (MAE) for $T_{\mathrm{PNO}} = 10^{-7}$ in the range of 0.02 eV and, hence, similar to that of Laplace-transformed PNO-CC3 and within the intrinisic error range of canonical CC3. However, for states with larger double excitation contributions the T0 approximation is found to yield significantly less accurate results even with rather tight PNO and TNO selection thresholds while the Laplace-transformed variant of PNO-CC3 shows a uniform accuracy for singly and doubly excited states (MAE and maximum errors of 0.02 eV and 0.05 eV for $T_{\mathrm{PNO}} = 10^{-7}$, respectively).

[a)] Corresponding author: Marius.Frank@rub.de

[b)] Gunnar.Schmitz@rub.de

[c)] christof.haettig@rub.de

I. INTRODUCTION

State-of-the art coupled cluster models that include connected triple excitations are able to accurately reproduce experimental results with high accuracy, e.g. for reactions energies often within the chemical accuracy of ≈ 1 kcal/mol and excitation energies for one-electron transitions within 0.1 eV. Unfortunately, the applicability of such accurate (triple excitations including) coupled cluster methods is with canonical implementations restricted to rather small molecular systems because of the high computational costs in terms of floating point operations (FLOPs), memory and disk space usage. For example, the costs for the widely used and highly accurate approximate triples models CCSD(T), CCSDR(3) and CC3 scale as $\mathcal{O}(\mathcal{N}^7)$ in terms of FLOPs and as $\mathcal{O}(\mathcal{N}^4)$ in terms of disk space demands with the system size $\mathcal{N}$. This steep scaling makes it impossible to apply these methods routinely to molecules with more than about twenty heavy atoms with basis sets that allow to exploit the accuracy these methods.

Fortunately, approaches to avoid the inherently steep scaling of the canonical coupled cluster methods without sacrificing their accuracy have come up during the past decades. Most of these approaches have in common that they makes use of the fact that the nature of dynamic electron correlation is local. This locality is difficult to exploit when canonical molecular orbitals (MOs) are used. Therefore, these methods employ localized molecular orbitals (LMOs) which allow to restrict the excitation space to local correlation domains and are, hence, called local correlation methods.

Over the past decades many different flavors of these local correlation methods have been proposed and shown to be efficient and accurate[1–27]. One of the nowadays most popular and promising local correlation approaches is based on the representation of the virtual orbital space by pair natural orbitals (PNOs) and has its roots in the 1970s where it was developed and refined by Maier[28–31],Ahlrichs[32,33], Staemmler[32,34], Kutzelnigg[32] and co-workers. About 10 years ago, it has been revived and since then refined[35–40] by Neese and co-workers who recognized that the bottleneck of the early PNO-based methods — the integral transformations to the PNO basis — can be circumvented using the resolution-of-the-identity (RI) approximation[41,42]. Within the PNO approximation local correlation domains are obtained by diagonalization of approximate model densities. The eigenvalues (occupation numbers) are used to select the most important orbitals for the description of the electron correlation

of a LMO pair ij. Restriction of the correlation domains to PNOs with eigenvalues above a given threshold T_{PNO} leads to a size of the virtual spaces which increases eventually only linearly with the system size.

Highly efficient, linear scaling and accurate PNO-based implementations of single reference methods such as MP2, CCSD, CCSD(T) and their explicitly correlated[35–40,43–49] counterparts as well as of the multireference methods NEVPT2[50] and CASPT2[51] have already been presented by different groups for ground state energy calculations. Most of these implementations make use of projected atomic orbitals (PAOs)[52–57] or orbital specific virtuals (OSVs)[44,47–49] as an intermediate basis during the PNO construction in order to achieve a linear cost-scaling. Also first-order molecular properties and gradients (geometry optimizations) using PNOs have recently become available[58–60].

Especially, the computation of excitation energies and response properties in a truncated PNO space has become an active field of research recently. The description of excited states is a special challenge for local correlation methods since the excitation process often is non-local. The development of PAO-based response methods beyond second order such as CC2[61,62] which avoid an explicit treatment of the doubles space has been given up. This is due to the fact that huge correlation domains which grow with the number of excited states were needed what made these implementations rather inefficient[63,64]. Also, approaches based on natural orbital (NO)[65] and natural transition orbital (NTO)[66] which have recently become an active field of research lack yet either general applicability or efficiency.

A novel route to tackle the excited state problem with local correlation methods has recently been proposed by Dutta *et al*[67]. Their idea is to solve the ground state CC equations in the PNO basis and to transform these ground state PNOs afterwards back to the canonical MO basis in which the excited state eigenvalue problem is then solved. Combining this approach with similarity-transformed equation of motion CCSD (STEOM-CCSD) leads to a formal $\mathcal{O}(\mathcal{N}^5)$-scaling of the costs. Just recently, Dutta *et al.* presented (ground state) PNO-based implementations of CCSD ionization potentials[68] (IPs) and electron affinities[69] (EAs) which are necessary ingredients for lower-scaling variants of STEOM-CCSD. However, besides the advantage of having a common PNO basis and, hence, being able to use well-established multistate Block-Davidson algorithms for the solution of the excited state eigenvalue problem a major disadvantage of this approach is that also its local variants inherit the difficulties of STEOM-CCSD[70] and is difficult to generalize to methods accounting

for connected triples such as CCSDR(T), CCSDR(3)[71] or CC3[72].

Another method, which also bears the advantage of being able to use standard multistate solvers which, compared to single state (i.e. one-state-at-a-time) solvers, are more robust, has been developed by Valeev and co-workers[73]. They use state-averaged PNOs obtained from averaging densities from approximate configuration interaction singles with perturbative doubles CIS(D) over a given number of states. The wavefunctions of all excited states are then restricted to the same local correlation domains obtained from this density. Even though giving accurate excitation energies, the computational costs increase for this approach in particular for extended systems with several chromophores not only with the size of individual chromophores but also with the number of states included.

Hättig and Helmich, in contrast, proposed to use state-specific PNOs for the solution of the excited state eigenvalue problem. Here, a separate PNO basis is constructed for each excited state from approximate CIS(D) densities. The advantage of this approach is that the PNO basis adapts itself to the nature of the excited state and is, hence, as compact as possible for each state. Furthermore, the demands in computational resources such as FLOPs, memory and disk space scales linearly with the size of the chromophore. The state-specific PNO approach is in our view the most promising local correlation approach for excited state calculations of extended systems, in particular, if they contain multiple chromophores, and has already been proven to be efficient and accurate for CC2[74], ADC(2)-x[75] and CCSD[76] calculations.

The aim of the present paper is to extend PNO-based CC response theory to models including connected triples. We use for this in the current work the coupled cluster singles and doubles with approximate triples model CC3[72,77] together with state-specific PNOs[78]. We chose CC3 because of its simplicity and thorough grounding in perturbation theory. We did here not consider perturbative triples corrections even though they are similarly accurate as CC3 since they involve additional computational steps and pitfalls when implemented with PNOs. The most important feature a model including connected triples should have is that it systematically improves upon CCSD excitation energies for singly as well as for doubly excited states and can eventually approach the accuracy of the canonical CC3 method. In the following, the concept of triples natural orbitals (TNOs) and the selection scheme for LMO triples will be extended to excited states. After discussing the formal theory the accuracy and efficiency of the implementation will be discussed.

II. THEORY AND IMPLEMENTATION

A. The CC3 Model

In single-reference coupled cluster theory the wavefunction is parametrized as

$$|\mathrm{CC}\rangle = e^{T}|\mathrm{HF}\rangle \tag{1}$$

where $|\mathrm{HF}\rangle$ denotes the reference determinant (usually from a Hartree-Fock calculation) and $T = T_1 + T_2 + \ldots$ is the cluster operator, where $T_i = \sum_{\mu_i} t_{\mu_i}\tau_{\mu_i}$ are the contributions from the excitation classes i and τ_{μ_i} excitation operators and t_{μ_i} the corresponding amplitudes.

The CC3 model[72] is an iterative approximation to the coupled cluster singles, doubles and triples model CCSDT where only the leading nonvanishing order contributions from the connected triple excitations T_3 are kept. But in difference to approximate triples models for ground-state energies the singles amplitudes are in CC3 treated as zeroth-order parameters due to their special role in response theory[72]. The residuals of the CC3 cluster equations are:[72]

$$\Omega_{\mu_1} = \langle\mu_1|e^{-T_2}\hat{H}e^{T_2}|\mathrm{HF}\rangle + \langle\mu_1|[\hat{H}, T_3]|\mathrm{HF}\rangle \ , \tag{2}$$

$$\Omega_{\mu_2} = \langle\mu_2|e^{-T_2}\hat{H}e^{T_2}|\mathrm{HF}\rangle + \langle\mu_2|[\hat{H}, T_3]|\mathrm{HF}\rangle \ , \tag{3}$$

$$\Omega_{\mu_3} = \langle\mu_3|[F, T_3]|\mathrm{HF}\rangle + \langle\mu_3|[[\hat{H}, T_2]|\mathrm{HF}\rangle \ , \tag{4}$$

The energy is obtained as $E = \langle\mathrm{HF}|H|\mathrm{CC}\rangle$. Above, we have introduced $\hat{H}$ as short-hand notation for the T_1-similarity transformed Hamiltonian[79] $\hat{H} = \exp(-T_1)H\exp(T_1)$.

If we denote with Δ_{μ_3} the orbital energy differences $\Delta^{ijk}_{abc} = \epsilon_i + \epsilon_j + \epsilon_k - \epsilon_a - \epsilon_b - \epsilon_c$, we can for canonical molecular orbitals solve Eq. (4) formally as

$$t_{\mu_3} = \Delta^{-1}_{\mu_3}\langle\mu_3|[\hat{H}, T_2]|\mathrm{HF}\rangle \ . \tag{5}$$

This allows to compute and process, whenever needed, a batch of triples amplitudes t_{μ_3} on-the-fly and solve e.g. the CC3 amplitude equations without storing a full rank-6 triples tensor, which would otherwise limit the applicability of the method by huge storage and I/O demands.

In coupled cluster response theory, excitation energies are obtained as eigenvalues of the Jacobian $\mathbf{A}$ of the ground state residual or vector function Ω_{μ_i},

$$A_{\mu_i\nu_j} = \frac{\partial\Omega_{\mu_i}}{\partial t_{\nu_j}}. \tag{6}$$

For CC3 the Jacobian obtained from eqs. (2) – (4) is

$$\mathbf{A} = \begin{pmatrix} \langle\mu_1|[\hat{H}+[\hat{H},T_2],\tau_{\nu_1}]|\mathrm{HF}\rangle & \langle\mu_1|[\hat{H},\tau_{\nu_2}]|\mathrm{HF}\rangle & \langle\mu_1|[\hat{H},\tau_{\nu_3}]|\mathrm{HF}\rangle \\ \langle\mu_2|[\hat{H}+[\hat{H},T_2+T_3],\tau_{\nu_1}]|\mathrm{HF}\rangle & \langle\mu_2|[\hat{H}+[\hat{H},T_2],\tau_{\nu_2}]|\mathrm{HF}\rangle & \langle\mu_2|[\hat{H},\tau_{\nu_3}]|\mathrm{HF}\rangle \\ \langle\mu_3|[[\hat{H},T_2],\tau_{\nu_1}|\mathrm{HF}\rangle & \langle\mu_3|[\hat{H},\tau_{\nu_2}]|\mathrm{HF}\rangle & \langle\mu_3|[F,\tau_{\nu_3}]|\mathrm{HF}\rangle \end{pmatrix} \tag{7}$$

The eigenvalues are usually determined by iterative procedures which require the implementation of linear transformations of a trial vector $\mathbf{R}$ with the Jacobian:

$$\rho_{\mu_i} = \sum_{\nu_j} A_{\mu_i\nu_j} R_{\nu_j}. \tag{8}$$

With the auxiliary operators $R_i = \sum_{\mu_i} R_{\mu_i}\tau_{\mu_i}$ and the one-index transformed Hamiltoninan[80] $\bar{H} = \left[\hat{H}, R_1\right]$ the linear transformations with the CC3 Jacobian can be written as

$$\rho_{\mu_1} = \langle\mu_1|\bar{H} + [\bar{H},T_2] + [\hat{H},R_2] + [\hat{H},R_3]|\mathrm{HF}\rangle, \tag{9}$$

$$\rho_{\mu_2} = \langle\mu_2|\bar{H} + [\bar{H},T_2+T_3] + [\hat{H}+[\hat{H},T_2],R_2] + [\hat{H},R_3]|\mathrm{HF}\rangle, \tag{10}$$

$$\rho_{\mu_3} = \langle\mu_3|[\bar{H},T_2] + [\hat{H},R_2] + [F,R_3]|\mathrm{HF}\rangle. \tag{11}$$

The triples part of the CC3 eigenvectors, E_{μ_i} have to fulfill the relation[77]:

$$E_{\mu_3} = (\Delta_{\mu_3}+\omega)^{-1}\,\langle\mu_3|[\bar{H},T_2] + [\hat{H},E_2]|\mathrm{HF}\rangle\ , \tag{12}$$

where ω denotes the excitation energy. This can be used to reformulate the eigenvalue problem for the CC3 excitation energies from a linear eigenvalue problem in the singles, doubles, and triples space into a non-linear eigenvalue problem in the singles and doubles space only for the effective Jacobi matrix

$$\sum_{j=1}^{2}\sum_{\nu_j} A^{eff}_{\mu_i\nu_j}(\omega)E_{\nu_j} = \sum_{j=1}^{2}\sum_{\nu_j}\left(A_{\mu_i\nu_j} + \sum_{\kappa_3}\frac{A_{\mu_i\kappa_3}A_{\kappa_3\nu_j}}{\Delta_{\kappa_3}+\omega}\right)E_{\nu_j} = \omega E_{\mu_i}\ , \tag{13}$$

without storage of full triples vectors.

The time determining steps of the CC3 Jacobian right transformations scale for canonical implementations as $\mathcal{O}(\mathcal{N}^7)$ which restricts the applicability of them to small molecular systems. The aim of the present work is to reduce this steep scaling using pair and triple natural orbitals (PNOs and TNOs) which will be described in the following sections.

B. Ground and excited state PNOs

Pair natural orbitals (PNOs) are linear combinations of virtual molecular orbitals

$$|\bar{a}_{ij}\rangle = \sum_a d^{ij}_{a\bar{a}_{ij}} |a\rangle, \tag{14}$$

with expansion coefficients $d^{ij}_{a\bar{a}_{ij}}$ that are initially obtained from the eigenvectors of the correlation contribution of a pair ij to the virtual-virtual block of the one-electron density

$$\sum_{ab} d^{ij}_{a\bar{a}_{ij}} D^{ij}_{ab} d^{ij}_{b\bar{b}_{ij}} = n^{ij}_{\bar{a}_{ij}} \delta_{\bar{a}_{ij}\bar{b}_{ij}} \ . \tag{15}$$

Here and in the following, indices $i, j, k, l, \ldots$ denote occupied and $a, b, c, d, \ldots$ virtual MOs. General MOs will be denoted as $p, q, r, s, \ldots$ and PNOs and OSVs will be marked with, respectively, bar and tilde accents. The eigenvalues $n^{ij}_{\bar{a}_{ij}}$ of the density $\mathbf{D}^{ij}$ have the meaning of occupation numbers and correlate with the importance of a given PNO for the correlation contribution to the wavefunction. If the occupied orbital space is represented by localized molecular orbitals (LMOs) the eigenvalues decay rapidly with the index $\bar{a}_{ij}$ and with the distance between the LMOs. Hence, it becomes practical to define a truncation threshold T_{PNO} and discard PNOs (i.e. truncate the virtual space) with $n^{ij}_{\bar{a}_{ij}} < T_{\mathrm{PNO}}$. In this way, the accuracy of a calculation can in principle be controlled by a simple truncation threshold.

For the ground state, the PNOs are usually constructed from approximate MP2 densities[81]

$$D^{ij}_{ab} = \sum_c \left(\tilde{t}^{ij,(1)}_{ac} t^{ij,(1)}_{bc} + \tilde{t}^{ij,(1)}_{ca} t^{ij,(1)}_{cb} \right) \tag{16}$$

with $\tilde{t}^{ij,(1)}_{ab} = 2t^{ij,(1)}_{ab} - t^{ij,(1)}_{ba}$ and the approximate first-order amplitudes

$$t^{ij,(1)}_{ab} = \frac{(ai|bj)}{F_{ii} + F_{jj} - \epsilon_a - \epsilon_b} \tag{17}$$

where $(ai|bj)$ denote the electron repulsion integrals (ERIs), F_{ii} the diagonal Fock matrix elements in the LMO basis, and ϵ_a orbital energies for canonical virtual MOs.

For PNOs of excited states we use an approximate correlation contribution to the density[78]

$$D^{ij,ex}_{ab} = \sum_c \left(\tilde{R}^{ij,(1)}_{ac} R^{ij,(1)}_{bc} + \tilde{R}^{ij,(1)}_{ca} R^{ij,(1)}_{cb} \right) \tag{18}$$

which is calculated from CIS(D)-like excited state first-order amplitudes[78]

$$R_{ab}^{ij,(1)} = \frac{(ai\tilde{|}bj)}{F_{ii} + F_{jj} - \epsilon_a - \epsilon_b + \omega}. \tag{19}$$

and $\tilde{R}_{ab}^{ij,(1)} = 2R_{ab}^{ij,(1)} - R_{ba}^{ij,(1)}$. The excited-state singles-dressed integrals are computed as

$$(ai\tilde{|}bj) = \sum_{\mu\nu\kappa\lambda} P_{ab}^{ij} \left(\bar{\Lambda}_{\mu a}^{p} C_{\nu i} + C_{\mu a} \bar{\Lambda}_{\nu i}^{h}\right) C_{\kappa b} C_{\lambda j} (\mu\nu|\kappa\lambda), \tag{20}$$

where $\mathbf{C}$ denotes the LMO coefficients and $\bar{\Lambda}_{\mu a}^{p} = -\sum_i R_a^i C_{\mu i}$ and $\bar{\Lambda}_{\mu i}^{h} = \sum_a R_a^i C_{\mu a}$ are modified MO coefficients dressed with the singles part of the current trial vector R_a^i. The symmetrization operator P_{ab}^{ij} is defined as $P_{ab}^{ij} f_{ab}^{ij} = f_{ab}^{ij} + f_{ba}^{ji}$.

If the PNOs would be obtained from equations (16) and (18) without any further approximations, the computational complexity of the PNO construction would increase with the system size as $\mathcal{O}(\mathcal{N}^5)$. To reduce this scaling the densities are evaluated in a so-called pre-PNO basis[44] $\{\tilde{a}_{ij}\}$ which is obtained by merging the orbital specific virtual[82] (OSV) spaces $\{\tilde{a}_i\}$ and $\{\tilde{a}_j\}$ of the LMOs i and j using the first-order amplitudes:[48,74]

$$t_{\tilde{a}_{ij}\tilde{b}_{ij}}^{ij,(1)} = \frac{(\tilde{a}_{ij} i|\tilde{b}_{ij} j)}{F_{ii} + F_{jj} - \epsilon_{\tilde{a}_{ij}} - \epsilon_{\tilde{b}_{ij}}} \ , \tag{21}$$

$$R_{\tilde{a}_{ij}\tilde{b}_{ij}}^{ij,(1)} = \frac{(\tilde{a}_{ij} i|\tilde{\tilde{b}}_{ij} j)}{F_{ii} + F_{jj} - \epsilon_{\tilde{a}_{ij}} - \epsilon_{\tilde{b}_{ij}} + \omega} \ , \tag{22}$$

where $\epsilon_{\tilde{a}_{ij}}$ are the eigenvalues of the Fock matrix which is diagonalized in the pre-PNO basis.

The ground-state OSVs are obtained by diagonalizing the MP2-like densities (eq. (16)) for the diagonal pairs. The excited-state OSVs are obtained from densities, Eq. (18), that are calculated from modified pseudo-amplitudes[74]

$$R_{ab}^{\prime ii,(1)} = \frac{(ai|bi) + (\overline{ai|bj})}{2F_{ii} - \epsilon_a - \epsilon_b + \omega} \ , \tag{23}$$

with integrals

$$(\overline{ai|bj}) = \sum_{\mu\nu\kappa\lambda} \left[\bar{\Lambda}_{\nu i}^{h} \bar{\Lambda}_{\lambda j}^{h} C_{\mu a} C_{\kappa b} + \bar{\Lambda}_{\mu a}^{p} \bar{\Lambda}_{\kappa b}^{p} C_{\nu i} C_{\lambda j} + P_{ab}^{ij} \bar{\Lambda}_{\mu a}^{p} \bar{\Lambda}_{\lambda j}^{h} C_{\nu i} C_{\kappa b}\right] (\mu\nu|\kappa\lambda) \tag{24}$$

in order to obtain OSVs suitable for expanding the one-index transformed integrals $(ai\bar{|}bj)$ of LMO pairs.

Furthermore, we pre-screen the set of LMO pairs before the formation of pre-PNOs based on approximate second-order pair contributions to the correlation energy. The estimated

pair correlation energies $e_{ij}^{(2)}$ for the ground state and $\omega_{ij}^{(2)}$ for the excited state are calculated in the OSV basis sets $\{\tilde{a}_i\}$ and $\{\tilde{b}_j\}$ for the two LMOs i and j as:

$$e_{ij}^{(2)} = \sum_{\tilde{a}_{ij}\tilde{b}_{ij}} \frac{(\tilde{a}_i i|\tilde{b}_j j)}{F_{ii} + F_{jj} - \epsilon_{\tilde{a}_i} - \epsilon_{\tilde{b}_j}}, \tag{25}$$

$$\omega_{ij}^{(2)} = \sum_{\tilde{a}_{ij}\tilde{b}_{ij}} \frac{(\tilde{a}_i i|\tilde{\bar{b}}_j j)}{F_{ii} + F_{jj} - \epsilon_{\tilde{a}_i} - \epsilon_{\tilde{b}_j} + \omega}. \tag{26}$$

Ground state pairs with $e_{ij}^{(2)} < \frac{1}{3}T_{pair}$ and excited state pairs with $\omega_{ij}^{(2)} < \frac{1}{3}T_{pair}$ are discarded. For a more detailed description of our PNO construction we refer the reader to Refs. 48, 78 and 74.

The ground and excited state doubles are restricted to the respective PNO space. For methods including triple excitations there are additional contributions from triples amplitudes. The construction of a suitable basis for these amplitudes will be discussed in the following.

C. Triples Selection and TNO Construction for the Ground State

The construction of a triples-specific basis from approximate triples amplitudes using similar strategies as for the PNOs is at least for approximate triples models like CCSD(T) and CC3 unpractical since the computational costs for the required ERIs and their contration with the doubles amplitudes to approximate triples amplitudes are high. As an alternative, Riplinger *et al.*[83] proposed to restrict the ground state triples ijk amplitudes to triples where ij, ik, and jk are significant pairs. Only triples for which each of those pairs is part of the ground state pair list are considered to be important for the triples contribution of the CCSD(T) model. Furthermore, the triples list is further compressed by only including triples where at most one pair is a so-called weak pair. Such a weak pair is not screened out by the MP2 pair correlation estimate but also not included in the CCSD treatment for which these authors applied a tighter pair selection threshold.

The triples selection as described above can be rationalized by analyzing the explicit expression for the ground state CCSD(T) triples equations[84]

$$t_{abc}^{ijk} = -\frac{1}{\Delta_{abc}^{ijk}} P_{abc}^{ijk} \Big\{ \sum_d t_{ad}^{ij}(ck|bd) - \sum_l t_{ab}^{il}(ck|lj) \Big\}. \tag{27}$$

where the operator P_{abc}^{ijk} acts as $P_{abc}^{ijk} f_{abc}^{ijk} = f_{abc}^{ijk} + f_{acb}^{ikj} + f_{bac}^{jik} + f_{cab}^{kij} + f_{bca}^{jki} + f_{cba}^{kji}$. Here and in the following, we restrict the discussion to the spin-free closed-shell case. The multipole expansion of two-electron integrals

$$|(pq|rs)| \leq \frac{M_{pq}^{(0)} M_{rs}^{(0)}}{R} + \frac{M_{pq}^{(1)} M_{rs}^{(0)} + M_{pq}^{(0)} M_{rs}^{(1)}}{R^2} + \frac{M_{pq}^{(2)} M_{rs}^{(0)} + 2M_{pq}^{(1)} M_{rs}^{(1)} + M_{pq}^{(0)} M_{rs}^{(2)}}{R^3} + \mathcal{O}(R^{-4}) \tag{28}$$

holds for (approximately) non-overlapping charge-distributions which in local correlation treatments is a reasonable assumption for weak and distant pairs[85]. In Eq. (28) upper indeces 0, 1 and 2 denote the monopoles, dipoles, and quadrupoles of the charge clouds pq and $R = |\vec{R}_{pq} - \vec{R}_{rs}|$ is the distance between the expansion centers $\vec{R}_{pq}$ and $\vec{R}_{rs}$ of these charge distributions. The $M^{(n)}$ denote the absolute values of the corresponding multipole integrals

$$M_{pq}^{(l)} = \sqrt{\sum_m \left| \int \phi_\mu(\mathbf{r}) \phi_\nu(\mathbf{r}) r^l \sqrt{\frac{4\pi}{2n+1}} Y_{lm}(\mathbf{r}) d\mathbf{r} \right|^2} \tag{29}$$

where Y_{lm} are the spherical harmonics of order l with $-l \leq m \leq l$. The monopole is directly related to the overlap, $M_{pq}^{(0)} = -S_{pq}$, and reduces for orthonormal orbitals to $M_{pq}^{(0)} = -\delta_{pq}$.

Applying the multipole expansion to the two terms in equation (27) separately gives

$$\left| \sum_d t_{ad}^{ij} (ck|bd) \right| \leq \sum_d |t_{ad}^{ij}| \left(\frac{M_{ck}^{(1)} M_{bd}^{(0)}}{R^2} + \frac{M_{ck}^{(2)} M_{bd}^{(0)} + 2M_{ck}^{(1)} M_{bd}^{(1)}}{R^3} \right) + \mathcal{O}(\mathcal{R}^{-7}), \tag{30}$$

$$\left| \sum_l t_{ab}^{il} (ck|lj) \right| \leq \sum_l |t_{ab}^{il}| \left(\frac{M_{ck}^{(1)} M_{lj}^{(0)}}{R^2} + \frac{M_{ck}^{(2)} M_{lj}^{(0)} + 2M_{ck}^{(1)} M_{lj}^{(1)}}{R^3} \right) + \mathcal{O}(\mathcal{R}^{-7}) \ , \tag{31}$$

where on the right hand side is was used that for weak or distant pairs the amplitudes t_{ab}^{ij} decay as $1/R_{ij}^3$ with the distance between the LMOs i and j. In equations (30) and (31) R refers to the distance between $\vec{R}_{ck}$ and, respectively, $\vec{R}_{bd}$ and $\vec{R}_{lj}$ and $\mathcal{R} = \min(R_{ij}, R)$.

These equations suggest that the triples amplitudes would have rather long-ranging non-negligible contributions since the leading terms of the multipole expansion of the integrals decays only as $\mathcal{O}(R^{-2})$. This would imply that only two LMOs of a triple ijk have to be close to each other; those for which the indeces appear in the amplitude t_{ab}^{ij} or in a charge distribution with a common index with the amplitude $t_{ab}^{il} M_{lj}^{(n)}$. But the third LMO could be rather far away from both of them as the contribution to the nominator of the triples

amplitude would decay only as $1/R^2$ with the distance between the charge centers in the ERI.

If both terms in Eq. (27) are combined, the long-range $\mathcal{O}(R^{-2})$ contributions cancel each other out and the dipole-dipole contribution of the integrals which decays as $\mathcal{O}(R^{-3})$ becomes the leading non-vanishing term in the multipole expansion of the triples amplitudes:

$$\left|\sum_d t_{ad}^{ij}(ck|bd) - \sum_l t_{ab}^{il}(ck|lj)\right| \leq 2\sum_d |t_{ad}^{ij}| \frac{M_{ck}^{(1)} M_{bd}^{(1)}}{R^3} + 2\sum_l |t_{ab}^{il}| \frac{M_{ck}^{(1)} M_{lj}^{(1)}}{R^3} + \mathcal{O}(\mathcal{R}^{-7}). \tag{32}$$

From equation (32) it can, thus, be concluded that the three LMOs of a triple ijk are in the long-range regime coupled by dipole interactions. Hence, for a non-vanishing contribution from a strong pair ij, for which the contractions $\sum_d t_{ab}^{ij}\phi_b(\mathbf{r})\phi_d(\mathbf{r})$ and $\sum_l t_{ab}^{il}\phi_l(\mathbf{r})\phi_j(\mathbf{r})$ are large, the LMO k must be close to either i or j and, hence, in addition to the pair ij also one of the pairs ik or jk has to be a strong pair.

This forms the basis for the pre-screening of LMO triples used in local correlation methods[18,83]. The PNO-CCSD(T) implementation[46] which we used as starting point for the current developments, employed as estimator for the magnitude of the correlation energy contribution from a LMO triple ijk:

$$E_{\text{guess}}^{ijk} = 3.5 \left[\frac{(e_1^{ijk} - e_2^{ijk})(e_2^{ijk} - e_3^{ijk})(e_3^{ijk} - e_1^{ijk})}{2\left\{(e_2^{ijk} - e_3^{ijk})\log e_1^{ijk} + (e_3^{ijk} - e_1^{ijk})\log e_2^{ijk} + (e_1^{ijk} - e_2^{ijk})\log e_3^{ijk}\right\}} \right]^{0.4} \tag{33}$$

with $e_x^{ijk} = e^{ij}e^{ik}\delta_{x,1} + e^{ij}e^{jk}\delta_{x,2} + e^{ik}e^{jk}\delta_{x,3}$ calculated from the CCSD pair energies if all three of the e_x^{ijk} differ by at least by 10^{-12}. If only two of these products of pair energies differ, the importance of a triple is estimated from these two products as

$$E_{\text{guess}}^{ijk} = 3.5 \left[\frac{e_1^{ijk} - e_2^{ijk}}{\log e_1^{ijk} - \log e_2^{ijk}} \right]^{0.9}. \tag{34}$$

Triples with E_{guess}^{ijk} below a threshold T_{trip} are discarded. In the meantime we have replaced the CCSD pair energies by the estimate for the MP2 correlation energies $e_{ij}^{(2)}$ from eq. (25) to avoid artificial difference e.g. between spin-orbital and spin-free calculations. Since E_{guess}^{ijk} is a rather empirical estimate for the size of the triples energy the selection threshold T_{trip} is chosen rather tight relative to the TNO selection threshold T_{TNO} (*vide infra*) to not affect the accuracy of a calculation.

For the selected triples ijk an initial pre-TNO basis $\{\tilde{a}_{ijk}\}$ is constructed by merging the ground state OSVs sets of the LMOs i, j, and k. Then, a density for ijk is calculated by averaging the approximate MP2 pair densities (c.f. equations (16) and (17)) for the three pairs in this basis,

$$D^{ijk,\mathrm{MP2}}_{\tilde{a}_{ijk}\tilde{b}_{ijk}} = \frac{1}{3}\left(S^{ijk,ij}_{\tilde{a}^0\bar{a}} D^{ij,\mathrm{MP2}}_{\bar{a}\bar{b}} S^{ij,ijk}_{\bar{b}\tilde{b}} + S^{ijk,ik}_{\tilde{a}\bar{a}} D^{ik,\mathrm{MP2}}_{\bar{a}\bar{b}} S^{ik,ijk}_{\bar{b}\tilde{b}} + S^{ijk,jk}_{\tilde{a}\bar{a}} D^{jk,\mathrm{MP2}}_{\bar{a}\bar{b}} S^{jk,ijk}_{\bar{b}\tilde{b}}\right). \tag{35}$$

In the above equation the pre-TNO/PNO overlap matrix

$$S^{ijk,ij}_{\tilde{a}\bar{a}} = \sum_c d^{ijk}_{c\tilde{a}} d^{ij}_{c\bar{a}} \tag{36}$$

with the PNO and pre-TNO coefficients $d^{ij}_{c\bar{a}}$ and $d^{ijk}_{c\tilde{a}}$ was used to transform the densities from the PNO to the pre-TNO basis. Similar as in the PNO construction, the initial TNO coefficients are obtained from the eigenvectors of this density where only the TNOs for eigenvalues $\eta^{ijk}_{\tilde{a}_{ijk}}$ above a threshold T_{TNO} are kept. Thereafter, the selected TNOs for a pair ijk are transformed to a semi-canonical basis in which the Fock matrix is diagonal.

D. Triples Selection and TNOs for Excited States

To arrive at a reasonable selection of the triples for excited states, we follow a similar multipole analysis-based strategy as used in the preceeding section for the ground state triples. For simplicity we assume that the reference wavefunction fulfills the Brillouin condition so that the ground state singles t_{μ_1} vanish in first-order and can be ignored for qualitative considerations. Before discussing the amplitude equations, we analyse the multipole expansion of the integrals dressed with the singles part of the eigenvector E^i_a that appears in the nominators of the triples equations:

$$(pq\bar{|}rs) = P^{qs}_{pr} \sum_t \left[E^q_t(pt|rs) - E^t_p(tq|rs)\right], \tag{37}$$

with the understanding that E_q^t is nonzero only if t is an index of an occupied and p of a virtual MO. A separate multipole expansion of the two terms in equation (37) gives

$$\left|\sum_t E_t^q(pt|rs)\right| \leq \sum_t |E_t^q| \left(\frac{M_{pt}^{(0)} M_{rs}^{(0)}}{R} + \frac{M_{pt}^{(1)} M_{rs}^{(0)} + M_{pt}^{(0)} M_{rs}^{(1)}}{R^2} + \frac{M_{pt}^{(2)} M_{rs}^{(0)} + 2M_{pt}^{(1)} M_{rs}^{(1)} + M_{pt}^{(0)} M_{rs}^{(2)}}{R^3} \right) + \mathcal{O}(R^{-4}) \tag{38}$$

$$\left|\sum_t E_p^t(tq|rs)\right| \leq \sum_t |E_p^t| \left(\frac{M_{tq}^{(0)} M_{rs}^{(0)}}{R'} + \frac{M_{tq}^{(1)} M_{rs}^{(0)} + M_{tq}^{(0)} M_{rs}^{(1)}}{R'^2} + \frac{M_{tq}^{(2)} M_{rs}^{(0)} + 2M_{tq}^{(1)} M_{rs}^{(1)} + M_{tq}^{(0)} M_{rs}^{(2)}}{R'^3} \right) + \mathcal{O}(R'^{-4}), \tag{39}$$

where R and R' denote the distances between the center of the orbital product rs and the centers of pt or tq, respectively. The first contribution is non-zero only if q is an occupied MO contributing to E_{μ_1} and the second contribution only if p is a virtual MO contributing to E_{μ_1}. Long-ranging charge-charge terms arise if p is a virtual MO located at or close to the electron-accepting chromophore and at the same time q an occupied MO at or close to the electron-donating chromophore. If the two terms are considered together the long-ranging $\mathcal{O}(R^{-1})$ and $\mathcal{O}(R'^{-1})$ contributions eventually cancel each other out if both distances are large compared to the distance between the centers of pt and tq and the dipole-monopole interactions become the leading non-vanishing terms in the multipole expansion of the dressed integrals:

$$\left|(pq\bar{|}rs)\right| \leq P_{pr}^{qs} \sum_t |E_t^q| \left(\frac{M_{pt}^{(1)} M_{rs}^{(0)}}{R^2} + \frac{M_{pt}^{(2)} M_{rs}^{(0)} + 2M_{pt}^{(1)} M_{rs}^{(1)}}{R^3} \right) + P_{pr}^{qs} \sum_t |E_p^t| \left(\frac{M_{tq}^{(1)} M_{rs}^{(0)}}{R^2} + \frac{M_{tq}^{(2)} M_{rs}^{(0)} + 2M_{tq}^{(1)} M_{rs}^{(1)}}{R^3} \right) + \mathcal{O}(R^{-4}) \tag{40}$$

For a long-range charge transfer state where the occupied and virtual natural transition orbitals (NTOs) are located on separate chromophores this will, however, only happen for rather large distances.

For the dressed integrals $(ai\bar{|}bj)$ appearing in the nominator of excited state doubles amplitudes of transitions dominated by one-electron excitations, the undressed orbital pair is always charge free and, hence, $\mathcal{O}(\mathcal{R}^{-3})$-decaying dipole-dipole interactions become the lowest non-vanishing order contributions to the multipole expansion for distances fulfilling

the above condition:

$$\left|(ai|\bar{b}j)\right| \leq 2P_{ab}^{ij}\left[\sum_c |E_c^i|\frac{M_{ac}^{(1)}M_{bj}^{(1)}}{R^3} + \sum_k |E_a^k|\frac{M_{ki}^{(1)}M_{bj}^{(1)}}{R^3}\right] + \mathcal{O}(R^{-4}) \tag{41}$$

$$\approx 2P_{ab}^{ij}\left[|\beta_{i\sigma^o}|\frac{M_{a\sigma^v}^{(1)}M_{bj}^{(1)}}{R^3} + |\beta_{a\sigma^v}|\frac{M_{\sigma^o i}^{(1)}M_{bj}^{(1)}}{R^3}\right] + O(R^{-4}) \tag{42}$$

In equation (42) we assumed for simplicity that E_{μ_1} is dominanted by a single pair of virtual $|\sigma^v\rangle$ and occupied NTOs $|\sigma^o\rangle$ with corresponding coefficients $\beta_{a\sigma^v}$ and $\beta_{i\sigma^o}$, i.e. that $E_a^i \approx \beta_{a\sigma^v}\beta_{i\sigma^o}$.

For local excitations where occupied and virtual NTOs are close to each other, only pairs ij contribute which are part of or close to the same chromophore and also the corresponding PNOs are close to this chromophore. However, for charge transfer excitations where occupied and virtual NTOs are spatially separated two different types of pairs ij are significant: Those where both LMOs i and j are close to the occupied NTO. For them the doubles amplitude matrices E_{ab}^{ij} have a rank of 1 (in the following called rank-1 pairs[74]) and one of their PNOs is close to the virtual NTO while the other is close to the occupied NTO. For the second class of pairs one LMO is close the occupied NTO while the other is close to the virtual NTO. Their doubles amplitude matrices have (for small molecular systems) a rank which can be as large as the number of virtual orbitals (in the following called rank-v pairs[74]) and all of their PNOs are located close to the virtual NTO.

We can now apply this for arriving at a scheme for selecting non-negligible LMO triples for the excited state eigenvectors. For this, we start from the (closed-shell) expression for the excited-state triples in the CCSDR(T) model:

$$\begin{aligned} R_{abc}^{ijk} =& \frac{1}{\Delta_{abc}^{ijk}+\omega}P_{abc}^{ijk}\Big\{\sum_{d\neq b} R_{ad}^{ij}(ck|bd) - \sum_{l\neq j} R_{ab}^{il}(ck|lj) + R_{ab}^{ij}[(ck|bb) - (ck|jj)] \\ &+ \sum_{d\neq b} t_{ad}^{ij}(ck|\bar{b}d) - \sum_{l\neq j} t_{ab}^{il}(ck|\bar{l}j) + t_{ab}^{ij}[(ck|\bar{b}b) - (ck|\bar{j}j)]\Big\}. \end{aligned} \tag{43}$$

The contributions obtained by applying the multipole expansion to the individual contributions to the excited state triples amplitudes are summarized in table I.

An analysis of the contributions given in table I leads to the following conclusions:

- Since the ground state doubles amplitudes are only significant if the virtuals are close to one of the LMOs ij, the long-ranging contributions to the integrals that arise from

TABLE I. Multipole expansion of the individual contributions to the excited state triples amplitudes. R_1 refers to the distance between the centers lk and bd, R_1' to the distance between ce abd bd, R_1'' to the distance between ck and ld, R_2 to the distance between mk and lj, R_2' to the distance between cd and lj, R_2'' to the distance between ck and le, R to the distance between ck and bd, R' to the distance between ck and lj.

Excited State Doubles Contributions

$$\left|\sum_d R^{ij}_{ad}(ck|bd)\right| \leq \sum_d |R^{ij}_{ad}| \left(\frac{M^{(1)}_{ck}M^{(0)}_{bd}}{R^2} + \frac{M^{(2)}_{ck}M^{(0)}_{bd} + 2M^{(1)}_{ck}M^{(1)}_{bd}}{R^3}\right) + \mathcal{O}(\mathcal{R}^{-7}),$$

$$\left|\sum_l R^{il}_{ab}(ck|lj)\right| \leq \sum_l |R^{il}_{ab}| \left(\frac{M^{(1)}_{ck}M^{(0)}_{lj}}{R'^2} + \frac{M^{(2)}_{ck}M^{(0)}_{lj} + 2M^{(1)}_{ck}M^{(1)}_{lj}}{R'^3}\right) + \mathcal{O}(\mathcal{R}^{-7})$$

Contributions to $t^{ij}_{ad}(ck\bar{|}bd)$

$$\left|\sum_d t^{ij}_{ad}\sum_l E^l_c(lk|bd)\right| \leq \sum_d |t^{ij}_{ad}| \sum_l |E^l_c| \left(\frac{M^{(0)}_{lk}M^{(0)}_{bd}}{R_1} + \frac{M^{(1)}_{lk}M^{(0)}_{bd} + M^{(0)}_{lk}M^{(1)}_{bd}}{R_1^2} + \frac{M^{(2)}_{lk}M^{(0)}_{bd} + 2M^{(1)}_{lk}M^{(1)}_{bd} + M^{(0)}_{lk}M^{(2)}_{bd}}{R_1^3}\right) + \mathcal{O}(\mathcal{R}^{-7})$$

$$\left|\sum_d t^{ij}_{ad}\sum_e E^k_e(ce|bd)\right| \leq \sum_d |t^{ij}_{ad}| \sum_e |E^k_e| \left(\frac{M^{(0)}_{ce}M^{(0)}_{bd}}{R_1'} + \frac{M^{(1)}_{ce}M^{(0)}_{bd} + M^{(0)}_{ce}M^{(1)}_{bd}}{R_1'^2} + \frac{M^{(2)}_{ce}M^{(0)}_{bd} + 2M^{(1)}_{ce}M^{(1)}_{bd} + M^{(0)}_{ce}M^{(2)}_{bd}}{R_1'^3}\right) + \mathcal{O}(\mathcal{R}^{-7})$$

$$\left|\sum_d t^{ij}_{ad}\sum_l E^l_b(ck|ld)\right| \leq 2\sum_d |t^{ij}_{ad}| \sum_l |E^l_b| \frac{M^{(1)}_{ck}M^{(1)}_{ld}}{R_1''^3} + \mathcal{O}(\mathcal{R}^{-7})$$

Contributions to $t^{il}_{ab}(ck\bar{|}lj)$

$$\left|\sum_l t^{il}_{ab}\sum_m E^m_c(mk|lj)\right| \leq \sum_l |t^{il}_{ab}| \sum_m |E^m_c| \left(\frac{M^{(0)}_{mk}M^{(0)}_{lj}}{R_2} + \frac{M^{(1)}_{mk}M^{(0)}_{lj} + M^{(0)}_{mk}M^{(1)}_{lj}}{R_2^2} + \frac{M^{(2)}_{mk}M^{(0)}_{lj} + 2M^{(1)}_{mk}M^{(1)}_{lj} + M^{(0)}_{mk}M^{(2)}_{lj}}{R_2^3}\right) + \mathcal{O}(\mathcal{R}^{-7})$$

$$\left|\sum_l t^{il}_{ab}\sum_d E^k_d(cd|lj)\right| \leq \sum_l |t^{il}_{ab}| \sum_d |E^k_d| \left(\frac{M^{(0)}_{cd}M^{(0)}_{lj}}{R_2'} + \frac{M^{(1)}_{cd}M^{(0)}_{lj} + M^{(0)}_{cd}M^{(1)}_{lj}}{R_2'^2} + \frac{M^{(2)}_{cd}M^{(0)}_{lj} + 2M^{(1)}_{cd}M^{(1)}_{lj} + M^{(0)}_{cd}M^{(2)}_{lj}}{R_2'^3}\right) + \mathcal{O}(\mathcal{R}^{-7})$$

$$\left|\sum_l t^{il}_{ab}\sum_e E^j_e(ck|le)\right| \leq 2\sum_l |t^{ij}_{ad}| \sum_e |E^j_e| \frac{M^{(1)}_{ck}M^{(1)}_{le}}{R_2''^3} + \mathcal{O}(\mathcal{R}^{-7})$$

the charge-carrying undressed orbital products bb and jj cancel mutually when the product ck is further away from j than the virtuals contributing to t^{ij}.

- The term $\sum_d t^{ij}_{ad}(ck|\bar{b}d)$ is only significant if ij is a strong GS and kj or ki a strong ES pair.

- Term $\sum_l t^{il}_{ab}(ck|\bar{l}j)$ is non-negligible if kj is a strong ES pair and i makes a strong GS pairs with any LMOs l for which $\int |\phi_l(\mathbf{r})\phi_j(\mathbf{r})|d\mathbf{r}$ or $\int |\phi_l \sum_d E^j_d(\mathbf{r})\phi_d(\mathbf{r})|d\mathbf{r}$ are non-negligible.

- $\sum_d R^{ij}_{ad}(ck|bd)$ is non-negligible for all triples where ij is a strong ES pair, but a restriction of k is not easily possible because of the long-ranging contribution from the charge-carrying orbital product bb.

- $\sum_l R^{il}_{ab}(ck|lj)$ is non-negligible for all ij for which there exists LMOs l for which $||\mathbf{R}^{il}||_F$ and $\int |\phi_l(\mathbf{r})\phi_j(\mathbf{r})|d\mathbf{r}$ are non-negligible, but again a restriction of k is not easily possible because of the charge-carrying orbital product jj

The fact that the distances R and R' (the terms involving the excited state doubles amplitudes) need to be large compared to the distance between the occupied and virtual NTO (for a cancellation of the long-range contributions) makes it difficult to restrict the index k of a LMO triple ijk to a local correlation domain. At least, it is not possible to restrict this index to form a pair ik or jk. We did not yet find an efficient way to restrict the index k of triples ijk for the general case where occupied and virtual NTO are spatially distant. However, for local excitations it is possible to construct the excited state triples list from the excited state pair information, since in such a case the occupied and virtual NTOs are very close and, hence, all LMOs ijk of the excited state triples amplitudes should be close to each other and close the chromophore. Hence, for the current first investigations only local excitations will be considered.

Furthermore, Eq. (43) shows that the excited state TNO basis has to describe the ground state doubles amplitudes t_{μ_2}, the excited state doubles amplitudes R_{μ_2}, and the undressed and R_1-dressed ERIs equally well. To achieve this we construct the approximate triples

density

$$D^{ijk}_{\tilde{a}\tilde{b}} = \frac{1}{6}\Big(S^{ijk,ij}_{\tilde{a}\bar{a}^0} D^{\mathrm{MP2},ij}_{\bar{a}^0\bar{b}^0} S^{ij,ijk}_{\bar{b}^0\tilde{b}} + S^{ijk,ik}_{\tilde{a}\bar{a}^0} D^{\mathrm{MP2},ik}_{\bar{a}^0\bar{b}^0} S^{ik,ijk}_{\bar{b}^0\tilde{b}} + S^{ijk,jk}_{\tilde{a}\bar{a}^0} D^{\mathrm{MP2},jk}_{\bar{a}^0\bar{b}^0} S^{jk,ijk}_{\bar{b}^0\tilde{b}} + S^{ijk,ij}_{\tilde{a}\bar{a}} D^{ex,ij}_{\bar{a}\bar{b}} S^{ij,ijk}_{\bar{b}\tilde{b}} + S^{ijk,ik}_{\tilde{a}\bar{a}} D^{ex,ik}_{\bar{a}\bar{b}} S^{ik,ijk}_{\bar{b}\tilde{b}} + S^{ijk,jk}_{\tilde{a}\bar{a}} D^{ex,jk}_{\bar{a}\bar{b}} S^{jk,ijk}_{\bar{b}\tilde{b}} \Big). \tag{44}$$

where $\mathbf{D}^{ex}$ refers to the approximate CIS(D) density (c.f. equations (18) and (19)) evaluated in the excited state PNO basis $\{\bar{a}\}$ and $\mathbf{D}^{\mathrm{MP2}}$ are the approximate MP2 densities (c.f. equations (16) and (17)) evaluated in the ground state PNO basis $\{\bar{a}^0\}$. Hence, the excited state TNO basis also needs to account for ground state information to be able to to approximate the ground state doubles amplitudes. The excited state pre-TNO basis is, thus, obtained by merging the excited state OSVs of the LMOs i, j and k. Since the excited state OSVs are already constructed such that they represent a suitable basis for integrals $(ai|bj)$ and $(ai\bar{|}bj)$ the pre-TNO basis obtained this way is also an adequate basis for the ground and excited state pair densities. The excited state TNOs are then obtained by diagonalizing the triples density $\mathbf{D}^{ijk}$. Afterwards, the Fock matrix is diagonalized in the excited state TNO basis.

Having selected a suitable basis for the excited state triples amplitudes (here: only for local excitations) the next step is to compute the excited state triples amplitudes in this local basis. Different strategies for their efficient computation will be discussed in the next section.

E. Evaluation of the Excited State Triples Amplitudes: T0 Approximation and Laplace Transformation

In a localized MO basis the evaluation of the triples amplitudes is complicated by the fact that the Fock matrix is no longer diagonal in a LMO basis so that instead of multiplying with the inverse of some orbital energy differences Δ^{ijk}_{abc} one has to solve (formally) a set of coupled linear equations. This problems appears already in local variants of CCSD(T) and several strategies have been proposed to tackle this: The neglect of the off-diagonal elements in the occupied/occupied block of the Fock matrix a simple and computationally inexpensive approximation, denoted as T0 approximation, for the triples amplitudes in local methods[17]. Even though, the T0 approximation performs well in many cases the neglect of F_{ij} can in certain cases lead to relatively large errors[18,46,86] which makes it desirable to have a possibility to include the triples correction in a more accurate way to verify results obtained

with the T0 approximation. This led Schütz[18] to the development of the T1 approximation which includes the couplings through F_{ij} to first order and corresponds to a modified first iteration of an iterative algorithm which can also be used to solve for the local CCSD(T) triples amplitudes. Even though, the T1 approximation, in contrast to the iterative solution, still avoids the I/O of triples amplitudes it is computationally far more expensive than the T0 approximation. In the context of a PNO-CCSD(T)(F12*) implementation[46] we proposed recently to use a numerical Laplace transformation to approximate the energy denominator. This leads to a systematically improvable accuracy (via the number of quadrature grid points) and also avoids the I/O of triples amplitudes which can even in a local implementation result in a severe computational bottleneck. Since these issues have not yet been studied for excitation energies, we implemented for the present work both the T0 approximation (CC3(T0)) and the Laplace transformation (LT-CC3) technique to investigate their performance for excitation energies.

Within the T0 approximation the excited state triples amplitudes are in the LMO and TNO basis approximated as:

$$\begin{aligned} R_{\bar{a}\bar{b}\bar{c}}^{ijk} = \frac{1}{\Delta_{\bar{a}\bar{b}\bar{c}}^{ijk} + \omega} P_{\bar{a}\bar{b}\bar{c}}^{ijk} \Big\{ & \sum_{\bar{d}} (\bar{c}k\hat{|}\bar{b}\bar{d}) \sum_{\bar{a}'\bar{d}'} S_{\bar{a}\bar{a}'}^{ijk,ij} R_{\bar{a}'\bar{d}'}^{ij} S_{\bar{d}'\bar{d}}^{ij,ijk} \\ & - \sum_{l} (\bar{c}k\hat{|}lj) \sum_{\bar{a}\bar{b}} S_{\bar{a}\bar{a}}^{ijk,il} R_{\bar{a}\bar{b}}^{il} S_{\bar{b}\bar{b}}^{il,ijk} \\ & + \sum_{\bar{d}} (\bar{c}k\bar{|}\bar{b}\bar{d}) \sum_{\bar{a}^0\bar{d}^0} S_{\bar{a}\bar{a}^0}^{ijk,ij} t_{\bar{a}^0\bar{d}^0}^{ij} S_{\bar{d}^0\bar{d}}^{ij,ijk} \\ & - \sum_{l} (\bar{c}k\bar{|}lj) \sum_{\bar{a}_{il}^0\bar{b}^0} S_{\bar{a}\bar{a}^0}^{ijk,il} t_{\bar{a}^0\bar{b}^0}^{il} S_{\bar{b}^0\bar{b}}^{il,ijk} \Big\}. \end{aligned} \tag{45}$$

with $\Delta_{\bar{a}\bar{b}\bar{c}}^{ijk} = F_{ii} + F_{jj} + F_{kk} - \epsilon_{\bar{a}} - \epsilon_{\bar{b}} - \epsilon_{\bar{c}}$ where $\epsilon_{\bar{a}}$ and F_{ii} denote the Fock matrix eigenvalues in the excited state TNO basis and the diagonal Fock matrix elements in the LMO basis, respectively. The PNO/TNO overlap matrices which are used to transform the virtual indices of the doubles amplitudes from the PNO to the TNO basis are defined as:

$$S_{\bar{a}\bar{b}}^{ijk,ij} = \sum_{a} d_{a\bar{a}}^{ijk} d_{a\bar{b}}^{ij} \, . \tag{46}$$

The implementation of the excited state triples amplitudes using a super matrix formulation as proposed by Noga and Valiron[87] is very similar to our previously published triples correction to PNO-CCSD(F12*). Thus, we do not repeat these equations here but refer to Ref. 46 for the details.

The Laplace transform of the energy denominator[88] can be expressed as

$$\frac{1}{\epsilon_i+\epsilon_j+\epsilon_k-\epsilon_a-\epsilon_b-\epsilon_c} = \int_0^\infty e^{-(\epsilon_i+\epsilon_j+\epsilon_k-\epsilon_a-\epsilon_b-\epsilon_c)x}dx \tag{47}$$

$$\approx \sum_z^{n_z} w_z e^{-(\epsilon_i+\epsilon_j+\epsilon_k-\epsilon_a-\epsilon_b-\epsilon_c)t_z} \tag{48}$$

where w_z denotes the quadrature weights, t_z the position and n_z the number of the grid points.[89,90] The advantage of using the Laplace transformation is that also the off-diagonal Fock matrix elements can be included without the need of an iterative solution scheme because the right hand side of Eq. (48) factorizable. For the excited state triples amplitudes we determne a new set of Laplace grid points in each CC3 iteration to account for the shift by the excitation energy ω which can have an influence on the accuracy of the Laplace transformation[89]. Applying the Laplace transformation to the excited state triples amplitudes leads to the expression:

$$\begin{aligned} R^{ijk}_{\bar{a}\bar{b}\bar{c}} = P^{ijk}_{\bar{a}\bar{b}\bar{c}} \sum_z^{n_L} w_z \Big\{ & \sum_{\bar{d}_{ijk}} (\bar{c}^z k^z \hat{|} \bar{b}^z \bar{d}) \sum_{\bar{a}'\bar{d}'} S^{ijk,ij,z}_{\bar{a}\bar{a}'} R^{i^z j^z}_{\bar{a}'\bar{d}'} S^{ij,ijk}_{\bar{d}'\bar{d}} \\ & - \sum_l (\bar{c}^z k^z \hat{|} l j^z) \sum_{\bar{a}'\bar{b}'} S^{ijk,il,z}_{\bar{a}\bar{a}'} R^{i^z l}_{\bar{a}'\bar{b}'} S^{il,ijk,z}_{\bar{b}'\bar{b}} \\ & + \sum_{\bar{d}} (\bar{c}^z k^z \bar{|} \bar{b}^z \bar{d}) \sum_{\bar{a}^0\bar{d}^0} S^{ijk,ij,z}_{\bar{a}\bar{a}^0} t^{i^z j^z}_{\bar{a}^0\bar{d}^0} S^{ij,ijk}_{\bar{d}^0\bar{d}} \\ & - \sum_l (\bar{c}^z k^z \bar{|} l j^z) \sum_{\bar{a}^0\bar{b}^0} S^{ijk,il,z}_{\bar{a}\bar{a}^0} t^{i^z l}_{\bar{a}^0\bar{b}^0} S^{il,ijk,z}_{\bar{b}^0\bar{b}} \Big\}. \end{aligned} \tag{49}$$

The grid point dependent LMOs $|i^z\rangle$ and TNOs $|\bar{a}^z\rangle$ are generated using grid point dependent transformation matrices

$$Y^z_{\mu\bar{a}_{ijk}} = \sum_a Y_{\mu a} e^{-(\epsilon_a+\frac{\omega}{6})t_z} d^{ijk}_{a\bar{a}_{ijk}}, \tag{50}$$

$$X^z_{\mu i} = \sum_j X_{\mu j} e^{(\epsilon_j-\frac{\omega}{6})t_z} T_{ij} m \tag{51}$$

where the matrices $\mathbf{Y}$ and $\mathbf{X}$ can contain the (unmodified) MO coefficients $C_{\mu p}$, or the coefficients for t_{μ_1} or R_{μ_1}-dressed particle and hole transformation matrices. The matrix T_{ij} transforms from the canonical MO to the LMO basis.

The grid point dependent PNO/TNO overlap matrices are defined as

$$S^{ijk,ij,z}_{\bar{a}_{ijk}\bar{b}_{ij}} = \sum_a d^{ijk}_{a\bar{a}_{ijk}} e^{-(\epsilon_a+\frac{\omega}{6})t_z} d^{ij}_{a\bar{b}_{ij}} \ , \tag{52}$$

and transform from the unmodified PNO to the grid point dependent TNO basis. Additionally, ground and excited state doubles amplitudes with one and two grid point dependent LMO indices are needed. Amplitudes with one grid point dependent LMO index are, similar as in the PNO-CCSD(T) implementation[46], calculated as

$$R^{ij^z}_{\bar{a}_{ij}\bar{b}_{ij}} = R^{ij}_{\bar{a}_{ij}\bar{b}_{ij}} T^z_{jj} + \sum_{k\neq j} T^z_{kj} \sum_{\bar{a}_{ik}\bar{b}_{ik}} S^{ij,ik}_{\bar{a}_{ij}\bar{a}_{ik}} t^{ik}_{\bar{a}_{ik}\bar{b}_{ik}} S^{ik,ij}_{\bar{a}_{ik}\bar{a}_{ij}} \tag{53}$$

and amplitudes with two grid point dependent LMO indices are obtained by applying the above equation to the remaining untransformed LMO index of $R^{ij^z}_{\bar{a}_{ij}\bar{b}_{ij}}$. The transformation matrix T^z_{ij} which transforms in equation (53) from the unmodified LMO basis to the grid point dependent LMO basis is given by

$$T^z_{ij} = \sum_k T_{ik} e^{(\epsilon_k - \omega)t_z} T_{jk} \ . \tag{54}$$

F. Triples Contributions to the Residual and the Transformations with the Jacobian

Since the triples contributions to the residual of the ground state cluster equations and the contraction of the Jacobian with a trial vector from the right are similar, we discuss them together with a focus on the latter case. We only describe the contributions beyond CCSD and refer the reader for the implementation of the CCSD vector function and Jacobian transformations in a PNO basis to Refs. 45,76.

Table II summarizes the CC3 contributions to the singles and doubles parts of the transformed vector. It can be seen that the time-determining $\mathcal{O}(\mathcal{N}^7)$-scaling steps of the canonical implementation become in the local implementation linear scaling in the limit that the number of significant LMO pairs and triples grows only linear with the system size and the number of PNOs and TNOs per, respectively, pair and triple is constant. For the terms $\rho^{ij,G_{DT}}_{\bar{a}\bar{b}}$,$\rho^{ij,I}_{\bar{a}\bar{b}}$ this is a natural consequence from the use of TNOs where the summations over occupied orbitals can be restricted to LMOs which are part of the sparse triples list $\{ijk\}$. For $\rho^{ij,H}_{\bar{a}\bar{b}}$ the contributions from the ground state wave function can be restricted to triples jkl where at least one LMO forms an excited state pair with i. Similarly, the excited state contribution can be restricted to triples jkl where at least one LMO forms an excited state or a ground state pair with i. Similar considerations make it possible to restrict the summation over LMOs l in the equations for the excited state triples amplitudes.

We follow in the implementation of the triples contribution for PNO-CC3 a similar strategy as for PNO-CCSD(T) and PNO-CCSD where only compact intermediates and integrals are stored on disc. For PNO-CC3, a large number of different two-electron integrals would have to be stored on disc since the integrals $(ck\hat{|}bd)$ and $(ck\hat{|}lj)$ are cubic in t_{μ_1} and, additionally, the integrals $(ck\bar{|}bd)$ and $(ck\bar{|}lj)$ contain three R_{μ_1}-dressed indices, respectively. Instead, we compute all integrals needed for the CC3 contributions from the AO basis in each iteration.

TABLE II. Explicit expressions for the PNO-CC3 contributions to the singles and doubles part of the Jacobian transformed vector ρ_{μ_1} and ρ_{μ_2}. For ease of notation the triples and pair indices of PNOs and TNOs are not given explicitly. To differentiate between PNOs and TNOs the PNOs are denoted by a tilde.

	formal scaling	
Contribution	CC3	PNO-CC3
$\rho^I_{ai} = 2\sum_{jk}\sum_{\bar{a}} d^{ijk}_{a\bar{a}} \sum_{\bar{b}\bar{c}} \left(R^{ijk}_{\bar{a}\bar{b}\bar{c}} - R^{ijk}_{\bar{c}\bar{b}\bar{a}}\right)\left(2(j\bar{b}\|k\bar{c}) - (j\bar{c}\|k\bar{b})\right)$	$\mathcal{O}(\mathcal{N}^6)$	$\mathcal{O}(\mathcal{N}^2)$
$\rho^{ij,G}_{\bar{a}'\bar{b}'} = 2\sum_{\bar{a}\bar{b}}\sum_{k} S^{ij,ijk}_{\bar{a}'\bar{a}} S^{ij,ijk}_{\bar{b}'\bar{b}} P^{ij}_{\bar{a}\bar{b}} \sum_{\bar{c}\bar{d}} \left(2R^{ijk}_{\bar{c}\bar{b}\bar{d}} - R^{ijk}_{\bar{c}\bar{d}\bar{b}} - R^{ijk}_{\bar{d}\bar{c}\bar{b}}\right)(\bar{a}\bar{c}\hat{\|}k\bar{d})$ $+ 2\sum_{\bar{a}^0\bar{b}^0}\sum_{k} S^{ij,ijk}_{\bar{a}'\bar{a}^0} S^{ij,ijk}_{\bar{b}'\bar{b}^0} P^{ij}_{\bar{a}^0\bar{b}^0} \sum_{\bar{c}^0\bar{d}^0} \left(2t^{ijk}_{\bar{c}^0\bar{b}^0\bar{d}^0} - t^{ijk}_{\bar{c}^0\bar{d}^0\bar{b}^0} - t^{ijk}_{\bar{d}^0\bar{c}^0\bar{b}^0}\right)(\bar{a}^0\bar{c}^0\bar{|}k\bar{d}^0)$	$\mathcal{O}(\mathcal{N}^7)$	$\mathcal{O}(\mathcal{N})$
$\rho^{ij,H}_{\bar{a}'\bar{b}'} = -2\sum_{\bar{a}\bar{b}} P^{ij}_{\bar{a}\bar{b}} \sum_{kl} S^{ij,jkl}_{\bar{a}'\bar{a}} S^{ij,jkl}_{\bar{b}'\bar{b}} \sum_{\bar{c}} \left(2R^{jkl}_{\bar{b}\bar{a}\bar{c}} - R^{jkl}_{\bar{c}\bar{a}\bar{b}} - R^{jkl}_{\bar{b}\bar{c}\bar{a}}\right)(ki\hat{\|}l\bar{c})$ $- 2\sum_{\bar{a}^0\bar{b}^0} P^{ij}_{\bar{a}^0\bar{b}^0} \sum_{kl} S^{ij,jkl}_{\bar{a}'\bar{a}^0} S^{ij,jkl}_{\bar{b}'\bar{b}^0} \sum_{\bar{c}} \left(2t^{jkl}_{\bar{b}^0\bar{a}^0\bar{c}^0} - t^{jkl}_{\bar{c}^0\bar{a}^0\bar{b}^0} - t^{jkl}_{\bar{b}^0\bar{c}^0\bar{a}^0}\right)(ki\bar{|}l\bar{c}^0)$	$\mathcal{O}(\mathcal{N}^7)$	$\mathcal{O}(\mathcal{N})$
$\rho^{ij,I}_{\bar{a}'\bar{b}'} = 2\sum_{\bar{a}\bar{b}}\sum_{k} S^{ij,ijk}_{\bar{a}'\bar{a}} S^{ij,ijk}_{\bar{b}'\bar{b}} P^{ij}_{\bar{a}\bar{b}} \sum_{\bar{c}} \left(R^{ijk}_{\bar{a}\bar{b}\bar{c}} - R^{ijk}_{\bar{c}\bar{b}\bar{a}}\right)\hat{F}_{k\bar{c}}$ $2\sum_{\bar{a}\bar{b}}\sum_{k} S^{ij,ijk}_{\bar{a}'\bar{a}^0} S^{ij,ijk}_{\bar{b}'\bar{b}^0} P^{ij}_{\bar{a}^0\bar{b}^0} \sum_{\bar{c}^0} \left(t^{ijk}_{\bar{a}^0\bar{b}^0\bar{c}^0} - t^{ijk}_{\bar{c}^0\bar{b}^0\bar{a}^0}\right)\bar{F}_{k\bar{c}^0}$	$\mathcal{O}(\mathcal{N}^6)$	$\mathcal{O}(\mathcal{N})$

G. Solution of the Eigenvalue Problem in a State-Specific Basis

The excited state PNO basis depends on the nature of the excited state through the excited state single amplitudes R_{μ_1} and the excitation energy ω. Since these quantities are at the beginning not known, the eigenvalue problem is solved self-consistently, i.e. a new

PNO basis is constructed and the Davidson algorithm is restarted if the excitation energy or the excited state singles amplitudes deviate significantly from those used for the PNO construction[74]. To trace the change of the singles amplitudes the overlap

$$^{(j)}s = \frac{^{(0)}R_{\mu_1} \cdot {}^{(j)}R_{\mu_1}}{||^{(0)}R_{\mu_1}|| \cdot ||^{(j)}R_{\mu_1}||} \tag{55}$$

between the initial singles $^{(0)}R_{\mu_1}$ from which the PNOs were constructed and the singles amplitudes $^{(j)}R_{\mu_1}$ in the j-th iteration is computed. If it does not fulfill

$$1 - {}^{(j)}s \geq 10 \cdot ||^{(j)}\sigma|| \tag{56}$$

the Davidson algorithm is restarted with new PNOs which are constructed from the current guess of ω and R_{μ_1}.

To avoid a quadratic scaling with respect to the number of states to be computed we employ a single state Davidson solver. In order to converge for singles and doubles methods (CC2, ADC(2), CCSD, etc.) to higher-lying eigenvalues Wielandt deflation is applied as a rank-1 update to the Jacobian as described in Ref. 74.

For PNO-CC3, however, a non-linear eigenvalue problem has to be solved if the I/O of triples amplitudes should be avoided. For a non-linear eigenvalue problem the (standard) deflation techniques as described in Ref. 74 cannot be used anymore.

On the other hand, the solution of a nonlinear eigenvalue problem could be avoided by solving the eigenvalue problem for the full Jacobian in the singles, doubles, and triples space. This would, however, require that the triples basis vectors as well as their linear transformations with $\mathbf{A}$ are stored on disc for several iterations and states. For the singles and doubles amplitudes this is in a PNO-based implementation not a problem. But even in a local implementation the storage requirements and the I/O for the triples amplitudes can become demanding, if not prohibitive.

Hence, in our implementation we follow a different route for solving the excited state eigenvalue problem which is similar to strategies used in canonical CC3 implementations: First, the PNO-CCSD eigenvalue problem ist solved using the Davidson algorithm described above and the eigenvectors and corresponding state-specific PNO information is ordered according to the PNO-CCSD excitation energies. Subsequently, the PNO-CC3 ground state equations are solved and the PNO-CCSD eigenvectors are used as start guess for the PNO-CC3 eigenvectors. After contruction of a new state-specific PNO basis from the converged

PNO-CCSD singles vector and excitation energy the doubles part of the PNO-CCSD doubles amplitudes is projected onto this basis and the nonlinear PNO-CC3 eigenvalue problem is solved in this basis by refining the PNO-CCSD vectors using a direct inversion of the iterative subspace (DIIS) algorithm.

III. COMPUTATIONAL DETAILS

Our implementation is part the pnoccsd program[45,48] in the development version of the TURBOMOLE quantum chemistry program package[91]. All calculations employ the frozen core approximation with the $1s$ orbitals of second-row elements excluded from the post-Hartree-Fock calculations. The Hartree-Fock calculations have been done with the dscf[92] and the canonical CC3 reference calculations with the ccsdf12 program of TURBOMOLE. For the benchmark calculations on the Schreiber test set[93] as well as for the calculations on alkene chains we used the def2-TZVP basis sets[94]. If not otherwise noted the corresponding standard auxiliary basis sets have been used[95,96] for the resolution-of-the-identity (RI) approximation of the two-electron integrals in post-HF calculations. The geometries of Schreibers test set have been taken from Ref. 93.

For the PNO-CC3 and PNO-CC3(T0) calculations we used intrinsic bond orbitals[97] (IBOs) as localization scheme for the occupied orbital space and carried out calculations with PNO thresholds of $-\log(T_{\mathrm{PNO}}) = 6, \ldots, 9$. The OSV, TNO and pair thresholds are directly coupled to the PNO threshold as $T_{\mathrm{OSV}} = 0.1 \cdot T_{\mathrm{PNO}}$, $T_{\mathrm{TNO}} = T_{\mathrm{PNO}}$ and $T_{pair} = (0.1 \cdot T_{\mathrm{PNO}})^{\frac{2}{3}}$. The list of LMO triples for the triple excitation part of the eigenvectors are selected as described in section II E. If not noted otherwise, a fixed number of four Laplace grid points ($n_L = 4$) has been used (*vide infra*) for the Laplace transformation of the triples amplitudes.

IV. RESULTS AND DISCUSSION

A. Choice of the Laplace Grid

To investigate the dependence of the accuracy on the number of Laplace grid points the first three excited states of a subset of molecules from Schreibers test set (Ethene, Butadiene, Cyclopropene, Formaldehyde, Acetone and Formamide) have been computed with a varying number of Laplace grid points ($n_L = 1, \ldots, 5$) as well as with the T0 approximation.

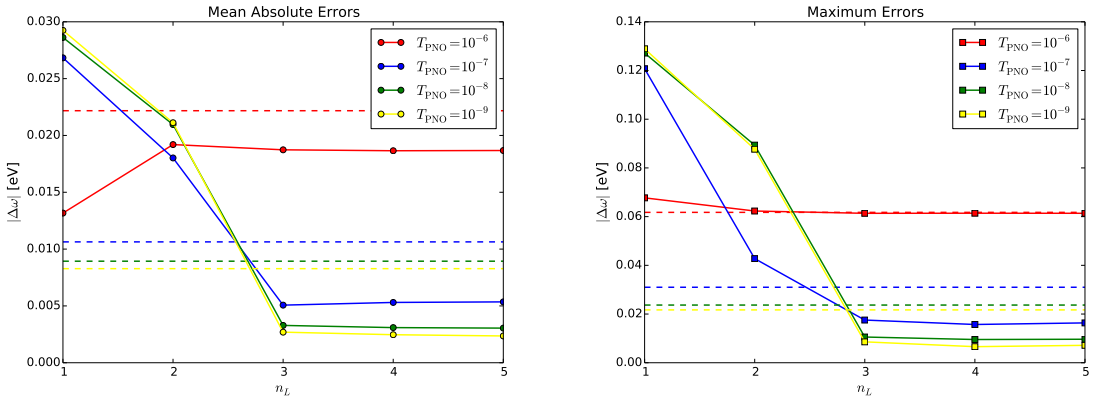


FIG. 1. Mean absolute and maximum errors for PNO-CC3 as function of the number of Laplace grid points. Dotted lines indicate the PNO-CC3(T0) errors for the respective PNO-threshold.

For these calculations the def2-TZVP in combination with the large def2-QZVPP auxiliary basis[98] has been used in order to reduce the errors arising from the different use of the RI approximation in canonical and PNO-based CC3. The errors have been computed with respect to canonical CC3.

Figure 1 shows the results of the statistical analysis of these states and molecules based on the mean absolute errors (MAE) and maximum errors (MAX). It can be seen that for PNO-CC3 the errors are already converged with $n_L = 3$ for all investigated PNO thresholds. For the loose threshold $T_{\mathrm{PNO}} = 10^{-6}$ the benefit from the Laplace transformation is small, irrespective of the number of grid points. The maximum errors for PNO-CC3 and PNO-CC3(T0) are basically identical since the errors are dominated for this PNO threshold by the PNO and TNO approximations. For the remaining PNO thresholds we find with $n_L = 3$ a decrease of the errors by a factor of up to 4. For $n_L < 3$ the errors are larger than for the T0 approximation since in this case the largest error arises from the non-converged Laplace transformation.

The fact that the MAE for PNO-CC3 is for the loose threshold $T_{\mathrm{PNO}} = 10^{-6}$ lowest with $n_L = 1$ may be explained by a fortunate unsystematic error compensation. Figure 1 suggests that for $n_L < 3$ the errors for $T_{\mathrm{PNO}} = 10^{-7}$ are lower than for the tighter PNO thresholds $T_{\mathrm{PNO}} = 10^{-8}$ and $T_{\mathrm{PNO}} = 10^{-9}$. This is due to the fact that the truncation

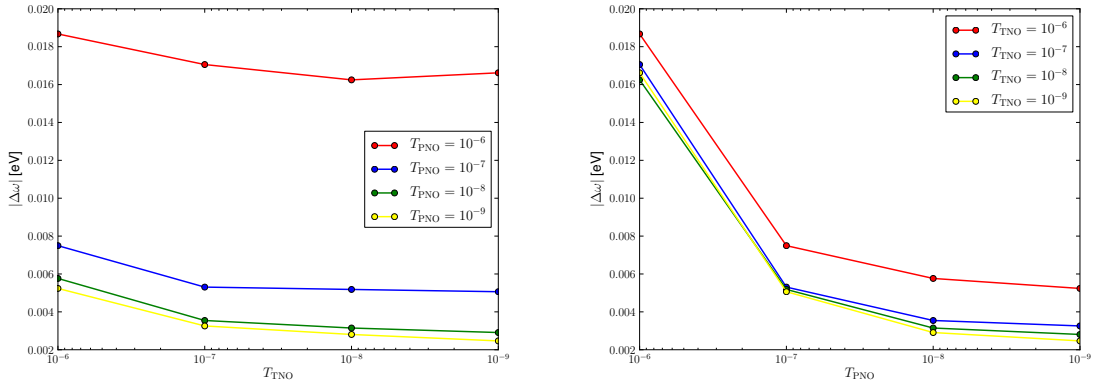


FIG. 2. Mean absolute errors of a subset of Schreibers test set as function of the TNO threshold (left side) and as function of the PNO threshold (right side).

of the virtual space does for these settings not cause the dominant errors for such few Laplace grid points but the errors of the Laplace transformation of the triples amplitudes are dominating. In combination with an error compensation this might lead to the fact that the errors for $T_{\mathrm{PNO}} = 10^{-7}$ are lower than for tighter thresholds. However, as soon as the Laplace transformation errors are converged the expected behavior (tighter PNO thresholds yield smaller errors) is recovered.

B. Choice of the TNO threshold

After having defined a suitable number of Laplace grid points, the next essential step is to investigate the definition of a TNO threshold for the truncation of the excited state (ES) TNO expansion. To investigate the dependence of the errors on the ES TNO threshold we performed PNO-CC3 ($n_L = 4$) calculations with different combinations of PNO and TNO thresholds (the same thresholds were used for ground and excited state calculations) using the same set of molecules and excited states as described in the previous section. Again, the calculations have been performed in the def2-TZVP orbital basis and the def2-QZVPP auxiliary basis.

The results are presented in figure 2. The dependence of the errors on the TNO threshold with a fixed PNO threshold (left side of figure 2) is rather weak compared to the errors as

function of the PNO threshold with a fixed TNO threshold (right side of figure 2). This can be explained by the fact that the TNO space is already restricted by the PNO truncation but the opposite is not the case. Lowering the PNO threshold also yields to an enlarged TNO space. Figure 2 suggests that the PNO-CC3 results are not significantly improved if the TNO threshold is chosen tighter than the corresponding PNO threshold. This is the same finding as made by Schmitz and Hättig[46]in the context of their (ground state) PNO-CCSD(T) implementation. Hence, we suggest to set the threshold for the selection of the excited state TNOs to the same value as the ground state TNO selection threshold $T_{\mathrm{TNO}} = T_{\mathrm{PNO}}$.

C. Benchmark Results for PNO-CC3 Excitation Energies

For benchmarking the accuracy of PNO-CC3 and PNO-CC3(T0) we chose Schreibers test set[93] which consists of 160 excited states in 27 and molecules. Since no CC3 calculations were in Schreibers study carried out for the nucleobases Adenine, Thymine, Uracil and Cytosine we chose the states added to Schreibers test set in Ref. 99 for these molecules. At the time this manuscript was written, the calculations on Benzoquinone were not finished and, hence, this molecule has been excluded from the statistical analysis.

Figure 3 shows the results obtained from a statistical analysis over all states included in Schreibers test set. For comparison, we also show our previously published results for PNO-CCSD. It can be seen that the MAE and maximum errors over all states show a rapid convergence towards the canonical result for PNO-CC3 ($n_L = 4$) . While the MAE for PNO-CC3 behaves very similar to the one of PNO-CCSD the maxium errors are approximately twice as large. PNO-CC3(T0) in contrast, shows significantly larger errors and a slower convergence than PNO-CC3. While the errors of PNO-CC3 and PNO-CC3(T0) are very similar for the loose threshold $T_{PNO} = 10^{-6}$, the deviations between both methods become larger as the PNO threshold decreases. This is especially pronounced for states with a significant doubles contribution ($\%T_1 \leq 80\%$) where the maximum error for PNO-CC3(T0) does not drop below 0.15 eV even for tight thresholds such as $T_{PNO} = 10^{-8}$. Apparently, the errors arising from the T0 approximation are for doubly excited states in a similar regime as the PNO/TNO truncation errors and, hence, hinder a rapid convergence with respect to the PNO threshold. For singly excited states ($\%T_1 > 80\%$), in contrast, the T0 approximation

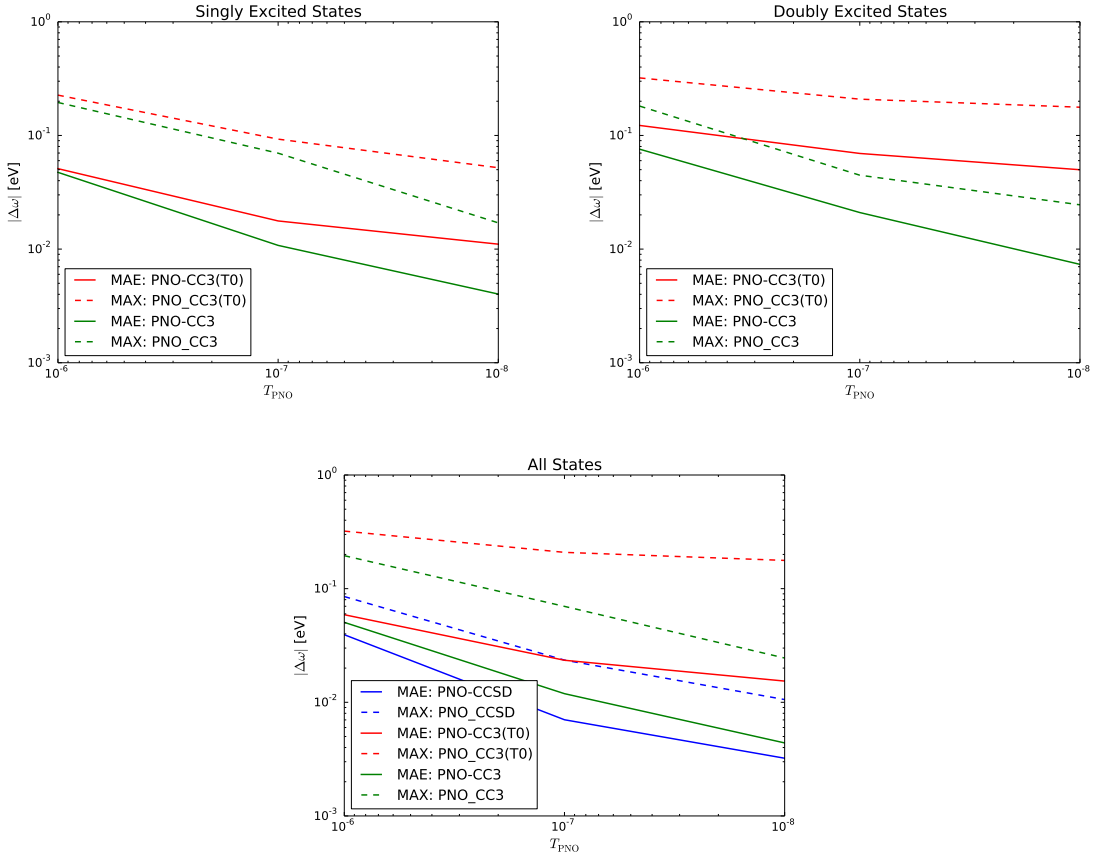


FIG. 3. Mean absolute and maximum errors for PNO-CC3 and PNO-CC3(T0) with respect to the canonical method obtained by a statistical analysis over the excited states included in Schreibers test set. Additionally, singly excited states ($\%T_1 > 80\%$) and states with a significant doubles contribution ($\%T_1 \leq 80\%$) are analyzed separately in the upper figures

shows a MAE of about 0.01 eV and a maximum error which is approximately twice as large than for its Laplace transformed counterpart and, hence, performs significantly better than for doubly excited states.

Even though the T0 approximation yields for single replacement dominated transitions results within the CC3 error bar (MAE of 0.01 eV) when tight PNO thresholds such as $T_{PNO} = 10^{-8}$ are used, it is only applicable with prudence and the more important double replacements become for the description of an excited state the less reliable the results become even when tight PNO thresholds are used.

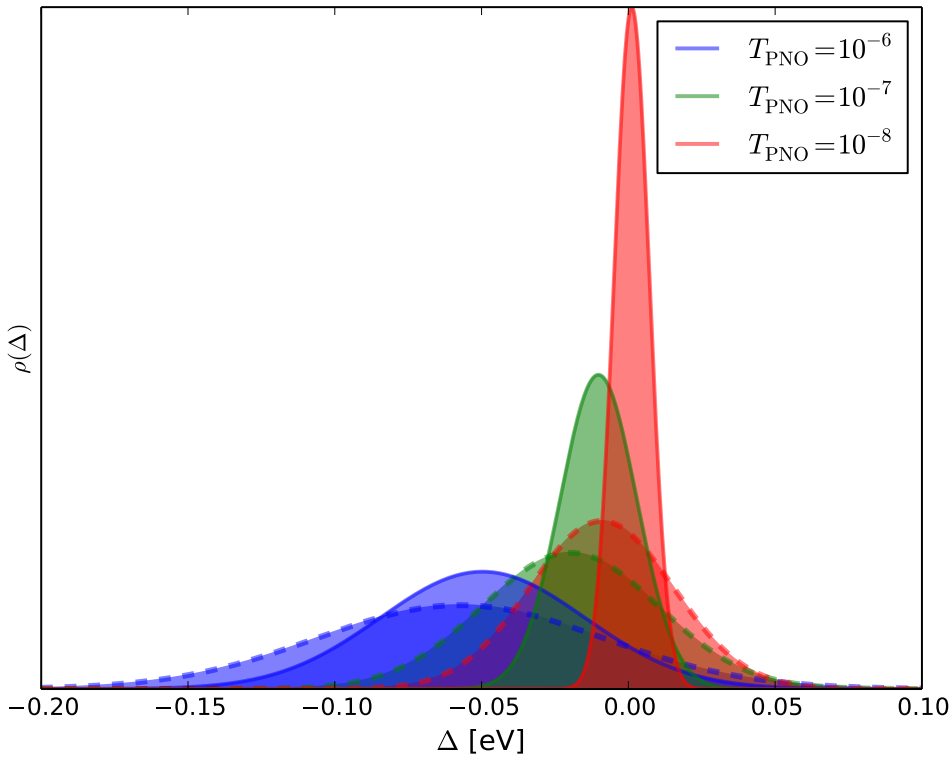


FIG. 4. Normal distributions of the deviations from the canonical reference results centered around the ME. Dashed lines indicate the PNO-CC3(T0) results while solid lines denote the PNO-CC3 results.

D. Efficiency of the Implementation

Having investigated the errors introduced by the PNO-CC3(T0) and PNO-CC3 approximations, the next step is the investigation of the efficiency of these methods. For this, it should first be investigated how the number of excited state TNOs depends on the chromophore and system size.

1. Scaling of the Number of Excited State TNOs

To investigate how the number of excited state TNOs scales with the chromophore size and how this compares to the GS TNOs and GS and ES PNOs and OSVs, we performed

calculations on increaslingly large alkene chains (C_nH_{n+2}) in the def2-TZVP basis using a PNO threshold of 10^{-7} and plotted the total numbers of these virtual orbitals against the system size. The first excited state of these alkene chains was used since it is delocalized over the whole molecule and, hence, suitable for comparing the number of virtual orbitals for the ground state against those for the excited state. The results are shown in table III and the left side of figure 5. Obviously, the number of TNOs is generally larger than the number of PNOs and OSVs due to the larger correlation domains needed for the triples while the total number of OSVs is the least. Furthermore, the number of TNOs generally increases far more rapid than the number of PNOs and OSVs for small systems (up to C_8H_{10}). For larger systems, all types of virtual orbitals behave very similar and in the asymptotic limit the virtual space spanned by these orbitals increases linearly with the system size (see table III). However, the number of GS and ES TNOs converges significantly slower towards this limit than the number of PNOs and OSVs. Furthermore, the ES TNOs converge slower towards this asympotic limit than GS TNOs while the number of GS and ES PNOs and OSVs show a more similar convergence behavior.

We have also carried out calculations on increaslingly large carboxylic acids where the first excitation only takes place on the π-system of the carboxylic group. The results are shown at the right-hand side of figure 5 which shows that the number of GS virtual orbitals shows in the asymptotic limit the same linear scaling as for the alkene chains. The number of ES TNOs and ES PNOs, however, converges towards a constant number since these are

TABLE III. Exponential laws for the dependence of the number of different virtual orbitals on the system/chromophore size for the alkene chains obtained from a linear regression analysis ($C_{20}H_{22}$ - $C_{24}H_{26}$).

Orbital type	Scaling
ES TNOs	$10^{3.19} \cdot \mathcal{N}^{1.45}$
GS TNOs	$10^{4.32} \cdot \mathcal{N}^{1.22}$
ES PNOs	$10^{3.25} \cdot \mathcal{N}^{0.97}$
GS PNOs	$10^{2.55} \cdot \mathcal{N}^{1.13}$
ES OSVs	$10^{2.08} \cdot \mathcal{N}^{0.98}$
GS OSVs	$10^{1.55} \cdot \mathcal{N}^{1.04}$

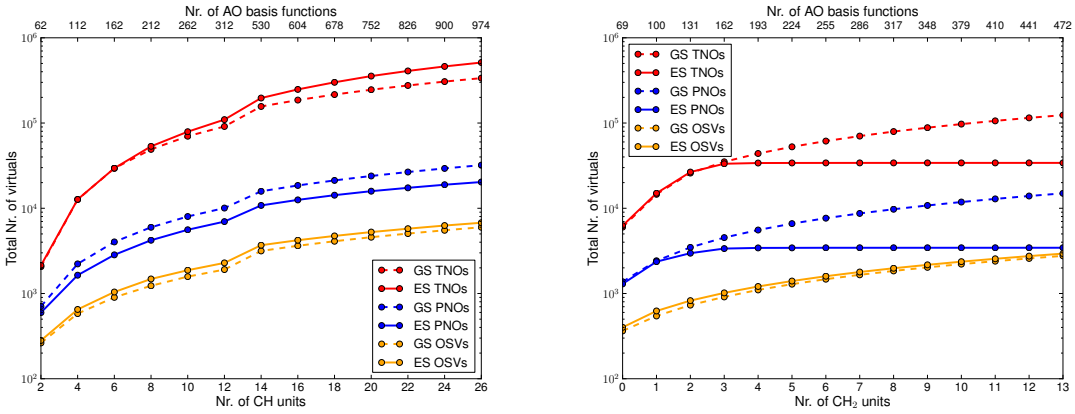


FIG. 5. Increase of the total number of different virtual orbitals with respect to the system size. The left figure shows the results obtained for alkene chains (C_nH_{n+2}) and the right figure shows the results for the carboxylic acids ($C_nH_{2n+1} - COOH$).

constructed such that they are spatially restricted to the chromophore region, which in this case is independent of the system size. The excited state OSVs do not share this feature since they are constructed by merging the excited state and ground state OSV correlation domains.

It can be summarized that the TNOs for excited states show similar features as excited state PNOs[78]: The number of excited state TNOs grows in the asymptotic limit linearly with the system size. Similar as for the ground state TNOs, also the number of excited state TNOs is significantly larger than the respective number of PNOs and OSVs. However, the number of TNOs for excited states is not significantly larger than for the ground state, even though the convergence towards a linear scaling is slightly slower.

2. Scaling of the Jacobian Right Transformation

In the previous section it was shown that the number of excited state TNOs scales linearly with the size of the chromophore as it is required for a linear scaling number of excited state triples amplitudes. It is now of interest how the actual wall-time for the Jacobian right transformation scales with the system size and how the Laplace transformation for PNO-CC3 affects the efficiency. Therefore, we performed calculations on increasingly large alkene

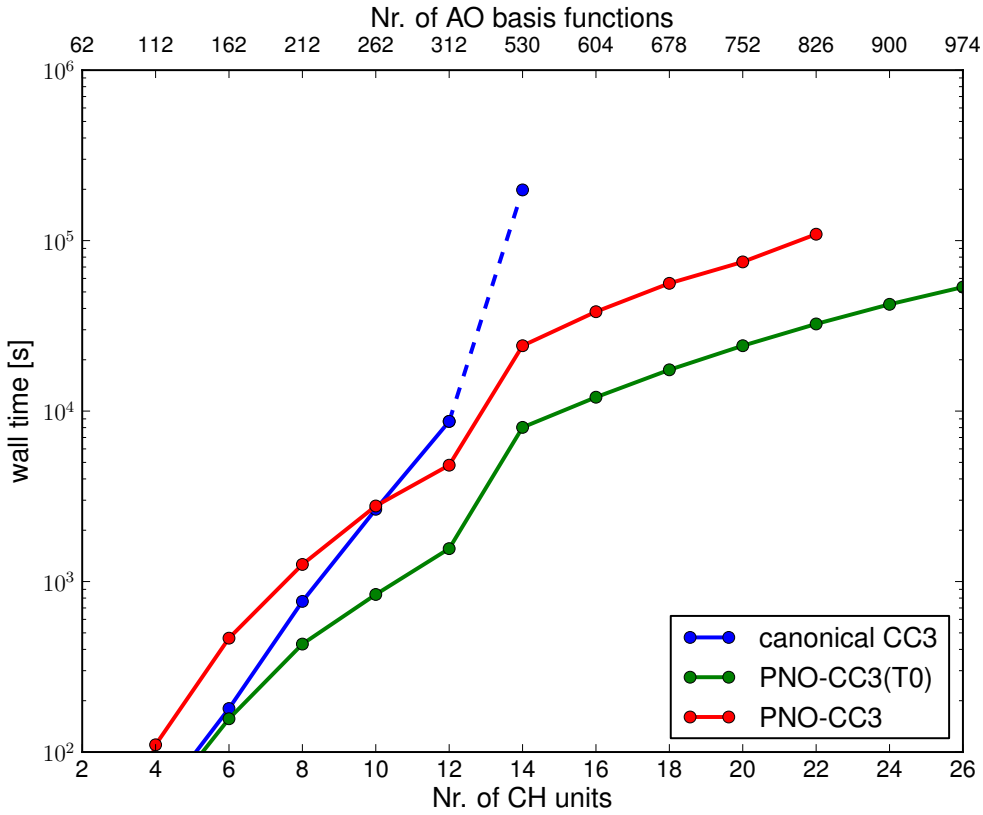


FIG. 6. The total wall-time as function of the system size obtained from canonical CC3, PNO-CC3(T0) and PNO-CC3 calculations on alkene chains. For canonical CC3 the last point was obtained by considering the fraction between the wall-time needed for the computation of the ground state vector function T_{GS} and the wall-time needed for the Jacobian right transformation T_{ES} for $C_{12}H_{14}$: $\frac{T_{\mathrm{ES}}}{T_{\mathrm{GS}}} = 1.88$. Since for canonical CC3 the computation of the Jacobian right transformation for $C_{14}H_{16}$ was not possible, the last point the exponential law was obtained from, was computed according to $T_{\mathrm{GS}} * 1.88 = T_{\mathrm{ES}}$.

chains in the TZVP basis. A PNO threshold of 10^{-7} was chosen and for the PNO-CC3 calculations three Laplace grid points ($n_L = 3$) were used. All calculations were performed on nodes with two Dual AMD EPYC 7000-Series CPUs (16 cores were used), 256 GB of DDR4 RAM and 3.8 TB SSD Micron 5200 hard discs.

For canonical CC3 we were not able to perform excited state calculations on molecules larger than $C_{12}H14$. Therefore, we estimated the wall-time of the next larger alkene molecule

TABLE IV. Exponential laws of the computational time for a Jacobian right transformation for canonical CC3, PNO-CC3(T0) and PNO-CC3 obtained from a linear regression of the curves shown in figure 6. For details it is referred to the text and figure 6.

Method	Scaling
Canonical CC3	$10^{-24.82} \cdot \mathcal{N}^{5.90}$
PNO-CC3(T0)	$10^{-10.52} \cdot \mathcal{N}^{3.11}$
PNO-CC3	$10^{-10.92} \cdot \mathcal{N}^{3.35}$

$C_{14}H_{16}$ by taking the ratio of the wall-time needed for the computation of the ground state vectors function and the Jacobian right transformation of $C_{12}H_{14}$. This ratio was then used to estimate the wall-time for a Jacobian right transformation based on the wall-time needed for the computation of the ground state vector function of $C_{14}H_{16}$. It was found by a linear regression analysis between $C_{12}H_{14}$ and $C_{14}H_{16}$ that for such rather small molecules the scaling of the canonical method with respect to the system size is in the order of $\mathcal{O}(\mathcal{N}^{5.90})$. Hence, the scaling of canonical CC3 is in this regime still dominated by the $\mathcal{O}(\mathcal{N}^6)$-scaling CC3 contributions to the Jacobian transformed vector, i.e. the ρ^{I} contributions to the transformed singles and doubles vectors, while the $\mathcal{O}(\mathcal{N}^7)$-scaling regime is not accessible for us.

However, for PNO-CC3 and PNO-CC3(T0) the scaling of the Jacobian right transformation is in the range of $\mathcal{O}(\mathcal{N}^3)$ and, hence, significantly larger systems are accessible. Even for $C_{24}H_{26}$, the PNO implementation is significantly faster than canonical CC3 is for $C_{14}H_{16}$. Furthermore, figure 6 shows that PNO-CC3 with $n_L = 3$ is approximately by a factor of three more expensive than the T0 approximation. For both methods the transformation of 3-index integrals from the AO to the TNO basis is the time-determining step since in our preliminary implementation since we do not screen the TNO coefficients yet for the R_{μ_1}-dressed integrals. Nevertheless, our implementation of the PNO based CC3 Jacobian right transformation shows a similar scaling as our previously published PNO-CCSD implementation for excitation energies[76]. It is only restricted to smaller systems due to the fact that the TNO basis is larger than the PNO basis.

V. SUMMARY AND CONCLUSIONS

We presented the first implementation of a local correlation based triples model for excitation energies. Performing a multipole based analysis of the excited state triples amplitudes revealed that a TNO basis for excited states can for non-local excitations not be constructed from the excited state (and ground state) PNO basis since this would lead to a neglect of important triples contributions. A solution to this problem for non-local excitations is subject to on-going work in our group. Consequently, for a first implementation and testing, we only considered local excitations. For these excitations the excited state TNO basis can be obtained from ground and excited state pair/PNO information.

However, applying our implementation of PNO-CC3 excitation energies to a large and diiverse test set, showed that PNO-CC3 already yields with moderate PNO/TNO thresholds of 10^{-7} mean absolute errors below the CC3 intrinsic error bar of about 0.01 eV. To obatin such an accuracy we had to employ the Laplace transformation of the energy denominator of the excited state triples amplitudes to also take the coupling between triple excitations into account. Comparing the results of PNO-CC3 to PNO-CC3(T0) showed that the error of the T0 approximation is most severe for states with a significant double excitation contribution. Here, PNO-CC3(T0) shows a very slow convergence with respect to the PNO/TNO selection threshold. For singly excited states, in contrast, PNO-CC3 and PNO-CC3(T0) show similar results.

Concerning the efficiency of the implementation it could be shown that our PNO based implementation of CC3 excitation energies scales as $\mathcal{O}(\mathcal{N}^3)$ with the system size. PNO-CC3 seems to be by the factor of Laplace grid points more expensive than PNO-CC3(T0). Furtheremore, it could be shown that the number of excited state TNOs scales linearly with the system size. The excited state TNO basis, however, needs to be larger than the ground state TNO basis due to the combination of ground and excited state information.

The results presented here, pave the way for the application of PNO-based local correlation models including triple excitations to the computation of excitation energies. Once the left CCSD eigenvectors are obtained, excitation energies can also be computed using the computationally less demanding but similarly accurate perturbative triples corrections CCSDR(T) and CCSDR(3).

REFERENCES

[1]M. Ziolkwski, B. Jansik, T. Kjaergaard and P. Jørgensen, J. Chem. Phys. **133**, 014107 (2010).

[2]K. Kristensen, M. Ziolkowski, B. Jansik, T. Kjaergaard and P. Jørgensen, J. Chem. Theory Comput. **7**, 1677 (2011).

[3]I. M. Hoyvik, K. Kristensen, B. Jansik and P. Jørgensen, J. Chem. Phys. **136**, 014105 (2012).

[4]K. Kristensen, T. Kjaergaard, I. M. Hoyvik, P. Ettenhuber, P. Jørgensen, B. Jansik, S. Reine and J. Jakowski, Mol. Phys. **111**, 1196 and 1210 (2013).

[5]S. Li, J. Ma and Y. Jiang, J. Comput. Chem. **23**, 237 (2002).

[6]S. Li, J. S. W. Li and Y. Jiang, J. Chem. Phys. **125**, 074109 (2006).

[7]W. Li, P. Piecuch, J. R. Gour and L. S, J. Chem. Phys. **131**, 114109 (2009).

[8]W. Li and P. Piecuch, J. Phys. Chem. A. **114**, 8644 (2010).

[9]W. Li and P. Piecuch, J. Phys. Chem. A. **114**, 6721 (2010).

[10]Y. Guo, W. Li and S. Li, J. Phys. Chem. A. **118**, 8996 (2014).

[11]W. Li and S. Li, S. Sci. China. **57**, 78 (2014).

[12]G. Rauhut, P. Pulay and H.-J. Werner, J. Comput. Chem. **19**, 1241 (1998).

[13]M. Schütz, G. Hetzer and H.-J. Werner, J. Chem. Phys. **111**, 5691 (1999).

[14]C. Hampel and H.-J. Werner, J. Chem. Phys. **104**, 6286 (1996).

[15]M. Schütz, Phys. Chem. Chem. Phys. **4**, 3941 (2002).

[16]M. Schütz and F. R. Manby, Phys. Chem. Chem. Phys. **5**, 3349 (2003).

[17]M. Schütz and H.-J. Werner, Chem. Phys. Lett. **318**, 370 (2000).

[18]M. Schütz, Chem. Phys. Lett. **130**, 9986 (2000).

[19]H. Stoll, J. Chem. Phys. **97**, 8449 (1992).

[20]H. Stoll, Chem. Phys. Lett. **191**, 548 (1992).

[21]H. Stoll, Phys. Rev. B: Condens Matter Matter Phys. **46**, 6700 (1992).

[22]J. Friedrich, M. Hanrath and M. Dolg, J. Chem. Phys. **126**, 154110 (2007).

[23]J. Friedrich and M. Dolg, J. Chem. Phys. **129**, 244105 (2008).

[24]J. Friedrich and M. Dolg, J. Chem. Theory Comput. **5**, 287 (2009).

[25]J. Friedrich, J. Chem. Theory Comput. **8**, 1597 (2012).

[26]J. Friedrich and K. Walczak, J. Chem. Theory Comput. **9**, 408 (2013).

[27]J. Friedrich and J. Hähnchen, J. Chem. Theory. Comput. **9**, 5381 (2013).

[28]W. Meyer. Methods of Electronic Structure Theory. Plenum Press, New York, 3 edition, 1977.

[29]W. Meyer, Theor. Chem. Acc. **35**, 277 (1974).

[30]W. Meyer, J. Chem. Phys. **58**, 1017 (1973).

[31]W. Meyer, Int. J. Quantum Chem. **S5**, 341 (1971).

[32]R. Ahlrichs, F. Driessler, H. Lischka, V. Staemmler and W. Kutzelnigg, J. Chem. Phys. **62**, 1235 (1975).

[33]R. Ahlrichs and F. Driessler, Theor. Chem. Acc. **36**, 275 (1975).

[34]V. Staemmler and R. Jaquet, Theor. Chem. Acc. **59**, 487 (1981).

[35]F. Neese, A. Hansen and D. G. Liakos, J. Chem. Phys. **131**, 064103 (2009).

[36]F. Neese, A. Hansen and F. Wennmohs, S. Acc. Chem. Res. **42**, 641 (2009).

[37]F. Neese., Wennmohs and A. Hansen, J. Chem. Phys. **130**, 114108 (2009).

[38]D. G. Liakos, A. Hansen and F. Neese, J. Chem. Theory Comput. **7**, 76 (2011).

[39]A. Hansen, D. G. Liakos and F. Neese, J. Chem. Phys. **135**, 214102 (2011).

[40]C. Riplinger and F. Neese, J. Chem. Phys. **138**, 034106 (2013).

[41]J. L. Whitten, J. Chem. Phys. **58**, 4496 (1973).

[42]B. I. Dunlap, J. W. D. Conolly and J. R. Sabin, J. Chem. Phys. **71**, 3396 (1973).

[43]D. P. Tew and C. Hättig, Int. J. Quantum Chem. **113**, 224 (2013).

[44]C. Hättig, D. P. Tew and B. Helmich, J. Chem. Phys. **136**, 204105 (2012).

[45]G. Schmitz, C. Hättig and D. P. Tew, Phys. Chem. Chem. Phys. **16**, 22167 (2014).

[46]G. Schmitz and C. Hättig, J. Chem. Phys. **145**, 234107 (2016).

[47]C. Krause and H.-J. Werner, Phys. Chem. Chem. Phys. **14**, 7591 (2012).

[48]G. Schmitz, B. Helmich and C. Hättig, Mol. Phys. **111**, 2463 (2013).

[49]J. Yang, G. K. L. Chan, F. R. Manby, M. Schütz and H.-J. Werner, J. Chem. Phys. **136**, 144105 (2012).

[50]Y. Guo1, K. Sivalingam, E. F. Valeev, and F. Neese, J. Chem. Phys. **144**, 094111 (2016).

[51]F. Menezes, D. Kats and H.-J. Werner, J. Chem. Phys. **145**, 124115 (2016).

[52]P. Pulay, Chem. Phys. Lett. **100**, 151 (1983).

[53]S. Saebø and P. Pulay, Chem. Phys. Lett. **113**, 13 (1985).

[54]S. Saebø and P. Pulay, Ann. Rev. Phys. Chem. **44**, 213 (1993).

[55]P. Pulay and S. Saebø, Theor. Chim. Acta. **69**, 357 (1986).

[56]S. Saebø and P. Pulay, J. Chem. Phys. **86**, 914 (1987).

[57]S. Saebø and P. Pulay, J. Chem. Phys. **88**, 1884 (1988).

[58]M. S. Frank, G. Schmitz and C. Hättig, Mol. Phys. **115**, 343 (2017).

[59]P. Pinski and F. Neese, J. Chem. Phys. **148**, 031101 (2018).

[60]P. Pinski and F. Neese, J. Chem. Phys. **150**, 164102 (2019).

[61]O. Christiansen, H. Koch and P. Jørgensen, Chem. Phys. Lett. **243**, 409 (1995).

[62]D. Kats, T. Korona and M. Schütz, J. Chem. Phys. **125**, 104106 (2006).

[63]T. Korona and H.-J. Werner, J. Chem. Phys. **118**, 3006 (2003).

[64]T. D. Crawford and R. A. King, Chem. Phys. Lett. **366**, 611 (2002).

[65]D. Mester, P. R. Nagy and M. Kállay, J. Chem. Phys. **146**, 194102 (2017).

[66]P. Baudin and K. Kristensen, J. Chem. Phys. **144**, 224106 (2016).

[67]A. K. Dutta, F. Neese and R. Izsák, J. Chem. Phys. **145**, 034102 (2016).

[68]A. K. Dutta, M. Saitow, C. Riplinger, F. Neese and R. Izsák, J. Chem. Phys. **148**, 244101 (2018).

[69]A. K. Dutta, M. Saitow, B. Demoulin, F. Neese and R. Izsák, J. Chem. Phys. **150**, 164123 (2019).

[70]M. Nooijen and R. J. Bartlett, J. Chem. Phys. **107**(17), 6812 (1997).

[71]O. Christiansen, H. Koch and P. Jørgensen, J. Chem. Phys. **105**, 1451 (1996).

[72]H. Koch, O. Christiansen, P. Jørgensen, A. M. J. Sánchez de Méras and T. Helgaker, J. Chem. Phys. **106**, 1808 (1997).

[73]C. Peng, M. C. Clement and E. F. Valeev, J. Chem. Theory Comput. **14**, 5597 (2018).

[74]B. Helmich and C. Hättig, J. Chem. Phys. **139**, 084114 (2013).

[75]B. Helmich and C. Hättig, Comput. Theor. Chem. **1040 - 1041**, 35 (2014).

[76]M. S. Frank and C. H. ttig, J. Chem. Phys. **148**, 134102 (2018).

[77]O. Christiansen, H. Koch and P. Jørgensen, J. Chem. Phys. **103**, 7429 (1995).

[78]B. Helmich and C. Hättig, J. Chem. Phys. **135**, 214106 (2011).

[79]H. Koch, O. Christiansen, , R. Kobayashi, P. Jørgensen and T. Helgaker, Chem. Phys. Lett. **228**, 233 (1994).

[80]O. Christiansen, H. Koch, A. Halkier, P. Jørgensen, T. Helgaker and A. Sánchez de Merás, J. Chem. Phys. **105**, 6921 (1996).

[81]F. Neese., Wennmohs and A. Hansen, J. Chem. Phys. **130**, 114108 (2009).

[82]J. Yang, Y. Kurashige, F. R. Manby and G. K. L. Chan, J. Chem. Phys. **134**(4), 044123

(2011).

[83]C. Riplinger and F. Neese, J. Chem. Phys. **139**, 134101 (2013).

[84]K. Raghavachari, G. W.Trucks, J. A. Pople and M. Head-Gordon, Chem. Phys. Lett. **157**, 479 (1989).

[85]G. Hetzer, P. Pulay and H.-J. Werner, J. Chem. Phys. **290**, 143 (1998).

[86]G. Schmitz and C. Hättig, J. Chem. Theory Comput. **13**, 2623 (2017).

[87]J. Noga and P. Valiron, Mol. Phys. **103**, 2123 (2005).

[88]J. Almlöf, Chem. Phys. Lett. **181**, 319 (1991).

[89]M. Häser and J. Almlöf, J. Chem. Phys. **96**, 489 (1992).

[90]A. K. Wilson and J. Almlöf, Theor. Chim. Acta. **95**, 49 (1997).

[91]R. Ahlrichs, M. Bär, M. Häser, H. Horn and C. Kälmel, Chem. Phys. Lett. **162**, 165 (1989).

[92]M. Häser and R. Ahlrichs, J. Comput. Chem. **10**, 104 (1989).

[93]M. Schreiber, M. R. Silva-Junior, S. P. A. Sauer and W. Thiel, J. Chem. Phys. **128**, 134110 (2008).

[94]F. Weigend and R. Ahlrichs, Phys. Chem. Chem. Phys. **7**, 3297 (2005).

[95]F. Weigend, A. Köhn and C. Hättig, J. Chem. Phys. **116**, 3175 (2002).

[96]F. Weigend, M. Häser, H. Patzelt and R. Ahlrichs, Chem. Phys. Lett. **294**, 143 (1998).

[97]G. Knizia, J. Chem. Theory Comput. **9**, 4834 (2013).

[98]A. Hellweg, C. Hättig, S. Höfener and W. Klopper, Theor. Chem. Acc. **117**, 587 (2007).

[99]D. Kánnár and P. G. Szalay, J. Chem. Theory Comput. **10**(9), 3757 (2014). PMID: 26588520.

VII. CONCLUSIONS AND OUTLOOK

In this work the PNO framework has been extended towards gradients (geometry optimizations) and excited state triples methods.

For the PNO-MP2 gradient the Lagrangian has been augmented by localization constraint (here: for Forster-Boys[184] localization) to take the missing invariance of rotations among the occupied MOs into account (if the PNO basis is truncated or pairs are neglected). However, even neglecting the relaxation of the PNOs and OSVs as well as the gradient of the PNO-related energy corrections led to accurate geometries (with respect to canonical MP2) even for systems whose geometry is entirely determined by weak interactions such as water clusters. For such systems it was also found that tighter PNO thresholds are required to obtain reasonable geometries. While rather loose thresholds such as $T_{\mathrm{PNO}} = 10^{-6}$ are sufficient to determine geometries of systems without weak interactions quite accurately they completely fail for describing weak interactions. For such systems thresholds of at least $T_{\mathrm{PNO}} = 10^{-7}$ are required. Another important finding is that for PNO-based geometry optimizations the convergence thresholds have to be mainly energy based and less coordinate based and that loose PNO thresholds show in many cases (especially for molecules with floppy groups such as methyl groups with low rotational barriers) convergence problems if the convergence thresholds are not adapted. At the time when our PNO-MP2 gradient results were published it was unclear whether this was due to the aforementioned approximations in the PNO-MP2 gradient which cause small mismatches between the calculated gradient and actual PES or due to an intrinsic roughness of the PES for loose PNO thresholds. However since Pinski and Neese[151,152] reported similar convergence difficulties for loose PNO thresholds with their DLPNO-MP2 gradient[151,152], it suggests that this is an intrinsic feature of the PNO approximation itself, i.e. it can be attributed to a slight roughness of the PNO-MP2 PES.

Concerning the efficiency, it was found that the time-determining step in the PNO-

MP2 gradient calculation arises from non-correlated HF contributions (solution of the CPHF equations). While the correlation contribution to the gradient scales as $\mathcal{O}(\mathcal{N}^3)$ the HF contribution scales as $\mathcal{O}(\mathcal{N}^4)$. This is due to the use of the RI approximation for the HF exchange integrals and prevents the PNO-MP2 gradient from being applied to large molecular systems. The time-determining step in the correlation contribution to the gradient is the computation of some three-index integrals since at the time the PNO-MP2 gradient was published it was not adapted for making use of a local-RI approximation. For this reason, we also implemented the use of exact exchange integrals making use of Kohns conjecture[185] which states that the HF exchange contribution can be implemented in a linear-scaling fashion[186] if the HOMO-LUMO gap is sufficiently large. Furthermore, we also adapted the correlation contribution to the gradient such that the local-RI approximation can be used. However, a thorough testing of these two additional implementations is remaining.

The HF Coulomb integrals are currently computed using the RI approximation (RI-J). A significant reduction of the computational costs could be obtained by combining the RI-J approximation with the multipole accelaration for the HF Coulomb integrals where the Coulomb operator is split into a far-field and a near-field part and only the near-field part is computed analytically while the far-field contribution is computed using multipole estimates of the Coulomb integrals[187]. Using PAOs as intermediate basis in the PNO construction may also make it possible to compute the correlation contribution in a linear-scaling fashion. Combining these two techniques could in the future then lead to linear-scaling and accurate PNO-MP2 gradients.

Since this work shows the general applicability of PNO-based local correlation methods for molecular geometry optimizations, it would be highly desirable to implement PNO-based gradients for higher-order methods such as CCSD and CCSD(T). In the long term it might also be interesting to investigate the applicability of the PNO

approximation in the computation of vibrational frequencies which require the calculation of the second derivative with respect to nuclear coordinates. Furthermore, the accuracy of the PNO-MP2 gradient in molecular dynamics simulations should be investigated in the future. Combining the accuracy of MP2 with the speed-up of the PNO approximation would enable the simulation of systems which are currently only treatable accessible with DFT methods. This would especially be interesting for the investigation of solvent effects and biologically relevant system due to the ability of MP2 to describe weak interactions accurately.

For excitation energies this work has first shown that the PNO approximation with state-specific PNOs is able to reproduce the canonical CCSD results with high precision and efficiency. Already moderate PNO threshold yielded mean absolute errors (MAEs) of below 0.01 eV in a large and diverse test set consisting of local and Rydberg excitations. It could also be shown that the implementation of the PNO-CCSD Jacobian right transformation is highly efficient, i.e. molecules with about 100 atoms could be calculated within a few days (on a single node) which is by far out-of-reach for a canonical CCSD implementation (without making use of MPI parallelization).

It was found that charge-transfer states need to be treated with special care. The previously found difficulty of PNO-CC2 in describing charge-transfer states[23] reappear in PNO-CCSD. A solution could be presented (the use of the pre-PNO basis for certain LMO pairs) which does neither deterioate the accuracy nor the efficiency of the implementation. Hence, this work is represents the first implementation of CCSD excitation energies in a local framework which is equally efficient for local and charge-transfer states while preserving the accuracy ($\approx$ 0.01 eV) needed to retain the accuracy of higher-order methods which also include connected triples excitations.

To investigate the performance of the PNO approximation for such triples models we chose the CC3 model since it was shown to significantly improve CCSD results

for single and double excitations (in contrast to CCSDT-1 and CCSDT-2) and is, from a perturbation theory point-of-view, the most thoroughly derived one among the existing iterative triples models.

A suitable local (TNO) basis could be derived by a thorough analysis of the excited triples amplitudes based on multipole expansion-based arguments. This analysis showed that the extension of the ground state TNO approximation is not straightforward since the excited state TNOs on the one side, should be restricted to the chromophore region but, on the other side, they also have to approximate the ground and excited state doubles amplitudes equally well. This results in the fact that the excited state TNO basis cannot simply obtained from information in the excited state PNO basis but that also ground state information has to be taken into account.

Furthermore, we used Laplace transformation techniques to derive an excited state triples method (PNO-CC3) which is able to converge towards the canonical result arbitrarily close (depending on the number of Laplace grid points) since the use of the T0 approximation[188] (PNO-CC3(T0)) for the triples amplitudes prevents such a convergence. We found that three Laplace grid points are usually sufficient to obtain converged results (with respect to the number of Laplace grid points) such that the errors of a PNO-CC3 approximation are not dominated by the numerical Laplace transformation. This results in an increase of the computational time roughly by a factor of three. However, it is still far more efficient than the iterative solution of the excited triples amplitudes as proposed by Werner and coworkers[189] which is approximately by a factor of ten more expensive than the T0 approximation[189]. The T1 approximation[189], in contrast, carries the same problem as the T0 approximation, i.e. it is not able to generally converge towards the canonical result.

We applied the methods PNO-CC3 and PNO-CC3(T0) to a large and diverse test set to investigate the accuracy and limitations of these methods. It was found that the errors arising from the T0 approximations are for excited states much

more pronounced than they are for the ground state (in case of PNO-CCSD(T0)). Especially for excited states with a significant double excitation character it was found that PNO-CC3 yields significantly more accurate results than PNO-CC3(T0). Already moderate PNO thresholds yield for PNO-CC3 errors below the method-intrinsic error bar. However, considering the error bar of CCSD with respect to CC3 it could be concluded that also the T0 approximation is able to significantly improve the CCSD results with moderate PNO thresholds.

For charge-transfer states we met some difficulties (large, slowly convergent errors) with our current definition of relevant excited state LMO triples. It could be shown that the large errors obtained for such states arise solely from the triples selection but not from the representation of the virtual space for a triple. A thorough analysis showed that important LMO triples are not considered if the excited state triples list is solely obtained from pair information (ground and/or excited state pairs). A solution to this problem could not be implemented up to now. But one possibility might be to construct a specialized and larger PNO basis which the excited state triples are then determined from.

Nonetheless, it was possible to present the first implementation of an excited state triples methods within a local correlation framework. Calculations with more than 50 atoms and approximately 1000 basis functions were possible. A more efficient implementation might be possible by using PAOs as an intermediate basis. The adaptive PAO construction presented by Schmitz and Hättig, which does not require any real-space cutoffs, should also be extendable to excited-state calculations and could increase the computational efficiency of CC3 calculations significantly.

In the long term also the computation of excited-state properties and gradients as well as transition moments and oscillator strengths with PNO-based methods would be highly desirable. For this, the computation of the left eigenvectors is required which have to be consistent with the right eigenvectors in terms of the PNO, local RI, ... basis. Once the left CCSD eigenvectors are available, the computationally

less demanding but similarly accurate (as compared to CC3) non-iterative triples models CCSDR(T), CCSDR(3) and CCSDR(T)(a*) could also be implemented.

REFERENCES

[1]M. Born and J. R. Oppenheimer. Zur Quantentheorie der Molekeln. Ann. Phys. **84**, 457 (1927).

[2]J. C. Slater. Notes on Hartree's method. Phys. Rev. **35**, 210 (1930).

[3]V. Fock. Näherungsmethode zur Lösung des quantenmechanischen Mehrkörperproblems. Zeitschrift für Physik. **61**, 126 (1930).

[4]C. C. J. Roothaan. Self-Consitent Field Theory for Open Shells of Electronic Systems. Rev. Mod. Phys. **32**, 179 (1960).

[5]P. Hohenberg and W. Kohn. Inhomogeneous Electron Gas. Phys. Rev. **136**, B864 (1964).

[6]W. Kohn and L. J. Sham. Self-Consistent Equations Including Exchange and Correlation Effects. Phys. Rev. **140**, A1133 (1965).

[7]S. Grimme, J. Antony, S. Ehrlich and H. Krieg. A consistent and accurate ab initio parametrization of density functional dispersion correction (DFT-D) for the 94 elements H-Pu. J. Chem. Phys. **132**, 154104 (2010).

[8]E. Caldeweyher, S. Ehlert, A. Hansen, H. Neugebauer, S. Spicher, C. Bannwarth and S. Grimme. A generally applicable atomic-charge dependent London dispersion correction. J. Chem. Phys. **150**, 154122 (2019).

[9]E. Runge and E. K. U. Gross. Density-functional theory for time-dependent systems. Phys. Rev. Lett. **52**, 997 (1984).

[10]E. K. U. Gross and W. Kohn. Local density-functional theory of frequency-dependent linear response. Phys. Rev. Lett. **55**, 2850 (1985).

[11]A. Dreuw and M. Head-Gordon. Single-reference ab initio methods for the calculation of excited states of large molecules. Chem. Rev. **105**, 4009 (2005).

[12]C. Lee, W. Yang and G. Parr. Development of the Colle-Salvetti correlation-energy formula into a functional of the electron density. Phys. Rev. B. **37**, 785 (1988).

[13]A. D. Becke. Density-functional exchange-energy approximation with correct asymptotic behaviour. Phys. Rev. A. **38**, 3098 (1988).

[14]A. D. Becke. Density-Functional Thermochemistry. III. The Role of Exact Exchange. J. Chem. Phys. **98**, 5648 (1993).

[15]T. Yanai, D. P. Tew and N. C. Handy. A new hybrid exchange-correlation functional using the Coulomb-attenuating method (CAM-B3LYP). Chem. Phys. Lett. **393**, 51 (2004).

[16]Q. Wu and T. V. Voorhis. Direct optimization method to study constrained systems within density-functional theory. Phys. Rev. A. **024502**, 72 (2005).

[17]F. Coester. Bound states of a many-particle system. Nucl. Phys. **7**, 421 (1958).

[18]F. Coester and H. Kümmel. Short-range correlations in nuclear wave functions. Nucl. Phys. **17**, 477 (1960).

[19]J. Da Providência. Variational approach to the many-body problem. Nucl. Phys. **61**, 87 (1965).

[20]J. Čížek. On the Correlation Problem in Atomic and Molecular Systems. Calculation of Wavefunction Components in Ursell-Type Expansion Using Quantum-Field Theoretical Methods. J. Chem. Phys. **45**, 4256 (1966).

[21]O. Sinanoğlu. Many-Electron Theory of Atoms and Molecules. I. Shells, Electron Pairs vs Many-Electron Correlations. J. Chem. Phys. **36**, 706 (1961).

[22]B. Helmich and C. Hättig. Local pair natural orbitals for excited states. J. Chem. Phys. **135**, 214106 (2011).

[23]B. Helmich and C. Hättig. A pair natural orbital implementation of the coupled cluster model CC2 for excitation energies. J. Chem. Phys. **139**, 084114 (2013).

[24]B. Helmich and C. Hättig. A pair natural orbital based implementation of ADC(2)-x: Perspectives and challenges for response methods for singly and

doubly excited states in large molecules. Comput. Theor. Chem. **1040 - 1041**, 35 (2014).

[25]J. Geertsen, M. Rittby and R. J. Bartlett. The equation-of-motion coupled-cluster method: Excitation energies of Be and CO. Chem. Phys. Lett. **164**, 57 (1989).

[26]H. Koch, H. J. A. Jensen, P. Jørgensen and T. Helgaker. Excitation energies from the coupled cluster singles and doubles linear response function (CCSDLR). Applications to Be, CH^+, CO, and H_2O. J. Chem. Phys. **93**(5), 3345 (1990).

[27]H. J. Monkhorst. Calculation of properties with the coupled-cluster method. Int. J. Quantum Chem. **12**(S11), 421 (1977).

[28]E. Dalgaard and H. J. Monkhorst. Some aspects of the time-dependent coupled-cluster approach to dynamic response functions. Phys. Rev. A. **28**, 1217 (1983).

[29]D. Mukherjee and P. Mukherjee. A response-function approach to the direct calculation of the transition-energy in a multiple-cluster expansion formalism. Chem. Phys. **39**(3), 325 (1979).

[30]S. Ghosh, D. Mukherjee and S. N. Bhattacharyya. A spin-adapted linear response theory in a coupled-cluster framework for direct calculation of spin-allowed and spin-forbidden transition energies. Chem. Phys. **72**(1), 161 (1982).

[31]S. Ghosh and D. Mukherjee. Use of cluster expansion techniques in quantum chemistry. A linear response model for calculating energy differences. Proc. Indian Acad. Sci. (Chem. Sci.). **93**(6), 947 (1984).

[32]H. Koch and P. Jørgensen. Coupled cluster response functions. J. Chem. Phys. **93**(5), 3333 (1990).

[33]J. F. Stanton and R. J. Bartlett. The equation of motion coupled-cluster method. A systematic biorthogonal approach to molecular excitation energies, transition probabilities, and excited state properties. J. Chem. Phys. **98**, 7029 (1993).

[34]H. Sekino and R. J. Bartlett. A linear response, coupled-cluster theory for

excitation energy. Int. J. Quantum Chem. **S18**, 255 (1984).

[35]T. Helgaker and P. Jørgensen, Analytical calculation of geometrical derivatives in molecular electronic structure theory, in Advances in Quantum Chemistry, edited by P.-O. Løwdin, volume 19 of Advances in Quantum Chemistry, pp. 183 – 245. Academic Press, 1988.

[36]C. Møller, and M. S. Plesset. Note on an Approximation Treatment for Many-Electron Systems. Phys. Rev. **46**, 618 (1934).

[37]K. Raghavachari, G. W.Trucks, J. A. Pople and M. Head-Gordon. A fifth-order perturbation comparison of electron correlation theories. Chem. Phys. Lett. **157**, 479 (1989).

[38]T. Helgaker, P. Jørgensen and J. Olsen. Molecular Electronic-Structure Theory. Wiley, New York, 2000.

[39]O. Christiansen, C. Hättig and J. Gauss. Polarizabilities of CO, N_2, HF, Ne, BH, and CH^+ from ab initio calculations: Systematic studies of electron correlation, basis set errors, and vibrational contributions. J. Chem. Phys. **109**(12), 4745 (1998).

[40]O. Christiansen, P. Jørgensen and C. Hättig. Response functions from Fourier component variational perturbation theory applied to a time-averaged quasienergy. Int. J. Quantum Chem. **68**(1), 1 (1998).

[41]O. Christiansen, H. Koch and P. Jørgensen. The second-order approximate coupled cluster singles and doubles model CC2. Chem. Phys. Lett. **243**, 409 (1995).

[42]J. F. Stanton and J. Gauss. Perturbative treatment of the similarity transformed Hamiltonian in equation-of-motion coupled-cluster approximations. J. Chem. Phys. **103**(3), 1064 (1995).

[43]S. R. Gwaltney, M. Nooijen and R. J. Bartlett. Simplified methods for equation-of-motion coupled-cluster excited state calculations. Chem. Phys. Lett. **248**(3), 189 (1996).

[44]M. Head-Gordon, R. J. Rico, M. Oumi and T. J. Lee. A doubles correction to electronic excited states from configuration interaction in the space of single substitutions. Chem. Phys. Lett. **219**, 21 (1994).

[45]D. Kánnár, A. Tajti and P. G. Szalay. Accuracy of Coupled Cluster Excitation Energies in Diffuse Basis Sets. J. Chem. Theory Comput. **13**(1), 202 (2017).

[46]J. J. Goings, M. Caricato, M. J. Frisch and X. Li. Assessment of low-scaling approximations to the equation of motion coupled-cluster singles and doubles equations. J. Chem. Phys. **141**(16), 164116 (2014).

[47]O. Christiansen, H. Koch and P. Jørgensen. Perturbative triple excitation corrections to coupled cluster singles and doubles excitation energies. J. Chem. Phys. **105**, 1451 (1996).

[48]H. Koch, O. Christiansen, P. Jørgensen, A. M. J. Sánchez de Méras and T. Helgaker. The CC3 model: An iterative coupled cluster approach including connected triples. J. Chem. Phys. **106**, 1808 (1997).

[49]Y. S. Lee, S. A. Kucharski and R. J. Bartlett. A Coupled Cluster Apporach with Triple Excitations. J. Chem. Phys. **81**, 5906 (1984).

[50]M. Urban, J. Noga, S. J. Cole and R. J. Bartlett. Towards a full CCSDT model for electron correlation. J. Chem. Phys. **83**, 4041 (1985).

[51]J. D. Watts and R. J. Bartlett. Economical triple excitation equation-of-motion coupled-cluster methods for excitation energies. Chem. Phys. Lett. **233**(1), 81 (1995).

[52]O. Christiansen, H. Koch and P. Jørgensen. Response functions in the CC3 iterative triple excitation model. J. Chem. Phys. **103**, 7429 (1995).

[53]D. A. Matthews and J. F. Stanton. A new approach to approximate equation-of-motion coupled cluster with triple excitations. J. Chem. Phys. **145**(12), 124102 (2016).

[54]J. Noga, R. J. Bartlett and M. Urban. Towards a full CCSDT model for electron correlation: CCSDT-n models. J. Chem. Phys. **83**, 4041 (1985).

[55]J. D. Watts and R. J. Bartlett. Iterative and non-iterative triple excitation corrections in coupled-cluster methods for excited electronic states: the EOM-CCSDT-3 and EOM-CCSD($\tilde{\text{T}}$) methods. Chem. Phys. Lett. **258**(5), 581 (1996).

[56]P.-F. Loos, A. Scemama, A. Blondel, Y. Garniron, M. Caffarel and D. Jacquemin. A Mountaineering Strategy to Excited States: Highly Accurate Reference Energies and Benchmarks. J. Chem. Theory Comp. **14**(8), 4360 (2018).

[57]M. S. Frank and C. Hättig. A pair natural orbital based implementation of CCSD excitation energies within the framework of linear response theory. J. Chem. Phys. **148**, 134102 (2018).

[58]R. H. Myhre, A. M. J. Sánchez de Merás and H. Koch. Multi-level coupled cluster theory. J. Chem. Phys. **141**, 224105 (2014).

[59]R. H. Myhre and H. Koch. The multilevel CC3 coupled cluster model. J. Chem. Phys. **145**, 044111 (2016).

[60]D. G. Liakos and F. Neese. Is It Possible To Obtain Coupled Cluster Quality Energies at near Density Functional Theory Cost? Domain-Based Local Pair Natural Orbital Coupled Cluster vs Modern Density Functional Theory. J. Chem. Theory Comput. (2015).

[61]S. Li, J. Ma and Y. Jiang. Linear scaling local correlation approach for solving the coupled cluster equations of large systems. J. Chem. Phys. **23**(2), 237 (2002).

[62]W. Li, P. Piecuch, J. R. Gour and S. Li. Local correlation calculations using standard and renormalized coupled-cluster approaches. J. Chem. Phys. **131**(11), 114109 (2009).

[63]W. Li and P. Piecuch. Improved Design of Orbital Domains within the Cluster-in-Molecule Local Correlation Framework: Single-Environment Cluster-in-Molecule Ansatz and Its Application to Local Coupled-Cluster Approach with Singles and Doubles. J. Phys. Chem. A. **114**(33), 8644 (2010).

[64]Z. Rolik and M. Kállay. A general-order local coupled-cluster method based on

the cluster-in-molecule approach. J. Chem. Phys. **135**(10), 104111 (2011).

[65]M. Ziókowski, B. Jansík, T. Kjærgaard and P. Jørgensen. Linear scaling coupled cluster method with correlation energy based error control. J. Chem. Phys. **133**(1), 014107 (2010).

[66]K. Kristensen, M. Ziókowski, B. Jansk, T. Kjærgaard and P. Jørgensen. A Locality Analysis of the Divide-Expand-Consolidate Coupled Cluster Amplitude Equations. J. Chem. Theory Comput. **7**(6), 1677 (2011).

[67]I.-M. Høyvik, K. Kristensen, B. Jansik and P. Jørgensen. The divide-expand-consolidate family of coupled cluster methods: Numerical illustrations using second order Møller-Plesset perturbation theory. J. Chem. Phys. **136**(1), 014105 (2012).

[68]M. Kobayashi, Y. Imamura and H. Nakai. Alternative linear-scaling methodology for the second-order Mller-Plesset perturbation calculation based on the divide-and-conquer method. J. Chem. Phys. **127**(7), 074103 (2007).

[69]M. Kobayashi and H. Nakai. Extension of linear-scaling divide-and-conquer-based correlation method to coupled cluster theory with singles and doubles excitations. J. Chem. Phys. **129**(4), 044103 (2008).

[70]K. Kitaura, T. Sawai, T. Asada, T. Nakano and M. Uebayasi. Pair interaction molecular orbital method: an approximate computational method for molecular interactions. Chem. Phys. Lett. **312**(2), 319 (1999).

[71]T. Nakano, T. Kaminuma, T. Sato, Y. Akiyama, M. Uebayasi and K. Kitaura. Fragment molecular orbital method: application to polypeptides. Chem. Phys. Lett. **318**(6), 614 (2000).

[72]N. Flocke and R. J. Bartlett. A natural linear scaling coupled-cluster method. J. Chem. Phys. **121**(22), 10935 (2004).

[73]H. Stoll. The correlation energy of crystalline silicon. Chem. Phys. Lett. **191**(6), 548 (1992).

[74]H. Stoll. Correlation energy of diamond. Phys. Rev. B. **46**, 6700 (1992).

[75]B. Paulus, P. Fulde and H. Stoll. Electron correlations for ground-state properties of group-IV semiconductors. Phys. Rev. B. **51**, 10572 (1995).

[76]H. Stoll, B. Paulus and P. Fulde. On the accuracy of correlation-energy expansions in terms of local increments. J. Chem. Phys. **123**(14), 144108 (2005).

[77]J. Friedrich and M. Dolg. Implementation and performance of a domain-specific basis set incremental approach for correlation energies: Applications to hydrocarbons and a glycine oligomer. J. Chem. Phys. **129**(24), 244105 (2008).

[78]J. Friedrich. Incremental Scheme for Intermolecular Interactions: Benchmarking the Accuracy and the Efficiency. J. Chem. Theory Comput. **8**(5), 1597 (2012).

[79]J. J. Eriksen, P. Baudin, P. Ettenhuber, K. Kristensen, T. Kjærgaard and P. Jørgensen. Linear-Scaling Coupled Cluster with Perturbative Triple Excitations: The Divide-Expand-Consolidate CCSD(T) Model. J. Chem. Theory Comput. **11**(7), 2984 (2015).

[80]T. F. Hughes, N. Flocke and R. J. Bartlett. Natural Linear-Scaled Coupled-Cluster Theory with Local Transferable Triple Excitations: Applications to Peptides. J. Phys. Chem. A. **112**(26), 5994 (2008).

[81]D. G. Fedorov and K. Kitaura. Coupled-cluster theory based upon the fragment molecular-orbital method. J. Chem. Phys. **123**(13), 134103 (2005).

[82]J. Friedrich and M. Dolg. Fully Automated Incremental Evaluation of MP2 and CCSD(T) Energies: Application to Water Clusters. J. Chem. Theory Comput. **5**(2), 287 (2009).

[83]J. Friedrich and K. Walczak. Incremental CCSD(T)(F12)—MP2-F12A Method to Obtain Highly Accurate CCSD(T) Energies for Large Molecules. J. Chem. Theory Comput. **9**(1), 408 (2013).

[84]J. Friedrich and J. Hänchen. Incremental CCSD(T)(F12*)—MP2: A Black Box Method To Obtain Highly Accurate Reaction Energies. J. Chem. Theory Comput. **9**(12), 5381 (2013).

[85]S. Saebø and P. Pulay. Local configuration interaction: An efficient approach for

larger molecules. Chem. Phys. Lett. **113**, 13 (1985).

[86]S. Saebø and P. Pulay. Local Treatment of Electron Correlation. Ann. Rev. Phys. Chem. **44**, 213 (1993).

[87]P. Pulay. Localizability of dynamic electron correlation. Chem. Phys. Lett. **100**, 151 (1983).

[88]P. Pulay and S. Saebø. Orbital-invariant formulation and second-order gradient evaluation in Møller-Plesset perturbation theory. Theor. Chim. Acta. **69**, 357 (1986).

[89]S. Saebø and P. Pulay. Fourth-order Møller-Plessett perturbation theory in the local correlation treatment. I. Method. J. Chem. Phys. **86**, 914 (1987).

[90]S. Saebø and P. Pulay. The local correlation treatment. II. Implementation and tests. J. Chem. Phys. **88**, 1884 (1988).

[91]J. W. Boughton and P. Pulay. Comparison of the boys and Pipek-Mezey localizations in the local correlation approach and automatic virtual basis selection. Journal of Computational Chemistry. **14**(6), 736 (1993).

[92]M. Schütz, G. Hetzer and H.-J. Werner. Low-order scaling local electron correlation methods. I. Linear scaling local MP2. J. Chem. Phys. **111**, 5691 (1999).

[93]J. Almlöf. Elimination of energy denominators in Møller-Plesset perturbation theory by a Laplace transform approach. Chem. Phys. Lett. **181**, 319 (1991).

[94]M. Häser and J. Almlöf. Laplace transform techniques in Møller-Plesset perturbation theory. J. Chem. Phys. **96**, 489 (1992).

[95]A. K. Wilson and J. Almlöf. MøllerPlesset correlation energies in a localized orbital basis using a Laplace transform technique. Theor. Chim. Acta. **95**, 49 (1997).

[96]M. Häser. Møller-Plesset (MP2) perturbation theory for large molecules. Theor. Chim. Acta. **87**(1), 147 (1993).

[97]D. S. Lambrecht, B. Doser and C. Ochsenfeld. Rigorous integral screening for

electron correlation methods. J. Chem. Phys. **123**(18), 184102 (2005).

[98]B. Doser, D. S. Lambrecht and C. Ochsenfeld. Tighter multipole-based integral estimates and parallel implementation of linear-scaling AO-MP2 theory. Phys. Chem. Chem. Phys. **10**, 3335 (2008).

[99]B. Helmich-Paris, M. Repisky and L. Visscher. Laplace-transformed atomic orbital-based Møller-Plesset perturbation theory for relativistic two-component Hamiltonians. J. Chem. Phys. **145**(1), 014107 (2016).

[100]P. Y. Ayala and G. E. Scuseria. Linear scaling second-order Møller-Plesset theory in the atomic orbital basis for large molecular systems. J. Chem. Phys. **110**(8), 3660 (1999).

[101]D. S. Hollman, J. J. Wilke and H. F. Schaefer. Explicitly correlated atomic orbital basis second order Møller-Plesset theory. J. Chem. Phys. **138**(6), 064107 (2013).

[102]P.-O. Löwdin and H. Shull. Natural Orbitals in the Quantum Theory of Two-Electron Systems. Phys. Rev. **101**, 1730 (1956).

[103]R. Ahlrichs, F. Driessler, H. Lischka, V. Staemmler and W. Kutzelnigg. PNO-CI (pair natural orbital configuration interaction) and CEPA-PNO (coupled electron pair approximation with pair natural orbitals) calculations of molecular systems. II. The molecules BeH_2, BH, BH_3, CH_4, CH_3^-, NH_3 (planar and pyramidal), H_2O, OH_3^+, HF and the Ne atom. J. Chem. Phys. **62**, 1235 (1975).

[104]R. Ahlrichs and F. Driessler. Direct determination of pair natural orbitals. Theor. Chem. Acc. **36**, 275 (1975).

[105]R. Ahlrichs, H. Lischka, B. Zurawski and W. Kutzelnigg. PNO-CI (pair-natural-orbital configuration interaction) and CEPA-PNO (coupled electron pair approximation with pair natural orbitals) calculations of molecular systems. IV. The molecules N_2, F_2, C_2H_2, C_2H_4, and C_2H_6. J, Chem. Phys. **63**(11), 4685 (1975).

[106]V. Staemmler and R. Jaquet. CEPA calculations on open-shell molecules. I.

Outline of the method. Theor. Chem. Acc. **59**, 487 (1981).

[107]F. Neese., Wennmohs and A. Hansen. Efficient and accurate local approximations to coupled-electron pair approaches: An attempt to revive the pair natural orbital method. J. Chem. Phys. **130**, 114108 (2009).

[108]F. Neese, A. Hansen and D. G. Liakos. Efficient and accurate approximations to the local coupled cluster singles doubles method using a truncated pair natural orbital basis. J. Chem. Phys. **131**, 064103 (2009).

[109]J. L. Whitten. Coulombic potential energy integrals and approximations. J. Chem. Phys. **58**, 4496 (1973).

[110]C. Riplinger and F. Neese. An efficient and near linear scaling pair natural orbital based local coupled cluster method. J. Chem. Phys. **138**(3), 034106 (2013).

[111]M. Saitow, U. Becker, C. Riplinger, E. F. Valeev and F. Neese. A new near-linear scaling, efficient and accurate, open-shell domain-based local pair natural orbital coupled cluster singles and doubles theory. J. Chem. Phys. **146**(16), 164105 (2017).

[112]C. Riplinger, B. Sandhoefer, A. Hansen and F. Neese. Natural triple excitations in local coupled cluster calculations with pair natural orbitals. J. Chem. Phys. **139**(13), 134101 (2013).

[113]M. Saitow, U. Becker, C. Riplinger, E. F. Valeev and F. Neese. A new near-linear scaling, efficient and accurate, open-shell domain-based local pair natural orbital coupled cluster singles and doubles theory. J. Chem. Phys. **146**(16), 164105 (2017).

[114]Y. Guo, C. Riplinger, U. Becker, D. G. Liakos, Y. Minenkov, L. Cavallo and F. Neese. Communication: An improved linear scaling perturbative triples correction for the domain based local pair-natural orbital based singles and doubles coupled cluster method [DLPNO-CCSD(T)]. J. Chem. Phys. **148**(1), 011101 (2018).

[115]O. Demel, J. Pittner and F. Neese. A Local Pair Natural Orbital-Based

Multireference Mukherjee's Coupled Cluster Method. J. Chem. Theory Comput. **11**(7), 3104 (2015).

[116]J. Brabec, J. Lang, M. Saitow, J. Pittner, F. Neese and O. Demel. Domain-Based Local Pair Natural Orbital Version of Mukherjees State-Specific Coupled Cluster Method. J. Chem. Theory Comput. **14**(3), 1370 (2018).

[117]J. Lang, J. Brabec, M. Saitow, J. Pittner, F. Neese and O. Demel. Perturbative triples correction to domain-based local pair natural orbital variants of Mukherjee's state specific coupled cluster method. Phys. Chem. Chem. Phys. **21**, 5022 (2019).

[118]J. Yang, Y. Kurashige, F. R. Manby and G. K. L. Chan. Tensor factorizations of local second-order Møller-Plesset theory. J. Chem. Phys. **134**(4), 044123 (2011).

[119]J. Yang, G. K.-L. Chan, F. R. Manby, M. Schütz and H.-J. Werner. The orbital-specific-virtual local coupled cluster singles and doubles method. J. Chem. Phys. **136**(14), 144105 (2012).

[120]M. Schütz, J. Yang, G. K.-L. Chan, F. R. Manby and H.-J. Werner. The orbital-specific virtual local triples correction: OSV-L(T). J. Chem. Phys. **138**(5), 054109 (2013).

[121]C. Krause and H.-J. Werner. Scalable Electron Correlation Methods. 6. Local Spin-Restricted Open-Shell Second-Order Møller-Plesset Perturbation Theory Using Pair Natural Orbitals: PNO-RMP2. J. Chem. Theory Comput. **15**(2), 987 (2019).

[122]Q. Ma, M. Schwilk, C. Köppl and H.-J. Werner. Scalable Electron Correlation Methods. 4. Parallel Explicitly Correlated Local Coupled Cluster with Pair Natural Orbitals (PNO-LCCSD-F12). J. Chem. Theory Comput. **13**(10), 4871 (2017).

[123]M. Schwilk, Q. Ma, C. Köppl and H.-J. Werner. Scalable Electron Correlation Methods. 3. Efficient and Accurate Parallel Local Coupled Cluster with Pair Natural Orbitals (PNO-LCCSD). J. Chem. Theory Comput. **13**(8), 3650 (2017).

[124]Q. Ma and H.-J. Werner. Scalable Electron Correlation Methods. 5. Parallel Perturbative Triples Correction for Explicitly Correlated Local Coupled Cluster with Pair Natural Orbitals. J. Chem. Theory Comput. **14**(1), 198 (2018).

[125]Q. Ma and H.-J. Werner. Accurate Intermolecular Interaction Energies Using Explicitly Correlated Local Coupled Cluster Methods [PNO-LCCSD(T)-F12]. J. Chem. Theory Comput. **15**(2), 1044 (2019).

[126]D. P. Tew, B. Helmich and C. Hättig. Local explicitly correlated second-order Møller-Plesset perturbation theory with pair natural orbitals. J. Chem. Phys. **135**(7), 074107 (2011).

[127]D. P. Tew and C. Hättig. Pair natural orbitals in explicitly correlated second-order Møller-Plesset theory. Int. J. Quantum Chem. **113**(3), 224 (2013).

[128]C. Hättig, D. P. Tew and B. Helmich. Local explicitly correlated second- and third-order Møller-Plesset perturbation theory with pair natural orbitals. J. Chem. Phys. **136**(20), 204105 (2012).

[129]G. Schmitz, C. Hättig and D. P. Tew. Explicitly correlated PNO-MP2 and PNO-CCSD and their application to the S66 set and large molecular systems. Phys. Chem. Chem. Phys. **16**, 22167 (2014).

[130]G. Schmitz and C. Hättig. Perturbative triples correction for local pair natural orbital based explicitly correlated CCSD(F12*) using Laplace transformation techniques. J. Chem. Phys. **145**(23), 234107 (2016).

[131]F. Pavošević, F. Neese and E. F. Valeev. Geminal-spanning orbitals make explicitly correlated reduced-scaling coupled-cluster methods robust, yet simple. J. Chem. Phys. **141**(5), 054106 (2014).

[132]F. Menezes, D. Kats and H.-J. Werner. Local complete active space second-order perturbation theory using pair natural orbitals (PNO-CASPT2). J. Chem. Phys. **145**(12), 124115 (2016).

[133]D. Kats and H.-J. Werner. Multi-state local complete active space second-order perturbation theory using pair natural orbitals (PNO-MS-CASPT2). J. Chem.

Phys. **150**(21), 214107 (2019).

[134]Y. Guo, K. Sivalingam, E. F. Valeev and F. Neese. SparseMaps – A systematic infrastructure for reduced-scaling electronic structure methods. III. Linear-scaling multireference domain-based pair natural orbital N-electron valence perturbation theory. J. Chem. Phys. **144**(9), 094111 (2016).

[135]Y. Guo, U. Becker and F. Neese. Comparison and combination of direct and fragment based local correlation methods: Cluster in molecules and domain based local pair natural orbital perturbation and coupled cluster theories. J. Chem. Phys. **148**(12), 124117 (2018).

[136]B. Fiedler, G. Schmitz, C. Hättig and J. Friedrich. Combining Accuracy and Efficiency: An Incremental Focal-Point Method Based on Pair Natural Orbitals. J. Chem. Theory Comput. **13**(12), 6023 (2017).

[137]M. Schütz, H.-J. Werner, R. Lindh and F. R. Manby. Analytical energy gradients for local second-order Møller-Plesset perturbation theory using density fitting approximations. J. Chem. Phys. **121**(2), 737 (2004).

[138]K. Ledermüller and M. Schütz. Local CC2 response method based on the Laplace transform: Analytic energy gradients for ground and excited states. J. Chem. Phys. **140**(16), 164113 (2014).

[139]M. Schütz. Oscillator strengths, first-order properties, and nuclear gradients for local ADC(2). J. Chem. Phys. **142**(21), 214103 (2015).

[140]G. Rauhut and H.-J. Werner. Analytical energy gradients for local coupled-cluster methods. Phys. Chem. Chem. Phys. **3**, 4853 (2001).

[141]K. Ledermüller, D. Kats and M. Schütz. Local CC2 response method based on the Laplace transform: Orbital-relaxed first-order properties for excited states. J. Chem. Phys. **139**(8), 084111 (2013).

[142]K. Freundorfer, D. Kats, T. Korona and M. Schütz. Local CC2 response method for triplet states based on Laplace transform: Excitation energies and first-order properties. J. Chem. Phys. **133**(24), 244110 (2010).

[143]D. Kats, T. Korona and M. Schütz. Transition strengths and first-order properties of excited states from local coupled cluster CC2 response theory with density fitting. J. Chem. Phys. **127**(6), 064107 (2007).

[144]M. Dornbach and H.-J. Werner. Analytical energy gradients for local second-order Møller-Plesset perturbation theory using intrinsic bond orbitals. Mol. Phys. **117**(9-12), 1252 (2019).

[145]G. Knizia. Intrinsic Atomic Orbitals: An Unbiased Bridge between Quantum Theory and Chemical Concepts. J. Chem. Theory Comput. **9**, 4834 (2013).

[146]K. Kristensen, P. Jørgensen, B. Jansk, T. Kjærgaard and S. Reine. Molecular gradient for second-order Møller-Plesset perturbation theory using the divide-expand-consolidate (DEC) scheme. J. Chem. Phys. **137**(11), 114102 (2012).

[147]D. Bykov, K. Kristensen and T. Kjærgaard. The molecular gradient using the divide-expand-consolidate resolution of the identity second-order Møller-Plesset perturbation theory: The DEC-RI-MP2 gradient. J. Chem. Phys. **145**(2), 024106 (2016).

[148]Z. Ni, Y. Wang, W. Li, P. Pulay and S. Li. Analytical Energy Gradients for the Cluster-in-Molecule MP2 Method and Its Application to Geometry Optimizations of Large Systems. J. Chem. Theory Comput. **15**(6), 3623 (2019).

[149]S. Schweizer, B. Doser and C. Ochsenfeld. An atomic orbital-based reformulation of energy gradients in second-order Møller-Plesset perturbation theory. J. Chem. Phys. **128**(15), 154101 (2008).

[150]M. Maurer and C. Ochsenfeld. A linear- and sublinear-scaling method for calculating NMR shieldings in atomic orbital-based second-order Møller-Plesset perturbation theory. J. Chem. Phys. **138**(17), 174104 (2013).

[151]P. Pinski and F. Neese. Communication: Exact analytical derivatives for the domain-based local pair natural orbital MP2 method (DLPNO-MP2). J. Chem. Phys. **148**, 031101 (2018).

[152]P. Pinski and F. Neese. Analytical gradient for the domain-based local pair natural orbital second order Møller-Plesset perturbation theory method (DLPNO-MP2). J. Chem. Phys. **150**, 164102 (2019).

[153]T. Crawford and R. A. King. Locally correlated equation-of-motion coupled cluster theory for the excited states of large molecules. Chem. Phys. Lett. **366**(5), 611 (2002).

[154]T. Korona and H.-J. Werner. Local treatment of electron excitations in the EOM-CCSD method. J. Chem. Phys. **118**(7), 3006 (2003).

[155]D. Kats, T. Korona and M. Schütz. Local CC2 electronic excitation energies for large molecules with density fitting. J. Chem. Phys. **125**(10), 104106 (2006).

[156]R. A. Mata and H. Stoll. An incremental correlation approach to excited state energies based on natural transition/localized orbitals. J. Chem. Phys. **134**(3), 034122 (2011).

[157]D. Mester, P. R. Nagy and M. Kállay. Reduced-cost second-order algebraic-diagrammatic construction method for excitation energies and transition moments. J. Chem. Phys. **148**(9), 094111 (2018).

[158]D. Mester, P. R. Nagy and M. Kállay. Reduced-cost linear-response CC2 method based on natural orbitals and natural auxiliary functions. J. Chem. Phys. **146**(19), 194102 (2017).

[159]R. Send, V. R. I. Kaila and D. Sundholm. Reduction of the virtual space for coupled-cluster excitation energies of large molecules and embedded systems. J. Chem. Phys. **134**(21), 214114 (2011).

[160]P. Baudin and K. Kristensen. LoFEx A local framework for calculating excitation energies: Illustrations using RI-CC2 linear response theory. J. Chem. Phys. **144**(22), 224106 (2016).

[161]P. Baudin, D. Bykov, D. Liakh, , P. Ettenhuber and K. Kristensen. A local framework for calculating coupled cluster singles and doubles excitation energies (LoFEx-CCSD). Mol. Phys. **115**, 2135 (2017).

[162]P. Baudin and K. Kristensen. Correlated natural transition orbital framework for low-scaling excitation energy calculations (CorNFLEx). J. Chem. Phys. **146**(21), 214114 (2017).

[163]P. Baudin and K. Kristensen. LoFEx - A local framework for calculating excitation energies: Illustrations using RI-CC2 linear response theory. J. Chem. Phys. **144**, 224106 (2016).

[164]P. Baudin, D. Bykov, D. Liakh, P. Ettenhuber and K. Kristensen. A local framework for calculating coupled cluster singles and doubles excitation energies (LoFEx-CCSD). Mol. Phys. **115**(17-18), 2135 (2017).

[165]C. Kumar and T. D. Crawford. Frozen Virtual Natural Orbitals for Coupled-Cluster Linear-Response Theory. J. Chem. Phys. **121**, 708 (2017).

[166]Y. C. Park, A. Perera and R. J. Bartlett. Low scaling EOM-CCSD and EOM-MBPT(2) method with natural transition orbitals. J. Chem. Phys. **149**(18), 184103 (2018).

[167]A. K. Dutta, F. Neese and R. Izsák. Towards a Pair Natural Orbital Coupled Cluster Method for Excited States. J. Chem. Phys. **145**, 034102 (2016).

[168]M. Nooijen and R. J. Bartlett. A new method for excited states: Similarity transformed equation-of-motion coupled-cluster theory. J. Chem. Phys. **106**(15), 6441 (1997).

[169]A. K. Dutta, M. Saitow, C. Riplinger, F. Neese and R. Izsák. A near-linear scaling equation of motion coupled cluster method for ionized states. J. Chem. Phys. **148**, 244101 (2018).

[170]A. K. Dutta, M. Saitow, B. Demoulin, F. Neese and R. Izsák. A domain-based local pair natural orbital implementation of the equation of motion coupled cluster method for electron attached states. J. Chem. Phys. **150**, 164123 (2019).

[171]A. K. Dutta, M. Nooijen, F. Neese and R. Izsák. Automatic active space selection for the similarity transformed equations of motion coupled cluster method. J. Chem. Phys. **146**, 074103 (2017).

[172]L. M. J. Huntington, M. Krupička, F. Neese and R. Izsák. Similarity transformed equation of motion coupled-cluster theory based on an unrestricted Hartree-Fock reference for applications to high-spin open-shell systems. J. Chem. Phys. **147**, 174104 (2017).

[173]S. Pal, M. D. Prasad and D. Mukherjee. On certain correspondences among various coupled-cluster theories for closed-shell systems. Pramana. **18**(3), 261 (1982).

[174]T. Helgaker, P. Jørgensen and N. C. Handy. A numerically stable procedure for calculating Møller-Plesset energy derivatives, derived using the theory of Lagrangians. Theor. Chim. Acta. **76**, 227 (1989).

[175]M. S. Frank, G. Schmitz and C. Hättig. The PNO-MP2 gradient and its application to molecular geometry optimizations. Mol. Phys. **115**, 343 (2017).

[176]E. R. Davidson. Iterative Calculation of a few of Lowest Eigenvalues and Corresponding Eigenvectors of Large Real-Symmetric Matrices. J. Comput. Phys. **17**, 87 (1975).

[177]C. Hättig, D. P. Tew and B. Helmich. Local explicitly correlated second- and third-order Møller-Plesset perturbation theory with pair natural orbitals. J. Chem. Phys. **136**, 204105 (2012).

[178]G. Schmitz, B. Helmich and C. Hättig. A $\mathcal{O}(\mathcal{N}^3)$-scaling PNO-MP2 method using a hybrid OSV-PNO approach with an iterative direct generation of OSVs. Mol. Phys. **111**(16-17), 2463 (2013).

[179]C. Riplinger and F. Neese. Natural triple excitations in local coupled cluster calculations with pair natural orbitals. J. Chem. Phys. **139**, 134101 (2013).

[180]G. Schmitz and C. Hättig. Accuracy of Explicitly Correlated Local PNO-CCSD(T). J. Chem. Theory. Comput. **13**(6), 2623 (2017). PMID: 28514146.

[181]B. Helmich. Paarspezifische natrliche Orbitale zur effizienten Berechnung von Coupled-Cluster-Anregungsenergien. PhD thesis, Ruhr-Universität Bochum,

2014.

[182]C. Peng, M. C. Clement and E. F. Valeev. State-Averaged Pair Natural Orbitals for Excited States: A Route toward Efficient Equation of Motion Coupled-Cluster. J. Chem. Theory Comput. **14**, 5597 (2018).

[183]H. Wielandt. Beiträge zur mathematischen Behandlung komplexer Eigenwertprobleme, Teil V: Bestimmung höerer Eigenwerte durch gebrochene Iteration. Aerodynamische Versuchsanstalt Göttingen, B 44/J/37, 1944.

[184]S. F. Boys. Construction of Some Molecular Orbitals to Be Approximately Invariant for Changes from One Molecule to Another. Rev. Mod. Phys. **32**, 296 (1960).

[185]W. Kohn. Density functional theory for systems of very many atoms. Int. J. Quantum Chem. **56**(4), 229 (1995).

[186]E. Schwegler and M. Challacombe. Linear scaling computation of the Hartree-Fock exchange matrix. J. Chem. Phys. **105**(7), 2726 (1996).

[187]M. Sierka, A. Hogekamp and R. Ahlrichs. Fast evaluation of the Coulomb potential for electron densities using multipole accelerated resolution of identity approximation. The Journal of Chemical Physics. **118**(20), 9136 (2003).

[188]M. Schütz and H.-J. Werner. Local perturbative triples correction (T) with linear cost scaling. Chem. Phys. Lett. **318**, 370 (2000).

[189]M. Schütz. Low-order scaling local electron correlation methods. III. Linear scaling local perturbative triples correction. Chem. Phys. Lett. **130**, 9986 (2000).